DEPARTMENT OF PHYSICS

PERTURBATIVE STUDY OF QUARK AND GLUON OPERATORS WITH IMPROVED ACTIONS ON THE LATTICE

DOCTOR OF PHILOSOPHY DISSERTATION

MARIOS COSTA

2014

Department of Physics

Perturbative Study of Quark and Gluon Operators with Improved Actions on the Lattice

Doctor of Philosophy Dissertation

Marios Costa

Advisor

Haralambos Panagopoulos

A dissertation submitted to the University of Cyprus in partial fulfillment of the requirements for the degree of Doctor of Philosophy

May 2014

PhD Candidate: Marios Costa

Title of Dissertation: Perturbative study of quark and gluon operators with improved actions on the lattice

Dissertation Committee:

Prof. Haralambos Panagopoulos, Research Supervisor

Prof. Fotios Ptochos

Prof. Nicolas Toumbas, Committee Chairman

Prof. Ettore Vicari

Prof. Matthew Zervos

Defended on April 28, 2014

The present doctoral dissertation was submitted in partial fulfillment of the requirements for the degree of Doctor of Philosophy of the University of Cyprus. It is a product of original work of my own, unless otherwise mentioned through references, notes, or any other statements.

Marios Costa

Dedicated to my advisor, Haris Panagopoulos, for guiding and supporting me over the years.

Acknowledgments

First of all, I would like to thank my advisor, Professor Haris Panagopoulos, for his constant enthusiasm and encouragement. I express my sincerest gratitude to him, whose guidance made this Thesis possible. It was certainly a privilege to be his student and I will miss all the times we spent together in his office.

Secondly, I want to thank Martha Constantinou for our collaboration in all of the computations presented here.

I do not have enough words to thank my parents for their love, support and their sacrifices.

I also feel the need to thank those who contributed in different ways to the realization of this work:

⋆ Professor Nicolas Toumbas, for many useful discussions on Field Theory and Group Theory.

⋆ Fotos Stylianou, who encouraged me to join the Lattice QCD community.

⋆ My brother, Costantino Costa, who gave me solutions to various computational problems.

⋆ Salomi Demou, with her positive way of thinking that was transferring to me as well. Our brief lunch breaks were extremely refreshing for me.

⋆ Diomidi Papadiomidous for being a good friend with genuine interest on the progress of my work.

⋆ All those of you, who have been by my side during my graduate studies. Your support is definitely appreciated.

Lastly, I thank the Research Promotion Foundation of Cyprus for financial support over an year.

Περίληψη

Στα πλαίσια της παρούσας Διατριβής πραγματοποιούνται διαταρακτικοί υπολογισμοί στην Κβαντική Χρωμοδυναμική (ΚΧΔ), στο φορμαλισμό του Πλέγματος. Εφαρμόζουμε μία ποικιλία από βελτιωμένες φερμιονικές και γκλουονικές δράσεις, οι οποίες χρησιμοποιούνται ευρέως στις αριθμητικές προσομοιώσεις. Οι υπολογισμοί που παρουσιάζονται είναι οι ακόλουθοι:

• Υπολογίσαμε τον διαδότη για φερμιόνια staggered και τις συναρτήσεις Green με ένα εξωτερικό κουάρκ και ένα εξωτερικό αντικουάρκ για ένα πλήρες σύνολο από υπερτοπικούς (ultralocal) διγραμμικούς φερμιονικούς τελεστές, χρησιμοποιώντας θεωρία διαταραχών μέχρι ένα βρόγχο και στην χαμηλότερη τάξη ως προς την σταθερά του πλέγματος. Από τους υπολογισμούς μας προσδιορίσαμε τις συναρτήσεις επανακανονικοποίησης για το πεδίο κουάρκ και για όλους τους υπερτοπικούς taste-singlet διγραμμικούς φερμιονικούς τελεστές. Το καινούργιο στοιχείο αυτού του υπολογισμού ήταν ότι οι γκλουονικοί σύνδεσμοι (links), οι οποίοι εμφανίζονται στη φερμιονική δράση και στον ορισμό των διγραμμικών φερμιονικών τελεστών, είχαν βελτιωθεί με την εφαρμογή της διαδικασίας stout smearing έως δύο φορές, επαναληπτικά. Εφαρμόσαμε τα αποτελέσματα μας για τον υπολογισμό της μαγνητικής επιδεκτικότητας της ΚΧΔ σε μηδενική και σε πεπερασμένη θερμοκρασία.

• Μελετήσαμε τις συνέπειες της πεπερασμένης σταθέρας πλεγματός a, στην τάξη a^2, πάνω σε πινακοστοιχεία των τοπικών και εκτεταμένων διγραμμικών φερμιονικών τελεστών, χρησιμοποιώντας τη δράση SLiNC. Η συμπερίληψη όρων μέχρι και τάξης $\mathcal{O}(a^2)$ περιπλέκει δραματικά αυτήν την εργασία αν και πρόκειται για ενός βρόγχου υπολογισμό. Υπολογίσαμε τις συναρτήσεις πολλαπλασιαστικής επανακανονικοποίησης, οι οποίες απαιτούνται προκειμένου να συσχετίσουμε τα αριθμητικά αποτελέσματα για τα πινακοστοιχεία ρευμάτων όπως προέκυψαν από προσομοιώσεις στο πλέγμα, με τα πεπερασμένα φυσικά πινακοστοιχεία. Ειδικότερα μελετήσαμε μια μέθοδο για την καταστολή των τεχνουργημάτων του πλέγματος, αφαιρώντας τις συνεισφορές ενός βρόγχου στις συναρτήσεις επανακανονικοποίησης, οι οποίες υπολογίστηκαν με θεωρία διαταραχών, από μη διαταρακτικές συνεισφορές. Συγκρίναμε αποτελέσματα, τα οποιά δημιουργήθηκαν από την πλήρη αφαίρεση των αποτελεσμάτων ενός βρόγχου, με εκείνα

όπου αφαιρέσαμε τη συνεισφορά τάξης a^2. Τα αποτελέσματα μας είναι σημαντικά για τη μελέτη των αδρονικών συναρτήσεων δομής, οι οποίες με την σειρά τους παρέχουν πληροφορίες σχετικά με τις κατανομές του σπιν, της ελικότητας και της ορμής των συστατικών σωματιδίων ενός αδρονίου.

• Υπολογίσαμε την επανακανονικοποίηση του χρωμομαγνητικού τελεστή, $\mathcal{O}_{CM}$. Ο υπολογισμός αυτός δεν ήταν καθόλου τετριμμένος. Μια σοβαρή επιπλοκή σ'αυτή την περίπτωση είναι ότι τελεστές με ίδιους κβαντικούς αριθμούς και με ίση ή μικρότερη διάσταση, μπορούν να αναμιχθούν με τον $\mathcal{O}_{CM}$ στο κβαντικό επίπεδο. Αυτό το φαινόμενο επιδεινώνεται όταν χρησιμοποιήσουμε πλεγματικές δράσεις χωρίς συμμετρία χείρος. Σε αυτήν την περίπτωση ακόμη και τελεστές με διαφορετική χειραλικότητα μπορούν να αναμιχθούν. Είναι όλο και πιο σημαντικό, ως εκ τούτου, να υπολογίσουμε τον πίνακα ανάμειξης των συναρτήσεων επανακανονικοποίησης, έτσι ώστε να ενισχυθεί όσο το δυνατό περισσότερο το αντίστοιχο φυσικό σήμα από τις μετρήσεις Monte Carlo. Τα αποτελέσματα μας για τα πινακοστοιχεία του $\mathcal{O}_{CM}$ εμφανίζονται, π.χ., σε μελέτες διασπάσεων βαρεών μεσονίων που εμπλέκουν αλλαγή γεύσης.

Abstract

In this Thesis we present results on perturbative calculations which we have performed in the context of Quantum Chromodynamics (QCD), formulated on the Lattice. We have employed a variety of improved fermion and gluon actions, which are currently used in numerical simulations. The calculations that we present are the following:

• We computed the staggered fermion propagator, as well as the Green's functions with one external quark-antiquark pair for a complete set of ultralocal staggered fermion bilinear operators, using perturbation theory up to one-loop and to lowest order in the lattice spacing. From our calculations we determined the renormalization functions for the quark field and for all ultralocal taste-singlet bilinear operators. The novel aspect of our calculations was that the gluon links, which appear both in the fermion action and in the definition of the bilinear operators, had been improved by applying a stout smearing procedure up to two times, iteratively. We apply our finding to the evaluation of the magnetic susceptibility of QCD at zero and finite temperature.

• We studied effects of finite lattice spacing a, to order a^2, on matrix elements of local and extended bilinear operators, using the SLiNC action. Carrying out calculations all the way to $\mathcal{O}(a^2)$ complicates dramatically the task at hand, even though our computations were at one loop. We computed the multiplicative renormalization functions, which are required in order to relate the current matrix elements, as extracted numerically from lattice simulations, to the physical finite matrix elements. In particular we investigated a method to suppress the lattice artifacts by subtracting one-loop contributions to renormalization functions, calculated in lattice perturbation theory, from nonperturbative results. We compared results obtained from a complete one-loop subtraction with those obtained via a subtraction of contributions proportional to the square of the lattice spacing. These results are relevant for the study of hadronic structure functions, which in turn provide information on the spin, helicity and momentum distributions of the constituent particles in a hadron.

• We calculated the renormalization of the chromomagnetic operator, $\mathcal{O}_{CM}$. This calculation was highly nontrivial. A serious complication in this case is that operators with the same quantum numbers and equal or lower dimensionality can mix with $\mathcal{O}_{CM}$ at the quantum level. This effect is exacerbated when using lattice actions with inexact chiral symmetry; in this case, even operators with different chiralities can mix. It becomes all the more important, therefore, to compute the mixing matrix of renormalization functions, so as to disentangle as much as possible the corresponding physical signals from Monte Carlo measurements. Our results for the matrix elements of $\mathcal{O}_{CM}$ appear, e.g., in the study of flavor-changing decays of heavy mesons.

Contents

List of Figures

List of Tables

Chapter 1

Introduction

1.1 Introduction to Quantum Chromodynamics

The most appropriate theory for the description of strong interactions is Quantum Chromodynamics (QCD). The theory of QCD has been introduced since the 1970s and is an integral part of the Standard Model. QCD is based on the non-Abelian group $SU(3)$, where the number 3 refers to the number of colors carried by quarks. This group has eight generators, the number 8 corresponding to the number of gluons. QCD has two fundamental properties, infrared (IR) slavery, which is an increase of the coupling constant g at low energies, and asymptotic freedom, which is the vanishing of the coupling at high energies. Asymptotic freedom was proven by David J. Gross, H. David Politzer and Frank Wilczek [1] (Nobel prize 2004), while infrared slavery has only been demonstrated numerically on the lattice. Given that both quarks and gluons have color charge as an additional degree of freedom, gluons interact with themselves.

The result of IR slavery is confinement, which means that quarks in experiments are never observed alone; rather they come in color-singlet combinations, which are called hadrons. Hadrons can be either mesons (quark-antiquark pairs) or baryons (3 quarks or 3 antiquarks). There exist six flavors of quarks: up (u), down (d), strange (s), charm (c), bottom (b) and top (t). The Hamiltonian eigenstates in QCD are hadrons, whose properties can fix the fundamental parameters of QCD: the coupling constant g (or $\alpha_s = g^2/4\pi$) and the quark masses m.

In order to obtain information on hadronic properties we study structure functions. These functions are a measure of the partonic composition of hadrons, which is important for hadronic collisions and decays. They are a key ingredient for deriving parton distribu-

tion functions (PDFs) of the nucleons. In recent years dramatic progress has been made in the understanding of nucleon structure and partonic content, due to important theoretical advances, and the availability of new high precision experiments.

In particular some particle colliders use two protons, or proton-antiproton pair, as initial state, thus reaching very high center-of-mass energies. Recent QCD related results were taken in the Fermilab Tevatron Collider and in the Large Hadron Collider (LHC). The data of these colliders leads to a better determination and detailed understanding of the partonic structure of the nucleon. Further detailed studies have been carried out on: inclusive photon and diphoton production, vector boson plus jets production, event shape variables, and other inclusive multijet productions. Comparisons of experimental measurements with QCD can be performed using a variety of theoretical approximations. Studying jets in experiments we test our understanding and predictions of high-energy QCD processes. Jet physics also provides a check of the strong coupling constant α_s. A recent determination of the strong coupling constant from jet data has been achieved at Fermilab. Further hadronic processes are investigated at LHC, in particular in the ATLAS, CMS and LHCb experiments.

Because of the strong force it is difficult to perform analytic calculations of scattering processes involving hadronic particles from first principles; it is only in the asymptotic-freedom regime that perturbation theory can be effectively applied. In this regime one may also make use of the Factorisation Theorem: the latter separates processes into non-perturbative PDFs which describe the composition of the proton and can be determined from experiment, and perturbative coefficient functions associated with higher scales which are calculated as a power-series in $\alpha_s(\mu)$. Thus, in order to understand any of the results of the above experiments one needs to understand how incoming hadrons are made up from constituent quarks and gluons, the interactions of which we then know how to calculate using perturbation theory as long as there is a large scale μ in the process so that perturbation theory is applicable. The production of any particle, say a Higgs boson at a hadron collider can be determined by the cross section of the parton-parton collision to produce the Higgs, convoluted with the probabilities to find these partons within the incoming hadrons. We can use deep inelastic scattering (DIS) experiments to probe the structure of hadrons and the fundamental interactions of quarks, gluons, and leptons. In DIS experiments a lepton probes a target nucleon or nucleus via exchange of an electroweak boson.

An additional physical process which is being investigated at LHC is the production of the deconfined quark-gluon plasma (QGP) phase in heavy-ion ($PbPb$) collisions at high

energies. Quarkonia ($c\bar{c}$ or $b\bar{b}$ bound states) are a useful means to probe QGP and to investigate the behavior of QCD in a high parton-density environment. A QGP state of matter would suggest a phase transition at some temperature. The existence of such phase transition was first exhibited in the strong coupling limit of QCD, and further corroborated by detailed numerical simulations.

1.2 Lattice QCD

The fact that perturbation theory alone cannot describe many aspects of strong interactions, makes quantitative studies of QCD a formidable task. For this purpose, an idea proposed in 1974 by Kenneth G. Wilson [2] was to formulate Gauge Theories on a spacetime lattice; such a formulation provides description of strongly coupled theories also nonperturbatively. Lattice theory is a way of regularizing quantum field theories. The regularization is achieved in the low-energy (InfraRed, IR) regime using a finite lattice size L. But in the end of every computation we will need to extrapolate our results to an infinite lattice size. The high-energy (UltraViolet, UV) regime is regularized by using a finite lattice spacing a. This introduces a momentum cutoff which is inverse to a, since the momenta are restricted to the finite interval $-\pi/a \leq p \leq \pi/a$ (first Brillouin zone). We could use other UV regulators (e.g. Pauli-Villars, Dimensional Regularization, momentum cutoff) but they are only applicable to perturbative calculations.

The subjects of lattice QCD are multidirectional. The subjects which are most actively pursued are listed below with some examples of recent research activity:

- Advances of lattice QCD algorithms have been in constant development over the years. These advances concern topics such as methods to simulate heavy quarks, the effects of quenching and the relevance of partial quenching, nonperturbative renormalization of operators, the role of chiral perturbation theory in extracting hadronic quantities from lattice QCD, the reduction of lattice-spacing artifacts, and the use of small-volume computations to extract infinite-volume physics.

- In order to study Hadron phenomenology, new methods and techniques are used. Some works are dedicated to improved computations of hadron masses, decay constants and weak transition matrix elements. Calculations of moments of structure functions, the running coupling and quark masses and many other physical quantities have also been reported. Lattice QCD also provides the best theoretical evidence that glueballs states exist.

- Some research teams are interested in analyzing the properties of QCD under extreme conditions. On one hand there is the goal of reaching a quantitative description of the behaviour of matter at high temperature and density. This does provide important input for a quantitative description of experimental signatures for the occurrence of a phase transition in heavy ion collisions. At high temperatures the interaction between quarks and gluons decreases due to asymptotic freedom, leading to deconfinement, and chiral symmetry is restored. On the other hand the analysis of a complicated quantum field theory like QCD at non-zero temperature can also help to improve our understanding of its nonperturbative properties at zero temperature. The low-temperature phase exhibits confinement and breaking of chiral symmetry. The introduction of external control parameters (temperature, chemical potential) allows to observe the response of different observables to this and may provide a better understanding of their interdependence.

- Using the lattice one can study, besides those transitions which we described, phase transitions that occurred during the early times of the evolution of the universe, such as the electroweak phase transition. The study of Quantum Fields on the Lattice also extends to Physics beyond the Standard Mondel, e.g. the study of quantum gravity and supersymmetric Yang-Mills theories.

- Calculations, using Lattice gauge theory, play a key role also in flavor physics: Flavor-changing amplitudes can be computed, providing information on the Cabibbo-Kobayashi-Maskawa (CKM) quark-mixing matrix. At the LHC, bottom baryons are being produced in unprecedented quantities, which opens up a new field for flavor physics. For example, the decay $\Lambda_b \to p\mu^-\bar{\nu_\mu}$ can be used to obtain a novel determination of the CKM matrix element $|V_{ub}|$, and the decay $\Lambda_b \to \Lambda\mu^+\mu^-$ probes the weak interactions beyond tree-level. The first lattice calculations of the relevant $\Lambda_b \to p$ and $\Lambda_b \to \Lambda$ form factors have recently been performed using domain-wall light quarks and static b quarks. In both cases, form factor calculations using lattice QCD are needed to interpret the experimental data.

- In the past few years there have been also a lot of theoretical developments. We mention here the Yang-Mills "gradient flow", which can be a powerful tool for non-perturbative studies of QCD. A key feature of the flow is certainly the fact that local fields constructed at positive flow time renormalize in a simple way, however complicated they may be. Correlation functions of such fields calculated in lattice QCD

therefore have a well-defined continuum limit and thus provide interesting probes of the universal properties of the theory.

These and other ideas are currently under intensive exploration. Given recent and future increases in computer power these advances will allow more reliable calculations of hadronic quantities.

1.3 Lattice Perturbation theory

The lattice is generally used in nonperturbative calculations but comparison with physical values often requires also perturbative calculations. Perturbation theory is an essential aspect of computations on the lattice, especially for investigating the behavior of lattice theories near the continuum limit. For a review in lattice perturbation theory see e.g., Ref. [3].

The role of perturbation theory on the lattice is very important since perturbative calculations connect the outcome of numerical simulations to the continuum physical results. Using perturbation theory we can determine the renormalization functions (RFs) of composite operators and of bare parameters of the Lagrangian, like coupling constant and masses. In many cases one could extract RFs nonperturbatively, but often a nonperturbative determination may turn out to be rather difficult (or impossible) to achieve. In cases where we can find RFs nonperturbatively we can always compare with the corresponding perturbative results, for a specific renormalization scale. This comparison can give significant cross-checks on the validity of perturbative and nonperturbative methods. We should also add that perturbative coefficients can be usually computed much more accurately than typical quantities in numerical simulations. A notetable exception regards mixing coefficients of operators of lower dimensionality. These coefficients necessarily contain inverse powers of the lattice spacing; consequently they diverge on $a \to 0$, and their perturbative estimation cannot be relied on. A specific instance of this behavior regards the vacuum expectation value of certain operators, i.e. their mixing coefficient with the identity operator.

Moreover, lattice perturbation theory is important for a number of other investigations, among which we can mention the study of anomalies on the lattice, the study of the general approach to the continuum limit, including the recovery of continuum symmetries broken by the lattice regularization (like Lorentz or chiral symmetry) in the limit where the lattice spacing goes to zero, and the scaling violations, the corrections to the continuum limit

which are of order a^n. An accurate treatment of such violations can greatly reduce the systematic error which is introduced by lattice artifacts in simulation results.

The mixing of lattice operators under renormalization can also be determined through perturbation theory. Generally operator mixing on the lattice is more complex than in the continuum. In fact, mixing patterns on the lattice become in general more transparent when looked at using perturbative renormalization than nonperturbatively.

In this thesis we concentrate on perturbative RFs. As we mentioned earlier RFs are necessary ingredients in the prediction of physical probability amplitudes from lattice matrix elements of operators. They relate observables computed on finite lattices to their continuum counterparts in specific renormalization schemes. On the lattice we have an infinite number of interaction vertices but, fortunately, only a finite number of vertices is needed at any given order in the bare coupling constant, g_0. The perturbative calculation of the relevant Green's functions in this thesis was carried out at one-loop order by computing the corresponding Feynman diagrams.

Analytic computations of Feynman diagrams in lattice QCD present quite a few new and interesting features with respect to the continuum. Of course general properties of the path integral, Wick's theorem, and gauge invariance continue to be valid on the lattice. The combinatorial rules are also similar to the continuum. But there are important differences, many of them connected to the breaking of Lorentz invariance. Lattice perturbation theory is much more complicated than continuum perturbation theory: there are more fundamental vertices and more diagrams. The propagators and vertices, with which one builds the Feynman diagrams, are also more complicated on the lattice than they are in the continuum, which can lead to expressions containing a huge number of terms. A typical "difficult" Feynman diagram contains $\sim 10^5$ terms before we integrate these expressions over the internal momenta.

Lattice perturbation theory may also be applied to systems at finite temperature: The euclidean Feynman rules at zero temperature are modified when relativistic systems of interacting fields are placed in contact with a heat bath. There are exact one-loop calculations of the equation of state within hard-thermal-loop perturbation theory, which employs an expansion in the ratios of thermal masses and the temperature [4]. In fact this expansion converges reasonably fast. There are also studies of the existence and properties of the transfer matrix using Chiral perturbation theory in the quenched approximation [5].

There have been only very few higher-loop results of lattice perturbation theory in the last decades, due to the fact that providing such results beyond one-loop order is

very demanding in human and CPU time. More precisely there are a few calculations of renormalization functions up to two-loops [6, 7, 8]. Numerical stochastic perturbation theory [9] might be a viable alternative to study higher-loops; for example, the lattice corrections up to three-loop order for the $SU(3)$ gluon and ghost propagators is achieved by numerical stochastic perturbation theory in Landau gauge.

Another application of lattice perturbation theory regards the Schrödinger functional (SF) [10]. This is a powerful and widely used tool for the treatment of a variety of problems in renormalization and related areas. Albeit offering many conceptual advantages, one major downside of the SF scheme is the fact that perturbative calculations quickly become cumbersome with the inclusion of higher orders in the gauge coupling and hence the use of an automated perturbation theory framework is desirable.

In recent years considerable efforts have also been made to improve lattice actions in order to reduce the dependence of the results on the lattice spacing. Results from lattice perturbation theory exist for a variety of improved lattice fermion actions: Wilson, Wilson-like (e.g. clover, SLiNC), Staggered, Overlap, domain wall fermions, Relativistic heavy quarks, NRQCD (Non-Relativistic QCD) and HQET (Heavy Quark Effective Theory) [11]. Other improvements of lattice actions are carried out using the background field method with an application to the hyperfine splitting of quarkonium states.

1.4 Overview of the Thesis

This Thesis contains work carried out over the past four years and it is laid out as follows. Chapter 2 provides a brief introduction to some lattice actions. We describe the discretization passage from continuum actions to a set of discrete space-time lattice actions.

In Chapter 3 we present the perturbative computation of the renormalization functions for the quark field and for a complete set of ultra-local fermion bilinears. The computation of the relevant Green's functions was carried out at 1-loop level for the staggered action using massive fermions. The gluon links which appear both in the fermion action and in the definition of the bilinears have been improved by applying a stout smearing procedure up to 2 times, iteratively. In the gluon sector we employed the Symanzik improved gauge action for different sets of values of the Symanzik coefficients. The renormalization functions are presented in (two variants of) the RI′ and in the $\overline{\text{MS}}$ renormalization schemes; the dependence on all stout parameters, as well as on the fermion mass, the gauge fixing parameter and the renormalization scale, is shown explicitly.

In Chapter 4 we apply our results of Chapter 3 to a nonperturbative study of the magnetic susceptibility of QCD at zero and finite temperature. We study the response of the QCD vacuum to a constant external (electro)magnetic field through the tensor polarization of the chiral condensate and the magnetic susceptibility at zero and at finite temperature. We determine these quantities using lattice configurations generated with the tree-level Symanzik improved gauge action and $N_f = 1+1+1$ flavors of stout smeared staggered quarks with physical masses. The magnetic susceptibilities χ_f reveal a spin-diamagnetic behavior; we obtain at zero temperature $\chi_u = -(2.08 \pm 0.08)$ GeV^{-2}, $\chi_d = -(2.02 \pm 0.09)$ GeV^{-2} and $\chi_s = -(3.4 \pm 1.4)$ GeV^{-2} for the up, down and strange quarks, respectively, in the $\overline{\text{MS}}$ scheme at a renormalization scale of 2 GeV. We also find the polarization to change smoothly with the temperature in the confinement phase and then to drastically reduce around the transition region.

In Chapter 5 we compute the one-loop 2-point perturbative bare Green's functions of the fermion propagator and of local and extended fermion bilinear operators on the lattice. The calculation is carried out up to $\mathcal{O}(a^2)$, where a is the lattice spacing. We employed the SLiNC action. Our results have been obtained for various choices of values for the Symanzik coefficients, c_i. The clover coefficient c_{SW}, the gauge parameter α, the stout parameter ω, the fermion masses m and the number of colors N_c are kept as free parameters. The Wilson parameter, r, is set equal to 1. Knowledge of these Green's functions allows us to determine renormalization functions for the quark field and each of the fermion bilinear operators which we studied.

In Chapter 6 we investigate a method to suppress the lattice artifacts from nonperturbative data by subtracting the one-loop contributions of perturbative renormalization factors using clover improved Wilson fermions with plaquette gauge action. We compare results obtained from a complete one-loop subtraction with those calculated by a subtraction of contributions proportional to the square of the lattice spacing.

In Chapter 7 we compute the Green's functions of the chromomagnetic operator $\mathcal{O}_{CM}$, with one external quark-antiquark pair and with zero or one external gluons, on the lattice and in the continuum using dimensional regularization. The lattice computation is carried out using the maximally twisted-mass action for fermions; for gluons we employ the Symanzik improved gauge action with different sets of values of the Symanzik coefficients. In order to find the mixing with other operators we examine the transformation properties of all candidate operators which could possibly mix with $\mathcal{O}_{CM}$. We have identified these operators and we construct a mixing matrix to find the renormalization of $\mathcal{O}_{CM}$. We also

calculate and present the renormalization of fermion field Z_ψ, gluon field Z_A, and of the coupling constant Z_g, which are required by the renormalization conditions.

Finally in Chapter 8 we summarize and conclude. The Appendices contain supplementary material that has been left out of the main body of the Thesis in order to improve readability.

Most of the results presented here have already been published in the following papers:

- G. S. Bali, F. Bruckmann, M. Constantinou, M. Costa, G. Endrődi, S. D. Katz, H. Panagopoulos and A. Schäfer, *"Magnetic susceptibility of QCD at zero and at finite temperature from the lattice"*, Phys. Rev. **D86** (2012) 094512.

- M. Constantinou, M. Costa, M. Göckeler, R. Horsley, H. Panagopoulos, H. Perlt, P. E. L. Rakow, G. Schierholz and A. Schiller, *"Perturbatively improving regularization-invariant momentum scheme renormalization constants"*, Phys. Rev. **D87** (2013) 096019.

- M. Constantinou, M. Costa and H. Panagopoulos, *"Perturbative renormalization functions of local operators for staggered fermions with stout improvement"*, Phys. Rev. **D88** (2013) 034504.

- M. Constantinou, M. Costa, R. Frezzotti, V. Lubicz, G. Martinelli, D. Meloni, H. Panagopoulos and S. Simula, *"The chromomagnetic operator: Hadronic Matrix Elements and the Mixing under Renormalization"*, to be submitted to Phys. Rev. D.

and conference proceedings:

- G. S. Bali, F. Bruckmann, M. Constantinou, M. Costa, G. Endrődi, Z. Fodor, S. D. Katz, S. Krieg, H. Panagopoulos, A. Schäfer and K. K. Szabo, *"Thermodynamic properties of QCD in external magnetic fields"*, PoS **Confinement X** (2012) 198.

- M. Constantinou, M. Costa, M. Göckeler, R. Horsley, H. Panagopoulos, H. Perlt, P. E. L. Rakow, G. Schierholz and A. Schiller, *"Perturbative subtraction of lattice artifacts in the computation of renormalization constants"*, PoS **LATTICE2012** (2012) 239.

- M. Constantinou, M. Costa, M. Göckeler, R. Horsley, H. Panagopoulos, H. Perlt, P. E. L. Rakow, G. Schierholz and A. Schiller, *"Perturbatively improving renormalization constants"*, PoS **LATTICE2013** (2013) 310.

- G. S. Bali, F. Bruckmann, M. Constantinou, M. Costa, G. Endrődi, S. D. Katz, H. Panagopoulos and A. Schäfer, *"Perturbative renormalization of staggered fermion operators with stout improvement: Application to the magnetic susceptibility of QCD"*, PoS **LATTICE2013** (2013) 458.

- M. Constantinou, M. Costa, R. Frezzotti, V. Lubicz, G. Martinelli, D. Meloni, H. Panagopoulos and S. Simula, *"The chromomagnetic operator on the lattice"*, PoS **LATTICE2013** (2013) 316.

Chapter 2

Actions on the lattice

There is a great variety of ways to discretize on the lattice a theory defined in the continuum. A number of symmetries of the continuum actions are necessarily violated when discretizing on a lattice, first and foremost Lorentz invariance. The Fermion and Gluon actions are written on the lattice using a discretization; such that the limit $a \to 0$ reproduces the continuum action. In recent years an appreciable effort has been invested in studying lattice actions which leave intact as many symmetries of the continuum theory as possible. We know that the renormalizability of Quantum Field Theories is based on gauge symmetry. Furthermore the existing proofs of perturbative renormalizability of QCD, defined on the lattice, rely on strict gauge invariance [12]. Thus the lattice actions are constructed to be gauge invariant. In this Chapter, we describe these actions which were used in our calculations. These actions are currently employed in large scale numerical simulations.

2.1 Wilson gluons

In this section we present the standard Wilson action for the gluons. To define the gluon action on the lattice we introduce the link variables, $U_\mu(x)$. They are unitary and connect two neighboring lattice sites. The index $\mu = 0, ..., 3$ labels the direction of the link and $\hat{\mu}$ is the unit vector in the μ^{th} direction.

For a gauge theory with N_c colors of fermion fields, the gauge group is $SU(N_c)$. The link variables are directly related to the gauge fields $A^a_\mu(x)$ in a nonlinear way; they are defined in a way that the continuum action is recovered when setting $a \to 0$.

$$U_\mu(x) \equiv U_\mu(x, x + a\hat{\mu}) = \exp\left[iag_0 T^a A^a_\mu(x + \frac{a\hat{\mu}}{2})\right], \tag{2.1}$$

where T^a $(a = 1, ..., N_c^2 - 1)$ are the $SU(N_c)$ generator matrices in the fundamental representation. By convention, the argument of A_μ^a is defined in the midpoint of the link (without affecting the continuum limit or the simulations) and U is an $N_c \times N_c$ unitary matrix satisfying:

$$U_{-\mu}(x) \equiv U(x, x - a\hat{\mu}) = e^{-iag_0 T^a A_\mu^a (x - \frac{a\hat{\mu}}{2})} = U^\dagger(x - a\hat{\mu}, x). \tag{2.2}$$

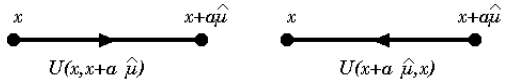

Figure 2.1: Schematic representation of link variables.

A local gauge transformation $G(x)$ acts on the fermion ($\psi(x)$, $\overline{\psi}(x)$) and gauge fields through the relations:

$$\begin{aligned}
\psi(x) &\rightarrow G(x)\psi(x) \\
\overline{\psi}(x) &\rightarrow \overline{\psi}(x)G^\dagger(x) \\
U_\mu(x) &\rightarrow G(x)U_\mu(x)G^\dagger(x + a\hat{\mu}) \qquad (2.3) \\
U_\mu^\dagger(x) &\rightarrow G(x + a\hat{\mu})U_\mu^\dagger(x)G^\dagger(x). \qquad (2.4)
\end{aligned}$$

One requires that the lattice action be invariant under the gauge transformations; thus, its gluon part must be constructed by gauge invariant objects. The simplest choice is the trace of the 1×1 loop, called plaquette:

$$U_P \equiv U_{\mu\nu}(x) = U_\mu(x)U_\nu(x + a\hat{\mu})U_\mu^\dagger(x + a\hat{\nu})U_\nu^\dagger(x), \tag{2.5}$$

U_P is the product of link variables along the perimeter of a square originating at x in the positive $\mu - \nu$ directions; it provides a natural discretization of the gauge field strength:

$$U_{\mu\nu}(x) \approx \exp\left[ia^2 g_0 F_{\mu\nu}(x)\right]. \tag{2.6}$$

As can be realized from Fig. 2.2, there are two different orientations for each plaquette, which are Hermitian conjugates to each other. Thus, a sum over all orientations involves only the real part of the loops. Taking the trace over color indices ensures gauge invariance.

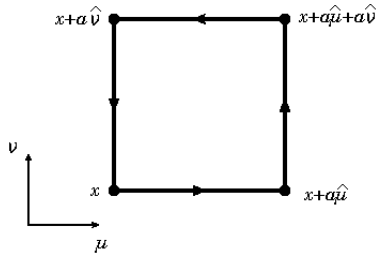

Figure 2.2: Schematic representation of a plaquette.

The Wilson gluon (plaquette) action is written as:

$$S_W^g = \frac{2N}{g_0^2} \sum_{\mu<\nu} \sum_x (1 - \frac{1}{N} \mathrm{ReTr}[U_P]). \tag{2.7}$$

The formulation of this action in terms of the link variables, rather than the gauge fields directly, serves to uphold gauge invariance.

In a naive continuum limit, where a goes to zero, one has:

$$S_W^g \to S_{cont.}^g = \frac{1}{2} \int d^4x \, \mathrm{Tr} \left(F_{\mu\nu} F_{\mu\nu} \right). \tag{2.8}$$

2.2 Naive fermion action and Wilson fermions

In the formulation of Lattice QCD, the fermion fields ($\psi(x)$, $\overline{\psi}(x)$) live on the lattice sites x and carry color ($i, j, ... = 1, ..., N_c$), flavor ($f = 1, ..., N_f$) and Dirac indices (α, $\beta, ... = 1, ..., 4$). We recall that N_c, N_f are the number of fermion colors and fermion flavors, respectively. To avoid heavy notation, the Dirac, flavor and color indices are not written.

The naive gauge invariant fermion action on the lattice in Euclidean space-time is:

$$\begin{aligned} S^f &= a^4 \sum_x \sum_\mu \frac{1}{2a} \overline{\psi}(x) \gamma_\mu^E \Big[U_\mu(x) \psi(x + a\hat{\mu}) - U_\mu^\dagger(x - a\hat{\mu}) \psi(x - a\hat{\mu}) \Big] \\ &+ a^4 \sum_x m_0 \overline{\psi}(x) \psi(x). \end{aligned} \tag{2.9}$$

This action has the correct continuum limit:

$$S_{cont.}^f = \int d^4x \overline{\psi}(x) \left(\gamma_\mu^E D_\mu + m_0 \right). \tag{2.10}$$

In order to find the naive propagator, it is convenient to work in momentum space. The Fourier transformation of the fields is:

$$\psi(x) = \int_{-\pi/a}^{\pi/a} \frac{d^4p}{(2\pi)^4}\, e^{iap\cdot x}\, \tilde{\psi}(p) \tag{2.11}$$

$$\overline{\psi}(x) = \int_{-\pi/a}^{\pi/a} \frac{d^4p}{(2\pi)^4}\, e^{-iap\cdot x}\, \tilde{\overline{\psi}}(p) \tag{2.12}$$

$$A_\mu(x) = \int_{-\pi/a}^{\pi/a} \frac{d^4p}{(2\pi)^4}\, e^{iap\cdot x}\, \tilde{A}_\mu(p). \tag{2.13}$$

The naive fermion propagator takes the form:

$$\langle \psi(x)\overline{\psi}(y)\rangle = \lim_{a\to 0} \int_{-\pi}^{\pi} \frac{d^4k}{(2\pi)^4}\, e^{ik(x-y)}\, \frac{-i\sum_\mu \gamma_\mu sin(k_\mu) + m_0}{\sum_\mu sin^2(k_\mu) + m_0^2} \tag{2.14}$$

The correct continuum limit in the naive fermionic case is destroyed due to the vanishing of $\sin(k_\mu)$ at the edges of the Brillouin zone. Thus there are sixteen regions, in momentum space rather than one $k_\mu \sim 0$, which contribute to the propagator, as if there were sixteen fermion species present. This is known as the doubling problem.

Kenneth G. Wilson in 1974 proposed in a famous paper [2] one of the most popular lattice actions to overcome the problem of the fermion doubling. The solution is to add a term (Wilson term) to the naive action. The Wilson term is:

$$-\frac{r}{2}\sum_x \overline{\psi}(x)\partial_\mu\partial_\mu\psi(x) \tag{2.15}$$

Below, we present Wilson's lattice action for fermions:

$$\begin{aligned} S_W^f &= a^4\Big\{\sum_x\sum_\mu \frac{-1}{2a}\,\overline{\psi}(x)\Big[(r-\gamma_\mu)U_\mu(x)\psi(x+a\hat{\mu}) \\ &+ (r+\gamma_\mu)U_\mu^\dagger(x-a\hat{\mu})\psi(x-a\hat{\mu})\Big] + (4r+m_0)\sum_x \overline{\psi}(x)\psi(x)\Big\} \end{aligned} \tag{2.16}$$

where the r is called Wilson parameter.

Besides the absence of fermion doublers and the existence of gauge symmetry, the Wilson action has a number of properties:

• It is invariant under translations by a.

• The transformations of charge conjugation $\mathcal{C}$, parity $\mathcal{P}$ and time reversal $\mathcal{T}$, leave the

action invariant.
• Eq. (2.16) includes only nearest-neighbor interactions, leading to vertices with compact form and easy to work with (locality).

The above properties of Eq. (2.16) go along with the following disadvantages:
• Chiral symmetry is explicitly broken at order a by the Wilson term, and it is restored only in the continuum limit. The axial current transformations are not an exact symmetry and the nonsinglet axial current requires a nontrivial multiplicative renormalization to restore current algebra up to $\mathcal{O}(a)$ effects.
• The lattice artifacts in the action are propotional to a, rather that a^2.

These properties and disadvantages are consistent with a famous No-Go theorem of Nielsen and Ninomiya [13] which says that *a lattice fermion formulation with locality, without species doubling and with an explicit continuous chiral symmetry is impossible.*

Other types of fermionic disretizations, notably "overlap" and "domain wall" fermions, bypass this theorem at the expense of not being "ultra local"; in particular these actions involve couplings between quarks and antiquarks which are at an arbitrary distance apart. As a result, numerical simulation of these actions is enormously more demanding in CPU time.

2.3 The Symanzik improved gluon action

The plaquette is not the only possibility for the construction of the discretized version of the gauge field strength. One can also consider larger closed Wilson loops. Rather than using only the smallest possible closed loops (1×1 plaquettes), we can generalize the Wilson action by including all loops with 4 and 6 links (*plaquette*, *rectangle*, *chair*, and *parallelogram* wrapped around an elementary 3-d cube), as shown in Fig. 2.3.

$$S_G = \frac{2}{g_0^2}\Big[\quad c_0 \sum_{\text{plaq.}} \mathrm{Re}\,\mathrm{Tr}\,\{1 - U_{\text{plaq.}}\} + c_1 \sum_{\text{rect.}} \mathrm{Re}\,\mathrm{Tr}\,\{1 - U_{\text{rect.}}\} \\ + \quad c_2 \sum_{\text{chair}} \mathrm{Re}\,\mathrm{Tr}\,\{1 - U_{\text{chair}}\} + c_3 \sum_{\text{paral.}} \mathrm{Re}\,\mathrm{Tr}\,\{1 - U_{\text{paral.}}\}\Big]\,. \tag{2.17}$$

The coefficients c_i can in principle be chosen arbitrarily, subject to the following nor-

malization condition which ensures the correct classical continuum limit of the action:

$$c_0 + 8c_1 + 16c_2 + 8c_3 = 1 \tag{2.18}$$

Some popular choices of values [14] for c_i used in numerical simulations will be considered in this work, and are listed in Table D.1 of Appendix D.1. They include the Wilson case ($c_0 = 1$, $c_1 = c_2 = c_3 = 0$), and the tree-level Symanzik ($c_0 = 5/3$, $c_1 = -1/12$, $c_2 = c_3 = 0$), TILW (tadpole improved Lüscher-Weisz), Iwasaki and DBW2 (doubly blocked Wilson) actions. The values for c_i used in numerical simulations are normally tuned in a way as to ensure $\mathcal{O}(a)$ improvement.

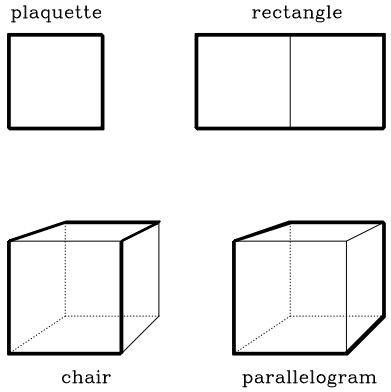

Figure 2.3: The 4 Wilson loops of the gluon action.

2.4 The clover fermion action

The widely used clover action was originally studied by Sheikholeslami and Wohlert [15] to remove the $\mathcal{O}(a)$ effects of the Wilson fermion action.

The improved action is written as:

$$S_{\rm sw} = S_W^f + a^5 \frac{ic_{\rm sw}}{4} \sum_f \sum_{x,\mu,\nu} \overline{\psi}^f(x) \sigma_{\mu\nu} \widehat{F}_{\mu\nu}(x) \psi^f(x) \tag{2.19}$$

where the first term of Eq. (2.19) is the fermion part of the Wilson action (Eq. (2.16)), $c_{\rm sw}$ is the clover parameter, $\sigma_{\mu\nu} = (i/2)\,(\gamma_\mu\gamma_\nu - \gamma_\nu\gamma_\mu)$, and the quantity $\widehat{F}_{\mu\nu}$ is a lattice discretization of the field tensor; more specifically, $\widehat{F}_{\mu\nu}$ is the sum of plaquettes in the $\mu-\nu$ plane, having x as their initial and final point:

$$\widehat{F}_{\mu\nu}(x) = \frac{1}{8a^2}(Q_{\mu\nu}(x) - Q^{\dagger}_{\mu\nu}(x)), \tag{2.20}$$

$Q_{\mu\nu}$ is the sum of the plaquette loops:

$$\begin{aligned} Q_{\mu\nu} &= U_{x,x+\mu}U_{x+\mu,x+\mu+\nu}U_{x+\mu+\nu,x+\nu}U_{x+\nu,x} \\ &+ U_{x,x+\nu}U_{x+\nu,x+\nu-\mu}U_{x+\nu-\mu,x-\mu}U_{x-\mu,x} \\ &+ U_{x,x-\mu}U_{x-\mu,x-\mu-\nu}U_{x-\mu-\nu,x-\nu}U_{x-\nu,x} \\ &+ U_{x,x-\nu}U_{x-\nu,x-\nu+\mu}U_{x-\nu+\mu,x+\mu}U_{x+\mu,x} \end{aligned} \tag{2.21}$$

as shown in Fig. 2.4.

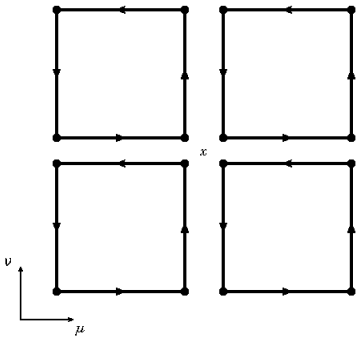

Figure 2.4: Graphical representation of $Q_{\mu\nu}$ (Eq. (2.21)) appearing in the clover action.

Given that the clover action is local, it does not introduce excessive complexity in neither perturbation theory nor numerical simulations. In particular, the addition of the clover term is only about a 15% overhead per update as compared to Wilson fermion simulations [16, 18]. Note that any value of $c_{\rm sw}$ is in principle allowed, since the corresponding term vanishes in the continuum limit. Specific choices for values of $c_{\rm sw}$ can be made by requiring, e.g. that $\mathcal{O}(a^1)$ effects are absent from the action, at the classical or quantum level.

2.5 SLiNC Action improved fermion and gluon action

The acronym SLiNC stands for the **S**tout **Li**nk **N**on-perturbative **C**lover action. It has been adopted by the QCDSF collaboration for their large scale simulations in recent years (see, e.g. [17]). The gluonic part of the SLiNC action is the tree-level Symanzik action

which reads:

$$S_G = \frac{2}{g_0^2}\left\{c_0 \sum_{\text{plaq.}} \text{Re}\,\text{Tr}\,(1 - U_{\text{plaq.}}) + c_1 \sum_{\text{rect.}} \text{Re}\,\text{Tr}\,(1 - U_{\text{rect.}})\right\} \tag{2.22}$$

with $c_0 = 5/3$ and $c_1 = -1/12$ ($c_0 + 8c_1 = 1$). This reduces to the standard plaquette action S_W^g for $c_1 = 0$.

The fermionic part of this action has the same form as the clover action but the links $U_\mu(x)$, connecting fermion fields on adjacent sites, are replaced by "stout" smeared links $\tilde{U}_\mu(x)$ and the Wilson parameter, r, is set to 1:

$$\begin{aligned} S^f \;=\; a^4 \sum_x \Big\{ & -\frac{1}{2a}\Big[\bar{\psi}(x)\widetilde{U}_\mu(x)\,(1-\gamma_\mu)\,\psi(x+a\hat{\mu}) \\ & + \bar{\psi}(x)\widetilde{U}_\mu^\dagger(x-a\hat{\mu})\,(1+\gamma_\mu)\,\psi(x-a\hat{\mu})\Big] \\ & + (4+m_0)\,\bar{\psi}(x)\psi(x) - c_{\text{sw}}\,g_0\,\frac{a}{4}\,\bar{\psi}(x)\,\sigma_{\mu\nu}\widehat{F}_{\mu\nu}(x)\,\psi(x)\Big\}. \end{aligned} \tag{2.23}$$

The links inside the clover term are not smeared. Stout links [19] are defined by:

$$\widetilde{U}_\mu(x) = e^{i\,Q_\mu(x)}\,U_\mu(x), \tag{2.24}$$

with

$$Q_\mu(x) = \frac{\omega}{2\,i}\left[V_\mu(x)U_\mu^\dagger(x) - U_\mu(x)V_\mu^\dagger(x) - \frac{1}{N_c}\text{Tr}\,\left(V_\mu(x)U_\mu^\dagger(x) - U_\mu(x)V_\mu^\dagger(x)\right)\right]. \tag{2.25}$$

$V_\mu(x)$ denotes the sum over all "staples" $U_\nu(x)U_\mu(x+a\hat{\nu})U_\nu^\dagger(x+a\hat{\mu})$ associated with the link $U_\mu(x)$ and ω is a tunable parameter; its value can be chosen using criteria similar to those which apply in the case of c_{sw}. Stout smearing is expandable as a power series in g_0^2, so we can use perturbation theory. Many other forms of smearing do not have this nice property since they lead to non-unitary links which, upon projection to $SU(N_c)$, cease to be Taylor expandable in g_0.

The reason for not smearing the clover term is that one wants to contain the physical extent of the fermion action in lattice units; this is relevant for non-perturbative calculations.

2.6 Staggered fermions

Another means of solving the fermion doubling problem is the introduction of "staggered" fermions.

In the staggered (or Kogut-Susskind) formulation [20], one is left with 4 fermion "tastes" whose 16 components are split over a unit hypercube by assigning only a single fermion field component to each lattice site. This construction can only be carried out in an even number of space-time dimensions.

The standard passage from the naive action for fermions (ψ, $\bar{\psi}$) to the staggered action entails the following change of basis:

$$\begin{aligned} \psi(x) = \gamma_x\,\chi(x) \quad , \qquad \bar{\psi}(x) = \bar{\chi}(x)\,\gamma_x^\dagger, \\ \gamma_x = \gamma_1^{n_1}\,\gamma_2^{n_2}\,\gamma_3^{n_3}\,\gamma_4^{n_4} \quad , \qquad x = (a\,n_1, a\,n_2, a\,n_3, a\,n_4), \quad n_i\,\epsilon\,\mathbb{Z}\,. \end{aligned} \tag{2.26}$$

Using the equalities:

$$\gamma_\mu\,\gamma_x = \eta_\mu(x)\gamma_{x+a\,\hat{\mu}} \quad \text{and} \quad \gamma_x^\dagger\,\gamma_x = \mathbb{1}\,, \qquad \eta_\mu(x) = (-1)^{\sum_{\nu<\mu} n_\nu}\,. \tag{2.27}$$

the naive fermion action takes the form:

$$S^f = a^4 \sum_x \sum_\mu \sum_i \frac{1}{2a}\,\overline{\chi}_i(x)\eta_\mu(x)\Big[U_\mu(x)\chi_i(x+a\hat{\mu}) - U_\mu^\dagger(x-a\hat{\mu})\chi_i(x-a\hat{\mu})\Big] + a^4 \sum_x m\overline{\chi}_i(x)\chi_i(x)\,. \tag{2.28}$$

Thus far, we have rewritten the usual lattice action. But the crucial step now is that the Dirac matrices have disappeared, and they have been replaced by the phase factors $\eta_\mu(x)$; in the new basis, the naive action consists of 4 identical parts, one for each value of the spinor index i carried by the spinor χ. Dropping this index altogether leads to the standard staggered fermion action, S_{stag}:

$$S_{\text{stag}} = a^4 \sum_x \sum_\mu \frac{1}{2a}\,\overline{\chi}(x)\eta_\mu(x)\Big[U_\mu(x)\chi(x+a\hat{\mu}) - U_\mu^\dagger(x-a\hat{\mu})\chi(x-a\hat{\mu})\Big] + a^4 \sum_x m\overline{\chi}(x)\chi(x)\,. \tag{2.29}$$

An advantage of staggered fermions is that a continuous subgroup of the original chiral transformations remains a symmetry of this lattice action even at finite lattice spacing, and thus no mass counterterms are needed for vanishing bare quark masses. All this is

achieved at the expense of taste and (partially) translational symmetry, which become in fact all mixed together.

2.7 Twisted mass action

As previously mentioned, the Wilson action breaks chiral symmetry, which can be restored with the introduction of an additive fermion mass renormalization as a counterterm. The result of the absence of chiral symmetry for nonzero lattice spacing, is that the Wilson-Dirac operator (Eq. (2.31)) is not protected against zero modes, unless the bare quark mass is positive. However, due to additive mass renormalization, the masses of the light quarks correspond to negative bare masses. One of the consequences of the zero modes is the following: After integration over the fermion and anti-fermion fields in the functional integral, there is a small eigenvalue of the Wilson-Dirac operator in the fermionic determinant and the fermion propagators appearing in the correlation functions. Thus, in the quenched approximation, where the fermionic determinant is ignored, this eigenvalue in the quark correlation is not canceled out upon division. The results are large fluctuations in particular measurables that compromise the ensemble average. The gauge field configurations at which this happens, are called exceptional.

A solution to the problem of exceptional configurations is the addition of a "twisted" mass term [21] to the standard Wilson action. The resulting action has the benefit that certain observables are automatically free of $\mathcal{O}(a)$ lattice artifacts.

Some additional advantages of this action are efficient simulations (as compared to other improved actions) and the fact that operator mixing resembles the continuum case. The twisted mass action can be used to study quarks at small masses, where the Wilson action would fail. Also, the properties and the interactions of hadrons can be probed nonperturbatively from first principles.

2.7.1 The lattice twisted mass action for degenerate quarks

The twisted mass lattice action [22] for a doublet of $N_f = 2$ mass degenerate quarks, written in the so called twisted basis $(\chi, \bar{\chi})$, is:

$$S_{tm}^{\{\chi\}} = a^4 \sum_x \bar{\chi}(x) \Big[D_W + m_0 + i\mu_q \gamma^5 \tau^3 \Big] \chi(x) \tag{2.30}$$

with m_0 real and positive. D_W is the Wilson-Dirac operator:

$$D_W = \frac{1}{2}\sum_{\mu=0}^{3}\{\gamma_\mu(\overrightarrow{\nabla}_\mu + \overleftarrow{\nabla}_\mu) - a\, r \overleftarrow{\nabla}_\mu \overrightarrow{\nabla}_\mu\} \tag{2.31}$$

The last term with the twisted mass parameter μ_q protects the Dirac operator against zero modes for any finite μ_q, since the twisted Dirac operator has positive determinant:

$$\det(D_W + m_0 + i\mu_q\gamma^5\tau^3) = \det(Q^2 + \mu_q^2) \tag{2.32}$$

where $Q = \gamma^5(D_W + m_0)$ is the hermitian Wilson operator; hence, the twisted Dirac operator does not have any zero eigenvalues. The isospin generator τ^3 acts in flavor space and its appearance means that isospin is no longer conserved (i.e. the up and down quark have opposite signs of the twisted mass leading to flavor symmetry breaking). Moreover, the twist term breaks parity symmetry (due to γ^5). These symmetries are restored in the continuum limit. The action remains invariant under the flavor-dependent axial transformations:

$$\begin{aligned} \psi &= e^{i\omega\gamma^5\frac{\tau^3}{2}}\chi \\ \bar{\psi} &= \bar{\chi}\, e^{i\omega\gamma^5\frac{\tau^3}{2}} \end{aligned} \tag{2.33}$$

with the mass parameters mixed to each other as:

$$\begin{aligned} m' &= \mu_q \sin(\omega) + m\cos(\omega) \\ \mu_q' &= \mu_q\cos(\omega) - m\sin(\omega) \end{aligned} \tag{2.34}$$

In the full twist case, $\omega = \pi/2$, the flavor symmetry is restored at a rate $\mathcal{O}(a^2)$. This case is useful, since there is automatic cancellation of $\mathcal{O}(a)$ effects in quantities like energies and on-shell operator matrix elements. The action can be written in the physical basis $(\psi, \bar{\psi})$, where the μ_q term has been eliminated:

$$S_{tm}^{\{\psi\}} = a^4 \sum_x \bar{\psi}(x)\Big[D_{Wtm} + M\Big]\psi \tag{2.35}$$

D_{Wtm} is the twisted Wilson operator:

$$D_{Wtm} = \frac{1}{2}\sum_{\mu=0}^{3}\{\gamma_\mu(\overrightarrow{\nabla}_\mu + \overleftarrow{\nabla}_\mu) - a\, r\, e^{-i\omega\gamma^5\tau^3}\overleftarrow{\nabla}_\mu \overrightarrow{\nabla}_\mu\} \tag{2.36}$$

and M is the polar mass:

$$M = \sqrt{m_0^2 + \mu_q^2} \tag{2.37}$$

In the continuum limit, where the last term of Eq. (2.36) vanishes, tmQCD can be seen as a change of variables which leaves the physical content of the theory unchanged if the rotation angle ω satisfies:

$$\tan(\omega) = \frac{\mu_q}{m_0} \tag{2.38}$$

Thus, in the continuum limit the axial rotation of the fermion fields (Eq. (2.33)) relates tmQCD to the standard QCD.

We are particularly interested in the action written in the twisted basis, because it is the one used in simulations. This is due to the fact that the renormalization of gauge invariant correlation functions is simpler for the twisted fields (χ, $\bar{\chi}$). The expression for the twisted mass propagator is:

$$G(p) = \frac{-i\gamma_\mu \mathring{p}_\mu + \mathcal{M}(p) - i\mu_q \gamma^5 \tau^3}{\mathring{p}_\mu^2 + \mathcal{M}(p)^2 + \mu_q^2} \tag{2.39}$$

with $\mathring{p}$ and $\mathcal{M}$ defined through:

$$\mathring{p}_\mu = \frac{1}{a}\sin(ap_\mu), \qquad \mathcal{M}(p) = m_0 + \frac{r}{2}a\hat{p}_\mu^2, \qquad \hat{p}_\mu = \frac{2}{a}\sin(\frac{ap_\mu}{2}) \tag{2.40}$$

The tree-level expression can be extracted by taking the Taylor expansion for small values of the lattice spacing a and keeping terms up to $\mathcal{O}(a)$, obtaining:

$$G_0(p) = p^2 + m_0^2 + \mu_q^2 + am_0 r p^2 \tag{2.41}$$

The first observation is that for zero bare mass (or even for $m_0 = a\tilde{m}_0$), the theory is free of $\mathcal{O}(a)$ effects, but this picture changes once we take into account the interactions between quarks. Moreover, the inclusion of the twisted mass parameter does not affect the $\mathcal{O}(a)$ improvement of the $m_0 = 0$, $a\tilde{m}_0$ cases.

2.7.2 The lattice twisted mass action for nondegenerate quarks

So far we have discussed the $N_f = 2$ case of degenerate light quarks, but the action can be generalized to include a further doublet of non-degenerate quarks [23, 24]. Such a generalization arises from the need to describe the heavier quarks, charm and strange.

Since we want to use this action in simulations of full tmQCD, we must maintain the reality and positivity of the quark determinant. Thus, in the action we add a flavor off-diagonal splitting:

$$S_{tm}^{\{\chi\}} = a^4 \sum_x \bar{\chi}(x)\Big[D_W + m_0 + i\mu_q\gamma^5\tau^3 + \epsilon_q\tau^1\Big]\chi(x) \tag{2.42}$$

where ϵ_q is the mass splitting parameter and we demand μ_q, $\epsilon_q > 0$. The additional term retains the properties of tmQCD at full twist and it keeps the quark determinant real and positive if $\sqrt{m_0^2 + \mu_q^2} > \epsilon_q$.

The transition to the physical basis is achieved with the following field transformations:

$$\psi = \Big(\exp(-i\omega\gamma^5\frac{\tau^1}{2})\Big)\Big(\frac{1}{\sqrt{2}}(1 + i\tau^2)\Big)\chi \tag{2.43}$$

$$\bar{\psi} = \bar{\chi}\Big(\frac{1}{\sqrt{2}}(1 - i\tau^2)\Big)\Big(\exp(-i\omega\gamma^5\frac{\tau^1}{2})\Big) \tag{2.44}$$

The action in this basis is now:

$$S_{tm}^{\{\psi\}} = a^4 \sum_x \bar{\psi}(x)\Big[D_{Wtm} + M\Big]\psi \tag{2.45}$$

where $M = \sqrt{m_q^2 + \mu_q^2}$ is again the polar mass. For the description of the heavy doublet charm and strange (c,s) we associate the physical quark mass with the mass parameter M, that is:

$$m_{charm} = M + \epsilon_q \qquad m_{strange} = M - \epsilon_q \tag{2.46}$$

and the fermion determinant is positive if $M > \epsilon_{\rm q}$.

Chapter 3

Perturbative renormalization functions of local operators for staggered fermions with stout improvement

3.1 Introduction

In recent years, significant improvements have been made in the use of matrix elements of operators made out of quark fields to extract mass spectra, decay constants, and a plethora of hadronic properties [25, 26, 27]. Although naive (unimproved) staggered fermions were introduced more than three decades ago [28], their discretization errors and their relatively large taste mixing posed a limit on the accuracy of results from simulations, despite their relatively low computational cost. This situation called for improvement; the outcome of such efforts was some of the most accurate discretizations used to date for high-precision simulations. One specific direction regards improving the fermion action (see, e.g. [29, 30]); in particular, the introduction of stout links in the action which has recently been put to use [31, 32] allows simulations to be carried out at near physical parameters. Compared to most other improved formulations of staggered fermions, the above action, as well as the HISQ action, lead to smaller taste violating effects [33, 34, 35].

Changes in the lattice action and in the discretization of operators imply that renormalization functions must be determined afresh, either perturbatively or non-perturbatively. In many cases non-perturbative estimates of renormalization functions are very difficult to obtain, due to complications such as possible mixing with operators of equal or lower

dimension, whose signals are hard to disentangle. For this reason, and in order to provide cross-estimates which have a reduced systematic error, the perturbative study of a variety of fermion operators is widely employed in numerical simulations of QCD on the lattice (see, e.g. [3] and references therein, also [36, 37, 38, 7, 8, 39]).

Within the staggered formulation using massive fermions we compute the fermion propagator and Green's functions of a set of local taste-singlet bilinears $\mathcal{O}$ (scalar (S), pseudoscalar (P), vector (V), axial (A) and tensor (T)). Our computation is performed to one loop and to lowest order in the lattice spacing, a. We also extract from the above the renormalization functions of the quark field $Z_{\rm q}$, quark mass $Z_{\rm m}$ and fermion bilinears $Z_{\mathcal{O}}$.

This is the first one-loop computation of these quantities, using staggered fermions with stout links. In the present work, we provide the details of the perturbative calculation and our results for the propagator and for the Green's functions, as well as the renormalization functions of all operators, including the vector, axial and pseudoscalar cases. Older results with staggered fermions [36] in the absence of stout smearing and for the Wilson gluon action are in complete agreement with our results; perturbartive results related to alternative improvements of the staggered action can be found, e.g., in Refs. [40, 41].

Stout links [19], rather than ordinary links, have been used both in the fermion action and in bilinear operators. Following Ref. [32], we use two steps of stout smearing with generic smearing parameters (ω_1, ω_2). We emphasize that the results for the bilinear Green's functions depend on four stout parameters, two due to the action smearing (ω_{A_1}, ω_{A_2}) and two more coming from the smearing of the operator ($\omega_{\mathcal{O}_1}$, $\omega_{\mathcal{O}_2}$); no numerical value needs to be specified for these parameters. The extension to further steps of stout smearing can be achieved with relative ease. For gluons we employ the Symanzik improved action. Our final expressions for the Green's functions exhibit a rather nontrivial dependence on the external momentum (p) and the fermion mass (m), and they are polynomial functions of the gauge parameter (α), stout parameters (ω_{A_i}, $\omega_{\mathcal{O}_i}$), and coupling constant (g); furthermore, most numerical coefficients in these expressions depend on the Symanzik parameters of the gluon action.

The one-loop expressions for the renormalization functions are presented in the mass-independent RI′ scheme; for the vector and axial renormalization functions we also employ an alternative RI′ scheme which might be more useful in renormalizing non-perturbative matrix elements. Furthermore, for comparison with experimental determinations and phenomenological estimates, it is useful to present our results also in the $\overline{\rm MS}$ scheme; we do so, paying particular attention to the possible alternative definitions of γ_5.

Results for $Z_{\rm q}$, $Z_{\rm m}$, $Z_{\mathcal{O}}$ exist for simpler actions to $\mathcal{O}(g^4)$ and/or $\mathcal{O}(g^2a^n)$, see e.g., Refs. [7, 8] for two-loop renormalization of flavor singlet and non-singlet local fermion bilinears, Ref. [38] for $Z_{\rm m}$ to two loops, Ref. [42] for one-loop renormalization of the fermion propagator and bilinears to $\mathcal{O}(a^1)$, and Refs. [43, 39, 14] for the fermion propagator and bilinears with 0 and 1 derivatives to one-loop and to $\mathcal{O}(a^2)$. The extension of the present computation beyond one loop and/or beyond $\mathcal{O}(a^0)$ becomes exceedingly complicated: One reason for this is the appearance of divergences in nontrivial corners of the Brillouin zone; also, a two-loop calculation requires vertices with up to four gluons, which are extremely lengthy in the presence of stout links (estimated length: $> 10^6$ terms).

We apply our results to a nonperturbative study of the magnetic susceptibility of QCD at zero and finite temperature in Chapter 4. In particular, we evaluate the "tensor coefficient", τ, which is relevant to the anomalous magnetic moment of the muon.

3.2 Formulation

3.2.1 Lattice actions

Our perturbative calculation makes use of the staggered fermion action.

Following the non-perturbative work of Ref. [32] we apply stout smearing according to Eq. (2.24), to all links appearing in $S_{\rm stag}$. In the present work we need the contributions of $Q_\mu(x)$ up to 2 gluons, to which the trace terms in Eq. (2.25) are irrelevant; the contributions can be read from the terms:

$$Q_\mu^{(2)}(x) = \frac{\omega}{2i}\sum_{\rho=\pm1}^{\pm4}\Big(U_\rho(x)U_\mu(x+a\hat\rho)U_\rho^\dagger(x+a\hat\mu)U_\mu^\dagger(x) - U_\mu(x)U_\rho(x+a\hat\mu)U_\mu^\dagger(x+a\hat\rho)U_\rho^\dagger(x)\Big) \tag{3.1}$$

($U_{-\rho}(y) \equiv U_\rho^\dagger(y-a\hat\rho)$, $\rho > 0$). The above procedure can be performed iteratively, by dressing the links more than once, in order to improve the convergence to the continuum limit. In the framework of our calculation we use "doubly-stout" links:

$$\widetilde{\widetilde{U}}_\mu(x) = e^{i\,\widetilde{Q}_\mu(x)}\,\widetilde{U}_\mu(x)\,, \tag{3.2}$$

where $\widetilde{Q}$ is defined as in Eq. (2.25), but using $\widetilde{U}$ as links (also in the construction of V_μ). Such links have been employed in numerical simulations in Refs. [31, 34]. To obtain results that are as general as possible, we use different stout parameters, ω, in the first (ω_1) and

the second (ω_2) smearing iteration. This allows for further optimization of improvement, by separate tuning of the two parameters; it also provides a check of the perturbative calculation by comparing the limit $\omega_1 = 0$ (or $\omega_2 = 0$) to the case of a single step of stout smearing. We smear both the links in $S_{\rm stag}$ and those in bilinear operators (see following subsection), so that we have a total of 4 stout parameters that we keep different from one another. In Appendix A we present the one-gluon link, $U^{(1)}$, for general ω_1 and ω_2, as well as the 2-gluon link, $U^{(2)}$; due to space limitations, the lengthy expression for $U^{(2)}$ (a total of $\sim$500 terms) has been presented only for $\omega_2 = 0$.

For gluons we employ the Symanzik improved action, Eq. (2.22).

3.2.2 Definition of operators

In the staggered formalism one defines fields that live on the corners of 4-dimensional elementary hypercubes of the lattice [44, 36, 45]. The position of a hypercube inside the lattice is denoted by the index y, where y is a 4-vector whose components y_μ are even integers ($y_\mu \,\epsilon\, 2\mathbb{Z}$). The position of a fermion field component within a specific hypercube is defined by one additional 4-vector index, C ($C_\mu \in \{0, 1\}$).

To be able to obtain the correct continuum limit, both for the action and for operators containing fermions, we relate χ with the physical field $Q_{\beta,b}$ (β: Dirac index, b: taste index). In standard notation:

$$\chi(y)_C \equiv \chi(ay + aC)/4 = \sum_{\beta,b} \left(\frac{1}{2}\xi_C\right)_{\beta,b} Q_{\beta,b}(y)\,, \quad Q_{\beta,b}(y) \equiv \frac{1}{2}\sum_C (\gamma_C)_{\beta,b}\ \chi(y)_C\,, \quad (3.3)$$

where ξ_C is defined similarly to γ_C (Eq. (2.26)), that is: $\xi_C = \xi_1^{C_1}\,\xi_2^{C_2}\,\xi_3^{C_3}\,\xi_4^{C_4}$, $\quad \xi_\mu = \left(\gamma_\mu^\star\right)$. In terms of the field Q one can now define fermion bilinear operators as follows:

$$\mathcal{O}_{\Gamma,\xi} = \bar{Q}\ (\Gamma \otimes \xi)\ Q\,, \quad (3.4)$$

where Γ and ξ are arbitrary 4×4 matrices acting on the Dirac and taste indices of $Q_{\beta,b}$, respectively. After rotating into the staggered basis, the operator $\mathcal{O}_{\Gamma,\xi}$ can be written as [36]:

$$\mathcal{O}_{\Gamma,\xi} = \sum_{C,D} \bar{\chi}(y)_C\ \left(\overline{\Gamma \otimes \xi}\right)_{CD}\ \chi(y)_D\,, \quad (3.5)$$

$$\left(\overline{\Gamma \otimes \xi}\right)_{CD} \equiv \frac{1}{4}\,\mathrm{Tr}\left[\gamma_C^\dagger\,\Gamma\,\gamma_D\,\xi\right]\,. \quad (3.6)$$

In this work we focus on taste-singlet operators, thus $\xi = \mathbb{1}$.

The operator of Eq. (3.5) is clearly not gauge invariant, since $\bar{\chi}$ and χ are defined at different points of the hypercube. To restore gauge invariance, we insert the average of products of gauge link variables along all possible shortest paths connecting the sites $y+C$ and $y+D$. This average is denoted by $U_{C,D}$ and the gauge invariant operator is now

$$\mathcal{O}_\Gamma \equiv \mathcal{O}_{\Gamma,\mathbb{1}} = \sum_{C,D} \bar{\chi}(y)_C \, \left(\overline{\Gamma \otimes \mathbb{1}}\right)_{CD} U_{C,D} \, \chi(y)_D \,. \tag{3.7}$$

From the definition of Eq. (3.6), as well as the equalities of Eq. (2.27), we can further simplify the expression for the operator $\mathcal{O}_\Gamma$, using:

$$\begin{aligned}
\frac{1}{4}\mathrm{Tr}\left[\gamma_C^\dagger \, \mathbb{1} \, \gamma_D\right] &= \delta_{C,D} \,, \\
\frac{1}{4}\,\mathrm{Tr}\left[\gamma_C^\dagger \, \gamma_\mu \, \gamma_D\right] &= \delta_{C,D+\hat{\mu}} \; \eta_\mu(D) \,, \\
\frac{1}{4}\mathrm{Tr}\left[\gamma_C^\dagger \, \sigma_{\mu\nu} \, \gamma_D\right] &= \frac{1}{i} \, \delta_{C,D+\hat{\mu}+\hat{\nu}} \; \eta_\nu(D) \; \eta_\mu(D+\hat{\nu}) \,, \\
\frac{1}{4}\,\mathrm{Tr}\left[\gamma_C^\dagger \, \gamma_5 \, \gamma_\mu \, \gamma_D\right] &= \delta_{C,D+\hat{\mu}+(1,1,1,1)} \; \eta_\mu(D) \, \eta_1(D+\hat{\mu}) \, \eta_2(D+\hat{\mu}) \, \eta_3(D+\hat{\mu}) \, \eta_4(D+\hat{\mu}) \,, \\
\frac{1}{4}\,\mathrm{Tr}\left[\gamma_C^\dagger \, \gamma_5 \, \gamma_D\right] &= \delta_{C,D+(1,1,1,1)} \; \eta_1(D) \, \eta_2(D) \, \eta_3(D) \, \eta_4(D) \,.
\end{aligned} \tag{3.8}$$

where $\sigma_{\mu\,\nu} = [\gamma_\mu, \gamma_\nu]/(2i)$. Here and below, in expressions such as $D+\hat{\mu}$ the sum is to be taken modulo 2. Using Eqs. (3.8), the operators can be written as:

$$\mathcal{O}_S(y) = \sum_D \bar{\chi}(y)_D \, \chi(y)_D \,, \tag{3.9}$$

$$\mathcal{O}_V(y) = \sum_D \bar{\chi}(y)_{D+\hat{\mu}} \, U_{D+\hat{\mu},D} \, \chi(y)_D \, \eta_\mu(D) \,, \tag{3.10}$$

$$\mathcal{O}_T(y) = \frac{1}{i} \sum_D \bar{\chi}(y)_{D+\hat{\mu}+\hat{\nu}} \, U_{D+\hat{\mu}+\hat{\nu},D} \, \chi(y)_D \, \eta_\nu(D) \, \eta_\mu(D+\hat{\nu}) \,, \tag{3.11}$$

$$\begin{aligned}
\mathcal{O}_A(y) = \sum_D & \bar{\chi}(y)_{D+\hat{\mu}+(1,1,1,1)} \, U_{D+\hat{\mu}+(1,1,1,1),D} \, \chi(y)_D \, \eta_\mu(D) \times \\
& \eta_1(D+\hat{\mu}) \, \eta_2(D+\hat{\mu}) \, \eta_3(D+\hat{\mu}) \, \eta_4(D+\hat{\mu}) \,,
\end{aligned} \tag{3.12}$$

$$\mathcal{O}_P(y) = \sum_D \bar{\chi}(y)_{D+(1,1,1,1)} \, U_{D+(1,1,1,1),D} \, \chi(y)_D \, \eta_1(D) \, \eta_2(D) \, \eta_3(D) \, \eta_4(D) \,. \tag{3.13}$$

With the exception of the scalar operator, the remaining operators contain averages of

products of up to 4 links (in orthogonal directions) between the fermion and the antifermion fields. For example, the average entering the tensor operator of Eq. (3.11) is:

$$U_{D+\hat{\mu}+\hat{\nu},D} = \frac{1}{2}\left[\,\tilde{\tilde{U}}^{\dagger}_{\nu}(ay+aD+a\hat{\mu})\;\tilde{\tilde{U}}^{\dagger}_{\mu}(ay+aD) + \{\mu \leftrightarrow \nu\}\,\right], \tag{3.14}$$

valid when $(D+\hat{\mu}+\hat{\nu})_i \geq D_i$, $i = 1,2,3,4$, and similarly for all other cases.

3.3 Calculation of Green's functions

In this section we describe some of the technical aspects of the calculation and present our results for one-loop Green's functions. As a starting point one must derive the vertices for the staggered action and the operators, up to 2 gluons, as required in our one-loop computation. For this reason one may use an equivalent expression of $\eta_\mu(x)$ appearing in the action:

$$\eta_\mu(x) = e^{i\pi\bar{\mu}\,n}\,, \quad x = an\,, \quad \bar{\mu} = \sum_{\nu=1}^{\mu-1}\hat{\nu}\,. \tag{3.15}$$

Using this form of $\eta_\mu(x)$, instead of the definition of Eq. (2.27), simplifies the expression for $\mathcal{O}_\Gamma$ in terms of Fourier transformed fields, $\tilde{\chi}(k)$, $\tilde{A}_\rho(k) \equiv \tilde{A}^c_\rho(k)\,T^c$:

$$\begin{aligned}
\mathcal{O}_\Gamma \;&=\; \int_{-\pi}^{\pi}\frac{d^4k_1}{(2\pi)^4}\int_{-\pi}^{\pi}\frac{d^4k_2}{(2\pi)^4}\,\tilde{\tilde{\chi}}(k_1)\,V_\Gamma(k_1,k_2)\,\tilde{\chi}(k_2) \\
&+\; \sum_{c,\rho}\int_{-\pi}^{\pi}\frac{d^4k_1}{(2\pi)^4}\int_{-\pi}^{\pi}\frac{d^4k_2}{(2\pi)^4}\int_{-\pi}^{\pi}\frac{d^4k_3}{(2\pi)^4}\,\tilde{\tilde{\chi}}(k_1)\,V^{c,\rho}_\Gamma(k_1,k_2,k_3;\omega_1,\omega_2)\,\tilde{\chi}(k_2)\,\tilde{A}^c_\rho(k_3) \\
&+\; \text{two}-\text{gluon terms} + \cdots
\end{aligned} \tag{3.16}$$

Thus, after Fourier transformation, the quark-antiquark vertices of Eqs. (3.9) - (3.13),

become:

$$V_S(k_1,k_2) = \delta\left(k_2-k_1\right) \tag{3.17}$$

$$V_V(k_1,k_2) = \delta\left(k_2-k_1+\pi\bar{\mu}\right)e^{-ik_{1\mu}}\,, \tag{3.18}$$

$$V_T(k_1,k_2) = \delta\left(k_2-k_1+\pi\bar{\mu}+\pi\bar{\nu}\right)e^{-ik_{1\mu}}e^{-ik_{1\nu}}\ (\nu>\mu)\,, \tag{3.19}$$

$$V_A(k_1,k_2) = \eta_\mu(\bar{\mu})\delta\left(k_2-k_1+\pi\sum_{\nu=1}^{4}\bar{\nu}+\pi\bar{\mu}\right)e^{-i(k_{1_1}+k_{1_2}+k_{1_3}+k_{1_4}-k_{1_\mu})}\,, \tag{3.20}$$

$$V_P(k_1,k_2) = \delta\left(k_2-k_1+\pi\sum_{\nu=1}^{4}\bar{\nu}\right)e^{-i(k_{1_1}+k_{1_2}+k_{1_3}+k_{1_4})}\,. \tag{3.21}$$

As for vertices containing gluons, we give here as an example the 1-gluon vertex of the vector operator, including double stout smearing:

$$\begin{aligned} V_V^{c,\rho}(k_1,k_2,k_3;\omega_1,\omega_2) \quad &= igT^c\Bigg[\cos\left(\tfrac{k_{3\mu}}{2}+k_{1\mu}\right)\delta\left(k_3-k_2+k_1+\pi\bar{\mu}+\pi\mu\right) \\ &\qquad +i\delta\left(k_3-k_2+k_1+\pi\bar{\mu}\right)\sin\left(\tfrac{k_{3\mu}}{2}+k_{1\mu}\right)\Bigg] \\ &\times\Bigg\{4\sin\left(\tfrac{k_{3\rho}}{2}\right)\sin\left(\tfrac{k_{3\mu}}{2}\right)\left(\omega_1+\omega_2+2\,\omega_1\,\omega_2\left(-4+\textstyle\sum_\sigma\cos\left(k_{1\sigma}\right)\right)\right) \\ &\qquad +\delta_{\rho\mu}\Bigg((8\omega_1-1)(8\omega_2-1) \\ &\quad +2\textstyle\sum_\sigma\cos\left(k_{3\sigma}\right)\left(\omega_1+\omega_2+2\,\omega_1\,\omega_2\left(-8+\sum_\tau\cos\left(k_{3\tau}\right)\right)\right)\Bigg)\Bigg\}\,, \end{aligned} \tag{3.22}$$

where μ is the index of the inserted Dirac matrix (γ_μ) and ρ is the index of the gluon.

Given that the argument y of the operators $\mathcal{O}_\Gamma$ runs only over even integers, summation over the position of $\mathcal{O}_\Gamma$, followed by Fourier transformation, leads to expressions of the form:

$$\sum_{y_\mu\,\epsilon\,2\mathbb{Z}} e^{i\,y\cdot k} = \frac{1}{16}(2\pi)^4\sum_C \delta_{2\pi}\left(k+\pi\,C\right)\,, \tag{3.23}$$

where $\delta_{2\pi}\left(k\right)$ stands for the standard periodic δ-function with non-vanishing support at $k\,\mathrm{mod}2\pi=0$. Since contributions to the continuum limit come from the neighborhood of

each of the 16 poles of the external momenta p, at $p_\mu = (\pi/a)C_\mu$, it is useful to define p'_μ and C_μ through

$$p_\mu = p'_\mu + \frac{\pi}{a} C_\mu \quad (\,\mathrm{mod}(\frac{2\pi}{a})\,), \quad (C_\mu \,\epsilon\, \{0,1\})\,, \tag{3.24}$$

where the "small" (physical) part p' has each of its components restricted to one half of the Brillouin zone: $-\pi/(2a) \le p'_\mu \le \pi/(2a)$. Thus, conservation of external momenta takes the form:

$$\delta_{2\pi}(a\,p_1 - a\,p_2 + \pi D) = \frac{1}{a}\delta(p'_1 - p'_2) \prod_\mu \delta_{C_{1\mu} - C_{2\mu} + D_\mu, 0}\,. \tag{3.25}$$

For the algebraic operations involved in evaluating the Feynman diagrams relevant to this calculation, we make use of our symbolic package in Mathematica; a description of this can be found, e.g., in Ref. [43].

3.3.1 Fermion propagator

We compute the one-loop correction to the fermion propagator in order to obtain the renormalization function of the fermion field, an essential ingredient for the renormalization of the operators $\mathcal{O}_\Gamma$. The tree-level fermion propagator in the basis of the χ fields can be written as:

$$S_{tree}(p_1, p_2) = (2\pi)^4\, \frac{-\frac{i}{a}\sum_\mu \sin(a\,p_{1\mu})\delta(p_1 - p_2 + \frac{\pi\bar{\mu}}{a}) + m\,\delta(p_1 - p_2)}{\frac{1}{a^2}\sum_\mu \sin^2(a\,p_{1\mu}) + m^2}\,. \tag{3.26}$$

The one-loop Feynman diagrams that enter the calculation of the 2-point, 1-particle irreducible (1PI), amputated Green's function, $S^{-1}(p)$, are illustrated in Fig. 3.1.

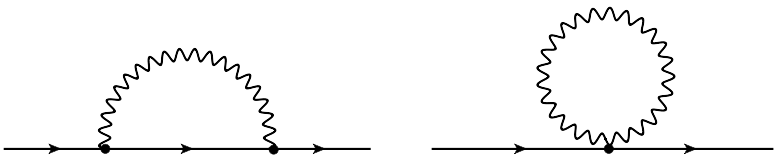

Figure 3.1: One-loop diagrams contributing to the fermion propagator. Wavy (solid) lines represent gluons (fermions).

We have computed $S^{-1}(p)$ for general values of: the gauge parameter α ($\alpha = 0$: Landau

gauge, $\alpha = 1$: Feynman gauge), the stout smearing parameters ω_{A_1}, ω_{A_2}, the Lagrangian mass m, the number of colors N_c and the external momenta p_1, p_2. We have obtained results using different sets of values for the Symanzik coefficients (shown in Table D.1). In presenting our result, Eq. (3.27), for $S^{-1}(p)$ up to one loop, the values of the quantities e_1, e_2 depend on the Symanzik coefficients and the stout smearing parameters. In all expressions the systematic errors (coming from an extrapolation to infinite lattice size of our numerical loop-integrals) are smaller than the last digit we present.

$$
\begin{aligned}
S^{-1}_{1-loop} = & \, i \sum_{\rho} \delta(p_1 - p_2 + \frac{\pi}{a}\bar{\rho})\, p_\rho\, (-1)^{C_{1\rho}} \\
& \left\{ 1 + \frac{g^2\, C_F}{16\pi^2} \left[(e_1 - \alpha \left(-4.79201 + \log\left(a^2 m^2 + a^2 p^2\right) + \frac{m^2}{p^2} - \frac{m^4}{p^4} \log\left(1 + \frac{p^2}{m^2}\right)\right) \right] \right\} \\
& + \delta(p_1 - p_2)\, m \\
& \left\{ 1 + \frac{g^2\, C_F}{16\pi^2} \left[e_2 + 5.79201\, \alpha - (3 + \alpha) \left(\log\left(a^2 m^2 + a^2 p^2\right) + \frac{m^2}{p^2} \log\left(1 + \frac{p^2}{m^2}\right)\right) \right] \right\}
\end{aligned}
\tag{3.27}
$$

p_1, p_2 : external momenta, $a\, p_\rho \equiv \left(a\, p_{1\rho} + \frac{\pi}{2}\right)_{\mathrm{mod}\pi} - \frac{\pi}{2} = \left(a\, p_{2\rho} + \frac{\pi}{2}\right)_{\mathrm{mod}\pi} - \frac{\pi}{2}$, and C_1 is defined in Eq. (3.24). Eq. (3.27) does have the expected structure of an inverse propagator, once one identifies, in the continuum limit:

$$
\sum_{\rho} \delta(p_1 - p_2 + \frac{\pi}{a}\bar{\rho})\, p_\rho\, (-1)^{C_{1\rho}} \underset{a \to 0}{\longrightarrow} \delta(p'_1 - p'_2) \not{p}'_1 \tag{3.28}
$$

For the tree-level Symanzik gauge action we obtain:

$$
\begin{aligned}
e_1 = & - 7.21363 + 124.515\, (\omega_{A_1} + \omega_{A_2}) - 518.433\, (\omega^2_{A_1} + \omega^2_{A_2}) - 2073.733\, \omega_{A_1}\, \omega_{A_2} \\
& + 9435.35\, (\omega^2_{A_1}\omega_{A_2} + \omega_{A_1}\, \omega^2_{A_2}) - 45903.1\, \omega^2_{A_1}\omega^2_{A_2}\,, \qquad (3.29) \\
e_2 = & \quad 27.1081 - 264.695\, (\omega_{A_1} + \omega_{A_2}) + 885.215\, (\omega^2_{A_1} + \omega^2_{A_2}) + 3540.86\, \omega_{A_1}\, \omega_{A_2} \\
& - 13960.0(\omega^2_{A_1}\omega_{A_2} + \omega_{A_1}\, \omega^2_{A_2}) + 60910.8\, \omega^2_{A_1}\omega^2_{A_2}\,. \qquad (3.30)
\end{aligned}
$$

In Appendix B.1 we provide the expressions of e_1, e_2 for the case of Wilson gluons. We denote the expression in curly brackets, in the last line of Eq. (3.27), as $\Sigma_m(q^2, m)$; from this we will extract the multiplicative renormalization of the Lagrangian mass, Z_{m}.

3.3.2 Fermion bilinears

In the context of this work we also study the 1PI, amputated, 2-point Green's functions of the operators $\mathcal{O}_\Gamma$, defined in Eqs. (3.9)-(3.13), up to one-loop: $\Lambda_{\mathcal{O}_\Gamma}^{1-loop}$. The 1PI Feynman diagrams that enter the calculation of the above Green's functions are shown in Fig. 3.2, and include up to two-gluon vertices extracted from the operator (the cross in the diagrams). The appearance of gluon lines on the operator stems from the product $U_{C,D}$ in the operator definition (Eq. (3.7))[1].

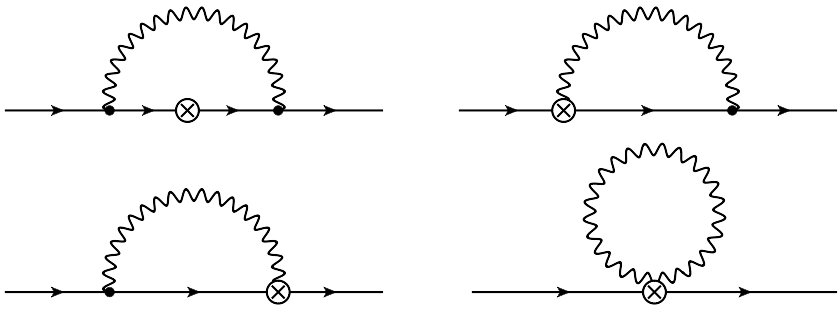

Figure 3.2: One-loop diagrams contributing to the fermion-antifermion Green's functions of the bilinear operators. A wavy (solid) line represents gluons (fermions). A cross denotes an insertion of the operator $\mathcal{O}_\Gamma$.

Analogous expressions to Eq. (3.27) arise for the bilinears as well. We note that the extraction of $Z_{\mathcal{O}_\Gamma}$ in a mass-independent scheme, such as RI′, necessitates evaluation of $\Lambda_{\mathcal{O}_\Gamma}^{1-loop}$ for $m = 0$ only. Nevertheless, we have included a nonzero Lagrangian mass in our computations; this allows us to derive the renormalized Green's functions at $m \neq 0$. Comparing the latter with results using a different regularization scheme (e.g. dimensional regularization) provides another check in our computation.

Although computing the diagrams of Fig. 3.2 does not use the expression for the propagator (Eq. (3.27)), all our results shown in Eqs. (3.31) - (3.35) are expressed in terms of e_1 (see Eqs. (3.27), (B.1)). The reason for that is to show explicitly the contribution to the quantities $\lambda_\mathcal{O}$ (Eqs. (3.36) - (3.40)) which appear in the renormalization functions $Z_\mathcal{O}$ (Eqs. (3.52) - (3.56)).

Dropping an overall Dirac δ-function of momentum conservation, and denoting the

[1]For $\mathcal{O}_S$ only the top right diagram of Fig. 3.2 contributes, since $U_{C,D} = \mathbb{1}$.

physical momentum of the fermion and antifermion by p, we obtain $\Lambda_{\mathcal{O}}^{1-loop}$:

$$\begin{aligned}
\Lambda_S^{1-loop} &= \mathbb{1} + \frac{g^2\,C_F}{16\pi^2}\Bigg[e_1 - \lambda_S + 5.79201\,\alpha + i\,\not{p}\left(4\alpha\,\frac{m^3}{(p^2)^2}\log\left(1+\frac{p^2}{m^2}\right) - 4\alpha\,\frac{m}{p^2}\right) \\
&- (\alpha+3)\left(3\,\frac{m^2}{p^2}\log\left(1+\frac{p^2}{m^2}\right) + \log\left(a^2m^2+a^2p^2\right)\right)\Bigg] \qquad (3.31)
\end{aligned}$$

$$\begin{aligned}
\Lambda_V^{1-loop} &= \gamma_\mu + \frac{g^2\,C_F}{16\pi^2}\Bigg[\gamma_\mu\Big(e_1 - \lambda_V + 4.79201\,\alpha - \alpha\frac{m^2}{p^2} - \alpha\log\left(a^2m^2+a^2p^2\right) \\
&+ \alpha\frac{m^4}{(p^2)^2}\log\left(1+\frac{p^2}{m^2}\right)\Big) \\
&+ ip_\mu\left(2\alpha\frac{m}{p^2} + 6\frac{m}{p^2} - \left(2\alpha\frac{m^3}{(p^2)^2} + 6\frac{m^3}{(p^2)^2}\right)\log\left(1+\frac{p^2}{m^2}\right)\right) \\
&- \not{p}p_\mu\left(2\alpha\frac{1}{p^2} - 4\alpha\frac{m^2}{(p^2)^2} + 4\alpha\frac{m^4}{(p^2)^3}\log\left(1+\frac{p^2}{m^2}\right)\right)\Bigg] \qquad (3.32)
\end{aligned}$$

$$\begin{aligned}
\Lambda_T^{1-loop} &= \sigma_{\mu\nu} + \frac{g^2\,C_F}{16\pi^2}\Bigg[\gamma_\mu\,\gamma_\nu\left(e_1 - \lambda_T + 3.79201\,\alpha - (1-\alpha)\Big(2\,\frac{m^2}{p^2} - \log\left(a^2m^2+a^2p^2\right)\right. \\
&\qquad \left. - \left(2\,\frac{m^4}{(p^2)^2} + \frac{m^2}{p^2}\right)\log\left(1+\frac{p^2}{m^2}\right)\Big)\right) \\
&- (\gamma_\mu\not{p}p_\nu - \gamma_\nu\not{p}p_\mu)(1-\alpha)\left(\left(4\,\frac{m^4}{(p^2)^3} + 2\,\frac{m^2}{(p^2)^2}\right)\log\left(1+\frac{p^2}{m^2}\right) - 4\,\frac{m^2}{(p^2)^2}\right) \\
&- i\,\gamma_\mu\,\gamma_\nu\not{p}\left(4\,\frac{m^3}{(p^2)^2}\log\left(1+\frac{p^2}{m^2}\right) - 4\,\frac{m}{p^2}\right) \\
&- i\,(\gamma_\mu p_\nu - \gamma_\nu p_\mu)\left(4\,\frac{m}{p^2} - 4\,\frac{m^3}{(p^2)^2}\log\left(1+\frac{p^2}{m^2}\right)\right)\Bigg] \qquad (3.33)
\end{aligned}$$

$$\begin{aligned}
\Lambda_A^{1-loop} &= \gamma_5\,\gamma_\mu + \frac{g^2\,C_F}{16\pi^2}\gamma_5\Bigg[\gamma_\mu\Bigg(e_1 - \lambda_A + 4.79021\,\alpha - (2-\alpha)\frac{m^2}{p^2} - \alpha\log\left(a^2m^2+a^2p^2\right) \\
&\qquad + \left(2\,(1-\alpha)\frac{m^4}{(p^2)^2} - 2\,(1+\alpha)\frac{m^2}{p^2}\right)\log\left(1+\frac{p^2}{m^2}\right)\Bigg) \\
&- i\,p_\mu(1-\alpha)\left(2\frac{m}{p^2} - 2\frac{m^3}{(p^2)^2}\log\left(1+\frac{p^2}{m^2}\right)\right) \\
&+ i\gamma_\mu\not{p}(1-\alpha)\left(2\frac{m}{p^2} - 2\frac{m^3}{(p^2)^2}\log\left(1+\frac{p^2}{m^2}\right)\right) \\
&- \not{p}p_\mu\Bigg(-8\frac{m^2}{(p^2)^2} + 2\alpha\frac{1}{p^2} + 4\alpha\frac{m^2}{(p^2)^2} \\
&\qquad + \left(8\frac{m^4}{(p^2)^3} - 4\alpha\frac{m^4}{(p^2)^3} + 4\frac{m^2}{(p^2)^2} - 4\alpha\frac{m^2}{(p^2)^2}\right)\log\left(1+\frac{p^2}{m^2}\right)\Bigg)\Bigg] \qquad (3.34)
\end{aligned}$$

$$\Lambda_P^{1-loop} = \gamma_5 + \frac{g^2\, C_F}{16\pi^2}\gamma_5 \quad \Bigg[\quad e_1 - \lambda_P + 5.79201\,\alpha - (\alpha+3)\frac{m^2}{p^2}\log\left(1+\frac{p^2}{m^2}\right) \\ - \quad (\alpha+3)\log\left(a^2m^2 + a^2p^2\right) \Bigg] \tag{3.35}$$

The quantities $\lambda_{\mathcal{O}}$ are independent of the mass, gauge parameter, external momentum and lattice spacing; they depend on the coefficients of the gluon action and on the stout parameters. As discussed earlier, we have employed different parameters for the 2 smearing steps; in fact, we have also kept the parameters of the action's smearing procedure (ω_{A_1}, ω_{A_2}) distinct from those of the operator smearing ($\omega_{\mathcal{O}_1}$, $\omega_{\mathcal{O}_2}$). For the tree-level Symanzik action and for general values of the stout parameters we obtained:

$$\begin{aligned} \lambda_S &= -34.3217 + 389.210\,(\omega_{A_1}+\omega_{A_2}) - 1403.65\,\left(\omega_{A_1}^2+\omega_{A_2}^2\right) - 5614.59\,\omega_{A_1}\,\omega_{A_2} \\ &+ 23395.4\,\left(\omega_{A_1}^2\,\omega_{A_2}+\omega_{A_1}\,\omega_{A_2}^2\right) - 106814\,\omega_{A_1}^2\,\omega_{A_2}^2 \end{aligned} \tag{3.36}$$

$$\begin{aligned} \lambda_V &= 86.7568\,[(\omega_{A_1}+\omega_{A_2}) - (\omega_{\mathcal{O}_1}+\omega_{\mathcal{O}_2})] - 337.383\,\left[\left(\omega_{A_1}^2+\omega_{A_2}^2\right) - \left(\omega_{\mathcal{O}_1}^2+\omega_{\mathcal{O}_2}^2\right)\right] \\ &- 1349.53\,(\omega_{A_1}\,\omega_{A_2} - \omega_{\mathcal{O}_1}\,\omega_{\mathcal{O}_2}) + 5950.81\,\Big[\left(\omega_{A_1}^2\,\omega_{A_2}+\omega_{A_1}\,\omega_{A_2}^2\right) \\ &- \left(\omega_{\mathcal{O}_1}^2\,\omega_{\mathcal{O}_2}+\omega_{\mathcal{O}_1}\,\omega_{\mathcal{O}_2}^2\right)\Big] - 28627.2\,\left(\omega_{A_1}^2\,\omega_{A_2}^2 - \omega_{\mathcal{O}_1}^2\,\omega_{\mathcal{O}_2}^2\right) \end{aligned} \tag{3.37}$$

$$\begin{aligned} \lambda_T &= 8.88342 + 116.579\,(\omega_{A_1}+\omega_{A_2}) - 200.588\,(\omega_{\mathcal{O}_1}+\omega_{\mathcal{O}_2}) - 531.759\,\left(\omega_{A_1}^2+\omega_{A_2}^2\right) \\ &+ 780.590\,\left(\omega_{\mathcal{O}_1}^2+\omega_{\mathcal{O}_2}^2\right) - 2095.16\,\omega_{A_1}\,\omega_{A_2} + 3154.24\,\omega_{\mathcal{O}_1}\,\omega_{\mathcal{O}_2} \\ &+ 31.8743\,(\omega_{A_1}+\omega_{A_2})\,(\omega_{\mathcal{O}_1}+\omega_{\mathcal{O}_2}) + 9877.233\,\left(\omega_{A_1}^2\,\omega_{A_2}+\omega_{A_1}\,\omega_{A_2}^2\right) \\ &- 13993.1\,\left(\omega_{\mathcal{O}_1}^2\,\omega_{\mathcal{O}_2}+\omega_{\mathcal{O}_1}\,\omega_{\mathcal{O}_2}^2\right) - 284.001\,\Big(\,(\omega_{A_1}+\omega_{A_2})\,\omega_{\mathcal{O}_1}\,\omega_{\mathcal{O}_2} \\ &+ \omega_{A_1}\,\omega_{A_2}\,(\omega_{\mathcal{O}_1}+\omega_{\mathcal{O}_2})\Big) - 48519.3\,\omega_{A_1}^2\,\omega_{A_2}^2 \\ &+ 68237.1\,\omega_{\mathcal{O}_1}^2\,\omega_{\mathcal{O}_2}^2 + 2709.49\,\omega_{A_1}\,\omega_{A_2}\omega_{\mathcal{O}_1}\,\omega_{\mathcal{O}_2} \end{aligned} \tag{3.38}$$

$$\begin{aligned}
\lambda_A &= 17.0363 + 117.584\,(\omega_{A_1}+\omega_{A_2}) - 314.355\,(\omega_{\mathcal{O}_1}+\omega_{\mathcal{O}_2}) - 518.419\,\left(\omega_{A_1}^2+\omega_{A_2}^2\right)\\
&+ 1223.79\,\left(\omega_{\mathcal{O}_1}^2+\omega_{\mathcal{O}_2}^2\right) - 2041.80\,\omega_{A_1}\,\omega_{A_2} + 4927.06\,\omega_{\mathcal{O}_1}\,\omega_{\mathcal{O}_2}\\
&+ 31.8758\,(\omega_{A_1}+\omega_{A_2})\,(\omega_{\mathcal{O}_1}+\omega_{\mathcal{O}_2}) + 9559.98\,\left(\omega_{A_1}^2\,\omega_{A_2}+\omega_{A_1}\,\omega_{A_2}^2\right)\\
&- 21823.5\,\left(\omega_{\mathcal{O}_1}^2\,\omega_{\mathcal{O}_2}+\omega_{\mathcal{O}_1}\,\omega_{\mathcal{O}_2}^2\right) - 210.274\,\Big(\,(\omega_{A_1}+\omega_{A_2})\,\omega_{\mathcal{O}_1}\,\omega_{\mathcal{O}_2}\\
&+ \omega_{A_1}\,\omega_{A_2}\,(\omega_{\mathcal{O}_1}+\omega_{\mathcal{O}_2})\,\Big) - 47154.2\,\omega_{A_1}^2\,\omega_{A_2}^2\\
&+ 105754.\,\omega_{\mathcal{O}_1}^2\,\omega_{\mathcal{O}_2}^2 + 1396.94\,\omega_{A_1}\,\omega_{A_2}\omega_{\mathcal{O}_1}\,\omega_{\mathcal{O}_2}
\end{aligned} \tag{3.39}$$

$$\begin{aligned}
\lambda_P &= 25.7425 + 119.062\,(\omega_{A_1}+\omega_{A_2}) - 428.120\,(\omega_{\mathcal{O}_1}+\omega_{\mathcal{O}_2}) - 518.541\,\left(\omega_{A_1}^2+\omega_{A_2}^2\right)\\
&+ 1667.00\,\left(\omega_{\mathcal{O}_1}^2+\omega_{\mathcal{O}_2}^2\right) - 2042.29\,\omega_{A_1}\,\omega_{A_2} + 6699.88\,\omega_{\mathcal{O}_1}\,\omega_{\mathcal{O}_2}\\
&+ 31.8765\,(\omega_{A_1}+\omega_{A_2})\,(\omega_{\mathcal{O}_1}+\omega_{\mathcal{O}_2}) + 9435.40\,\left(\omega_{A_1}^2\,\omega_{A_2}+\omega_{A_1}\,\omega_{A_2}^2\right)\\
&- 29654.0\,\left(\omega_{\mathcal{O}_1}^2\,\omega_{\mathcal{O}_2}+\omega_{\mathcal{O}_1}\,\omega_{\mathcal{O}_2}^2\right) - 210.274\,\Big(\,(\omega_{A_1}+\omega_{A_2})\,\omega_{\mathcal{O}_1}\,\omega_{\mathcal{O}_2}\\
&+ \omega_{A_1}\,\omega_{A_2}\,(\omega_{\mathcal{O}_1}+\omega_{\mathcal{O}_2})\,\Big) - 44803.9\,\omega_{A_1}^2\,\omega_{A_2}^2\\
&+ 143482.\,\omega_{\mathcal{O}_1}^2\,\omega_{\mathcal{O}_2}^2 + 1657.76\,\omega_{A_1}\,\omega_{A_2}\omega_{\mathcal{O}_1}\,\omega_{\mathcal{O}_2}
\end{aligned} \tag{3.40}$$

In Appendix B.2 we provide the expressions for $\lambda_{\mathcal{O}}$ in the case of the Wilson gluon action. We note in passing that in the absence of stout smearing ($\omega_{A_i}=\omega_{\mathcal{O}_i}=0$) $\lambda_V=0$ which implies that $Z_{\rm V}^{\rm RI'}=Z_{\rm V}^{\overline{\rm MS}}=1$ (cf. Eqs. (3.54), (3.63)), as is well known from current conservation. In addition, Eqs. (3.37),(B.4) show that non-renormalization of $\mathcal{O}_V$ applies also when $\omega_{A_i}=\omega_{\mathcal{O}_i}$; this follows from the fact that the stout link version of $\mathcal{O}_V$ mimics that of the action, and thus current conservation applies equally well in this case.

The dependence of the Green's functions of Eqs. (3.31) - (3.35) on mass and external momentum is regularization independent and agrees for instance with the results of Refs. [42, 14]. As is well known, in the limit of zero mass the vector and axial Green's functions beyond tree level are not multiples of their tree-level values: There appear additional, finite contributions with tensor structures which are distinct from those at tree level. These contributions, denoted as $\Sigma_V^{(2)}$ and $\Sigma_A^{(2)}$, can be read off Eqs. (3.32), (3.34):

$$\Sigma_V^{(2)} = \frac{g^2\,C_F}{16\pi^2}\Big[-2\,\alpha\frac{\not{p}\,p_\mu}{p^2}\Big] \tag{3.41}$$

$$\Sigma_A^{(2)} = \frac{g^2\,C_F}{16\pi^2}\Big[-2\,\alpha\frac{\gamma_5\,\not{p}\,p_\mu}{p^2}\Big] \tag{3.42}$$

A similar contribution for the tensor bilinear does not appear up to, and including, three

loops [46]. The role of $\Sigma_V^{(2)}$ and $\Sigma_A^{(2)}$ in the renormalization of $\mathcal{O}_V$ and $\mathcal{O}_A$ will be discussed in the next section.

3.4 Renormalization functions

3.4.1 Renormalization functions in the RI′ scheme

Renormalization functions (RFs), for operators and action parameters, relate bare quantities, regularized on the lattice, to their renormalized continuum counterparts:

$$\psi^R = Z_{\rm q}^{\frac{1}{2}}\psi^B\,, \qquad m^R = Z_{\rm m} m^B\,, \qquad \mathcal{O}_\Gamma^R = Z_{\mathcal{O}_\Gamma}\mathcal{O}_\Gamma^B\,. \tag{3.43}$$

The RFs of lattice operators are necessary ingredients in the prediction of physical probability amplitudes from lattice matrix elements. In this section we present the multiplicative RFs, in the RI′ scheme, of the fermion field ($Z_{\rm q}$), the fermion mass ($Z_{\rm m}$) and the fermion bilinears.

The RI′ renormalization scheme consists in requiring that the renormalized forward amputated Green's function $\Lambda(p)$, computed in the chiral limit and at a given (large Euclidean) scale $p^2 = \mu^2$, be equal to its tree-level value. Since renormalization conditions are typically imposed on amputated renormalized Green's functions, let us relate the latter to the bare ones. For the quark-antiquark Green's functions:

$$\begin{aligned}
\langle \psi^R\,\overline{\psi}^R\rangle &= Z_{\rm q}\langle \psi^B\,\overline{\psi}^B\rangle & (3.44)\\
\langle \psi^R\,\mathcal{O}_\Gamma^R\,\overline{\psi}^R\rangle_{\rm amp} &= \langle \psi^R\,\overline{\psi}^R\rangle^{-1}\,\langle \psi^R\,\mathcal{O}_\Gamma^R\,\overline{\psi}^R\rangle\,\langle \psi^R\,\overline{\psi}^R\rangle^{-1}\\
&= \left(Z_{\rm q}^{-1}\,\langle \psi^B\,\overline{\psi}^B\rangle^{-1}\right)\left(Z_{\rm q}\,Z_{\mathcal{O}_\Gamma}\langle \psi^B\,\mathcal{O}_\Gamma\,\overline{\psi}^B\rangle\right)\left(Z_{\rm q}^{-1}\,\langle \psi^B\,\overline{\psi}^B\rangle^{-1}\right)\\
&= Z_{\rm q}^{-1}Z_{\mathcal{O}_\Gamma}\langle \psi^B\,\mathcal{O}_\Gamma\,\overline{\psi}^B\rangle_{\rm amp}. & (3.45)
\end{aligned}$$

These requirements (along with the definition of Σ_m, Eq. (3.27)) lead to the following

definitions for $Z_{\rm q}^{\rm RI'}$, $Z_{\rm m}^{\rm RI'}$, $Z_{\mathcal{O}_\Gamma}^{\rm RI'}$:

$$S_{1-loop}^{-1}\Big|_{p^2=\mu^2,\, m=0} = S_{tree}^{-1}\Big|_{p^2=\mu^2,\, m=0} Z_{\rm q}^{\rm RI'}(\mu) \tag{3.46}$$

$$\Sigma_m\Big|_{p^2=\mu^2,\, m=0} = Z_{\rm m}^{\rm RI'}(\mu)\, Z_{\rm q}^{\rm RI'}(\mu) \tag{3.47}$$

$$\Lambda_{\mathcal{O}_\Gamma}^{1-loop}\Big|_{p^2=\mu^2,\, m=0} = \Lambda_{\mathcal{O}_\Gamma}^{tree}\, Z_{\rm q}^{\rm RI'}(\mu)\, \left(Z_{\mathcal{O}_\Gamma}^{\rm RI'}(\mu)\right)^{-1}, \quad (\Gamma = S,\, T,\, P) \tag{3.48}$$

where S_{tree}^{-1} is the tree-level result for the inverse propagator, and $\Lambda_{\mathcal{O}_\Gamma}^{tree}$ is the tree-level value of the Green's function for $\mathcal{O}_\Gamma$.

The presence of $\Sigma_V^{(2)}$ and $\Sigma_A^{(2)}$ in the one-loop Green's functions of $\mathcal{O}_V$ and $\mathcal{O}_A$ makes a prescription such as Eq. (3.48) inapplicable in those cases. Instead we employ:

$$\left(\Lambda_{V,\,A}^{1-loop} - \Sigma_{V,\,A}^{(2)}\right)\Big|_{p^2=\mu^2,\, m=0} = \Lambda_{V,\,A}^{tree} Z_{\rm q}^{\rm RI'}(\mu)\, \left(Z_{V,\,A}^{\rm RI'}(\mu)\right)^{-1}, \tag{3.49}$$

and thus take into account only the terms in $\Lambda_{V,\,A}$ which are proportional to their corresponding tree-level values.

The expressions we obtain using our results for $\Lambda_{\mathcal{O}_\Gamma}^{1-loop}$ are shown here only for the tree-level improved Symanzik gauge action. The quantities $\lambda_{\mathcal{O}}$ are defined in Eqs. (3.36) - (3.40). We note that the results for $Z_{\rm m}$ and $Z_{\rm S}$ are related by $Z_{\rm m} = Z_{\rm S}^{-1}$ as expected. Our results for the RFs are presented for arbitrary values of the renormalization scale μ.

$$Z_{\rm q}^{\rm RI'} = 1 + \frac{g^2\, C_F}{16\pi^2}\left[e_1 - \alpha\, \log\left(a^2\,\mu^2\right) + 4.79201\,\alpha\right] \tag{3.50}$$

$$Z_{\rm m}^{\rm RI'} = 1 + \frac{g^2\, C_F}{16\pi^2}\left[-e_1 + e_2 - 3\, \log\left(a^2\,\mu^2\right) + \alpha\right] \tag{3.51}$$

$$Z_{\rm S}^{\rm RI'} = 1 + \frac{g^2\,C_F}{16\pi^2}\left[\lambda_S - \alpha + 3\,\log\left(a^2\,\mu^2\right)\right] \tag{3.52}$$

$$Z_{\rm V}^{\rm RI'} = 1 + \frac{g^2\,C_F}{16\pi^2}\left[\lambda_V\right] \tag{3.53}$$

$$Z_{\rm T}^{\rm RI'} = 1 + \frac{g^2\,C_F}{16\pi^2}\left[\lambda_T + \alpha - \log\left(a^2\,\mu^2\right)\right] \tag{3.54}$$

$$Z_{\rm A}^{\rm RI'} = 1 + \frac{g^2\,C_F}{16\pi^2}\left[\lambda_A\right] \tag{3.55}$$

$$Z_{\rm P}^{\rm RI'} = 1 + \frac{g^2\,C_F}{16\pi^2}\left[\lambda_P - \alpha + 3\,\log\left(a^2\,\mu^2\right)\right]. \tag{3.56}$$

(e_1, e_2, $\lambda_{\mathcal{O}}$: are as defined in the previous Subsection).

In order to compare perturbative and non-perturbative estimates of RFs one clearly needs to employ the same renormalization prescription in both cases. In the context of a numerical simulation the term $\Sigma^{(2)}$ for the vector and axial cases is often not removed from the Green's functions, contrary to what is done perturbatively in Eq. (3.49). Therefore, an alternative RI′ renormalization prescription appears more natural:

$$Z_q^{-1}\,Z_{V,A}^{\rm RI'\,alter}\,{\rm Tr}\left[\Lambda_{V,A}^{1-loop}\,\Lambda_{V,A}^{tree}\right] = {\rm Tr}\left[\Lambda_{V,A}^{tree}\,\Lambda_{V,A}^{tree}\right]. \tag{3.57}$$

Using the above prescription, the extracted $Z_{\rm V}^{\rm RI'\,alter}$ and $Z_{\rm A}^{\rm RI'\,alter}$ take the form (to one loop):

$$Z_{\rm V}^{\rm RI'\,alter} = Z_{\rm V}^{\rm RI'} + \frac{g^2\,C_F}{16\pi^2}\,\frac{\alpha}{2}, \tag{3.58}$$

$$Z_{\rm A}^{\rm RI'\,alter} = Z_{\rm A}^{\rm RI'} + \frac{g^2\,C_F}{16\pi^2}\,\frac{\alpha}{2}. \tag{3.59}$$

3.4.2 Conversion to the $\overline{\rm MS}$ scheme

In this section we provide the expressions for the RFs in the $\overline{\rm MS}$ continuum scheme, using conversion factors adapted from Ref. [46]. These conversion factors do not depend on the regularization scheme (and, thus, they are independent of the lattice discretization), when expressed in terms of the renormalized coupling constant. However, expressing them in terms of the bare coupling constant introduces a dependence on the action. In our analysis we use one-loop formulae, which are action independent. The definition for the conversion factors $C_{\mathcal{O}}$, is as follows:

$$Z_{\mathcal{O}_\Gamma}^{\overline{\rm MS},\,\rm NDR} = C_{\mathcal{O}}\, Z_{\mathcal{O}_\Gamma}^{\rm RI'}\,. \tag{3.60}$$

The above conversion factors refer to the Naive Dimensional Regularization (NDR) of the $\overline{\rm MS}$ scheme (see e.g., Ref. [47]), in which $C_P = C_S$ and $C_A = C_V$. From Eq. (3.60) one obtains[2]:

$$Z_{\rm q}^{\overline{\rm MS},\,\rm NDR} = Z_{\rm q}^{\rm RI'} - \frac{g^2\,C_F}{16\pi^2}\,\alpha + \mathcal{O}(g^4) \tag{3.61}$$

$$Z_{\rm S,P}^{\overline{\rm MS},\,\rm NDR} = Z_{\rm S,P}^{\rm RI'} + \frac{g^2\,C_F}{16\pi^2}\,(4+\alpha) + \mathcal{O}(g^4) \tag{3.62}$$

$$Z_{\rm V,A}^{\overline{\rm MS},\,\rm NDR} = Z_{\rm V,A}^{\rm RI'} \tag{3.63}$$

$$Z_{\rm T}^{\overline{\rm MS},\,\rm NDR} = Z_{\rm T}^{\rm RI'} - \frac{g^2\,C_F}{16\pi^2}\,\alpha + \mathcal{O}(g^4)\,. \tag{3.64}$$

Other modified minimal subtraction schemes are related to NDR via additional finite renormalization and affect the operators which include a γ_5, due to the nonunique generalization of γ_5 to D dimensions. Thus, the treatment of the pseudoscalar and axial operators in the $\overline{\rm MS}$ scheme requires special attention. The $\overline{\rm MS}$ renormalized pseudoscalar and axial operators, as defined in the scheme of 't Hooft and Veltman (HV) [48], involve extra finite factors, Z_5^P, Z_5^A, in addition to the conversion factors of Eqs. (3.62) - (3.63) [49]:

$$Z_5^P = 1 - \frac{g^2}{16\pi^2}\,(8\,C_F) \tag{3.65}$$

$$Z_5^A = 1 - \frac{g^2}{16\pi^2}\,(4\,C_F)\,. \tag{3.66}$$

[2]Note that, at variance with Eq. 3.63, the conversion factors $C_{A,V}$ will not be equal to 1 if one uses, e.g., the "alternative" RI′ renormalization scheme of Eq. (3.57)

The relation between the NDR and the HV schemes is:

$$Z_{\rm P}^{\overline{\rm MS},\,\rm HV} = Z_{\rm P}^{\overline{\rm MS},\,\rm NDR}\, Z_5^P \tag{3.67}$$

$$Z_{\rm A}^{\overline{\rm MS},\,\rm HV} = Z_{\rm A}^{\overline{\rm MS},\,\rm NDR}\, Z_5^A\,. \tag{3.68}$$

We would like to point out that although the expressions for Z_5^A and Z_5^P are, in general, different for the singlet and non-singlet operators, at one-loop level they coincide.

Other variants of $\overline{\rm MS}$ include the DR$\overline{\rm EZ}$ and DRED schemes; the conversion from one scheme to another can be found in Section 4 of Ref. [36]. Our results for the fermion bilinears using the Wilson gauge action and without stout smearing, converted in the DR$\overline{\rm EZ}$ scheme, agree with the corresponding results of Ref. [36].

Having obtained $Z_{\mathcal{O}_\Gamma}^X$ in some renormalization scheme ($X = ({\rm RI}'), ({\rm RI}'{\rm alter}), (\overline{\rm MS}{\rm ,NDR}), (\overline{\rm MS}{\rm ,HV})$, etc.) the expression for the renormalized Green's functions in that scheme, $\Lambda_{\mathcal{O}_\Gamma}^{\rm renorm,X}(p,m)$, follow immediately:

$$\Lambda_{\mathcal{O}_\Gamma}^{R,X}(p,m) = \Lambda_{\mathcal{O}_\Gamma}^{B,X}(p,m)\ \left(Z_q^X\right)^{-1}\ Z_{\mathcal{O}_\Gamma}^X\,. \tag{3.69}$$

3.5 Summary

In this chapter we presented the calculation of the fermion propagator and the Green's functions for the ultra-local fermion bilinear operators: scalar, pseudoscalar, vector, axial and tensor. The computations were performed to one loop in lattice perturbation theory, using staggered fermions and Symanzik improved gluons, parameterized by 3 independent Symanzik coefficients; explicit results have been obtained for some of the most commonly used actions in this family: Wilson, Tree-level Symanzik, Tadpole improved Lüscher-Weisz, Iwasaki and DBW2.

The novelty in our calculations is the stout smearing of the links that we apply in both the fermion action and in the bilinear operators. More precisely, we use 2 steps of stout smearing with distinguishable parameters. To make our results as general as possible we also distinguish between the stout parameters appearing in the fermion action and in the bilinears.

Our expressions for the fermion propagator and the Green's functions of the bilinear operators exhibit a rather nontrivial dependence on the external momentum (q) and the fermion mass (m), and they are polynomial functions of the gauge parameter (α), stout parameters (ω_{A_i}, $\omega_{\mathcal{O}_i}$), and coupling constant (g). The numerical coefficients appearing in

these expressions depend on the Symanzik parameters of the gluon action and are presented for the Wilson and for the tree-level Symanzik improved gluon action.

Using the aforementioned results we extract the renormalization function of the fermion field and those of the fermion bilinears in the RI′ scheme and we provide the appropriate conversion factors to the $\overline{\text{MS}}$ scheme; we pay particular attention to the operators which include a γ_5 in their definition. Moreover, for the case of the vector and axial operators we give an alternative prescription to obtain the renormalizations in the RI′ scheme.

There are several directions in which the present work could be extended:

- A natural extension would be the computation of the Green's functions for operators including covariant derivatives, such as the one-derivative vector and axial operators[3]: $\overline{\psi}\gamma_{\{\mu}\overleftrightarrow{D}_{\nu\}}\psi$, $\overline{\psi}\gamma_5\gamma_{\{\mu}\overleftrightarrow{D}_{\nu\}}\psi$. The corresponding renormalization functions may be applied to the nonperturbative lattice evaluation of the momentum fraction of the nucleon, $\langle x\rangle_q$, and the moment of the polarized quark distribution of the nucleon, $\langle x\rangle_{\Delta q}$.

- A related further work using staggered fermions with stout improvement would be a computation of Green's functions for 4-fermi operators; a work in this direction can be found in Ref. [50].

- A possible improvement to the action may involve further iterations of stout smearing; such a procedure has been applied to Wilson fermions [51].

- It would be also interesting to calculate the Green's functions up to second order in the lattice spacing; such an extension would not only be useful in order to construct improved versions of the operators, but also to remove $\mathcal{O}(g^2\,a^2)$ contributions from the non-perturbative estimates of the renormalization functions. Similar computations have been performed recently with Wilson/clover/twisted mass fermions [39, 52, 43].

[3] Curly brackets denote symmetrization and subtraction of the trace.

Chapter 4

Magnetic susceptibility of QCD at zero and at finite temperature from the lattice

In the previous chapter we computed the matrix elements of staggered fermion operators. The extension to stout improvement on staggered fermions had never been explored until this computation. The necessity to calculate the perturbative renormalization functions of the scalar and tensor operator in the staggered formulation was dictated by the simulations run by our collaborators in University of Regensburg, University of Wuppertal and Eötvös University. They implemented the MILC code v7.6 [53] in order to obtain the zero-temperature magnetic susceptibilities at physical quark masses.

4.1 Introduction

An external (electro)magnetic field is an excellent probe of the dynamics of the QCD vacuum. Strong magnetic fields affect fundamental properties of QCD like chiral symmetry breaking and restoration, deconfinement, the hadron spectrum or the phase diagram, just to name a few. Chiral symmetry breaking has long been known to be enhanced by magnetic fields at zero temperature, signalled by an increasing chiral condensate (see e.g. Ref. [54]). The particle spectrum may undergo drastic changes (see e.g. the ongoing discussion in Refs. [55, 56, 57]) with some strong decay channels becoming unavailable and others opening up. The transitions at non-vanishing temperature related to chiral sym-

metry breaking and deconfinement are also affected by the magnetic field B. The phase diagram of QCD in the temperature-magnetic field plane was determined recently in lattice simulations [31, 58, 59] by analyzing the dependence of the chiral condensate and of other observables on B, with the main result that the transition temperature T_c decreases[1] with growing B and the transition remains an analytic crossover just as at $B = 0$ [62]. These effects are relevant in several physical situations as strong magnetic fields are expected to play a significant role, e.g., in early cosmology [63], in non-central heavy ion collisions [64] and in dense neutron stars [65].

Another fundamental characteristic of the QCD vacuum is the response of the free energy density (which at zero temperature is the vacuum energy density) to magnetic fields,

$$f = -\frac{T}{V}\log \mathcal{Z}, \tag{4.1}$$

where $\mathcal{Z}$ is the partition function of the system and V the (three-dimensional) volume. Due to rotational invariance the B-dependence of f is to leading order quadratic, characterized by the magnetic susceptibility of the QCD vacuum,

$$\xi = -\left.\frac{\partial^2 f}{\partial (eB)^2}\right|_{eB=0}, \tag{4.2}$$

which is a dimensionless quantity (here $e > 0$ denotes the elementary charge). A positive susceptibility indicates a decrease in f due to the magnetic field, that is to say, a *paramagnetic* response. On the other hand $\xi < 0$ is referred to as *diamagnetism* [66]. Clearly, the sign of ξ is a fundamental property of the QCD vacuum.

In the functional integral formalism of QCD the susceptibility is readily split into spin- and orbital angular momentum-related terms, according to

$$\xi = \sum_f \xi_f, \qquad \xi_f = \xi_f^S + \xi_f^L, \tag{4.3}$$

with contributions from each quark flavor f with electric charge q_f and mass m_f. For a

[1] Employing physical quark masses in the simulation and extrapolating the results to the continuum limit, as was done in Refs. [31, 58, 59], proved to be essential. Studies where these ingredients are missing produce qualitatively different results, namely an increasing $T_c(B)$ function [60, 61]. A possible explanation for this discrepancy and a comparison to effective theories was given recently in Ref. [59].

constant magnetic field $B = F_{xy}$ in the positive z direction,

$$\xi_f^S = \frac{q_f/e}{2m_f} \frac{\partial}{\partial(eB)} \left\langle \bar{\psi}_f \sigma_{xy} \psi_f \right\rangle \Big|_{eB=0}, \quad \sigma_{\mu\nu} = \frac{1}{2i}[\gamma_\mu, \gamma_\nu]. \tag{4.4}$$

ξ_f^L is given by an analogous expression with σ_{xy} replaced by a generalized angular momentum also present for spinless particles, cf. Eq. (B.14) of Appendix B.3. Eq. (4.4) constitutes an important relation which, to our knowledge, has not been recognized previously in this context. Its derivation from the quark determinant and the corresponding Dirac operator is given in Appendix B.3.

In the present work we concentrate on the spin contributions, and thus the expectation value of the tensor polarization operator $\bar{\psi}_f \sigma_{\mu\nu} \psi_f$. To leading order this is proportional to the field strength and thus can be written as [67]

$$\left\langle \bar{\psi}_f \sigma_{xy} \psi_f \right\rangle = q_f B \cdot \left\langle \bar{\psi}_f \psi_f \right\rangle \cdot \chi_f \equiv q_f B \cdot \tau_f, \tag{4.5}$$

where the expectation value is the quark condensate $\left\langle \bar{\psi}_f \psi_f \right\rangle$. Corrections to the right hand side are expected to be of $\mathcal{O}(B^3)$, so that Lorentz invariance is maintained. In the literature χ_f is referred to as the *magnetic susceptibility of the condensate* (for the quark flavor f). In what follows we will also use the term "magnetic susceptibility". Again we stress that it constitutes only one of the two contributions to the total susceptibility. We also define the *tensor coefficient* τ_f as the product of $\left\langle \bar{\psi}_f \psi_f \right\rangle$ and χ_f. Both quantities will depend on the temperature T at which the expectation values of Eq. (4.5) are determined. At finite quark masses it is advantageous to work with τ_f instead of χ_f for reasons related to renormalization (see below).

The magnetic susceptibility χ_f, in the context of QCD, was first introduced in Ref. [67]. Since then its experimental relevance has been growing steadily. In particular, this quantity appears in the description of radiative D_s meson transitions [68], of the anomalous magnetic moment of the muon [69] and of chiral-odd photon distribution amplitudes [70, 71]. Moreover, vector-tensor two-point functions at zero momentum are related to χ_f [72].

Since χ_f acts as an input parameter in various strong interaction processes [73], a high-precision determination of its value is of importance. In the past, it has been calculated using QCD sum rules [74, 75, 76], in the holographic approach [77, 78], using the operator product expansion [79], in the instanton liquid model and chiral effective models [80, 81, 82, 83], using the zero modes of the Dirac operator [84], and in low-energy models of QCD like the quark-meson model and the Nambu-Jona-Lasinio (NJL) model [85]. The numerical

value of χ_f was also determined recently on the lattice in the quenched approximation of two- [86] and of three-color QCD [87], in both cases without renormalization. We mention that the quenched approach can lead to large systematic errors at strong magnetic fields [88].

In this work we determine $\tau_f(T)$ and $\chi_f(T)$ for a wide range of temperatures around the transition region between the hadronic and the quark-gluon plasma phases and at $T = 0$. We apply fully dynamical lattice simulations, i.e. both the fermionic degrees of freedom and the external field are taken into account in the generation of the gauge ensembles. We perform the renormalization of the tensor coefficient and carry out the continuum extrapolation using results obtained at different lattice spacings. One main result will be that the tensor coefficient at $T = 0$ is negative for each quark flavor f, indicating the spin-diamagnetic nature of the QCD vacuum. Moreover we observe that τ_f decreases around the QCD crossover temperature similarly to other order parameters like the condensate.

This chapter is organized as follows. We define the lattice implementation of the magnetic field and the observables in Sec. 4.2 and discuss their renormalization in Sec. 4.3. The multiplicative renormalization is carried out perturbatively; the determination of renormalization constants is detailed in Chapter 3. After a brief summary of the simulation setup in Sec. 4.4 we present the results in Sec. 4.5 for the tensor coefficients and in Sec. 4.6 for the susceptibilities, before we conclude.

4.2 Magnetic field and observables

We study the effect of an external magnetic field B on the expectation value of the tensor polarization, Eq. (4.5). To realize such an external field on the lattice we implement the continuum U(1) gauge field A_μ satisfying $\partial_x A_y - \partial_y A_x = B$ using space-dependent complex phases [89, 90, 60, 31] in the following way,

$$\begin{aligned} u_y(n) &= e^{ia^2 q_f B n_x}, \\ u_x(N_x - 1, n_y, n_z, n_t) &= e^{-ia^2 q_f B N_x n_y}, \\ u_x(n) &= 1, \qquad n_x \neq N_x - 1, \\ u_\nu(n) &= 1, \qquad \nu \notin \{x, y\}, \end{aligned} \tag{4.6}$$

where the sites are labeled by integers $n \equiv (n_x, n_y, n_z, n_t)$, with $n_\nu = 0 \ldots N_\nu - 1$ and a is the lattice spacing. This prescription for the links corresponds to a covariant derivative for

the flavor f of the form[2] $D_{\mu,f} = \partial_\mu + iq_f A_\mu + igA^a_\mu T^a$. This discretization satisfies periodic boundary conditions in the spatial directions and ensures that the magnetic flux across the $x-y$ plane is constant. It is well known that the magnetic flux in a finite volume is quantized [91, 92], which on the lattice implies

$$qB \cdot a^2 = \frac{2\pi N_b}{N_x N_y}, \quad N_b \in \mathbb{Z}, \quad 0 \leq N_b < N_x N_y, \tag{4.7}$$

where q is the smallest charge in the system, in our case $q = q_d = q_s = -e/3$. Due to the periodicity of the links of Eq. (4.6) in N_b with period $N_x N_y$, one expects lattice artefacts to become large if $N_b > N_x N_y/4$. In the following we use lattices with $N_x = N_y = N_z \equiv N_s$.

We consider three quark flavors u, d and s. Since the charges and masses of the quarks differ we have to treat each flavor separately; $q_u = -2q_d = -2q_s$. We assume $m_u = m_d \neq m_s$. The partition function in the staggered formulation then reads,

$$\mathcal{Z} = \int \mathcal{D}U e^{-\beta S_g} \prod_{f=u,d,s} \left[\det M(U, q_f B, m_f)\right]^{1/4}, \tag{4.8}$$

with $M(U, qB, m) = \not{D}(U, qB) + m\mathbb{1}$ being the fermion matrix and $\beta = 6/g^2$ the gauge coupling. The exact form of the action we use is described in Refs. [33, 93], and further details of the simulation setup are given in Sec. 4.4. Since the external field couples directly only to quarks, B just enters the fermion determinants through the U(1) links of Eq. (4.6). The volume of the system is given as $V \equiv (aN_s)^3$ and the temperature as $T = (aN_t)^{-1}$.

In this formulation the expectation value of the quark condensate for the flavor f can be written as

$$\langle \bar{\psi}_f \psi_f \rangle \equiv \frac{T}{V} \frac{\partial \log \mathcal{Z}}{\partial m_f} = \frac{T}{4V} \left\langle \mathrm{Tr}\, M^{-1}(U, q_f B, m_f) \right\rangle. \tag{4.9}$$

Likewise, the expectation value of the tensor Dirac structure reads,

$$\langle \bar{\psi}_f \sigma_{\mu\nu} \psi_f \rangle = \frac{T}{4V} \left\langle \mathrm{Tr}\, (M^{-1}(U, q_f B, m_f)\sigma_{\mu\nu}) \right\rangle. \tag{4.10}$$

At this point a few comments regarding the sign of the expectation values in Eq. (4.5) are in place. In continuum calculations a negative sign for the condensate is customary, see e.g. Ref. [76], in contrast to our convention in Eq. (4.9). This sign convention applies for any fermionic bilinear expectation value, therefore it does not affect the sign of χ_f, but

[2]Note that we do not include in the action the corresponding photon kinetic term $F_{\mu\nu}F_{\mu\nu}/4 = B^2/2$. This means that in the discussion we will never encounter B alone but only the combination $q_f B \sim eB$.

only that of τ_f. Further possible differences in the sign can arise from the definition of $\sigma_{\mu\nu}$ and from that of the U(1) part of the covariant derivative. We note that our notation is consistent with that of Ref. [76] in terms of $\sigma_{\mu\nu}$, but differs by a minus sign in the covariant derivative (see the paragraph below Eq. (4.6)), implying an overall relative minus sign of χ_f.

4.3 Renormalization

In order to determine the continuum limit of the observables defined in Eqs. (4.9) and (4.10), their renormalization has to be performed. The quark condensate (at finite mass) is subject to additive and multiplicative renormalization, due to the divergent terms in the free energy density f of Eq. (4.1) and in the bare mass m_f. The former divergence is (to leading order) quadratic in the cutoff $1/a$ [94]. Therefore, the bare observable can be written as

$$\left\langle \bar{\psi}_f \psi_f \right\rangle (B,T) = \frac{1}{Z_{\mathrm{S}}} \left\langle \bar{\psi}_f \psi_f \right\rangle^r (B,T) + \zeta_S m_f/a^2 + \ldots, \tag{4.11}$$

where Z_{S} is the renormalization constant of the scalar operator and the ellipses denote subleading (logarithmic) divergences in a. Here the superscript r indicates the renormalized observable. The divergences in $\left\langle \bar{\psi}\psi \right\rangle$ depend neither on the temperature nor on the external field[3]. Therefore, in mass-independent renormalization schemes, ζ_S and Z_{S} are just functions of the gauge coupling. The conventional way to cancel the additive divergences is to consider the difference, for example, between the condensate at $T \neq 0$ and at $T = 0$.

The situation is somewhat different for the tensor polarization. As a calculation in the free theory shows, an additive divergence of the form $q_f B m_f \log(m_f^2 a^2)$ appears in $\left\langle \bar{\psi}\sigma_{\mu\nu}\psi \right\rangle$ (see Appendix B.4). This divergence vanishes in the chiral limit (or at zero external field) and is not related to the multiplicative divergence of the tensor operator to which we will return below. Altogether the bare observable can thus be written as

$$\begin{aligned} &\left\langle \bar{\psi}_f \sigma_{\mu\nu} \psi_f \right\rangle (B,T) \\ &\quad = \frac{1}{Z_{\mathrm{T}}} \left\langle \bar{\psi}_f \sigma_{xy} \psi_f \right\rangle^r (B,T) + \zeta_T q_f B m_f \log(m_f^2 a^2) + \ldots, \end{aligned} \tag{4.12}$$

where Z_{T} is the renormalization constant of the tensor operator (its perturbative determination is detailed in Chapter. 3) and ζ_T the coefficient of the divergent logarithm. Both

[3] For a detailed argumentation about the absence of B-dependent divergences in the condensate see Ref. [31] and references therein.

are independent of T and B (and in mass-independent schemes of m_f). In Eq. (4.12) the ellipses denote finite terms. In the free theory we calculate $\zeta_T(g=0) = 3/(4\pi^2)$ (see Appendix B.4). For our non-perturbative work, we used $Z_S^{\overline{\rm MS}}$ and $Z_T^{\overline{\rm MS}}$, with parameters $\omega_{\mathcal{O}_i} = \omega_{A_i} = 0.15$:

$$\begin{aligned} Z_S^{\overline{\rm MS}} &= 1 + \frac{g^2 C_F}{16\pi^2}\left[0.7929 + 3\log\left(a^2\mu^2\right)\right], \\ Z_T^{\overline{\rm MS}} &= 1 + \frac{g^2 C_F}{16\pi^2}\left[1.3136 - \log\left(a^2\mu^2\right)\right]. \end{aligned} \tag{4.13}$$

From these considerations it is clear that the magnetic susceptibility χ_f, being proportional to the ratio of Eq. (4.12) over Eq. (4.11), at non-vanishing quark mass contains additive divergences which depend both on T and on B (and also on the quark flavor f). This means that these singular contributions cannot be removed by subtracting the same operator, measured at different T or B (or flavor f).

Therefore, in the following we consider the tensor coefficient τ_f defined in Eq. (4.5). We notice that the operator $1 - m_f\partial/\partial m_f$ eliminates the logarithmic divergence and thus can be used to define an observable with a finite continuum limit,

$$\tau_f^r \equiv \left(1 - m_f \frac{\partial}{\partial m_f}\right)\tau_f \cdot Z_{\rm T} \equiv \tau_f Z_{\rm T} - \tau_f^{\rm div}. \tag{4.14}$$

At finite quark mass this is one possible prescription to cancel the additive logarithmic term. It has the advantages that the chiral limit of τ_f is left unaffected, and that, together with the logarithmic divergence, scheme-dependent finite terms also cancel in this difference (see Eq. (B.24)), such that the scheme- and renormalization scale-dependence of τ_f resides solely in $Z_{\rm T}$.

Since the subtracted divergence is independent of the temperature, we are able to determine $\tau_f^{\rm div}$ at zero temperature where we systematically study the dependence of τ_f on m_f and a, and then perform the subtraction at nonzero temperatures as well. As we will see, the subtraction in Eq. (4.14) amounts to a $5-10$ per cent effect for the lattice spacings we use.

4.4 Simulation setup

For our measurements we used the gauge ensembles of Refs. [31, 59] augmented by additional new ensembles. All configurations were generated with the tree-level improved

Symanzik gauge action and stout smeared staggered fermions, at physical quark masses. We use lattices at both $T = 0$ and at $T > 0$, at various values of the external magnetic field. We employ two steps of stout smearing with parameter $\omega_A = \omega_O = 0.15$ both in the action and in the operators. The zero temperature ensembles consist of $24^3 \times 32$, $32^3 \times 48$ and $40^3 \times 48$ lattices at five different lattice spacings, while at finite temperature we carried out measurements on lattices with $N_t = 6, 8$ and 10, allow for a continuum limit extrapolation. We studied finite volume effects on $N_t = 6$ lattices, using three different aspect ratios. The light ($m_u = m_d \equiv m_{ud}$) and strange (m_s) quark masses are set to their physical values, along the line of constant physics (LCP) as $m_{ud} = m_{ud}(\beta)$, and $m_s/m_{ud} = 28.15$. The LCP was determined by keeping f_K/M_π and f_K/M_K physical, and the lattice scale is set using f_K. More details about the lattice action, the determination of the scale and the LCP, and the lattice ensembles can be found in Refs. [33, 93, 31]. At each temperature and external magnetic field we measured the observables of interest on $\mathcal{O}(100)$ thermalized configurations which were separated by 5 trajectories to reduce autocorrelations. The measurements were carried out using the noisy estimator method, with 20–40 random vectors.

We define the coupling g in the "E" scheme [95], using the nonperturbative plaquette expectation value,

$$g_E^2 = \frac{1}{c}\left(1 - \frac{1}{3}\left\langle \mathrm{Tr}\, U_\Box \right\rangle^{\mathrm{nonper}}\right), \tag{4.15}$$

which is found to be 10−20% larger than the bare coupling g^2. We compute c perturbatively from the plaquette expectation value up to one-loop:

$$\left\langle \mathrm{Tr}\, U_\Box \right\rangle^{\mathrm{per}} = N_c(1 - g^2 c). \tag{4.16}$$

For the tree-level improved Symanzik gauge action we obtain $c = 0.183131340(2) \cdot C_F$, thereby confirming Ref. [96].

We allow for a systematic error of 50% in $1 - Z_{\mathrm{T}}^{\overline{\mathrm{MS}}}$ for the effect of higher order terms in the perturbative calculation.

4.5 Results

We measure the tensor polarizations as functions of the external field at various temperatures for the three different flavors. We observe that $\left\langle \bar{\psi}_u \sigma_{xy} \psi_u \right\rangle$ is negative, indicating that $\chi_u < 0$, in accordance with Ref. [76] and the discussion about the sign convention below Eq. (4.10). Whether this corresponds to a para- or a diamagnetic response will be

discussed in Sec. 4.6.

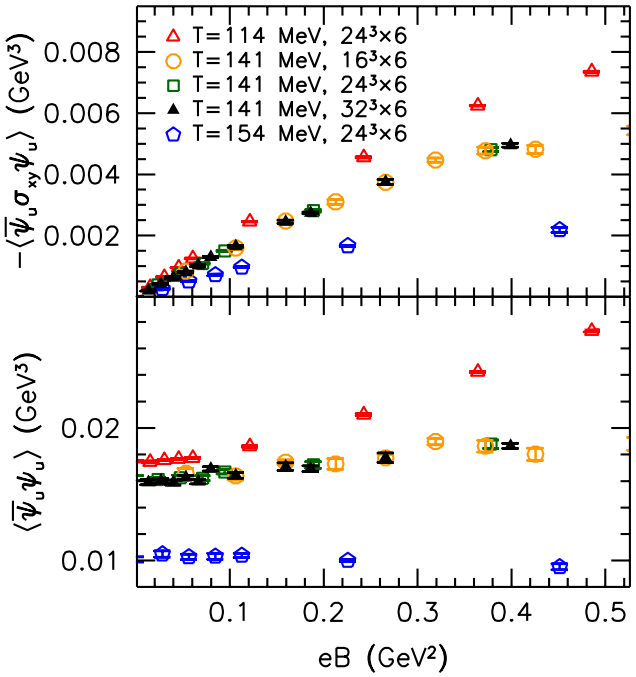

Figure 4.1: Minus the bare tensor polarization (upper panel) and the bare condensate (lower panel) for the up quark, for three temperatures on the $N_t = 6$ lattices.

In the upper panel of Fig. 4.1 we show minus the bare tensor polarization as a function of the magnetic field for $N_t = 6$. We confirm the linear trend to leading order in B, in agreement with Ref. [86]. However, the slope at small B is also observed to change significantly with temperature. We find that nonlinear effects are always below 5% for magnetic fields $eB < 0.2$ GeV^2 and they reduce as the temperature decreases. In the lower panel of Fig. 4.1 we also show how the bare condensate itself changes with B for different temperatures. We observe that the dependence of the condensate on B varies strongly with the temperature in the transition region. This behavior was found to be the reason for the decrease of the chiral transition temperature with growing B, and was investigated in detail in Refs. [31, 58, 59]. We study finite volume effects at one temperature $T = 141$ MeV, for $N_t = 6$ ensembles with $N_s = 16, 24$ and 32, see Fig. 4.1. The largest lattice corresponds to a linear extent of 7 fm. Since we see no deviation for the tensor polarization or the condensate between the different volumes, we conclude that finite size effects are smaller than our statistical errors.

Next, we concentrate on the leading linear trend in $\langle\bar{\psi}_f\sigma_{xy}\psi_f\rangle$, i.e. on the slope characterized by the tensor coefficient τ_f, as defined in Eq. (4.5). We perform the multiplicative

renormalization of τ_f according to Eq. (4.14), using the tensor renormalization constant, Eq. (4.13) in the $\overline{\text{MS}}$ scheme at a renormalization scale $\mu = 2$ GeV. The dependence of the results on the renormalization scale μ is found to be mild, as can be seen below.

We measure $Z_{\text{T}} \cdot \tau_f$ at zero temperature for several lattice spacings and quark masses. Here we fix the strange quark mass to its physical value and tune only the light mass such that $R \equiv m_{ud}/m_{ud}^{\text{phys}}$ varies between 0.5 and 28.15. For the latter ratio all three quarks have equal masses. (Note that these measurements are also fully dynamical and no partial quenching is applied.) In Fig. 4.2 we plot minus the tensor coefficient for the up quark as a function of R for five different lattice spacings. Motivated by the behavior of the tensor coefficient in the free case, Eq. (B.23), and by the scaling properties of the action we use, we consider the following fit function for $Z_{\text{T}}\tau_f$:

$$c_{f0} + c_{f1}R + c_{f2}R\log(R^2a^2), \quad c_{fi} = c_{fi}^{(0)} + c_{fi}^{(1)}a^2. \tag{4.17}$$

Here a is to be understood in units of GeV^{-1}. This form describes the data very well; we obtain χ^2/d.o.f. ≤ 1.5 for both the up and down flavors. The fitted values for $c_{fi}^{(j)}$ are listed in Table 4.1. We remark that the coefficients of the logarithms, $c_{u2}^{(0)}/m_{ud}^{\text{phys}} = 0.055(5)$ and $c_{d2}^{(0)}/m_{ud}^{\text{phys}} = 0.072(6)$ are quite close to the free-field value of $3/(4\pi^2)$ (see Appendix B.4). We perform the fit both for all lattice spacings and for only the finest four lattices. Moreover we consider the inclusion of an R^2 term in the fit and vary the fit range to exclude points with largest masses. The difference between these fits is used to estimate the systematic error of this combined extrapolation.

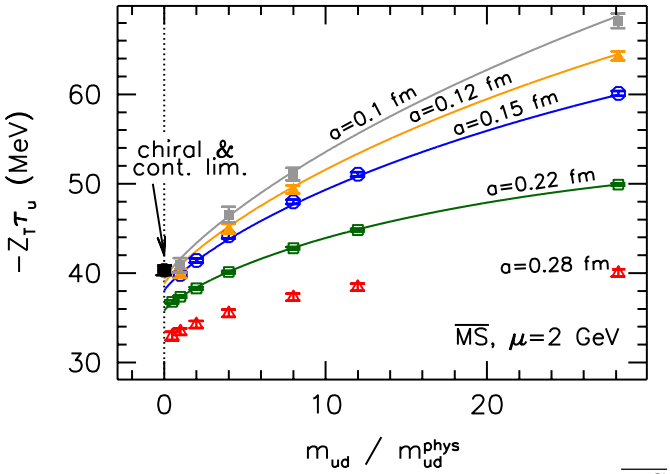

Figure 4.2: Mass dependence of the combination $-Z_{\text{T}} \cdot \tau_u$ in the $\overline{\text{MS}}$ scheme at renormalization scale $\mu = 2$ GeV. The coefficient of the logarithmic divergence is determined by fitting the data by a lattice spacing-dependent function (solid lines).

f	$c_{f0}^{(0)}$	$c_{f0}^{(1)}$	$c_{f1}^{(0)}$	$c_{f1}^{(1)}$	$c_{f2}^{(0)}$	$c_{f2}^{(1)}$
u	-40.3	3.8	-2.1	0.5	0.19	-0.03
d	-38.9	2.8	-2.5	0.7	0.25	-0.07

Table 4.1: Central values for the fit parameters of Eq. (4.17) in units of MeV.

At zero quark mass the additive divergence is absent and therefore, applying the combined fit, the continuum limit of the chiral limit of $Z_{\mathrm{T}}\tau_f$ can be extracted (it equals the $c_{f0}^{(0)}$ parameter). This corresponds to the black point in Fig. 4.2. However, since we are interested in the tensor coefficient at physical quark masses, we now follow the scheme of Eq. (4.14), subtracting the logarithmic divergence. We apply the operator $1 - m_f\partial_{m_f} = 1 - R\partial_R$, which acting on the fit function of Eq. (4.17) yields

$$\tau_f^r = c_{f0} - 2c_{f2}R. \tag{4.18}$$

As already emphasized in Sec. 4.3, the subtraction of the divergent term τ_f^{div} does not affect the chiral continuum limit since it vanishes at $m_f = 0$. Moreover, this subtraction eliminates the scheme-dependent finite terms (cf. Eq. (B.24)), making the conversion to the $\overline{\mathrm{MS}}$ scheme trivial.

For the strange quark we do not perform a similar analysis with modified strange quark masses, but subtract the logarithmic divergence by using the fit parameters for the down quark and $R = 28.15$. We find that the dependence of the strange quark tensor polarization on the light quark masses is below a few per cent (1% for the coarsest and 4% for the finest lattice). Therefore this approximation introduces errors smaller than those already present due to statistics and renormalization.

After the subtraction, the renormalized tensor coefficient τ_f^r has a well defined continuum limit even for finite quark masses. We find that for physical light quark masses $|\tau_{u,d}^{\mathrm{div}}| < 2.5$ MeV for our range of lattice spacings. For the strange quark the divergent contribution is larger in magnitude, giving rise to larger errors due to this subtraction.

Our final results for the zero temperature renormalized tensor coefficients in the $\overline{\mathrm{MS}}$ scheme at a renormalization scale $\mu = 2$ GeV are summarized in Table 4.2. For the light flavors this Table contains the results both for physical quark masses and for the chiral limit. These values may be compared to the unrenormalized quenched SU(2) lattice result $-\tau_{ud} = 46(3)$ MeV of Ref. [86] and to a similar study in the quenched SU(3) theory, 52 MeV [87]. Our results are in reasonable agreement with the QCD sum rule result 50(15)

MeV of Ref. [76], which was calculated at $\mu = 1$ GeV (note that the scale dependence of τ_f is small due to its small anomalous dimension, see Eq. (4.13)). We also compare our results to the NJL and quark-meson model predictions of 69 MeV and 65 MeV [85], respectively, which were obtained at an even lower renormalization scale of $\mu \sim 0.6$ GeV. We remark that a lower value of 44 MeV is obtained in the renormalized version of the quark meson model [85].

f	m	τ_f^r	error				
			stat.	mult.	cont.	scale	total
u	phys.	-40.7	0.2	0.3	1.0	0.8	1.3
	chir.	-40.3	0.2	0.3	1.1	0.8	1.4
d	phys.	-39.4	0.3	0.3	1.1	0.8	1.4
	chir.	-38.9	0.3	0.3	1.3	0.8	1.5
s	phys.	-53.0	0.5	0.3	7.1	1.1	7.2

Table 4.2: Results and error budget for the renormalized tensor coefficients for physical quark masses (phys.) and in the chiral limit (chir.). Given are (in units of MeV) the errors related to statistics, the multiplicative renormalization, the combined continuum fit, the lattice scale and, finally, the total error.

Next, one uses the fact that the τ_f^{div} contribution is independent of T to perform the additive renormalization of the tensor coefficient at finite temperatures. In Fig. 4.3 $-\tau_u^r$ is plotted as a function of the temperature for three lattice spacings. A simultaneous fit of the results is performed for different lattice spacings to an N_t-dependent spline function. This dependence is of the form N_t^{-2}, once again to reflect the scaling properties of our lattice action. We can read off the continuum extrapolation at $N_t^{-2} = 0$, which is shown in the figure by the hatched yellow band. The systematic error of the continuum extrapolation is estimated to be 1 MeV based on our experience at $T = 0$ (see Table 4.2) and is added to the statistical error in quadrature. Moreover, the uncertainty in the determination of the lattice scale (for details see Ref. [93]) propagates into this result and gives rise to an additional systematic error of 2%. Since this latter error is uniform and does not influence the shape of the $\tau_f^r(T)$ curve, it is not included in the plot.

In the same manner the tensor coefficient is determined for the down quark at $T > 0$, and obtain results which are within errors consistent with τ_u^r, just as was observed at $T = 0$. For the strange quark this procedure leads to a qualitatively similar temperature-dependence too. The dependence of $\tau_{u,d}^r$ on the temperature in the transition region can be used to define a transition temperature at $B = 0$. We determine the inflection point

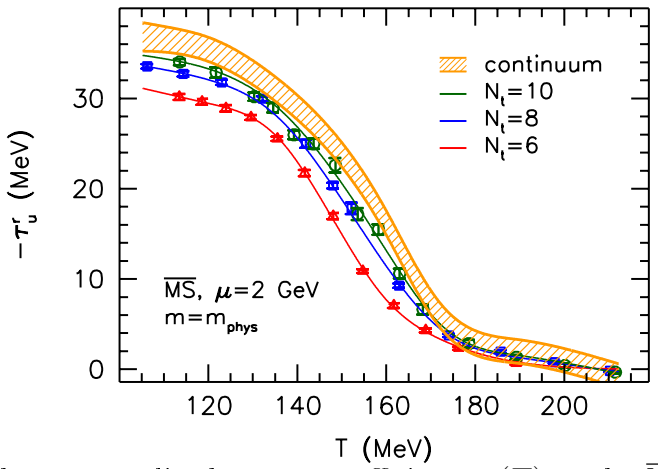

Figure 4.3: Minus the renormalized tensor coefficient $\tau_u^r(T)$ in the $\overline{\text{MS}}$ scheme at a renormalization scale $\mu = 2$ GeV for three lattice spacings and the continuum extrapolation.

of $\tau_{u,d}^r(T)$ and obtain $T_c = 162(3)(3)$ MeV in the continuum limit. Here the first error combines the statistical error and the error coming from the continuum extrapolation, and the second one is due to the uncertainty in the lattice scale. In conclusion, the tensor coefficient acts as a quasi-order parameter for the chiral transition, and gives a similar transition temperature as the chiral condensate at $B = 0$, $T_c = 159(3)(3)$ MeV, cf. Refs. [31, 97].

Finally, the dependence of τ_f^r is studied on the renormalization scale μ at $T = 0$. We carry out the analysis for a range of renormalization scales in the window 1 GeV $\leq \mu \leq$ 4 GeV. We find a very mild dependence on μ such that the tensor coefficients remain within the total errors given in Table 4.2.

4.6 Magnetic susceptibility

We can translate the result for τ_f^r to the magnetic susceptibility χ_f of Eq. (4.5) using the (scale- and scheme-dependent) value of the quark condensate. We recall the Gell-Mann-Oakes-Renner relation,

$$M_\pi^2 F^2 = (m_u + m_d) \cdot \langle \bar{\psi}_l \psi_l \rangle + \ldots, \tag{4.19}$$

which, at zero external field and in the chiral limit, relates the light condensate $l = u, d$ to the quark masses and to the pion mass and decay constant, with $F = 86.2(5)$ MeV [98]. We make use of a recent lattice determination [99] of the quark masses in the $\overline{\text{MS}}$ scheme at $\mu = 2$ GeV, $m_u + m_d = 6.94(13)$ MeV, to extract $\langle \bar{\psi}_l \psi_l \rangle = (269(2)\ \text{MeV})^3$. (We mention

that multiplying the lattice bare mass along the LCP [93] and the inverse of the scalar renormalization constant of Eq. (4.13), we get a compatible value for the renormalized quark mass in the $\overline{\text{MS}}$ scheme, albeit with large uncertainties.) For the strange condensate we employ the QCD sum rule prediction [100], $\langle\bar{\psi}_s\psi_s\rangle / \langle\bar{\psi}_l\psi_l\rangle = 0.8(3)$. Using these values for the quark condensates, the zero-temperature magnetic susceptibilities at physical quark masses are calculated as

$$\overline{\text{MS}},\ \mu = 2\ \text{GeV}: \qquad \begin{aligned} \chi_u &= -(2.08 \pm 0.08)\ \text{GeV}^{-2}, \\ \chi_d &= -(2.02 \pm 0.09)\ \text{GeV}^{-2}, \\ \chi_s &= -(3.4 \pm 1.4)\ \text{GeV}^{-2}. \end{aligned} \tag{4.20}$$

The magnetic susceptibilities at different values of μ can be obtained by running down with the ratio of renormalization constants $Z_{\text{T}}^{\overline{\text{MS}}}/Z_{\text{S}}^{\overline{\text{MS}}}$. Using the four-loop running to $\mu = 1$ GeV one has to multiply the above values by $r = 1.49(7)$. We remark furthermore that running down with $Z_{\text{S}}^{\overline{\text{MS}}}$ to a renormalization scale of $\mu = 1$ GeV we obtain $\langle\bar{\psi}_l\psi_l\rangle = (245(5)\ \text{MeV})^3$.

Our results in Eq. (4.20) are in good agreement with the QCD sum rule calculations[4] summarized and updated in Ref. [76]: $\chi_l = -2.11(23)\ \text{GeV}^{-2}$ at $\mu = 2$ GeV, and also compare well with the vector dominance estimate of $\chi_l = -2/m_\rho^2 \approx -3.3\ \text{GeV}^{-2}$. We remark that for the strange susceptibility, QCD sum rules predict $\chi_s \approx \chi_l$ [101], which is somewhat smaller than our result in Eq. (4.20).

Comparing the temperature-dependence of the light tensor coefficient (Fig. 4.3) and that of the light quark condensate from Ref. [59], we conclude that the ratio of the two renormalized observables is compatible with a constant, resulting in a magnetic susceptibility $\chi_l(T)$ depending only weakly on the temperature, at least for temperatures $T < 170$ MeV. Moreover, we remark that since χ_f is given in terms of the chiral condensate (which has a large anomalous dimension), the magnetic susceptibility has a stronger scale dependence than τ_f^r.

As anticipated in the introduction, the magnetic susceptibility χ_f of the condensate is intimately connected to the spin contribution ξ^S to the total magnetic susceptibility. Using this equivalence (which we prove in Appendix B.3), one sees that with our sign conventions $\chi_f > 0$ corresponds to paramagnetism and $\chi_f < 0$ to diamagnetism. Thus we conclude that the response of the QCD quark condensate to external magnetic fields is in its nature

[4] The value given in Ref. [76] is $\chi_l = 3.15(30)\ \text{GeV}^{-2}$ at $\mu = 1$ GeV. We divided this by $-1.49(7)$, running the value to the scale $\mu = 2$ GeV and accounting for the different sign convention we employ, see the remark after Eq. (4.10).

diamagnetic.

In conclusion, in this Chapter we studied the response of the QCD vacuum to a constant external magnetic field at zero and at finite temperature. We determined the tensor polarizations of the quark condensates for various temperatures and external fields. We observed that the polarization of the flavor f at a temperature T is a linear function of B for fields $eB < 0.2$ GeV^2, with a coefficient $\tau_f(T)$, defined in Eq. (4.5). The renormalization of this tensor coefficient requires two steps. The additive divergences (which are present for finite quark masses) were fitted explicitly at $T = 0$ and then subtracted using the operator $1 - m\partial_m$, at $T = 0$ and at $T > 0$. The multiplicative renormalization was performed perturbatively. We obtained results in the $\overline{\text{MS}}$ scheme at a renormalization scale $\mu = 2$ GeV, and extrapolated these to the continuum limit using several lattice spacings. Our final results for the renormalized τ_f^r are given in Table 4.2 for $T = 0$ and are shown in Fig. 4.3 for $T > 0$. Combining the results for τ_f^r and the quark condensates we also determined the magnetic susceptibilities χ_f, see Eq. (4.20) for the zero temperature values. We found χ_f to remain constant within errors as the temperature is increased up to $T \approx 170$ MeV.

We showed furthermore that there is a simple relation between the tensor coefficients τ_f^r and the spin contribution ξ^S to the total magnetic susceptibility, see Eq. (4.4). The negative sign of ξ^S reveals a diamagnetic response, i.e., that the spin magnetization of the medium aligns itself antiparallel to the external field. The magnitude of this effect reduces as the temperature grows, since ξ^S is proportional to τ_f^r which is plotted in Fig. 4.3. For the free case ξ^S and ξ^L are known to have opposite signs [102], implying a partial cancellation between the two sectors. Therefore, a determination of the orbital angular momentum contribution is necessary to arrive at a definite conclusion on whether the total response of the QCD vacuum to external magnetic fields is para- or diamagnetic.

Chapter 5

Perturbative calculation of local and extended fermion bilinear operators with the SLiNC action

In this Chapter we calculate corrections to the fermion propagator and to the Green's functions of all local and one-derivative vector, axial and tensor fermion bilinear operators, to one-loop in perturbation theory. We employ the SLiNC action. This action is presently being used by the QCDSF Collaboration, in simulations of QCD with dynamical quark flavors. The novel aspect of our calculations is that they are carried out to second order in the lattice spacing, $\mathcal{O}(a^2)$. Consequently, they have addressed a number of new issues, most notably the appearance of loop integrands with strong IR divergences (convergent only beyond 6 dimensions). Such integrands are not present in $\mathcal{O}(a^1)$ improvement calculations; there, IR divergent terms are seen to have the same structure as in the $\mathcal{O}(a^0)$ case, by virtue of parity under integration, and they can thus be handled by well-known techniques [43]. The $\mathcal{O}(a^2)$ corrections to the quark propagator and Green's functions computed in this Chapter are useful to improve the nonperturbative RI-MOM determination of renormalization constants for quark bilinear operators. Our results depend on a large number of parameters: coupling constant, number of colors, lattice spacing, external momentum, clover parameter, Symanzik coefficients, stout and gauge parameter.

5.1 Introduction

One fundamental aim in simulations of hadronic states is the accurate evaluation of moments of parton momentum, helicity and transversity distributions as a function of the momentum fraction, as well as moments of generalized parton distributions (GPDs) of meson and baryon states. These quantities contain a very rich spectrum of physical information on nucleons, and are thus at the forefront of research in Strong Interaction Physics. Beyond the information that GPDs yield, such as size, magnetization and shape, GPDs encode additional information, relevant for experimental investigations, such as the decomposition of the total hadron spin into angular momentum and spin carried by quarks and gluons. GPDs are single particle matrix elements of the light-cone operator [103, 104], which can be expanded in terms of local twist-two operators. Lattice QCD allows us to extract hadron matrix elements for the twist-two operators, which can be expressed in terms of generalized form factors.

In order to evaluate moments of GPDs from numerical simulations of QCD on the Lattice, one must measure nucleon matrix elements of a series of composite fermion operators, both local and extended. These operators must be renormalized, before one can compare results from simulations to physical, experimentally measurable quantities. Sophisticated techniques in Quantum Field Theory will be applied to compute the perturbative renormalization of the fermion propagator, local bilinears and higher-twist operators, beyond leading order in g (coupling constant) and a (lattice spacing). These terms are subtracted from the non-perturbative results as we are going to see in Chapter 6 in the case of clover fermions and Wilson gluons. This subtraction suppresses lattice artifacts considerably, depending on the operator under study, and leads to a more accurate determination of the renormalization constants [39].

In the Bjorken limit[1], involved in studies of deep inelastic scattering, the Operator Product Expansion (OPE) for a product of hadronic currents takes the form:

$$J(x)J(0) \sim \sum_{n,i} C^{(n,i)}(x^2)\, x^{\mu_1} \cdots x^{\mu_n}\, \mathcal{O}^{(n,i)}_{\mu_1 \cdots \mu_n}(0) \tag{5.1}$$

The forward matrix elements of the local operators $\mathcal{O}(x; N, i)$ appearing in this expansion are directly related to the moments of hadron structure functions [107]. The dominant

[1] In the Bjorken limit [105, 106] structure functions have factorization properties, which follow from the renormalizability of the theory.

contribution in the expansion is given by operators whose twist (dimension minus spin) equals two, which in the flavor non-singlet case means the following traceless operators [108] (curly brackets denote symmetrization over Lorentz indices and subtraction of the traces; T^a are flavor matrices):

$$\mathcal{O}^{\{\mu\,\mu_1\cdots\mu_n\}} = \overline{\psi}\gamma^{\{\mu} D^{\mu_1}\cdots D^{\mu_n\}}\frac{T^a}{2}\psi \tag{5.2}$$

$$\mathcal{O}_5^{\{\mu\,\mu_1\cdots\mu_n\}} = \overline{\psi}\gamma^{\{\mu}\gamma_5 D^{\mu_1}\cdots D^{\mu_n\}}\frac{T^a}{2}\psi \tag{5.3}$$

The matrix elements of local operators we studied are given by:

$$\langle p's'|\mathcal{O}_\Gamma^{\{\mu_1\cdots\mu_n\}}|ps\rangle \tag{5.4}$$

where s, s' are the initial and final spin 4-vectors of the nucleon, p, p' are the corresponding momenta and $D \equiv \overleftrightarrow{D} = (\overrightarrow{D} - \overleftarrow{D})/2$ is the covariant derivative.

The extended bilinear operators, which we study, are symmetrized over two Lorentz indices and are made traceless:

$$\mathcal{O}^{\{\sigma\,\tau\}} \equiv \frac{1}{2}\Big(\mathcal{O}^{\sigma\,\tau} + \mathcal{O}^{\tau\,\sigma}\Big) - \frac{1}{4}\delta^{\sigma\,\tau}\sum_\lambda \mathcal{O}^{\lambda\,\lambda}, \quad \mathcal{O}^{\sigma\,\tau} \equiv \overline{\psi}\gamma^\sigma D^\tau\psi. \tag{5.5}$$

This definition avoids mixing with lower dimension operators. In a massless renormalization scheme the renormalization constants are defined in the chiral limit, where flavor symmetry is exact. Hence, the same value for Z is obtained independently of the value of T^a and therefore we drop $(T^a/2)$ on the operators from here on. One should however keep in mind the fact that the values of Z for flavor singlet and nonsinglet operators will be different beyond one-loop in perturbation theory and also nonperturbatively.

Concentrating on one derivative operators, there are three types of forward matrix elements, $(p = p')$ according to the choice of the γ-structure of the operator $\mathcal{O}$; in the flavor singlet case, these three types correspond to:

- Unpolarized quark distributions:
  The operator is $\mathcal{O}^{\{\mu_1\,\mu_2\}} = \overline{\psi}(0)\gamma^{\{\mu_1} D^{\mu_2\}}\psi(0)$ and it is related to the moment:

$$\langle x^n\rangle_q = \int_{-1}^{1} dx\, x^n\left[q(x) + (-1)^{n+1}\bar{q}(x)\right],\ q = q_\downarrow + q_\uparrow \tag{5.6}$$

  where $q(x)$ is the quark density distribution.

- Longitudinal spin distributions:
  The operator $\mathcal{O}_5^{\{\mu_1\,\mu_2\}} = \overline{\psi}(0)\gamma_5\,\gamma^{\{\mu_1} D^{\mu_2\}}\psi(0)$ is related to the moment:

$$\langle x^n\rangle_{\Delta q} = \int_{-1}^{1} dx\, x^n \left[\Delta q(x) + (-1)^n \Delta\bar{q}(x)\right],\ q = q_\downarrow - q_\uparrow \tag{5.7}$$

  where $\Delta q(x)$ is the quark helicity distribution.

- Transversity distribution: The operator is $\mathcal{O}_{5\,\sigma}^{\mu\,\{\mu_1\,\mu_2\}} = \overline{\psi}(0)\gamma_5\,\sigma^{\mu\{\mu_1} D^{\mu_2\}}\psi(0)$ and the corresponding moment is:

$$\langle x^n\rangle_{\delta q} = \int_{-1}^{1} dx\, x^n \left[\delta q(x) + (-1)^{n+1} \delta\bar{q}(x)\right],\ q = q_\perp - q_\parallel \tag{5.8}$$

  where $\delta q(x)$ is the quark transversity distribution.

The quark density, helicity, and transversity distributions are related to the following matrix elements of twist-2 operators [109]:

$$\begin{aligned}
2\,\langle x^{n-1}\rangle_q\, p^{\mu_1}\cdots p^{\mu_n} &\equiv \frac{1}{2}\sum_s \langle ps|\left(\frac{i}{2}\right)^{n-1} \bar{\psi}\gamma^{\{\mu_1}\overleftrightarrow{D}^{\mu_2}\cdots\overleftrightarrow{D}^{\mu_n\}}\psi|ps\rangle \qquad (5.9)\\
\frac{2}{n+1}\,\langle x^n\rangle_{\Delta q}\, s^{\{\sigma} p^{\mu_1}\cdots p^{\mu_n\}} &\equiv -\langle ps|\left(\frac{i}{2}\right)^{n} \bar{\psi}\gamma_5\gamma^{\{\sigma}\overleftrightarrow{D}^{\mu_1}\cdots\overleftrightarrow{D}^{\mu_n\}}\psi|ps\rangle\\
\frac{2}{m_N}\,\langle x^n\rangle_{\delta q}\, s^{[\mu} p^{\{\nu]} p^{\mu_1}\cdots p^{\mu_n\}} &\equiv \langle ps|\left(\frac{i}{2}\right)^{n} \bar{\psi}\gamma_5\sigma^{\mu\{\nu}\overleftrightarrow{D}^{\mu_1}\cdots\overleftrightarrow{D}^{\mu_n\}}\psi|ps\rangle,
\end{aligned}$$

where the square brackets denote antisymmetrization.

5.2 Computation

The most laborious aspect of our calculation is the extraction of the dependence on lattice spacing a and external momentum p. This is a delicate task even at one-loop level, since we are interested in $\mathcal{O}(a^2)$ improvement; for this purpose, we cast algebraic expressions (typically involving thousands of summands) into terms which can be naively Taylor expanded in a to the required order, plus a smaller set of terms containing superficial divergences. The latter can be evaluated via analytical continuation to $D > 4$ or even $D > 6$ dimensions, and splitting each expression into a UV-finite part (which can thus be calculated in the continuum), and a part which is polynomial in a. A list of the divergent integrals appearing in this calculation can be found in Ref. [43].

Dealing with "strong" IR divergent terms, a typical example of integral is:

$$\int_{-\pi}^{\pi} \frac{d^4k}{(2\pi)^4} \frac{1}{\hat{k}^2 \widehat{k+a\,p}^{\,2}} \tag{5.10}$$

First we split the original integrand I into two parts

$$I \equiv \frac{1}{\hat{k}^2 \widehat{k+a\,p}^{\,2}} = I_1 + I_2 \tag{5.11}$$

where I_2 is obtained from I by a series expansion, with respect to the arguments of all trigonometric functions, to subleading order; I_1 is simply the remainder $I - I_2$

$$I_2 = \frac{1}{k^2\,(k+a\,p)^2} + \left[\frac{(k+a\,p)^4}{12\,k^2\,\left((k+a\,p)^2\right)^2} + \frac{k^4}{12\,\left(k^2\right)^2\,(k+a\,p)^2}\right] \tag{5.12}$$

$$\begin{aligned} I_1 &= \frac{k^2 - \frac{k^4}{12} - \hat{k}^2}{k^2\,\hat{k}^2\,\widehat{k+a\,p}^{\,2}} + \frac{k^4\left(k^2-\hat{k}^2\right)}{12\,\left(k^2\right)^2\,\hat{k}^2\,\widehat{k+a\,p}^{\,2}} + \frac{k^4\left((k+a\,p)^2 - \widehat{k+a\,p}^{\,2}\right)}{12\,\left(k^2\right)^2\,(k+a\,p)^2\,\widehat{k+a\,p}^{\,2}} \\ &+ \frac{(k+a\,p)^2 - \frac{(k+a\,p)^4}{12} - \widehat{k+a\,p}^{\,2}}{k^2\,(k+a\,p)^2\,\widehat{k+a\,p}^{\,2}} + \frac{(k+a\,p)^4\left((k+a\,p)^2 - \widehat{k+a\,p}^{\,2}\right)}{12\,k^2\,\left((k+a\,p)^2\right)^2\,\widehat{k+a\,p}^{\,2}} \end{aligned} \tag{5.13}$$

($q^4 \equiv \sum_\mu q_\mu^4$). I_2 is free of trigonometric functions, while I_1 has been written as a sum of terms, each of which is naively Taylor expandable to $\mathcal{O}(a^2)$; its integral equals

$$\int_{-\pi}^{\pi} \frac{d^4k}{(2\pi)^4} I_1 = 0.004210419649(1) + a^2\,p^2\,0.0002770631001(3) + \mathcal{O}(a^4, a^4 \ln a) \tag{5.14}$$

The errors appearing in the above equation come from extrapolations to infinite lattice size.

To evaluate the integral of I_2 we split the hypercubic integration region into a sphere of arbitrary radius μ about the origin ($\mu \leq \pi$) plus the rest

$$\int_{-\pi}^{\pi} = \int_{|k|\leq\mu} + \left(\int_{-\pi}^{\pi} - \int_{|k|\leq\mu}\right) \tag{5.15}$$

The integral outside the sphere is free of IR divergences and is thus Taylor expandable to

any order, giving (for $\mu = 3.14155$).

$$\left(\int_{-\pi}^{\pi} - \int_{|k|\leq\mu}\right) \frac{d^4k}{(2\pi)^4} I_2 = 6.42919(3)\, 10^{-3} + a^2\, p^2\, 6.2034(1)\, 10^{-5} + \mathcal{O}(a^4) \tag{5.16}$$

We are now left with the integral of I_2 over a sphere. The most infrared divergent part of I_2 is $1/(k^2\,(k + a\,p)^2)$, with IR degree of divergence -4, and can be integrated *exactly*, giving

$$\int_{|k|\leq\mu} \frac{d^4k}{(2\pi)^4} \frac{1}{k^2\,(k + a\,p)^2} = \frac{1}{16\pi^2}\left(1 - \ln(\frac{a^2\,p^2}{\mu^2})\right) \tag{5.17}$$

The remaining two terms comprising I_2 have IR degree of divergence -2, thus their calculation to $\mathcal{O}(a^2)$ can be performed in D-dimensions, with D slightly greater that 4. Let us illustrate the procedure with one of these terms: $k^4/((k^2)^2\ (k + a\,p)^4)$. By appropriate substitutions of

$$\frac{1}{(k+\bar{p})^2} = \frac{1}{k^2} + \frac{-2(k\cdot\bar{p}) - \bar{p}^2}{k^2\,(k+\bar{p})^2} \qquad (\bar{p} \equiv a\,p) \tag{5.18}$$

we split this term as follows

$$\begin{aligned} \frac{k^4}{(k^2)^2\ (k+\bar{p})^2} &= \left[\frac{k^4}{(k^2)^3} + \frac{k^4\,(-2(k\cdot\bar{p}) - \bar{p}^2)}{(k^2)^4} + \frac{4\,k^4(k\cdot\bar{p})^2}{(k^2)^5}\right] \\ &+ \left(\frac{k^4\,(4(k\cdot\bar{p})\bar{p}^2 + (\bar{p}^2)^2)}{(k^2)^4\ (k+\bar{p})^2} + \frac{4\,k^4(k\cdot\bar{p})^2\,(-2(k\cdot\bar{p}) - \bar{p}^2)}{(k^2)^5\ (k+\bar{p})^2}\right) \end{aligned} \tag{5.19}$$

The part in square brackets is polynomial in a and can be integrated easily, using D-dimensional spherical coordinates. The remaining part is UV-convergent; thus the integration domain can now be recast in the form

$$\int_{|k|\leq\mu} = \int_{|k|<\infty} - \int_{\mu\leq|k|<\infty} \tag{5.20}$$

The integral over the whole space can be performed using the methods of Ref. [110], whereas the integral outside the sphere of radius μ is $\mathcal{O}(a^3)$ and may be safely dropped. The same procedure is applied to the remaining term of I_2. Adding the contributions from all the steps described above, we check that the result is independent of μ.

5.3 Renormalization of the fermion propagator and of the bilinears

Perturbative calculations involving the SLiNC action will be used in forthcoming simulations. The fermion propagator with quantum corrections using the SLiNC action with non-zero bare mass, m, and the computation of the one-loop 2-point bare Green's functions of local and extended bilinear operators are the main objects that we are going to deal with in this Chapter.

We compute the one-loop 2-point bare Green's functions (amputated, $1PI$), $S^{1-loop} = \langle \psi(x)\overline{\psi}(y) \rangle$ (fermion self-energy). The clover coefficient $c_{\rm SW}$ and the stout parameter ω have been considered to be free parameters and our results are given as polynomials of $c_{\rm SW}$ and of ω. Moreover, the dependence on the number of colors N_c, the coupling constant g, the gauge fixing parameter α and the lattice spacing a, is shown explicitly.

The one-loop Feynman diagrams that enter the 2-point Green's function calculation, are the same as those illustrated in Fig. 3.1 (but, of course, with different expressions for the bare propagator and vertices).

Here we present the expression for the inverse propagator $(S^{1-loop})^{-1}$ (with zero quark masses):

$$
\begin{aligned}
\big(S^{1-loop}(p)\big)^{-1} \;=\; & \big(S^{tree}(p)\big)^{-1} + \frac{g^2\,C_F}{16\pi^2}\Big\{ \\
& \frac{1}{a}\big[-40.4432 + 4.6627\,c_{\rm SW}^2 + 11.9482\,c_{\rm SW} + \omega(455.514 - 37.3014\,c_{\rm SW}) - 1685.6\omega^2\big] \\
& + i\;\not{p}\big[13.0233 - 4.79201\alpha + \alpha\log\left(a^2p^2\right) - 2.01543\,c_{\rm SW} - 1.2422\,c_{\rm SW}^2 \\
& \quad + \omega(4.6734\,c_{\rm SW}\,i\not{p} - 152.564) + 541.381\omega^2\big] \\
& + a\,p^2\big[10.6964 - 3.8639\alpha + \alpha\log\left(a^2p^2\right) - \frac{3}{2}\log\left(a^2p^2\right) - 4.7529\,c_{\rm SW} \\
& \quad + \frac{3}{2}\,c_{\rm SW}\log\left(a^2p^2\right) - 0.0759\,c_{\rm SW}^2 + \omega\left(8.7722\,c_{\rm SW} - 90.6889\right) + 271.446\omega^2\big] \\
& + a^2\big[-\frac{1}{6}\alpha\,i\not{p}^3\log\left(a^2p^2\right) - \frac{3}{8}\alpha\,i\,p^2\not{p}\log\left(a^2p^2\right) - \frac{1}{4}\,c_{\rm SW}^2\,i\,p^2\not{p}\log\left(a^2p^2\right) \\
& \quad + \omega\big(-\,i\,p^2\not{p}\log\left(a^2p^2\right) - 0.5058\,c_{\rm SW}\,i\,p^2\not{p} - 0.4164\,c_{\rm SW}\,i\not{p}^3 + 12.0983\,i\,p^2\not{p} \\
& \quad + 29.509\,i\not{p}^3\big) - \frac{1}{4}\,c_{\rm SW}\,i\,p^2\not{p}\log\left(a^2p^2\right) + \frac{157}{180}\,i\not{p}^3\log\left(a^2p^2\right) + \frac{73}{360}\,i\,p^2\not{p}\log\left(a^2p^2\right) \\
& \quad - \frac{5\alpha\,i\,p4\not{p}}{48p^2} + 1.51605\alpha\,i\,p^2\not{p} + 0.507001\alpha\,i\not{p}^3 + 0.4978\,c_{\rm SW}^2\,i\,p^2\not{p} \\
& \quad + 0.0786\,c_{\rm SW}^2\,i\not{p}^3 + 0.6534\,c_{\rm SW}\,i\,p^2\not{p} + 0.0514\,c_{\rm SW}\,i\not{p}^3 \\
& \quad + \omega^2\left(-28.0799\,i\,p^2\not{p} - 74.1412\,i\not{p}^3\right) - \frac{7\,i\,p4\not{p}}{240p^2} - 1.1472\,i\,p^2\not{p} - 4.2478\,i\not{p}^3\big]\Big\}, \qquad (5.21)
\end{aligned}
$$

where $S^{tree}(p)$ is the tree-level propagator, and the contributions $\mathcal{O}(a^{-1})$ determine the additive renormalization of mass (critical mass).

A number of Lorentz non-invariant tensors ($p4 = \sum_\mu p_\mu^4$, $\not{p}^3 = \sum_\mu \gamma_\mu p_\mu^3$) appear in $\mathcal{O}(a^2)$ correction terms of S^{1-loop}; they are compatible with hypercubic invariance.

Using our results for the fermion propagator, we can compute the multiplicative renormalization function of the quark field in the RI′ renormalization scheme ($Z_{\rm q}^{\rm RI'}$). In order to find $Z_{\rm q}^{\rm RI'}$, we use a mass-independent renormalization condition:

$$
Z_{\rm q}^{\rm RI'} = \frac{1}{12}{\rm Tr}\left[\frac{-i\sum_\rho \gamma_\rho \sin(p_\rho)}{\sum_\rho \sin^2(p_\rho)}\,(S^{1-loop}(p))^{-1}\right]\Big|_{p_\rho=\mu_\rho}, \qquad (5.22)
$$

where μ is the renormalization scale 4-vector, the trace is taken over spin and color indices and $(S^{1-loop}(p))^{-1}$ is the inverse fermion propagator that we computed up to one-loop and up to $\mathcal{O}(a^2)$. Given the dependence of $\mathcal{O}(a^2)$ terms on the direction of the external momentum, p_ρ, alternative renormalization prescriptions, involving different directions of the renormalization scale $\mu_\rho = p_\rho$, treat lattice artifacts diversely.

Our result for $Z_{\rm q}^{\rm RI'}$ is:

$$\begin{aligned} Z_{\rm q}^{\rm RI'} &= 1+\frac{g^2\,C_F}{16\pi^2}\Big[-13.0233+4.7920\,\alpha+2.0154\;c_{\rm SW}+1.2422\;c_{\rm SW}^2 \\ &+ 152.5641\,\omega-4.6734\;c_{\rm SW}\,\omega-541.3805\,\omega^2-\alpha\;\log(a^2\mu^2) \\ &+ a^2\,\mu^2\Big(1.14716-1.51605\,\alpha-0.653431\;c_{\rm SW}-0.497834\;c_{\rm SW}^2 \\ &- 12.0983\,\omega+0.5059\;c_{\rm SW}\,\omega+28.0799\,\omega^2 \\ &+ \log(a^2\mu^2)\Big(-\frac{73}{360}+\frac{3}{8}\,\alpha+\frac{1}{4}\;c_{\rm SW}+\frac{1}{4}\;c_{\rm SW}^2+\omega\Big)\Big) \\ &+ a^2\frac{\mu 4}{\mu^2}\Big(2.1065+0.3958\,\alpha+0.2845\;c_{\rm SW}+0.1284\;c_{\rm SW}^2 \\ &- 4.0816\,\omega-0.3625\;c_{\rm SW}\,\omega-16.0889\,\omega^2-\frac{157}{180}\log(a^2\mu^2)\Big)\Big] \end{aligned} \tag{5.23}$$

We now turn to the one-loop $\mathcal{O}(a^2)$ corrections to Green's functions Λ_Γ^{1-loop} of local fermion operators that have the form $\bar\psi\Gamma\psi$. Γ corresponds to the following set of products of the Dirac matrices:

$$\Gamma = \mathbb{1},\ \gamma_5,\ \gamma_\mu,\ \gamma_5\gamma_\mu,\ \sigma_{\mu\nu}, \qquad \sigma_{\mu\nu}=\frac{1}{2}[\gamma_\mu,\gamma_\nu] \tag{5.24}$$

for the scalar (O^S), pseudoscalar (O^P), vector (O^V), axial (O^A) and tensor (O^T) operator, respectively. We restrict ourselves to forward matrix elements. We also considered the tensor operator $O^{T'}$, corresponding to $\Gamma=\gamma_5\sigma_{\mu\nu}$ and checked that its Green's function coincides with that of O^T; this is a nontrivial check for our calculational procedure. These operators are very important because from their matrix elements we can extract decay constants and hadronic masses.

The only one-particle irreducible Feynman diagram that enters the calculation of the above operators is shown in Fig. 5.1. Our results for the one-loop corrections to the

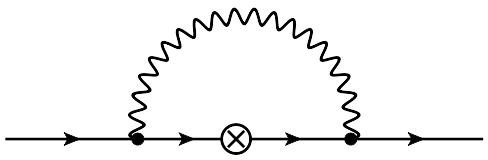

Figure 5.1: One-loop diagram contributing to the local bilinear operators. A wavy (solid) line represents gluons (fermions). A cross denotes the Dirac matrices $\mathbb{1}$ (scalar), γ_5 (pseudoscalar), γ_μ (vector), $\gamma_5\gamma_\mu$ (axial), $\sigma_{\mu\nu}$ (tensor T) and $\gamma_5\sigma_{\mu\nu}$ (tensor T').

amputated 2-point Green's function of each operator $\bar{\psi}\Gamma\psi$, at momentum p

$$\Lambda_\Gamma^{1-loop} = \langle\psi\ \left(\bar{\psi}\Gamma\psi\right)\ \bar{\psi}\rangle_{(p)}^{amp} \tag{5.25}$$

are a polynomial of $c_{\rm SW}$, a and ω, in a general covariant gauge. One might attempt to use the $\mathcal{O}(a)$ corrections computed above in order to devise an improved operator, with suppressed finite-a artifacts; it should be noted, however, that improvement by means of local operators, as permitted by Quantum Field Theory, is not sufficient to warrant a complete cancellation of $\mathcal{O}(a^2)$ terms in Green's functions, since the latter contain also terms with non-polynomial momentum dependence, such as $\sum_\mu p_\mu^4/p^2$. Thus, at best, one can achieve full $\mathcal{O}(a^2)$ improvement only on-shell, or approximate improvement near a given reference momentum scale. Such non-polynomial terms are not present at $\mathcal{O}(a^1)$. Our results for Λ_Γ^{1-loop} are:

$$\begin{aligned}
\Lambda_S^{1-loop}(p) &= \mathbb{1} + \frac{g^2\,C_F}{16\pi^2}\Big[0.5835 + 5.79201\alpha + 8.8507\,c_{\rm SW} - 0.1252\,c_{\rm SW}^2 \\
&- (3+\alpha)\log\left(a^2p^2\right) \\
&+ i\,a\,\not{p}\big(0.3394 - 3.93576\alpha - 3.76354\,c_{\rm SW} - 1.15006\,c_{\rm SW}^2 \\
&+ \frac{3}{2}(1 + c_{\rm SW} + \alpha)\log\left(a^2p^2\right)\big) \\
&+ \omega\big(12.3004 - 22.8948\,c_{\rm SW} - a\,14.6765\,i\,\not{p} + a\,8.44675\,c_{\rm SW}\,i\,\not{p} \\
&- a^2\,11.4484p^2 + a^2\,5.29756\,c_{\rm SW}p^2\big) \\
&+ \omega^2\left(-60.0198 + a\,52.0918\,i\,\not{p} + a^2\,27.3685p^2\right) \\
&+ a^2\left((2.35473 - 2.27359\alpha - 3.85278\,c_{\rm SW} + 0.196462\,c_{\rm SW}^2)p^2\right. \\
&- \left(\frac{1}{4} - \frac{3}{4}\alpha - \frac{3}{2}\,c_{\rm SW}\right)p^2\log\left(a^2p^2\right) \\
&+ \left.(13\alpha + 11)\frac{p4}{72p^2} + \frac{\not{p}^3\not{p} + \not{p}\not{p}^3}{p^2}\left(\frac{25}{144} - \frac{11}{72}\alpha\right)\right)\Big]
\end{aligned} \tag{5.26}$$

$$\begin{aligned}
\Lambda_P^{1-loop}(p) &= \gamma_5 + \frac{g^2\,C_F}{16\pi^2}\,\gamma_5\Big[8.7101 + 5.79201\alpha + 2.98701\,c_{\rm SW}^2 - (3+\alpha)\log\left(a^2p^2\right) \\
&+ \omega\big(48.6342 - a^2\,6.5059p^2\big) + \omega^2\big(108.487 + a^2\,29.2531p^2\big) \\
&+ a^2\left((0.7064 - 0.8381\alpha - 0.2756\,c_{\rm SW}^2)p^2 - \left(\frac{1}{4} - \frac{3}{4}\alpha\right)p^2\log\left(a^2p^2\right)\right. \\
&+ \left.(13\alpha + 11)\frac{p4}{72p^2} + \frac{\not{p}^3\not{p} + \not{p}\not{p}^3}{p^2}\left(\frac{25}{144} - \frac{11}{72}\right)\right)\Big]
\end{aligned} \tag{5.27}$$

$$
\begin{aligned}
\Lambda_V^{1-loop}(p) &= \gamma_\mu + \frac{g^2\,C_F}{16\pi^2}\Bigg\{\gamma_\mu\Big[3.5796 + 4.79201\alpha - 2.2127\,c_{\rm SW} + 0.7781\,c_{\rm SW}^2 \\
&- \alpha\log\left(a^2p^2\right) + \omega\big(-15.6991 + 5.72369\,c_{\rm SW} \\
&- a^2\left(8.1378 - 0.9433\,c_{\rm SW} - \log\left(a^2p^2\right)\right)p^2\big) \\
&+ \omega^2\big(43.4652 + a^2\,24.501p^2\big) - 2\alpha\frac{\not{p}\,p_\mu}{p^2} \\
&+ a^2\left((0.0214 - 0.8110\alpha + 0.8342\,c_{\rm SW} - 0.2874\,c_{\rm SW}^2)p^2\right. \\
&+ \left.\left(\frac{4}{45} + \frac{1}{8}\alpha - \frac{5}{12}\,c_{\rm SW} + \frac{1}{4}\,c_{\rm SW}^2\right)p^2\log\left(a^2p^2\right) + (55\alpha + 17)\frac{p4}{720p^2}\right) \\
&+ a^2p_\mu^2\big(1.6763 + 0.1249\alpha + 0.2260\,c_{\rm SW} + 0.02822\,c_{\rm SW}^2 \\
&- \omega\big(3.0079 + 1.6200\,c_{\rm SW} + 7.4373\omega\big) - \frac{8}{15}\log\left(a^2p^2\right)\big)\Big] \\
&+ i\,a\,p_\mu\Big[2.0974 - 0.9357\alpha - 1.5187\,c_{\rm SW} - 0.3851\,c_{\rm SW}^2 \\
&+ (\alpha - 3 + 3\,c_{\rm SW})\log\left(a^2p^2\right) \\
&- \omega\big(23.2135 - 6.1854\,c_{\rm SW} - 38.4633\omega\big) \\
&- i\,a\,\not{p}\big[1.0377 + 0.2436\alpha + 0.2896\,c_{\rm SW} - 0.3028\,c_{\rm SW}^2 \\
&- \omega\big(8.7521 + 0.09571\,c_{\rm SW} + 15.8859\omega\big) \\
&+ \left(-\frac{7}{120} - \frac{5}{24}\alpha\right)\frac{p4}{(p^2)^2} + \left(-\frac{52}{45} + \frac{1}{4}\alpha + \frac{1}{6}\,c_{\rm SW} + \frac{1}{2}\,c_{\rm SW}^2\right)\log\left(a^2p^2\right) \\
&+ 2\omega\left(a^2p^2\right)\big]\Big] + a^2\not{p}\frac{p_\mu^3}{p^2}\Big(-\frac{1}{20} + \frac{1}{12}\alpha\Big) - a^2\not{p}^3\frac{p_\mu}{p^2}\Big(\frac{157}{90} + \frac{1}{3}\alpha\Big) \\
&+ a^2\,\gamma_\mu\frac{\not{p}^3\not{p} + \not{p}\not{p}^3}{p^2}\left(\frac{1}{360} + \frac{1}{72}\alpha\right)\Bigg\}
\end{aligned}
\tag{5.28}
$$

$$
\begin{aligned}
\Lambda_A^{1-loop}(p) &= \gamma_5\gamma_\mu + \frac{g^2\,C_F}{16\pi^2}\gamma_5 \Bigg\{ \gamma_\mu \Big[-0.483698 + 4.79201\alpha + 2.2127\,c_{\rm SW} - 0.7781\,c_{\rm SW}^2 \\
&- \alpha \log\left(a^2p^2\right) + \omega\big(14.7682 - 5.72369\,c_{\rm SW} \\
&- a^2\left(14.4089 - 2.6709\,c_{\rm SW} - \log\left(a^2p^2\right)\right)p^2\big) \\
&+ \omega^2\big(40.7883 + a^2\,25.345p^2\big) - 2\alpha\frac{\not{p}\,p_\mu}{p^2} \\
&+ a^2\left((1.3008 - 1.7465\alpha - 1.4876\,c_{\rm SW} + 0.3141\,c_{\rm SW}^2)p^2\right. \\
&+ \left.\left(-\frac{37}{90} + \frac{5}{8}\alpha + \frac{7}{12}\,c_{\rm SW} - \frac{1}{4}\,c_{\rm SW}^2\right)p^2\log\left(a^2p^2\right) + (55\alpha + 17)\frac{p4}{720p^2}\right) \\
&+ a^2p_\mu^2\big(0.29617 + 0.1249\alpha + 1.7629\,c_{\rm SW} - 0.1113\,c_{\rm SW}^2 \\
&- \omega\big(1.0288 + 5.1342\,c_{\rm SW} - 10.4477\omega\big) - \frac{8}{15}\log\left(a^2p^2\right)\big)\Big] \\
&+ i\,a\,p_\mu\Big[-0.9254 + 2.9357\alpha - 1.5461\,c_{\rm SW} + 0.1283\,c_{\rm SW}^2 + \alpha\log\left(a^2p^2\right) \\
&+ \omega\big(17.5221 - 3.5991\,c_{\rm SW} - 47.5493\omega\big) \\
&- i\,a\,\not{p}\big[0.596635 + 1.1146\alpha + 0.3347\,c_{\rm SW} + 0.2787\,c_{\rm SW}^2 \\
&+ \omega\big(4.4682 - 0.25184\,c_{\rm SW} - 9.1428\omega\big) \\
&- \left(\frac{7}{120} + \frac{5}{24}\alpha\right)\frac{p4}{(p^2)^2} + \left(\frac{38}{45} - \frac{3}{4}\alpha - \frac{5}{6}\,c_{\rm SW} - \frac{1}{2}\,c_{\rm SW}^2\right)\log\left(a^2p^2\right) \\
&+ 2\omega\left(a^2p^2\right)\big]\Big] + a^2\not{p}\frac{p_\mu^3}{p^2}\Big(-\frac{1}{20} + \frac{1}{12}\alpha\Big) - a^2\not{p}^3\frac{p_\mu}{p^2}\Big(\frac{157}{90} + \frac{1}{3}\alpha\Big) \\
&+ a^2\,\gamma_\mu\frac{\not{p}^3\not{p} + \not{p}\not{p}^3}{p^2}\left(\frac{1}{360} + \frac{1}{72}\alpha\right)\Bigg\}
\end{aligned}
\tag{5.29}
$$

Note that the expressions for $\Lambda_V^{1-loop}(p)$ and $\Lambda_A^{1-loop}(p)$ are more complicated, compared to the scalar $\Lambda_S^{1-loop}(p)$ and pseudoscalar $\Lambda_P^{1-loop}(p)$ amputated Green's functions, in the sense that momentum dependence assumes a wider variety of functional forms.

The tensor Green's function $\Lambda_T^{1-loop}(p)$ (and $\Lambda_{T'}^{1-loop}(p)$) is the most complicated of all

the Green's functions that we studied.

$$
\begin{aligned}
\Lambda_T^{1-loop}(p) &= \sigma_{\mu\nu} + \frac{g^2\,C_F}{16\pi^2}\Bigg\{(\gamma_\mu\gamma_\nu - \gamma_\nu\gamma_\mu)\Big[0.2575 + 1.8961\alpha - 0.73755\,c_{\rm SW} - 0.2384\,c_{\rm SW}^2 \\
&+ \frac{1}{2}(1-\alpha)\log\left(a^2p^2\right) + \omega\big(2.7175 + 1.9079\,c_{\rm SW} - a^2\,(8.6127 + 0.0412\,c_{\rm SW})p^2\big) \\
&+ \omega^2\big(-3.1465 + a^2\,13.6028p^2\big) + a^2\big(0.5287 - 0.6097\alpha + 0.1233\,c_{\rm SW} - 0.0306\,c_{\rm SW}^2 \\
&+ \left(-\frac{31}{72} + \frac{1}{4}\alpha + \omega\right)\log\left(a^2p^2\right)\,)p^2 - \,a^2\,\frac{\not{p}^3\not{p} + \not{p}\not{p}^3}{p^2}\left(\frac{121}{1440} - \frac{13}{144}\alpha\right) \\
&- a^2\left(\frac{7}{360} + \frac{1}{72}\alpha\right)\frac{p4}{p^2}\Big] \\
&+ a\Big[2i\,(\gamma_\nu p_\mu - \gamma_\mu p_\nu)\big[0.7557 - 0.9678\alpha - 0.3988\,c_{\rm SW} + 0.1917\,c_{\rm SW}^2 \\
&+ \omega\big(-10.1839 + 1.4227\,c_{\rm SW} + 21.5031\omega\big) - \left(\frac{3}{4} - \frac{1}{2}\alpha - \frac{1}{4}\,c_{\rm SW}\right)\log\left(a^2p^2\right) \\
&+ a\frac{1}{2}\,(-i\,\gamma_\nu p_\mu + i\,\gamma_\mu p_\nu)\big(-0.06725 + 0.625\alpha + 0.3842\,c_{\rm SW} - 0.06573\,c_{\rm SW}^2 \\
&+ \omega\big(0.4947 - 0.8785\,c_{\rm SW} + 4.4712\omega\big)\big)\Big] \\
&+ a\,(i\,\gamma_\mu\gamma_\nu - i\,\gamma_\nu\gamma_\mu)\not{p}\Big[0.7557 - 0.9678\alpha - 0.3988\,c_{\rm SW} + 0.1916\,c_{\rm SW}^2 \\
&+ \omega\big(-10.1839 + 1.4227\,c_{\rm SW} + 21.5031\omega\big) + \left(-\frac{3}{4} + \frac{1}{2}\alpha + \frac{1}{4}\,c_{\rm SW}\right)\log\left(a^2p^2\right)\Big] \\
&- a^2\,(\gamma_\mu p_\nu - \gamma_\nu p_\mu)\not{p}\Big[0.3350 + -0.5604\alpha - 0.0225\,c_{\rm SW} - 0.0351\,c_{\rm SW}^2 \\
&- \omega\big(6.6101 - 0.1737\,c_{\rm SW} - 12.5144\omega\big) - \left(1 - \frac{1}{2}\alpha - \frac{1}{2}\,c_{\rm SW}\right)\log\left(a^2p^2\right)\Big] \\
&+ a^2\,\frac{101}{36}\left(\frac{p_\mu^3\,p_\nu}{p^2} - \frac{p_\nu^3\,p_\mu}{p^2}\right) - \,a^2\,\left(\gamma_\mu\frac{p_\mu^2\,p_\nu}{p^2} - \gamma_\nu\frac{p_\mu\,p_\nu^2}{p^2}\right)\not{p}\Big(\frac{10}{9} + \frac{1}{4}\alpha\Big) \\
&- a^2\,\frac{101}{72}\left(\gamma_\mu\frac{p_\nu\not{p}^3}{p^2} - \gamma_\nu\frac{p_\mu\not{p}^3}{p^2}\right) + \,a^2\,\left(\gamma_\nu\frac{p_\mu^3\not{p}}{p^2} - \gamma_\mu\frac{p_\nu^3\not{p}}{p^2}\right)\left(\frac{7}{24} + \frac{1}{4}\alpha\right)\Bigg\}
\end{aligned}
\tag{5.30}
$$

As a check of our calculation we also compute $\Lambda_{T'}^{1-loop}$ given below in Eq. (5.31). Indeed this expression becomes identical to Eq. (5.30), once it is expressed in terms of the coordinates p_ρ, p_σ which are complementary to p_μ, p_ν.

$$
\begin{aligned}
\Lambda_{T'}^{1-loop}(p) &= \gamma_5\sigma_{\mu\nu} + \frac{g^2\,C_F}{16\pi^2}\,\gamma_5\,\Bigg\{(\gamma_\mu\gamma_\nu-\gamma_\nu\gamma_\mu)\Big[0.2575 + 1.8961\alpha - 0.73755\,c_{\rm SW} - 0.2384\,c_{\rm SW}^2 \\
&+ \frac{1}{2}(1-\alpha)\log\left(a^2p^2\right) + \omega\big(2.7175 + 1.9079\,c_{\rm SW} - a^2\,(4.8128 + 0.9241\,c_{\rm SW})p^2\big) \\
&+ \omega^2\big(-3.1465 + a^2\,11.8168p^2\big) + a^2\big(0.07340 - 0.3919\alpha + 0.5188\,c_{\rm SW} - 0.01750\,c_{\rm SW}^2 \\
&+ \left(\frac{5}{72} - \frac{1}{4}\,c_{\rm SW} + \omega\right)\log\left(a^2p^2\right)\big)p^2 - \,a^2\,\frac{\not{p}^3\not{p} + \not{p}\not{p}^3}{p^2}\left(\frac{121}{1440} - \frac{13}{144}\alpha\right) \\
&- a^2\left(\frac{7}{360} + \frac{1}{72}\alpha\right)\frac{p4}{p^2}\Big] \\
&+ a\Big[2i\,(\gamma_\nu p_\mu - \gamma_\mu p_\nu)\big[-0.7557 + 0.9678\alpha + 0.3988\,c_{\rm SW} - 0.1917\,c_{\rm SW}^2 \\
&+ \omega\big(10.1839 - 1.4227\,c_{\rm SW} - 21.5031\omega\big) + \left(\frac{3}{4} - \frac{1}{2}\alpha - \frac{1}{4}\,c_{\rm SW}\right)\log\left(a^2p^2\right) \\
&+ a\frac{1}{2}\,(-\,i\,\gamma_\nu p_\mu + i\,\gamma_\mu p_\nu)\big(0.6228 + 0.625\alpha - 0.3842\,c_{\rm SW} + 0.06573\,c_{\rm SW}^2 \\
&+ \omega\big(-0.4947 + 0.8785\,c_{\rm SW} - 4.4712\omega\big)\big)\Big] \\
&- a^2\,(\gamma_\mu p_\nu - \gamma_\nu p_\mu)\not{p}\Big[-0.7761 + 0.3104\alpha + 0.0225\,c_{\rm SW} + 0.0351\,c_{\rm SW}^2 \\
&+ \omega\big(6.6101 - 0.1737\,c_{\rm SW} - 12.5144\omega\big) + \left(1 - \frac{1}{2}\alpha - \frac{1}{2}\,c_{\rm SW}\right)\log\left(a^2p^2\right)\Big] \\
&+ a^2\,\frac{101}{36}\left(\frac{p_\mu^3\,p_\nu}{p^2} - \frac{p_\nu^3\,p_\mu}{p^2}\right) - \,a^2\left(\gamma_\mu\frac{p_\mu^2\,p_\nu}{p^2} - \gamma_\nu\frac{p_\mu\,p_\nu^2}{p^2}\right)\not{p}\left(\frac{10}{9} + \frac{1}{4}\alpha\right) \\
&- a^2\,\frac{101}{72}\left(\gamma_\mu\frac{p_\nu\not{p}^3}{p^2} - \gamma_\nu\frac{p_\mu\not{p}^3}{p^2}\right) + \,a^2\left(\gamma_\nu\frac{p_\mu^3\not{p}}{p^2} - \gamma_\mu\frac{p_\nu^3\not{p}}{p^2}\right)\left(\frac{7}{24} + \frac{1}{4}\alpha\right)\Bigg\}
\end{aligned}
\tag{5.31}
$$

Starting from $\Lambda_\Gamma^{1-loop}(p)$, it is straightforward to write down the renormalization functions Z_Γ (for the operators $\mathcal{O}^\Gamma$) in the RI′ renormalization scheme, which uses the tree-level 2-pt Green's functions of the corresponding operators $\Lambda_\Gamma^{\rm tree}(p)$. $Z_\Gamma^{\rm RI'}$, as obtained from $\Lambda_\Gamma(p)$, differ from the corresponding expressions evaluated at $\mathcal{O}(a^0)$, by lattice artifacts, which are functions of $(a\mu)$, and vanish as $a \to 0$.

In order to determine the renormalization of the local bilinear operator $Z_\Gamma^{\rm RI'}$ we use the renormalization condition:

$$
\left(Z_\Gamma^{\rm RI'}\right)^{-1} Z_q^{\rm RI'} = \frac{{\rm Tr}\left[\Lambda_\Gamma^{1-loop}(p)\,\Lambda_\Gamma^{\rm tree}(p)^\dagger\right]}{{\rm Tr}\left[\Lambda_\Gamma^{\rm tree}(p)\,\Lambda_\Gamma^{\rm tree}(p)^\dagger\right]}\Big|_{p_\rho=\mu_\rho}\,, \tag{5.32}
$$

where the trace is taken again over spin and color indices, and the conditions are imposed on the massless theory. In Chapter 3, we discussed alternative renormalization schemes for $Z_{\rm V}$ and $Z_{\rm A}$, stemming from the fact that the corresponding one-loop Green's functions were not mere multiples of the bare ones; the latter property will hold for all Green's functions once $\mathcal{O}(a^2)$ corrections are included. Thus Eq. (5.32) corresponds to the alternative scheme discussed in Chapter 3.

Our results for $Z_\Gamma^{\rm RI'}$ are (the momentum p must be set equal to the renormalization scale 4-vector μ: $p_\rho = \mu_\rho$):

$$\begin{aligned}
Z_{\rm S}^{\rm RI'} &= 1 + \frac{g^2\,C_F}{16\pi^2}\Big[-13.6067 - \alpha - 6.8353\ c_{\rm SW} + 1.3674\ c_{\rm SW}^2 \\
&+ 140.2641\,\omega + 18.2213\ c_{\rm SW}\,\omega - 481.3605\,\omega^2 + 3\,\log(a^2p^2) \\
&+ a^2\,p^2\,\Big(- 1.2076 + 0.7575\,\alpha + 3.1993\ c_{\rm SW} - 0.6943\ c_{\rm SW}^2 \\
&- 0.6499\,\omega - 4.7917\ c_{\rm SW}\,\omega + 0.7114\,\omega^2 \\
&+ \log(a^2p^2)\,\Big(\frac{17}{360} + \frac{3}{8}\,\alpha - \frac{5}{4}\ c_{\rm SW} + \frac{1}{4}\ c_{\rm SW}^2 + \omega\Big)\Big) \\
&+ a^2\frac{p4}{p^2}\Big(1.6065 + 0.5208\,\alpha + 0.2845\ c_{\rm SW} + 0.1284\ c_{\rm SW}^2 \\
&- 4.0816\,\omega - 0.3625\ c_{\rm SW}\,\omega - 16.0889\,\omega^2 - \frac{157}{180}\log(a^2p^2)\Big)\Big] \qquad (5.33)
\end{aligned}$$

$$\begin{aligned}
Z_{\rm P}^{\rm RI'} &= 1 + \frac{g^2\,C_F}{16\pi^2}\Big[-21.7334 - \alpha + 2.0154\ c_{\rm SW} - 1.7448\ c_{\rm SW}^2 \\
&+ 201.1975\,\omega - 4.6734\ c_{\rm SW}\,\omega - 649.8675\,\omega^2 + 3\,\log(a^2p^2) \\
&+ a^2\,p^2\,\Big(0.4408 - 0.6779\,\alpha - 0.6534\ c_{\rm SW} - 0.2223\ c_{\rm SW}^2 \\
&- 5.5924\,\omega + 0.5059\ c_{\rm SW}\,\omega - 1.1732\,\omega^2 \\
&+ \log(a^2p^2)\,\Big(\frac{17}{360} + \frac{1}{8}\,\alpha + \frac{1}{4}\ c_{\rm SW} + \frac{1}{4}\ c_{\rm SW}^2 + \omega\Big)\Big) \\
&+ a^2\frac{p4}{p^2}\Big(1.6065 + 0.5208\,\alpha + 0.2845\ c_{\rm SW} + 0.1284\ c_{\rm SW}^2 \\
&- 4.0816\,\omega - 0.3625\ c_{\rm SW}\,\omega - 16.0889\,\omega^2 - \frac{157}{180}\log(a^2p^2)\Big)\Big] \qquad (5.34)
\end{aligned}$$

$$
\begin{aligned}
Z_{\mathrm{V}}^{\mathrm{RI}'} &= 1 + \frac{g^2\, C_F}{16\pi^2}\Big[-16.6029 + 4.2281\ c_{\mathrm{SW}} + 0.4641\ c_{\mathrm{SW}}^2 \\
&+ 168.2635\,\omega - 10.3971\ c_{\mathrm{SW}}\,\omega - 584.8465\,\omega^2 \\
&+ a^2\, p^2 \Big(1.1257 - 0.7050\,\alpha - 1.4877\ c_{\mathrm{SW}} - 0.2105\ c_{\mathrm{SW}}^2 \\
&- 3.9604\,\omega + 1.4492\ c_{\mathrm{SW}}\,\omega + 3.5785\,\omega^2 \\
&+ \log(a^2p^2)\left(\frac{-7}{24} + \frac{1}{4}\,\alpha + \frac{2}{3}\ c_{\mathrm{SW}}\right)\Big) \\
&+ a^2\frac{p4}{p^2}\Big(2.0773 + 0.2917\,\alpha + 0.2845\ c_{\mathrm{SW}} + 0.1284\ c_{\mathrm{SW}}^2 \\
&- 4.0816\,\omega - 0.3625\ c_{\mathrm{SW}}\,\omega - 16.0889\,\omega^2 - \frac{157}{180}\log(a^2p^2)\Big) \\
&+ a^2 p_\mu^2\Big(-2.7140 - 0.3686\,\alpha - 0.5157\ c_{\mathrm{SW}} + 0.2746\ c_{\mathrm{SW}}^2 \\
&+ 11.76\,\omega + 1.5243\ c_{\mathrm{SW}}\,\omega - 8.4485\,\omega^2 \\
&+ \log(a^2p^2)\left(\frac{76}{45} - \frac{1}{4}\,\alpha + \frac{1}{6}\ c_{\mathrm{SW}} - \frac{1}{2}\ c_{\mathrm{SW}}^2 + 2\,\omega\right)\Big) \\
&+ \frac{p_\mu^2}{p^2}(2\,\alpha) + a^2\frac{p4p_\mu^2}{(p^2)^2}\Big(\frac{7}{120} + \frac{5}{24}\,\alpha\Big) \\
&+ a^2\frac{p_\mu^4}{p^2}\Big(\frac{323}{180} - \frac{5}{12}\,\alpha\Big)\Big]
\end{aligned}
\tag{5.35}
$$

$$
\begin{aligned}
Z_{\mathrm{A}}^{\mathrm{RI}'} &= 1 + \frac{g^2\, C_F}{16\pi^2}\Big[-12.5396 - 0.1972\; c_{\mathrm{SW}} + 2.0203\; c_{\mathrm{SW}}^2 \\
&+ 137.796\,\omega + 1.0502\; c_{\mathrm{SW}}\,\omega - 500.593\,\omega^2 \\
&+ a^2\, p^2 \Big(-0.1537 + 0.2305\,\alpha + 0.8342\; c_{\mathrm{SW}} - 0.8120\; c_{\mathrm{SW}}^2 \\
&+ 2.3106\,\omega - 2.1650\; c_{\mathrm{SW}}\,\omega + 2.7349\,\omega^2 \\
&+ \log(a^2p^2)\,\Big(\frac{5}{24} - \frac{1}{4}\,\alpha + \frac{1}{3}\; c_{\mathrm{SW}} + \frac{1}{2}\; c_{\mathrm{SW}}^2\Big)\Big) \\
&+ a^2\frac{p4}{p^2}\Big(2.0773 + 0.2917\,\alpha + 0.2845\; c_{\mathrm{SW}} + 0.1284\; c_{\mathrm{SW}}^2 \\
&- 4.0816\,\omega - 0.3625\; c_{\mathrm{SW}}\,\omega - 16.0889\,\omega^2 - \frac{157}{180}\log(a^2p^2)\Big) \\
&+ a^2p_\mu^2\Big(-0.8928 - 1.2396\,\alpha - 2.0977\; c_{\mathrm{SW}} - 0.1673\; c_{\mathrm{SW}}^2 \\
&- 3.4394\,\omega + 5.3861\; c_{\mathrm{SW}}\,\omega - 1.3048\,\omega^2 \\
&+ \log(a^2p^2)\,\Big(\frac{14}{45} + \frac{3}{4}\,\alpha + \frac{5}{6}\; c_{\mathrm{SW}} + \frac{1}{2}\; c_{\mathrm{SW}}^2 - 2\,\omega\Big)\Big) \\
&+ \frac{p_\mu^2}{p^2}(2\,\alpha) + a^2\frac{p4\; p_\mu^2}{(p^2)^2}\Big(\frac{7}{120} + \frac{5}{24}\,\alpha\Big) \\
&+ a^2\frac{p_\mu^4}{p^2}\Big(\frac{323}{180} - \frac{5}{12}\,\alpha\Big)\Big]
\end{aligned}
\tag{5.36}
$$

$$
\begin{aligned}
Z_{\mathrm{T}}^{\mathrm{RI}'} &= 1 + \frac{g^2\, C_F}{16\pi^2}\Big[-13.5383 + \alpha + 3.4905\ c_{\mathrm{SW}} + 1.7192\ c_{\mathrm{SW}}^2 \\
&+ 147.129\,\omega - 8.4892\ c_{\mathrm{SW}}\,\omega - 535.088\,\omega^2 - \log(a^2p^2) \\
&+ a^2\,p^2\Big(0.0897 - 0.2966\,\alpha - 0.9001\ c_{\mathrm{SW}} - 0.5592\ c_{\mathrm{SW}}^2 \\
&+ 5.1271\,\omega + 0.4234\ c_{\mathrm{SW}}\,\omega + 0.8744\,\omega^2 \\
&+ \log(a^2p^2)\Big(\frac{79}{120} - \frac{1}{8}\,\alpha + \frac{1}{4}\ c_{\mathrm{SW}} + \frac{1}{4}\ c_{\mathrm{SW}}^2 - \omega\Big)\Big) \\
&+ a^2\frac{p4}{p^2}\Big(2.4815 + 0.06250\,\alpha + 0.2845\ c_{\mathrm{SW}} + 0.1284\ c_{\mathrm{SW}}^2 \\
&- 4.0816\,\omega - 0.3625\ c_{\mathrm{SW}}\,\omega - 16.0889\,\omega^2 - \frac{157}{180}\log(a^2p^2)\Big) \\
&+ a^2(p_\mu^2 + p_\nu^2)\Big(- 0.2005 - 0.6856\,\alpha - 0.7910\ c_{\mathrm{SW}} + 0.0964\ c_{\mathrm{SW}}^2 \\
&- 7.5997\,\omega + 1.9309\ c_{\mathrm{SW}}\,\omega + 3.5718\,\omega^2 \\
&+ \log(a^2p^2)\Big(- 1 + \frac{1}{2}\,\alpha + \frac{1}{2}\ c_{\mathrm{SW}}\Big)\Big) \\
&+ a^2\frac{p_\mu^4 + p_\nu^4}{p^2}\Big(\frac{10}{9} + \frac{1}{4}\,\alpha\Big) \\
&+ a^2\frac{p_\mu^2\,p_\nu^2}{p^2}\Big(\frac{20}{9} + \frac{1}{2}\,\alpha\Big)\Big]
\end{aligned}
\tag{5.37}
$$

These results are in complete agreement with clover fermions [14] in the absence of stout smearing.

Lastly, we compute the matrix elements of the extended bilinear operators of the form $\overline{\psi}(x)\Gamma D_\nu\psi(x)$. Here Γ corresponds to the Dirac matrices

$$\Gamma = \gamma_\mu,\ \gamma_5\gamma_\mu,\ \sigma_{\mu\nu} \tag{5.38}$$

and $D \equiv \overleftrightarrow{D} = (\overrightarrow{D} - \overleftarrow{D})/2$. More specifically, the extended bilinear operators are defined

as:

$$\mathcal{O}_{\rm DV}^{\{\mu\nu\}} = \frac{1}{2}\Big[\overline{\psi}\,\gamma_\mu \overleftrightarrow{D}_\nu \psi + \overline{\psi}\,\gamma_\nu \overleftrightarrow{D}_\mu \psi\Big] - \frac{1}{4}\delta_{\mu\nu}\sum_\tau \overline{\psi}\,\gamma_\tau \overleftrightarrow{D}_\tau \psi \tag{5.39}$$

$$\mathcal{O}_{\rm DA}^{\{\mu\nu\}} = \frac{1}{2}\Big[\overline{\psi}\,\gamma_5\gamma_\mu \overleftrightarrow{D}_\nu \psi + \overline{\psi}\,\gamma_5\gamma_\nu \overleftrightarrow{D}_\mu \psi\Big] - \frac{1}{4}\delta_{\mu\nu}\sum_\tau \overline{\psi}\,\gamma_5\gamma_\tau \overleftrightarrow{D}_\tau \psi \tag{5.40}$$

$$\mathcal{O}_{\rm DT}^{\mu\{\nu\rho\}} = \frac{1}{2}\Big[\overline{\psi}\,\gamma_5\sigma_{\mu\nu} \overleftrightarrow{D}_\rho \psi + \overline{\psi}\,\gamma_5\sigma_{\mu\rho} \overleftrightarrow{D}_\nu \psi\Big] - \frac{1}{4}\delta_{\nu\rho}\sum_\tau \overline{\psi}\,\gamma_5\sigma_{\mu\tau} \overleftrightarrow{D}_\tau \psi \tag{5.41}$$

The above operators, being symmetrized and traceless, have no mixing with lower dimension operators. In the flavor nonsinglet case, mixing with operators of the same dimension is also absent. However, in the flavor singlet case, $\mathcal{O}_{\rm DV}^{\{\mu\nu\}}$ will mix with the dimension-4 gluon operator:

$$\mathrm{Tr}\,(F_{\mu\rho}\,F_{\rho\nu}) - \frac{1}{4}\delta_{\mu\nu}\mathrm{Tr}\,(F_{\sigma\rho}\,F_{\rho\sigma}) \tag{5.42}$$

In our computation, μ, ν, ρ, τ are generic Lorentz indices. We denote the corresponding Z-factors by $Z_{\rm DV}$, $Z_{\rm DA}$, $Z_{\rm DT}$. In a massless renormalization scheme the renormalization constants are defined in the chiral limit, where isospin symmetry is exact. The one derivative operators fall into different irreducible representations of the hypercubic group, depending on the choice of indices. Hence, we distinguish between

$$\mathcal{O}_{\rm DV1} = \mathcal{O}_{\rm DV} \text{ with } \mu = \nu \tag{5.43}$$

$$\mathcal{O}_{\rm DV2} = \mathcal{O}_{\rm DV} \text{ with } \mu \neq \nu \tag{5.44}$$

$$\mathcal{O}_{\rm DA1} = \mathcal{O}_{\rm DA} \text{ with } \mu = \nu \tag{5.45}$$

$$\mathcal{O}_{\rm DA2} = \mathcal{O}_{\rm DA} \text{ with } \mu \neq \nu \tag{5.46}$$

$$\mathcal{O}_{\rm DT1} = \mathcal{O}_{\rm DT} \text{ with } \mu \neq \nu = \rho\,(\text{also}: \mu = \nu \neq \rho\,, \mu = \rho \neq \nu\,, \mu = \nu = \rho) \tag{5.47}$$

$$\mathcal{O}_{\rm DT2} = \mathcal{O}_{\rm DT} \text{ with } \mu \neq \nu \neq \rho \neq \mu \tag{5.48}$$

Thus, $Z_{\rm DV1}$ will be different from $Z_{\rm DV2}$, but renormalized matrix elements of the two corresponding operators will be components of the same tensor in the continuum limit.

The expressions for the matrix elements are functions of a general gauge parameter, coupling constant, external momentum, masses, stout parameter ω and clover parameter $c_{\rm SW}$. The Feynman diagrams involved in the computation of the Z-factors are the same as those illustrated in Fig. 3.2 (where now crosses denote the insertion of an extented

operator). The presence of a covariant derivative in the definition of these operators implies that the corresponding vertices may also contain gluons. This explains the appearance of more diagrams as compared to Fig. 5.1. The Z-factors for the extended operators are determined by setting the quark masses to zero and using Eq. (5.32), which is most amenable to non-perturbative treatment.

The tree-level expressions of the operators, including the $\mathcal{O}(a^2)$ terms, are:

$$\Lambda^{\text{tree}}_{\text{DV1}}(p) = i\gamma_\mu\Big(p_\mu - a^2\,\frac{p_\mu^3}{6}\Big) - \frac{i}{4}\sum_\tau \gamma_\tau\Big(p_\tau - a^2\,\frac{p_\tau^3}{6}\Big) + \mathcal{O}(a^4) \tag{5.49}$$

$$\Lambda^{\text{tree}}_{\text{DA1}}(p) = \gamma_5\,\Lambda^{\text{tree}}_{\text{DV1}}(p) \tag{5.50}$$

$$\Lambda^{\text{tree}}_{\text{DV2}}(p) = \frac{i}{2}\left(\gamma_\mu\Big(p_\nu - a^2\,\frac{p_\nu^3}{6}\Big) + \gamma_\nu\Big(p_\mu - a^2\,\frac{p_\mu^3}{6}\Big)\right) + \mathcal{O}(a^4) \tag{5.51}$$

$$\Lambda^{\text{tree}}_{\text{DA2}}(p) = \gamma_5\,\Lambda^{\text{tree}}_{\text{DV2}}(p) \tag{5.52}$$

$$\Lambda^{\text{tree}}_{\text{DT1}}(p) = i\gamma_5\,\sigma_{\mu\nu}\Big(p_\nu - a^2\,\frac{p_\nu^3}{6}\Big) - \frac{i}{4}\sum_\tau \gamma_5\,\sigma_{\mu\tau}\Big(p_\tau - a^2\,\frac{p_\tau^3}{6}\Big) + \mathcal{O}(a^4) \tag{5.53}$$

$$\Lambda^{\text{tree}}_{\text{DT2}}(p) = \frac{i}{2}\,\gamma_5\left(\sigma_{\mu\nu}\Big(p_\rho - a^2\,\frac{p_\rho^3}{6}\Big) + \sigma_{\mu\rho}\Big(p_\nu - a^2\,\frac{p_\nu^3}{6}\Big)\right) + \mathcal{O}(a^4) \tag{5.54}$$

We perform a Taylor expansion up to $\mathcal{O}(a^2)$ in the denominator of the renormalization condition Eq. (5.32) and it leads to the following:

$$\text{Tr}\Big[\Lambda^{\text{tree}}_{\text{DV1}}(p)\cdot\Lambda^{\text{tree}}_{\text{DV1}}(p)\Big] = -2\,p_\mu^2 - \frac{1}{4}p^2 + a^2(\frac{1}{12}p4 + \frac{2}{3}p_\mu^4) + \mathcal{O}(a^4) \tag{5.55}$$

$$= -\text{Tr}\Big[\Lambda^{\text{tree}}_{\text{DA1}}(p)\cdot\Lambda^{\text{tree}}_{\text{DA1}}(p)\Big] \tag{5.56}$$

$$\text{Tr}\Big[\Lambda^{\text{tree}}_{\text{DV2}}(p)\cdot\Lambda^{\text{tree}}_{\text{DV2}}(p)\Big] = -p_\mu^2 - p_\nu^2 + \frac{a^2}{3}(p_\mu^4 + p_\nu^4) + \mathcal{O}(a^4) \tag{5.57}$$

$$= -\text{Tr}\Big[\Lambda^{\text{tree}}_{\text{DA2}}(p)\cdot\Lambda^{\text{tree}}_{\text{DA2}}(p)\Big] \tag{5.58}$$

$$\text{Tr}\Big[\Lambda^{\text{tree}}_{\text{DT1}}(p)\cdot\Lambda^{\text{tree}}_{\text{DT1}}(p)\Big] = \frac{p^2}{4} + 2\,p_\nu^2 - \frac{p_\mu^2}{4} - a^2\left(\frac{p4}{12} + \frac{2\,p_\nu^4}{3} - \frac{p_\mu^4}{12}\right) + \mathcal{O}(a^4) \tag{5.59}$$

$$\text{Tr}\Big[\Lambda^{\text{tree}}_{\text{DT2}}(p)\cdot\Lambda^{\text{tree}}_{\text{DT2}}(p)\Big] = p_\nu^2 + p_\rho^2 - \frac{a^2}{3}\left(p_\nu^4 + p_\rho^4\right) + \mathcal{O}(a^4) \tag{5.60}$$

Bellow we present the numerator of Eq. (5.32), in each of the six cases Eqs. (5.43)-

(5.48). Since the expressions are extremely lengthy, we only show them for the special choices: $m_0 = 0$ and $\alpha = 0$ (Landau gauge).

$$
\begin{aligned}
\mathrm{Tr}\Big[\Lambda^{1-loop}_{\mathrm{DV1}}(p)\cdot\Lambda^{\mathrm{tree}}_{\mathrm{DV1}}(p)\Big] &= -2\,p_\mu^2 - \frac{1}{4}p^2 + a^2(\frac{1}{12}p4 + \frac{2}{3}p_\mu^4) \\
&+\frac{g^2\,C_F}{16\pi^2}\Big\{\frac{4}{3}\frac{p_\mu^4}{p^2} + p^2\Big[3.6101 + 0.4024\,c_{\mathrm{SW}} - 0.0877\,c_{\mathrm{SW}}^2 - 7.6866\,\omega - 0.9116\,c_{\mathrm{SW}}\;\omega \\
&\qquad + \;\; 0.6488\,\omega^2 - \frac{2}{3}\log(a^2\,p^2)\Big] \\
&\quad + p_\mu^2\Big[27.5472 + 3.2198\,c_{\mathrm{SW}} - 0.7021\,c_{\mathrm{SW}}^2 - 61.4926\,\omega - 7.2932\,c_{\mathrm{SW}}\;\omega + 5.1905\,\omega^2 \\
&\qquad - \;\; \frac{16}{3}\log(a^2\,p^2)\Big] \\
&\quad + a^2\Big[(p^2)^2\Big[0.1183 - 0.2026\,c_{\mathrm{SW}} + 0.0577\,c_{\mathrm{SW}}^2 + 2.4778\,\omega - 0.2136\,c_{\mathrm{SW}}\;\omega - 0.5638\,\omega^2 \\
&\qquad + \;\; \left(\frac{7}{288} + \frac{1}{4}\,c_{\mathrm{SW}} - \frac{5}{48}\,c_{\mathrm{SW}}^2 - \frac{1}{2}\,\omega\right)\log(a^2\,p^2)\Big] \\
&\quad + p^2\,p_\mu^2\Big[-0.6573 - 0.8958\,c_{\mathrm{SW}} + 0.2028\,c_{\mathrm{SW}}^2 + 10.0278\,\omega + 2.4515\,c_{\mathrm{SW}}\;\omega - 1.2017\,\omega^2 \\
&\qquad - \;\; \left(\frac{299}{180} + \frac{7}{6}\,c_{\mathrm{SW}} - \frac{1}{6}\,c_{\mathrm{SW}}^2 - \frac{4}{3}\,\omega\right)\log(a^2\,p^2)\Big] \\
&\quad + p4\Big[-1.7188 - 0.0970\,c_{\mathrm{SW}} + 0.0112\,c_{\mathrm{SW}}^2 + 3.1421\,\omega + 0.5376\,c_{\mathrm{SW}}\;\omega - 0.1729\,\omega^2 \\
&\qquad + \;\; \frac{397}{720}\log(a^2\,p^2) - \frac{43}{360}\frac{p_\mu^2}{p^2}\Big] \\
&\quad + p_\mu^4\Big[-16.1049 - 1.5015\,c_{\mathrm{SW}} + 0.3484\,c_{\mathrm{SW}}^2 + 34.9319\,\omega + 0.1408\,c_{\mathrm{SW}}\;\omega - 4.6922\,\omega^2 \\
&\quad + \left(\frac{94}{15} - \frac{2}{3}\,c_{\mathrm{SW}} - \frac{2}{3}\,c_{\mathrm{SW}}^2 - \frac{8}{3}\,\omega\right)\log(a^2\,p^2) + \frac{29}{90}\frac{p4}{(p^2)^2} + \frac{169}{45}\frac{p_\mu^2}{p^2}\Big]\Big]\Big\},
\end{aligned}
\tag{5.61}
$$

$$
\begin{aligned}
\mathrm{Tr}\Big[\Lambda^{1-loop}_{\mathrm{DV2}}(p)\cdot\Lambda^{\mathrm{tree}}_{\mathrm{DV2}}(p)\Big] &= -p_\mu^2 - p_\nu^2 + \frac{a^2}{3}(p_\mu^4 + p_\nu^4) \\
&+\frac{g^2\,C_F}{16\pi^2}\Big\{\frac{4}{3}\frac{p_\mu^2\,p_\nu^2}{p^2} + (p_\mu^2+p_\nu^2)\Big[15.0458 + 1.5496\,c_{\mathrm{SW}} - 0.6719\,c_{\mathrm{SW}}^2 - 37.1295\,\omega - 2.6765\,c_{\mathrm{SW}}\;\omega \\
&\qquad + \;\; 22.3039\,\omega^2 - \frac{8}{3}\log(a^2\,p^2)\Big] \\
&+a^2\Big[(p_\mu^4+p_\nu^4)\Big[-7.1429 - 0.3175\,c_{\mathrm{SW}} + 0.1395\,c_{\mathrm{SW}}^2 + 14.2793\,\omega + 0.9123\,c_{\mathrm{SW}}\;\omega - 8.4361\,\omega^2 \\
&\qquad + \;\; \frac{491}{360}\log(a^2\,p^2)\Big] \\
&+(p_\mu^2+p_\nu^2)\Big[p^2\Big(-0.13212 - 0.6358\,c_{\mathrm{SW}} + 0.2072\,c_{\mathrm{SW}}^2 + 7.5642\,\omega + 0.0782\,c_{\mathrm{SW}}\;\omega - 0.5418\,\omega^2 \\
&\qquad + \;\; \Big(-\frac{103}{360} + \frac{5}{12}\,c_{\mathrm{SW}} - \frac{1}{4}\,c_{\mathrm{SW}}^2 - \frac{4}{3}\,\omega\Big)\log(a^2\,p^2)\Big) + \frac{353}{720}\frac{p4}{p^2}\Big] \\
&+p_\mu^2\,p_\nu^2\Big[-4.0096 - 0.9718\,c_{\mathrm{SW}} + 0.2141\,c_{\mathrm{SW}}^2 + 8.0384\,\omega + 1.9856\,c_{\mathrm{SW}}\;\omega - 2.6169\,\omega^2 \\
&+\Big(\frac{1013}{180} - \frac{2}{3}\,c_{\mathrm{SW}} - \frac{2}{3}\,c_{\mathrm{SW}}^2 - \frac{8}{3}\,\omega\Big)\log(a^2\,p^2) + \frac{29}{90}\frac{p4}{(p^2)^2} + \frac{169}{90}\frac{(p_\mu^2+p_\mu^2)}{p^2}\Big]\Big]\Big\},
\end{aligned}
\tag{5.62}
$$

$$
\begin{aligned}
\mathrm{Tr}\Big[\Lambda^{1-loop}_{\mathrm{DA1}}(p)\cdot\Lambda^{\mathrm{tree}}_{\mathrm{DA1}}(p)\Big] &= 2\,p_\mu^2+\frac{1}{4}p^2+a^2(-\frac{1}{12}p4-\frac{2}{3}p_\mu^4)\\
&+\frac{g^2\,C_F}{16\pi^2}\Big\{-\frac{4}{3}\frac{p_\mu^4}{p^2}+p^2\Big[-4.1273+0.2230\,c_{\mathrm{SW}}-0.1390\,c_{\mathrm{SW}}^2+9.4907\,\omega+0.4476\,c_{\mathrm{SW}}\;\omega\\
&\qquad -\;2.9191\,\omega^2+\frac{2}{3}\log(a^2\,p^2)\Big]\\
&+p_\mu^2\Big[-31.6853+1.7842\,c_{\mathrm{SW}}-1.1120\,c_{\mathrm{SW}}^2+75.9257\,\omega+3.5816\,c_{\mathrm{SW}}\;\omega-23.3531\,\omega^2\\
&\qquad +\;\frac{16}{3}\log(a^2\,p^2)\Big]\\
&+a^2\Big[(p^2)^2\Big[0.1703-0.1565\,c_{\mathrm{SW}}+0.0439\,c_{\mathrm{SW}}^2-1.9315\,\omega+0.1725\,c_{\mathrm{SW}}\;\omega-0.2107\,\omega^2\\
&\qquad +\;\left(\frac{65}{288}-\frac{1}{48}\,c_{\mathrm{SW}}-\frac{5}{48}\,c_{\mathrm{SW}}^2-\frac{1}{2}\,\omega\right)\log(a^2\,p^2)\Big]\\
&+p^2\,p_\mu^2\Big[0.3982-1.1861\,c_{\mathrm{SW}}+0.3708\,c_{\mathrm{SW}}^2-21.8081\,\omega-1.1757\,c_{\mathrm{SW}}\;\omega+4.2720\,\omega^2\\
&\qquad +\;\left(-\frac{541}{180}+\frac{11}{6}\,c_{\mathrm{SW}}-\frac{1}{6}\,c_{\mathrm{SW}}^2+\frac{4}{3}\,\omega\right)\log(a^2\,p^2)\Big]\\
&+p4\Big[1.6923+0.1097\,c_{\mathrm{SW}}+0.0292\,c_{\mathrm{SW}}^2-3.7154\,\omega-0.3908\,c_{\mathrm{SW}}\;\omega+1.6098\,\omega^2\\
&\qquad -\;\frac{397}{720}\log(a^2\,p^2)+\frac{43}{360}\frac{p_\mu^2}{p^2}\Big]\\
&+p_\mu^4\Big[18.4613+0.8116\,c_{\mathrm{SW}}+0.2139\,c_{\mathrm{SW}}^2-23.3669\,\omega-0.5706\,c_{\mathrm{SW}}\;\omega+6.9208\,\omega^2\\
&+\left(\frac{2}{5}-2\,c_{\mathrm{SW}}-\frac{2}{3}\,c_{\mathrm{SW}}^2+\frac{8}{3}\,\omega\right)\log(a^2\,p^2)-\frac{29}{90}\frac{p4}{(p^2)^2}-\frac{169}{45}\frac{p_\mu^2}{p^2}\Big]\Big]\Big\},
\end{aligned}
\tag{5.63}
$$

$$
\begin{aligned}
\mathrm{Tr}\Big[\Lambda^{1-loop}_{\mathrm{DA2}}(p)\cdot\Lambda^{\mathrm{tree}}_{\mathrm{DA2}}(p)\Big] &= p_\mu^2+p_\nu^2-\frac{a^2}{3}(p_\mu^4+p_\nu^4)\\
&+\frac{g^2\,C_F}{16\pi^2}\Big\{-\frac{4}{3}\frac{p_\mu^2\,p_\nu^2}{p^2}+(p_\mu^2+p_\nu^2)\Big[-16.1020+0.8946\,c_{\mathrm{SW}}-0.4852\,c_{\mathrm{SW}}^2+33.2339\,\omega\\
&\qquad+\;1.0929\,c_{\mathrm{SW}}\;\omega+8.4372\,\omega^2+\frac{8}{3}\log(a^2\,p^2)\Big]\\
&+a^2\Big[(p_\mu^4+p_\nu^4)\Big[7.2286-0.2033\,c_{\mathrm{SW}}+0.0726\,c_{\mathrm{SW}}^2-13.1536\,\omega-0.5131\,c_{\mathrm{SW}}\;\omega-1.7577\,\omega^2\\
&\qquad-\;\frac{491}{360}\log(a^2\,p^2)\Big]\\
&+(p_\mu^2+p_\nu^2)\Big[p^2\Big(0.7587-0.6017\,c_{\mathrm{SW}}+0.2159\,c_{\mathrm{SW}}^2-9.5685\,\omega+0.2459\,c_{\mathrm{SW}}\;\omega+0.7202\,\omega^2\\
&\qquad+\;\Big(-\frac{137}{360}+\frac{5}{12}\,c_{\mathrm{SW}}-\frac{1}{4}\,c_{\mathrm{SW}}^2+\frac{4}{3}\,\omega\Big)\log(a^2\,p^2)\Big)-\frac{353}{720}\frac{p4}{p^2}\Big]\\
&+p_\mu^2\,p_\nu^2\Big[4.8509+1.1683\,c_{\mathrm{SW}}-0.0629\,c_{\mathrm{SW}}^2+7.8377\,\omega-2.3841\,c_{\mathrm{SW}}\;\omega-0.9413\,\omega^2\\
&+\Big(\frac{187}{180}+2\,c_{\mathrm{SW}}-\frac{2}{3}\,c_{\mathrm{SW}}^2+\frac{8}{3}\,\omega\Big)\log(a^2\,p^2)-\frac{29}{90}\frac{p4}{(p^2)^2}-\frac{169}{90}\frac{(p_\mu^2+p_\mu^2)}{p^2}\Big]\Big]\Big\}. \qquad (5.64)
\end{aligned}
$$

We present also the corresponding trace of the tensor operators for the special choices: $m_0=0,\ c_{\mathrm{SW}}=0,\ \omega=0$ and $\alpha=0$ (Landau gauge).

$$
\begin{aligned}
\mathrm{Tr}\Big[\Lambda^{1-loop}_{\mathrm{DT1}}(p)\cdot\Lambda^{\mathrm{tree}}_{\mathrm{DT1}}(p)\Big] &= \frac{p^2-p_\mu^2}{4}+2\,p_\nu^2+a^2\,(\frac{p_\mu^4-p4}{12}-\frac{2\,p_\nu^4}{3})\\
&+\frac{g^2\,C_F}{16\pi^2}\Big\{(p_\mu^2-p^2)\Big[4.2265-\log(a^2\,p^2)\Big]+p_\nu^2\Big[-29.1167\;+5\;\log(a^2\,p^2)\Big]\\
&+a^2\Big[p^4\Big[-0.14754-\frac{43}{1440}\;\log(a^2\,p^2)\Big]+p4\Big[1.9379-\frac{433}{720}\;\log(a^2\,p^2)\\
&\qquad-\;\frac{379}{720}\,\frac{p_\nu^2}{p^2}+\frac{17}{192}\,\frac{p_\mu^2}{p^2}\Big]\\
&+p^2\Big[1.7215\,p_\nu^2+\frac{61}{48}\;\log(a^2\,p^2)\,p_\nu^2+0.37022\,p_\mu^2-\frac{227}{1440}\;\log(a^2\,p^2)\,p_\mu^2\Big]\\
&+p_\nu^4\Big[14.9155-\frac{71}{15}\;\log(a^2\,p^2)-\frac{721}{90}\,\frac{p_\mu^2}{p^2}\Big]+p_\nu^2\,p_\mu^2\Big[2.4896-\frac{881}{240}\;\log(a^2\,p^2)-\frac{39}{10}\,\frac{p_\mu^2}{p^2}\Big]\\
&+p_\mu^4\Big[-2.2491+\frac{71}{90}\;\log(a^2\,p^2)\Big]-\frac{134}{45}\,\frac{p_\nu^6}{p^2}\Big]\Big\}, \qquad (5.65)
\end{aligned}
$$

$$
\begin{aligned}
\mathrm{Tr}\Big[\Lambda^{1-loop}_{\mathrm{DT2}}(p)\cdot\Lambda^{\mathrm{tree}}_{\mathrm{DT2}}(p)\Big] &= p_\rho^2+p_\nu^2+a^2\,(-\frac{p_\rho^4}{3}-\frac{p_\nu^4}{3})\\
&+\frac{g^2\,C_F}{16\pi^2}\,\Big\{(p_\nu^2+p_\rho^2)\,\Big[-15.8474+3\,\log(a^2\,p^2)\Big]\\
&+a^2\,\Big[(p_\nu^2+p_\rho^2)\,\Big[0.2213\,p^2+\frac{107}{360}\,\log(a^2\,p^2)\,p^2-\frac{41}{60}\,\frac{p4}{p^2}+0.7360\,p_\mu^2\\
&\qquad -\frac{301}{360}\,\log(a^2\,p^2)\,p_\mu^2-\frac{67}{90}\,\frac{p_\mu^4}{p^2}\Big]\\
&-\frac{67}{15}\,\frac{p_\rho^2\,p_\mu^2\,p_\nu^2}{p^2}+(p_\nu^4+p_\rho^4)\,\Big[7.3949-\frac{1051}{720}\,\log(a^2\,p^2)\Big]+p_\rho^2\,p_\nu^2\Big[2.9845\,-\frac{1609}{360}\,\log(a^2\,p^2)\Big]\\
&-\frac{67}{45}\,\frac{p_\rho^4\,p_\nu^2+p_\rho^2\,p_\nu^4}{p^2}\Big]\Big\}. \qquad (5.66)
\end{aligned}
$$

By inserting our results (Eqs. (5.61)-(5.66)) into Eq. (5.32) we immediately obtain the renormalization functions $Z_{\mathrm{DV1}}, Z_{\mathrm{DV2}}, Z_{\mathrm{DA1}}, Z_{\mathrm{DA2}}, Z_{\mathrm{DT1}}, Z_{\mathrm{DT2}}$.

5.4 Summary

In this Chapter we have calculated the fermion propagator and the Green's functions for the fermion bilinear operators up to one loop, using the SLiNC action. These matrix elements are used to extract mass spectra, decay rates and transition amplitudes in hadronic Physics; others are directly related to physical properties of quarks inside nucleons, such as moments of their helicity and momentum distributions [111, 112].

The truly novel feature in our calculations is that they were performed to second order in the lattice spacing a ($\mathcal{O}(a^2, a^2\log a)$). This fact introduces a number of complications, which are not present in lower order results. In a nutshell, the reason for these complications is as follows: The extraction of a further power of a from a Feynman diagram strengthens, by one unit, the superficial degree of infrared (IR) divergence of the corresponding integrand over loop momenta. Thus, a priori, in a $\mathcal{O}(a^1)$ calculation, loop integrals would be IR convergent only in $D > 5$ dimensions; however, as can be easily deduced by inspection, the most divergent parts of the integrands are odd functions of the loop momenta, and will thus vanish upon integration. What is left behind is a less divergent integrand which is IR convergent in $D > 4$, just as in the case of $\mathcal{O}(a^0)$ calculations, and can thus be treated by standard methods, such as those of Ref. [113]. For $\mathcal{O}(a^2)$ calculations, on the other hand, integrands are IR convergent only at $D > 6$, and their most divergent parts no longer vanish upon integration; a naive application of the procedure of Ref. [113] will

fail to produce all $\mathcal{O}(a^2)$ contributions. The procedure which we proposed in this work for handling the above difficulty is in fact applicable to any order in a. In brief, it recasts the integrands as a sum of two parts: The first part can be *exactly* evaluated as a function of a, while the second part is naively Taylor expandible, as a polynomial to the desired order in a.

The propagator and Green's functions have been obtained with massive fermions (including non-degenerate flavors). Nevertheless, even at vanishing masses, our final expressions are quite lengthy, since they exhibit a rather nontrivial dependence on several parameters. Our final results for the Z functions do not contain masses since we used the mass independent renormalization scheme.

One possible use of our results is in constructing improved versions of the operators O^Γ, with reduced lattice artifacts. In doing so, however, one must bear in mind that, unlike the $\mathcal{O}(a^1)$ case, corrections to $\mathcal{O}(a^2)$ include expressions which are non-polynomial in the external momentum and, therefore, cannot be eliminated by introducing admixtures of local operators. Full improvement can be achieved at best for on-shell matrix elements only.

At the nonzero values of a employed in numerical simulations, $\mathcal{O}(a^2)$ corrections are quite important. Ideally, one would prefer a nonperturbative determination of renormalization functions; while this is often possible, several sources of error must be dealt with. A very effective way to proceed is through a combination of perturbative and nonperturbative results. This procedure is carried out and explained in detail in the next Chapter. Briefly stated, nonperturbative data are "corrected" by the perturbative expressions for Green's functions, and then extrapolated towards small a. In the next Chapter we improve the nonperturbative renormalization constants in the RI′-MOM scheme using the clover action.

Chapter 6

Perturbatively improving RI-MOM renormalization constants using the Clover action

In this Chapter we compute the perturbative renormalization factors (Z factors) of local and extended (one derivative) fermion bilinear operators which are defined in Table 6.1. A novel feature in this one-loop perturbative calculation is that the relevant 2-point Green's functions are computed up to second order in the lattice spacing a. We employ the clover action for fermions and the Symanzik improved gauge action for gluons. We apply our results to data extracted from numerical simulations performed by the QCDSF collaboration using $N_f = 2$ clover improved Wilson fermions with plaquette gauge action; in particular, in order to suppress lattice artifacts from the nonperturbative Green's functions we subtract the one-loop, $\mathcal{O}(a^2)$ contributions of the renormalization factors calculated in lattice perturbation theory. We compare results obtained from a complete one-loop subtraction with those obtained by subtracting only contributions proportional to a^2.

6.1 Introduction

As mentioned in previous Chapters, renormalization factors in lattice Quantum Chromodynamics (QCD) relate observables computed on finite lattices to their continuum counterparts in specific renormalization schemes. Therefore, their determination should be as precise as possible in order to allow for a reliable comparison with experimental results.

Given that the approach based on lattice perturbation theory suffers from its intrinsic complexity, slow convergence and the impossibility to handle mixing with lower-dimensional operators, nonperturbative methods have been developed and applied. Among them the so-called Rome-Southampton method [114] (utilizing the RI-MOM scheme) is widely used because of its simple implementation,even though it requires gauge fixing.

Like (almost) all quantities evaluated in lattice QCD also renormalization factors suffer from discretization effects. One can attempt to cope with these lattice artifacts by extrapolating the nonperturbative scale dependence to the continuum (see Ref. [115]) or one can try to suppress them by a subtraction procedure based on perturbation theory. Here we shall deal with the latter approach.

In a recent work of the QCDSF/UKQCD collaboration [117] a comprehensive discussion and a comparison of perturbative and nonperturbative renormalization have been given. Particular emphasis was placed on the perturbative subtraction of the unavoidable lattice artifacts. For simple operators this can be done in one-loop order completely by computing the corresponding diagrams for finite lattice spacing numerically. While being very effective this procedure is rather involved and not suited as a general method for more complex operators, especially for operators with more than one covariant derivative, and complicated lattice actions. An alternative approach can be based on the subtraction of one-loop terms of order a^2, with a being the lattice spacing. The computation of those terms has been developed by our group [43] and applied to various operators for different actions. In this Chapter we use some of those results for the analysis of Monte Carlo data for renormalization coefficients.

We study the flavor-nonsinglet quark-antiquark operators given in Table 6.1. The corresponding renormalization factors have been measured (and chirally extrapolated[1]) at $\beta = 5.20, 5.25, 5.29$ and 5.40 using $N_f = 2$ clover improved Wilson fermions with plaquette gauge action [117]. All results are computed in the Landau gauge. Our perturbative results were obtained for generic values of the clover parameter c_{SW}; in order to apply these results to the nonperturbative calculation we set $c_{SW} = 1$.

[1]The chiral limit is reached when the masses of the light quarks assume their critical value, i.e., the value at which chiral symmetry is restored.

Operator (multiplet)	Notation	Repre-sentation	Operator basis
$\bar{u}\, d$	$\mathcal{O}^S$	$\tau_1^{(1)}$	$\mathcal{O}^S$
$\bar{u}\,\gamma_5\, d$	$\mathcal{O}^P$	$\tau_4^{(1)}$	$\mathcal{O}^P$
$\bar{u}\,\gamma_\mu\, d$	$\mathcal{O}^V_\mu$	$\tau_1^{(4)}$	$\mathcal{O}^V_1, \mathcal{O}^V_2, \mathcal{O}^V_3, \mathcal{O}^V_4$
$\bar{u}\,\gamma_\mu\gamma_5\, d$	$\mathcal{O}^A_\mu$	$\tau_4^{(4)}$	$\mathcal{O}^A_1, \mathcal{O}^A_2, \mathcal{O}^A_3, \mathcal{O}^A_4$
$\bar{u}\,\sigma_{\mu\nu}\, d$	$\mathcal{O}^T_{\mu\nu}$	$\tau_1^{(6)}$	$\mathcal{O}^T_{12}, \mathcal{O}^T_{13}, \mathcal{O}^T_{14}, \mathcal{O}^T_{23}, \mathcal{O}^T_{24}, \mathcal{O}^T_{34}$
$\bar{u}\,\gamma_\mu \overleftrightarrow{D}_\nu\, d$	$\mathcal{O}_{\mu\nu} \to \mathcal{O}^{v_{2,a}}$	$\tau_3^{(6)}$	$\mathcal{O}_{\{12\}}, \mathcal{O}_{\{13\}}, \mathcal{O}_{\{14\}}, \mathcal{O}_{\{23\}}, \mathcal{O}_{\{24\}}, \mathcal{O}_{\{34\}}$
$\bar{u}\,\gamma_\mu \overleftrightarrow{D}_\nu\, d$	$\mathcal{O}_{\mu\nu} \to \mathcal{O}^{v_{2,b}}$	$\tau_1^{(3)}$	$1/2(\mathcal{O}_{11}+\mathcal{O}_{22}-\mathcal{O}_{33}-\mathcal{O}_{44})$, $1/\sqrt{2}(\mathcal{O}_{33}-\mathcal{O}_{44}), 1/\sqrt{2}(\mathcal{O}_{11}-\mathcal{O}_{22})$

Table 6.1: Operators and their representations as investigated in the present Chapter. The symbol {...} means the totally symmetric and traceless part. A detailed group theoretical discussion is given in [118]. There are 20 (inequivalent) irreducible representations of H(4), which are denoted by $\tau_k^{(l)}$, where l is the dimension of the representation and $k = 1, 2, \ldots$ distinguishes inequivalent representations of the same dimension.

6.2 Renormalization group invariant operators

We define the renormalization constant Z of an operator $\mathcal{O}$ from its amputated Green function (or vertex function) $\Lambda(p)$, where p is the external momentum and the operator is taken at vanishing momentum. The corresponding renormalized vertex function and the tree-level (Born) term (with all lattice artifacts included) are denoted by $\Lambda_R(p)$ and $\Lambda^{\text{tree}}(p)$, respectively. Just as in Eq. (5.32), if there is no mixing, Z can then be obtained by imposing the condition

$$\frac{1}{12}\,\text{tr}\left[\Lambda_R(p)\,\Lambda^{\text{tree}}(p)^{-1}\right] = 1 \tag{6.1}$$

for vanishing quark mass at $p^2 = \mu^2$, where μ_ρ is the (4-vector) renormalization scale. The Z factor relates the renormalized and the unrenormalized vertex function through

$$\Lambda_R(p) = Z_q^{-1}\, Z\, \Lambda(p)\,, \tag{6.2}$$

with Z_q being the quark field renormalization constant determined by

$$Z_q(p) = \frac{\text{tr}\left[-\text{i}\sum_\lambda \gamma_\lambda \sin(ap_\lambda)\, aS^{-1}(p)\right]}{12\sum_\nu \sin^2(ap_\nu)} \tag{6.3}$$

in the chiral limit again at $p^2 = \mu^2$. Condition (6.1) together with (6.3) defines the RI′-MOM renormalization scheme. Here S^{-1} is the inverse quark propagator. The argument p appearing in all Z factors is meant to be set equal to the renormalization scale 4-vector μ. Using (6.1) we compute Z from

$$Z_q^{-1}\, Z\, \frac{1}{12}\, \mathrm{tr}\left[\Lambda(p)\, \Lambda^{\mathrm{tree}}(p)^{-1}\right] = 1\,. \tag{6.4}$$

For operators transforming as singlets under the hypercubic group $H(4)$, such as $\mathcal{O}^S$, Z can depend on the components of p only through $H(4)$ invariants.

For operators belonging to an $H(4)$ multiplet of dimension greater than 1 the condition (6.1) violates $H(4)$ covariance and would in general lead to different Z factors for each member of the multiplet. In Ref. [117] an averaging procedure has been proposed to calculate one common Z factor for every multiplet. Labeling the chosen operator basis by $i = 1, 2, \ldots, d$ the common Z was calculated from

$$Z_q^{-1}\, Z\, \frac{1}{d} \sum_{i=1}^{d} \frac{1}{12}\, \mathrm{tr}\left[\Lambda_i(p) \Lambda_i^{\mathrm{tree}}(p)^{-1}\right] = 1\,. \tag{6.5}$$

This condition leads to an $H(4)$-invariant Z for the operators without derivatives in Table 6.1. However, in general this is not the case.

It is not difficult to devise a renormalization condition that respects the hypercubic symmetry. Choosing a basis of operators (again labeled by i), transforming according to a unitary irreducible representation of $H(4)$, the relation

$$Z_q^{-1}\, Z\, \frac{\sum_{i=1}^{d} \mathrm{tr}\left[\Lambda_i(p) \Lambda_i^{\mathrm{tree}}(p)^{\dagger}\right]}{\sum_{j=1}^{d} \mathrm{tr}\left[\Lambda_j^{\mathrm{tree}}(p) \Lambda_j^{\mathrm{tree}}(p)^{\dagger}\right]} = 1 \tag{6.6}$$

defines a Z factor which is invariant under $H(4)$, provided that the quark field renormalization factor is also $H(4)$ invariant. The derivation of renormalization condition (6.6) is given in Appendix C. For the operators without derivatives the definitions (6.6) and (6.5) are equivalent. For the operators with one derivative the resulting differences turn out to be negligible. In the following the Z factors will be determined from (6.6) using the operator basis given in Table 6.1. This is our version of the RI′-MOM scheme.

We define a so-called RGI (renormalization group invariant) operator, which is inde-

pendent of scale M and scheme $\mathcal{S}$, by [116, 117]

$$\mathcal{O}^{\mathrm{RGI}} = \Delta Z^{\mathcal{S}}(M)\, \mathcal{O}^{\mathcal{S}}(M) = Z^{\mathrm{RGI}}(a)\, \mathcal{O}_{\mathrm{bare}} \tag{6.7}$$

with

$$\Delta Z^{\mathcal{S}}(M) = \left(2\beta_0 \frac{g^{\mathcal{S}}(M)^2}{16\,\pi^2}\right)^{-(\gamma_0/2\beta_0)} \exp\left\{\int_0^{g^{\mathcal{S}}(M)} dg' \left(\frac{\gamma^{\mathcal{S}}(g')}{\beta^{\mathcal{S}}(g')} + \frac{\gamma_0}{\beta_0 g'}\right)\right\} \tag{6.8}$$

and the RGI renormalization constant (depending on a via the lattice coupling)

$$Z^{\mathrm{RGI}}(a) = \Delta Z^{\mathcal{S}}(M)\, Z^{\mathcal{S}}_{\mathrm{bare}}(M, a)\,. \tag{6.9}$$

Here $g^{\mathcal{S}}$ is the coupling constant, $\beta^{\mathcal{S}}$ is the β-function which is defined by: $\beta^{\mathcal{S}} = \mu\, dg^{\mathcal{S}}/d\mu$; $\gamma^{\mathcal{S}}$ is the anomalous dimension of the renormalized operator $\mathcal{O}^{\mathrm{RGI}}$, which is defined by: $\mu\, dZ^{\mathcal{S}}/d\mu = -\gamma^{\mathcal{S}} Z^{\mathcal{S}}$ where μ is the renormalization scale. Relations (6.7), (6.8) and (6.9) allow us to compute the operator $\mathcal{O}$ in any scheme and at any scale we like, once Z^{RGI} is known. Therefore, the knowledge of Z^{RGI} is very useful for the renormalization procedure in general. Ideally, Z^{RGI} depends only on the bare lattice coupling, but not on the momentum p. Computed on a lattice, however, it suffers from lattice artifacts, e.g., it contains contributions proportional to a^2p^2, $(a^2p^2)^2$, $a^4\sum_\mu p_\mu^4$, etc. For a precise determination it is essential to have these discretization errors under control.

As the RI′-MOM scheme is in general not $O(4)$-covariant even in the continuum limit, it is not very suitable for computing the anomalous dimensions needed in (6.8). Therefore we use an intermediate scheme $\mathcal{S}$ with known anomalous dimensions and calculate Z^{RGI} as follows:

$$Z^{\mathrm{RGI}}(a) = \Delta Z^{\mathcal{S}}(M = \mu)\, Z^{\mathcal{S}}_{\mathrm{RI'-MOM}}(M = \mu)\, Z^{\mathrm{RI'-MOM}}_{\mathrm{bare}}(\mu, a)\,. \tag{6.10}$$

It turns out that a type of momentum subtraction scheme is a good choice for $\mathcal{S}$ (for details see Ref. [117]). The formula which is used to compute the transformation factor $Z^{\mathcal{S}}_{\mathrm{RI'-MOM}}(\mu)$ is given there together with all needed coefficients of the β-function and anomalous dimensions, which are based on continuum three-loop calculations such as those in [119, 120, 121].

On a lattice with linear extent L the scale μ should ideally fulfill the relation

$$1/L^2 \ll \Lambda^2_{\mathrm{QCD}} \ll \mu^2 \ll 1/a^2\,. \tag{6.11}$$

In that case $Z^{\mathrm{RGI}}(a)$ would be independent of μ, and from the resulting plateau we could read off the corresponding final value. However, in practice $a\mu$ is not necessarily small leading to non-negligible lattice artifacts that have to be tamed. A promising tool to control lattice artifacts in a systematic way is lattice perturbation theory: We expect that after subtracting these perturbative terms the calculation of the Z factors can be done more accurately.

6.3 Subtraction of all lattice artifacts in one-loop order

In standard lattice perturbation theory the one-loop renormalization constants are given in the form

$$Z(\mu, a) = 1 + \frac{g^2\, C_F}{16\,\pi^2}\,(\gamma_0\,\ln(a\mu) + \Delta)\,, \quad C_F = \frac{4}{3}\,. \tag{6.12}$$

This means that the a-dependence is retained only in the logarithm and implicitly in g, while in all other contributions the limit $a \to 0$ has been taken.

However, there is no need to do so. We can keep a finite everywhere and thus evaluate the lattice artifacts at one-loop order completely, proceeding as follows. Let us denote by $F(p, a)$ the total one-loop correction to the 2-pt Green's functions and by $\tilde{F}(p, a)$ the expression resulting from $F(p, a)$ by neglecting all contributions which vanish for $a \to 0$. The difference

$$D(p, a) = F(p, a) - \tilde{F}(p, a) \tag{6.13}$$

represents the lattice artifacts in one-loop perturbation theory and is used to correct for the discretization errors:

$$Z_{\mathrm{bare}}^{\mathrm{RI'-MOM}}(p, a)_{\mathrm{MC,sub}} = Z_{\mathrm{bare}}^{\mathrm{RI'-MOM}}(p, a)_{\mathrm{MC}} - \frac{g_\star^2}{16\,\pi^2} C_F\, D(p, a)\,. \tag{6.14}$$

There is a certain freedom in choosing the coupling $g_\star$ in (6.14). It turned out that the use of the boosted coupling

$$g_{\mathrm{B}}^2 = \frac{g^2}{P(g)} = g^2 + O(g^4) \tag{6.15}$$

($P(g)$ being the measured plaquette at $\beta = 6/g^2$) is quite successful in estimating the higher-order discretization effects. With the prescription (6.14) all lattice artifacts in one-loop order are subtracted.

In Fig. 6.1 we show the effect of subtraction on the RGI renormalization factors for selected operators of Table 6.1. For all operators we recognize after subtraction a remark-

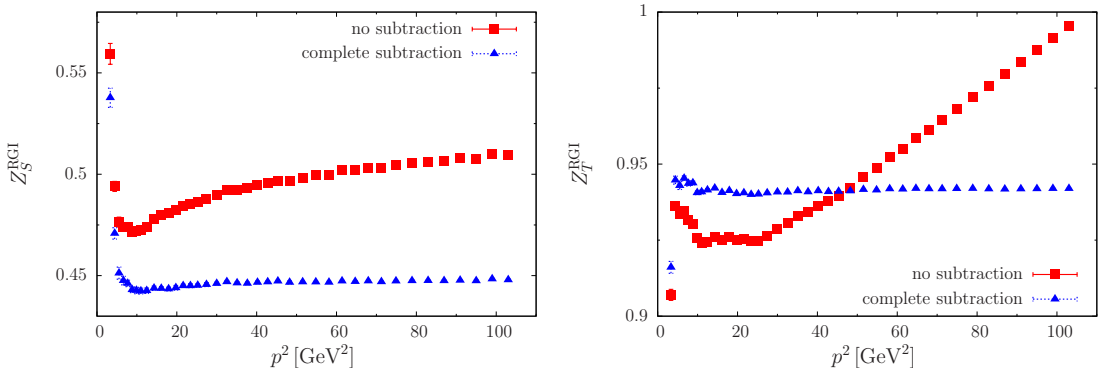

Figure 6.1: Z_S^{RGI} (left) and Z_T^{RGI} (right) for $\beta = 5.40$. The Z factors obtained without subtraction are shown as red squares, those with complete one-loop subtraction (6.14) as blue triangles. (The necessary scale transformation factors for the momenta are given at the end of Section 6.4.)

able smoothing and a pronounced plateau as a function of p^2 for $p^2 \gtrsim 10\,\mathrm{GeV}^2$. The large bending in the small p^2 region might indicate the breakdown of perturbation theory (cf. the discussion in [117]). The examples show that the one-loop subtraction of lattice artifacts (6.14) works very well and, moreover, is needed for a precise determination of the renormalization constants. The final values for Z^{RGI} from (6.10) are obtained by a fit with an ansatz [117]

$$Z^{\mathcal{S}}_{\mathrm{RI'-MOM}}(p)\, Z^{\mathrm{RI'-MOM}}_{\mathrm{bare}}(p,a)_{\mathrm{MC,sub}} = \frac{Z^{\mathrm{RGI}}(a)}{\Delta Z^{\mathcal{S}}(p)\ [1 + b_1\,(g^{\mathcal{S}})^8]} + c_1\, a^2 p^2\,. \tag{6.16}$$

The free parameter b_1 takes into account that the transformation factor $Z^{\mathcal{S}}_{\mathrm{RI'-MOM}}(p)$ is known to three-loop order $\left(g^{\mathcal{S}}\right)^6$ only. Further possible lattice artifacts are parametrized by $c_1\, a^2 p^2$.

For practical reasons the numerical calculation of $F(p,a)$ - and therefore the calculation of Z^{RGI} using (6.16) - is restricted to operators with at most one derivative and for $N_f = 2$ only. In order to perform the subtraction for a wider class of operators and/or for $N_f = 2{+}1$ (where the lattice action under consideration becomes more complicated) we have to look for an alternative method. One possibility which will be discussed in the next sections is a "reduced" subtraction: Instead of subtracting the complete one-loop lattice artifacts we subtract only the one-loop terms proportional to a^2, if they are known for the given action.

6.4 Subtraction of order a^2 one-loop lattice artifacts

6.4.1 Lattice perturbation theory up to order g^2a^2

The diagrammatic approach to compute the one-loop a^2 terms for the Z factors of local and one-link operators has been developed by some of us [43, 122]. The general case of Wilson type improved fermions is discussed in [14]. For details of the computations we refer to these references. Here we give explicitly the results for the operators and actions investigated in this work (massless improved Wilson fermions with $c_{\rm SW} = 1$, plaquette gauge action, Landau gauge).

Using the relation (6.6) we compute a common Z factor for each multiplet given in Table 6.1. The results are as follows:

$$
\begin{aligned}
Z_S &= 1+\frac{g^2\,C_F}{16\pi^2}\left\{-23.3099+3\,\log(a^2S_2)\right.\\
&\quad \left.+a^2\left[S_2\left(1.64089-\frac{239}{240}\log(a^2S_2)\right)+\frac{S_4}{S_2}\left(1.95104-\frac{101}{120}\log(a^2S_2)\right)\right]\right\},\\
Z_P &= 1+\frac{g^2\,C_F}{16\pi^2}\left\{-26.3832+3\,\log(a^2S_2)\right.\\
&\quad \left.+a^2\left[S_2\left(-6.31906+\frac{121}{240}\log(a^2S_2)\right)+\frac{S_4}{S_2}\left(1.95104-\frac{101}{120}\log(a^2S_2)\right)\right]\right\},\\
Z_V &= 1+\frac{g^2\,C_F}{16\pi^2}\left\{-15.3291\right.\\
&\quad \left.+a^2\left[S_2\left(-1.33855+\frac{151}{240}\log(a^2S_2)\right)+\frac{S_4}{S_2}\left(2.89896-\frac{101}{120}\log(a^2S_2)\right)\right]\right\},\\
Z_A &= 1+\frac{g^2\,C_F}{16\pi^2}\left\{-13.7927\right.\\
&\quad \left.+a^2\left[S_2\left(-0.92273+\frac{151}{240}\log(a^2S_2)\right)+\frac{S_4}{S_2}\left(2.89896-\frac{101}{120}\log(a^2S_2)\right)\right]\right\},\\
Z_T &= 1+\frac{g^2\,C_F}{16\pi^2}\left\{-11.1325-\log(a^2S_2)\right. \qquad (6.17)\\
&\quad \left.+a^2\left[S_2\left(-1.72760+\frac{221}{240}\log(a^2S_2)\right)+\frac{S_4}{S_2}\left(3.21493-\frac{101}{120}\log(a^2S_2)\right)\right]\right\},\\
Z_{v_{2,a}} &= 1+\frac{g^2\,C_F}{16\pi^2}\left\{6.93831-\frac{8}{3}\log(a^2S_2)-\frac{2}{9}\frac{S_4}{(S_2)^2}\right.\\
&\quad +a^2\left[S_2\left(-1.50680+\frac{167}{180}\log(a^2S_2)\right)\right.\\
&\quad \left.\left.+\frac{S_4}{S_2}\left(2.63125-\frac{197}{180}\log(a^2S_2)\right)-\frac{71}{540}\frac{{S_4}^2}{(S_2)^3}-\frac{82}{135}\frac{S_6}{(S_2)^2}\right]\right\},\\
Z_{v_{2,b}} &= 1+\frac{g^2\,C_F}{16\pi^2}\left\{5.78101-\frac{8}{3}\log(a^2S_2)+\frac{4}{9}\frac{S_4}{(S_2)^2}\right.\\
&\quad +a^2\left[S_2\left(-0.56888+\frac{1}{30}\log(a^2S_2)\right)\right.\\
&\quad \left.\left.+\frac{S_4}{S_2}\left(-0.51323+\frac{19}{30}\log(a^2S_2)\right)+\frac{71}{270}\frac{{S_4}^2}{(S_2)^3}+\frac{164}{135}\frac{S_6}{(S_2)^2}\right]\right\}.
\end{aligned}
$$

Here we have introduced the notation

$$S_n = \sum_{\lambda=1}^{4} p_\lambda^n \,, \tag{6.18}$$

with p_λ being the momentum components. Note that terms of type $(S_4/S_2)\log(a^2 S_2)$, appearing in $Z_S,\ Z_P,\ Z_V,\ Z_A,\ Z_T$, all have the same coefficient which arises solely from the quark wave function renormalization constant Z_q. The corresponding one-loop vertex functions $\Lambda_i(p)$ in (6.6) do not contain such a structure. For later purposes we write the Z factors generically as

$$Z = 1 + \frac{g^2\, C_F}{16\pi^2}\, Z_{1-\mathrm{loop}} + a^2 g^2 Z^{(a^2)}_{1-\mathrm{loop}}(p,a)\,. \tag{6.19}$$

We emphasize that the numerical coefficients in the above expressions are either exact rationals or can be computed to a very high precision.

Below we provide numerical values for the 1-loop renormalization constants $\frac{g^2\, C_F}{16\pi^2}\, Z_{1-\mathrm{loop}}$ at $\beta = 5.40$, so that we have an idea on the significance of $Z^{(a^2)}_{1-\mathrm{loop}}$ for the local operators.

$$\frac{g^2\, C_F}{16\pi^2}\, Z^S_{1-\mathrm{loop}} = -0.218684 + 0.028144\, \log(ap)^2 \tag{6.20}$$

$$\frac{g^2\, C_F}{16\pi^2}\, Z^P_{1-\mathrm{loop}} = -0.247511 + 0.028144\, \log(ap)^2 \tag{6.21}$$

$$\frac{g^2\, C_F}{16\pi^2}\, Z^V_{1-\mathrm{loop}} = -0.143811 \tag{6.22}$$

$$\frac{g^2\, C_F}{16\pi^2}\, Z^A_{1-\mathrm{loop}} = -0.129397 \tag{6.23}$$

$$\frac{g^2\, C_F}{16\pi^2}\, Z^T_{1-\mathrm{loop}} = -0.104440 - 0.009381\, \log(ap)^2 \tag{6.24}$$

In Figs. 6.2, 6.3 and 6.4 we present $a^2 g^2 Z^{(a^2)}_{1-\mathrm{loop}}(p,a)$ for selected operators as a function of a^2p^2 on a finite lattice, where we choose the lattice momenta as $p_\lambda = (2\pi\, i_\lambda)/(a\, L_\lambda)$. Here, i_λ are integers and L_λ is the lattice extension in direction λ. We compare the correction terms for a general set of momenta with those obtained for the momenta used in this investigation at $\beta = 5.40$ on $24^3 \times 48$ lattices and with "diagonal" momenta, i.e., momenta on the diagonal of the Brillouin zone.

The figures show that the momenta of the actually measured Z factors are very close to the diagonal. For clarity of presentation, only a subset of momentum choices have been

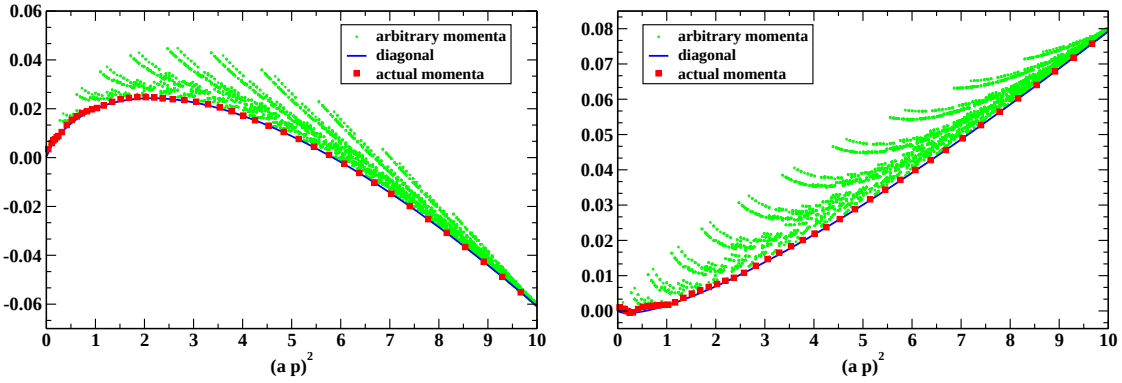

Figure 6.2: The $a^2 g^2 Z^{(a^2)}_{1-\mathrm{loop}}(p,a)$ for operators $\mathcal{O}^S$ (left) and $\mathcal{O}^P$ (right) as a function of a^2p^2 on a $24^3 \times 48$ lattice at $\beta = 5.40$. The green filled circles are the values for an arbitrary set of momenta, whereas the red filled squares are obtained from the momenta used in this investigation. The blue line is computed from diagonal momenta.

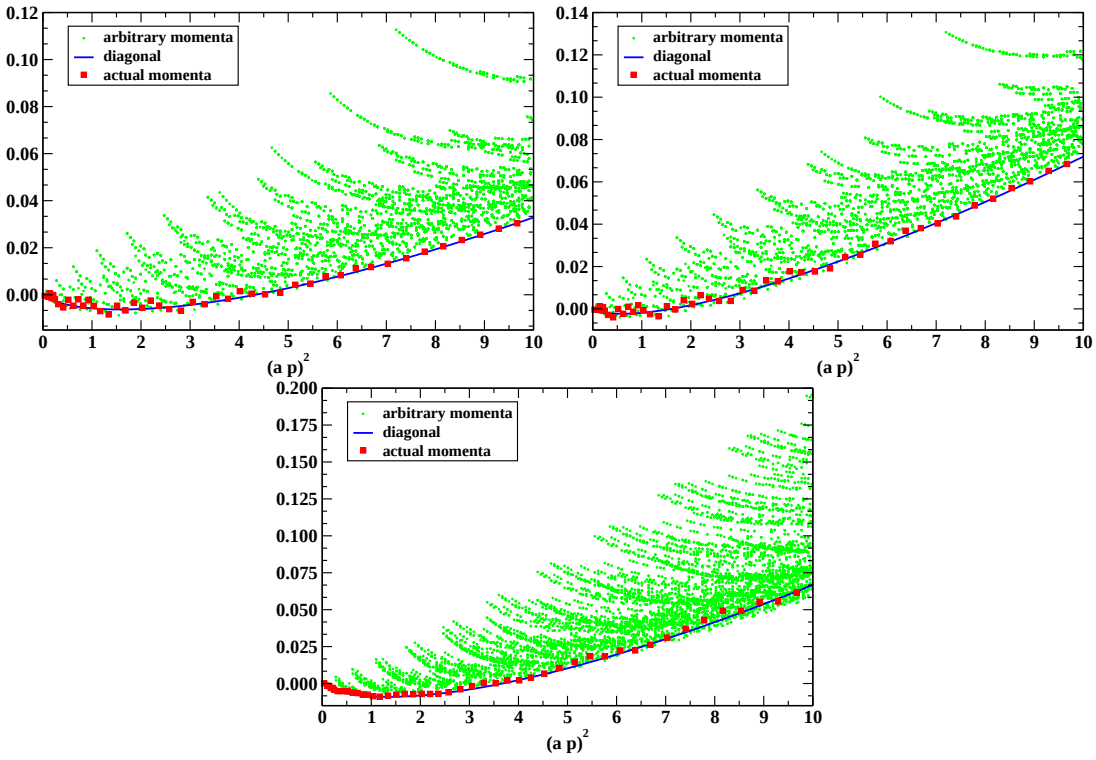

Figure 6.3: The same as Fig. 6.2 but for operators $\mathcal{O}^V$ (left), $\mathcal{O}^A$ (right) and $\mathcal{O}^T$ (lower).

included for $(ap)^2 > 5$. Furthermore, one recognizes that the magnitude of the calculated one-loop a^2 corrections in the used momentum range is small but not negligible compared to the measured values which are of order 1 (see also Fig. 6.1). Therefore, one can expect

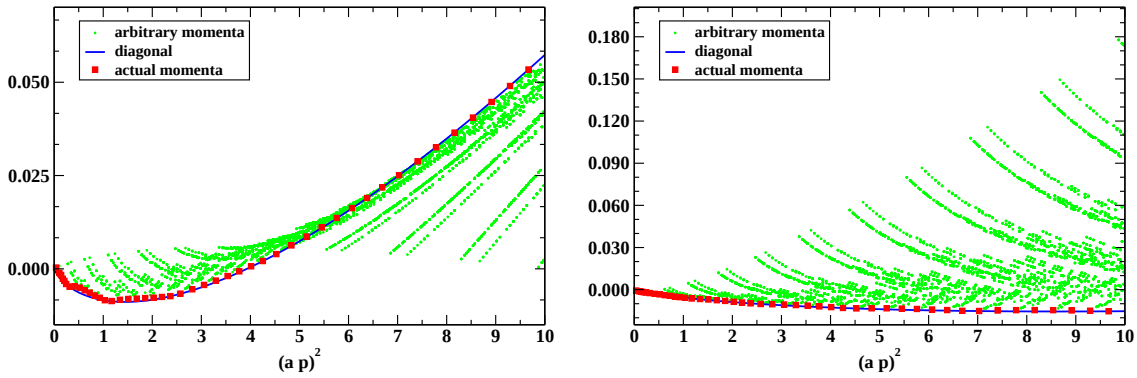

Figure 6.4: The same as Fig. 6.2 but for operators $\mathcal{O}^{v_{2,a}}$ (left) and $\mathcal{O}^{v_{2,b}}$ (right).

that the subtraction of those terms yields a noticeable effect.

6.4.2 Subtraction of lattice artifacts up to order a^2

The subtraction procedure of order a^2 terms is not unique - we can use different definitions. The only restriction is that at one-loop order different procedures should lead to the same estimates for the renormalization functions (treating $Z_{\rm bare}^{\rm RI'-MOM}(p,a)_{\rm MC}$ in perturbation theory). We investigate the following possibilities,

$$Z_{\rm bare}^{\rm RI'-MOM}(p,a)_{\rm MC,sub,s} = Z_{\rm bare}^{\rm RI'-MOM}(p,a)_{\rm MC} - a^2\, g_\star^2\, Z_{\rm 1-loop}^{(a^2)}(p,a)\,, \tag{6.25}$$

$$Z_{\rm bare}^{\rm RI'-MOM}(p,a)_{\rm MC,sub,m} = Z_{\rm bare}^{\rm RI'-MOM}(p,a)_{\rm MC} \times \left(1 - a^2\, g_\star^2\, Z_{\rm 1-loop}^{(a^2)}(p,a)\right)\,, \tag{6.26}$$

where $g_\star$ can be chosen to be either the bare lattice coupling g or the boosted coupling $g_{\rm B}$ (6.15). (In the following we denote subtraction type (6.25) by (**s**) and (6.26) by (**m**)). With ansatz (**s**) the one-loop a^2 correction is subtracted "directly" from $Z_{\rm bare}^{\rm RI'-MOM}(p,a)_{\rm MC}$. Subtraction type (**m**) factorizes the one-loop a^2 correction from the nonperturbative Z factor. We have not performed this procedure on the pseudoscalar operator, because chiral extrabolation of nonperturbative data is rather unstable in this case.

The $Z^{\rm RGI}$ are computed from (6.10) using (**s**) or (**m**), where we expect slightly different numbers depending on the choice of coupling $g_\star$. The only significant errors to $Z_{\rm bare}^{\rm RI'-MOM}(p,a)_{\rm MC,sub}$ are due to the Monte Carlo simulations.

In Fig. 6.5 we show how the subtraction of lattice artifacts (complete and a^2) affects the renormalization constants for the scalar and tensor operators. The complete one-loop subtraction results in a clear plateau for both $Z^{\rm RGI}$ factors. Using the a^2 subtractions

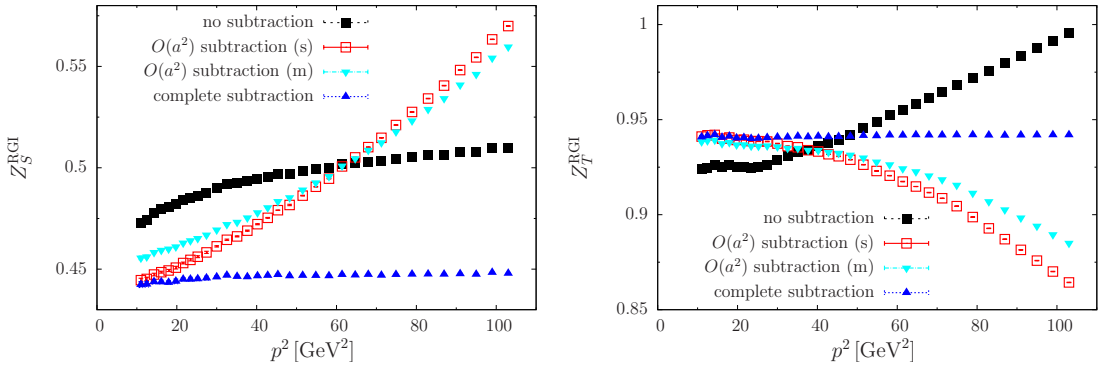

Figure 6.5: Unsubtracted and subtracted renormalization constants for the scalar operator $\mathcal{O}^S$ (left) and the tensor operator $\mathcal{O}^T$ (right) at $\beta = 5.40$, for $p^2 \gtrsim 10\,\mathrm{GeV}^2$ and $r_0\,\Lambda_{\overline{\rm MS}} = 0.700$. The complete subtraction is based on (6.14), whereas the a^2 subtractions are of type (**s**) and (**m**) with $g_\star = g_{\rm B}$.

there remains a more or less pronounced curvature which has to be fitted. From the definitions of the subtraction terms it is clear that they vanish at $a^2p^2 = 0$. Moreover, for small $p^2 \approx 10\,\mathrm{GeV}^2$ the subtraction methods (**s**) and (6.14) already agree, as they should. However, as discussed above, $Z^{\rm RGI}$ can only be determined from sufficiently large momenta ($p^2 \gtrsim 10\,\mathrm{GeV}^2$), where differences arise between the various procedures. Therefore the results for $Z^{\rm RGI}$ may differ depending on the kind of subtraction. As can be seen in Fig. 6.5, this effect varies strongly from operator to operator.

6.4.3 Fit procedure

Compared to the complete one-loop subtraction we expect that $Z^{\rm RI'-MOM}_{\rm bare}(p,a)_{\rm MC,sub}$ as computed from (**s**) or (**m**) contains terms proportional to a^{2n} ($n \geq 2$) even at order g^2, as well as the lattice artifacts from higher orders in perturbation theory, constrained only by hypercubic symmetry. Therefore, we parametrize the subtracted data for each β in terms of the hypercubic invariants S_n defined in (6.18) as follows

$$Z^{\mathcal{S}}_{\rm RI'-MOM}(p)\, Z^{\rm RI'-MOM}_{\rm bare}(p,a)_{\rm MC,sub} = \frac{Z^{\rm RGI}(a)}{\Delta Z^{\mathcal{S}}(p)\,\left[1 + b_1\,(g^{\mathcal{S}})^8\right]} + \tag{6.27}$$
$$a^2\left(c_1\,S_2 + c_2\,\frac{S_4}{S_2} + c_3\,\frac{S_6}{(S_2)^2}\right) + a^4\,\left(c_4\,(S_2)^2 + c_5\,S_4\right) + a^6\left(c_6\,(S_2)^3 + c_7\,S_4\,S_2 + c_8\,S_6\right)\,.$$

There are also further non-polynomial invariants at order a^4, a^6, but their behavior is expected to be well described by the invariants which have been included already. Ansatz

(6.27) is a generalization of (6.16): After the "reduced" one-loop subtraction of lattice artifacts the Z factors are expected to depend more strongly on a^4 or a^6 hypercubic invariants than after the complete one-loop subtraction (see Fig. 6.5). The parameters $c_1, \ldots, c_8$ describe the lattice artifacts.

Together with the target parameter $Z^{\mathrm{RGI}}(a)$ we have ten parameters for this general case. In view of the limited number of data points for each single β value (5.20, 5.25, 5.29, 5.40) we apply the ansatz (6.27) to several β values simultaneously with

$$\frac{Z^{\mathrm{RGI}}(a)}{\Delta Z^{\mathcal{S}}(p)\ [1 + b_1\,(g^{\mathcal{S}})^8]} \to \frac{Z^{\mathrm{RGI}}(a_k)}{\Delta Z_k^{\mathcal{S}}(p)\ [1 + b_1\,(g^{\mathcal{S}})^8]}\,, \tag{6.28}$$

where k labels the corresponding β value ($a_k = a(\beta_k)$). The parameters c_i are taken to be independent of β. This enhances the ratio (number of data points)/(number of fit parameters) significantly and we obtain several $Z^{\mathrm{RGI}}(a_k)$ at once. The fit is performed by a nonlinear model fit which uses - depending on the actual convergence - either the Nelder-Mead or a differential evolution algorithm [123]. Additionally, we have checked some of the fit results using MINUIT [124].

The renormalization factors are influenced by the choice[2] for $r_0\,\Lambda_{\overline{\mathrm{MS}}}$. This quantity enters $\Delta Z^{\mathcal{S}}(M)$ in (6.8) via the corresponding coupling $g^{\mathcal{S}}(M)$ (for details see [117]). We choose $r_0\,\Lambda_{\overline{\mathrm{MS}}} = 0.700$ [125]. In order to estimate the influence of the choice of $r_0\,\Lambda_{\overline{\mathrm{MS}}}$ we also use $r_0\,\Lambda_{\overline{\mathrm{MS}}} = 0.789$ calculated in [126]. The Sommer scale r_0 is chosen to be $r_0 = 0.501\,\mathrm{fm}$ and the relation between the lattice spacing a and the inverse lattice coupling β is given by $r_0/a = 6.050\,(\beta = 5.20), 6.603\,(\beta = 5.25), 7.004\,(\beta = 5.29)$ and $8.285\,(\beta = 5.40)$ [127].

6.5 Renormalization factors for local and one-link operators

The fit procedure as sketched above has quite a few degrees of freedom and it is essential to investigate their influence carefully. A criterion for the choice of the minimal value of p^2 is provided by the breakdown of perturbation theory at small momenta. The data suggest [117] that we are on the "safe side" when choosing $p^2_{\mathrm{min}} = 10\,\mathrm{GeV}^2$. As the upper end of the fit interval we take the maximal available momentum at given coupling β.

[2]The Sommer scale r_0 is a length scale (distance) defined in terms of the force, $F(r)$, between static quarks, satisfying: $r_0^2 F(r_0) = 1.65$.

Other important factors are

- **Type of subtraction:** As discussed above the procedure of the one-loop subtraction is not unique. We choose different definitions (**s**) and (**m**) with either bare g or boosted coupling g_B.
- **Selection of hypercubic invariants:** For the quality of the fit it is essential how well we describe the lattice artifacts which remain after subtraction [128, 129]. This is connected to the question whether the a^2 subtraction has been sufficient to subtract (almost) all a^2 artifacts. Therefore, we perform fits with various combinations of structures with coefficients c_i in (6.27). One should mention that the concrete optimal (i.e. minimal) set of c_i depends strongly on the momenta of the available Monte Carlo data - nearly diagonal momenta require fewer structures to be fitted than far off-diagonal ones.

The analysis should provide an optimal restricted set of parameters which can be used as a guideline for other classes of operators. Nevertheless, one has to inspect every new case carefully.

The results for Z^{RGI} will depend on the above mentioned factors. As a detailed presentation for all operators and β-values would be too lengthy, we select some operators and/or β values and take the corresponding results as a kind of reference. All results presented in this section are computed for $r_0\,\Lambda_{\overline{\mathrm{MS}}} = 0.700$. The choice $r_0\,\Lambda_{\overline{\mathrm{MS}}} = 0.789$ leads to qualitatively similar results. The large number of parameters in ansatz (6.27) calls for a combined use of the data sets at $\beta = (5.20, 5.25, 5.29, 5.40)$ for our fit analysis as indicated in (6.28). With the choice $p^2_{\mathrm{min}} = 10\,\mathrm{GeV}^2$ this results in 94 data points available for the corresponding fits. Additionally, we should note that the errors on our fit parameters are those obtained from the nonlinear model fit. They differ from the error calculation for the Z^{RGI} based on (6.16) and used in [117].

6.5.1 Dependence on the subtraction type

In Fig. 6.6 we present the Z^{RGI} for operators $\mathcal{O}^S$, $\mathcal{O}^V$, $\mathcal{O}^T$ and $\mathcal{O}^{v_{2,a}}$ for the different subtraction types using the fit ansatz (6.27) with all $c_i \neq 0$, i.e., we include a^2, a^4 and a^6 terms. From the discussion in Section 6.4.2 we expect that the resulting differences vary from operator to operator (cf. Fig. 6.5).

From Fig. 6.6 we observe that the complete one-loop subtraction (**1**) and the subtraction (**2**) agree within 1 %. This is not unexpected because the subtraction schemes are similar

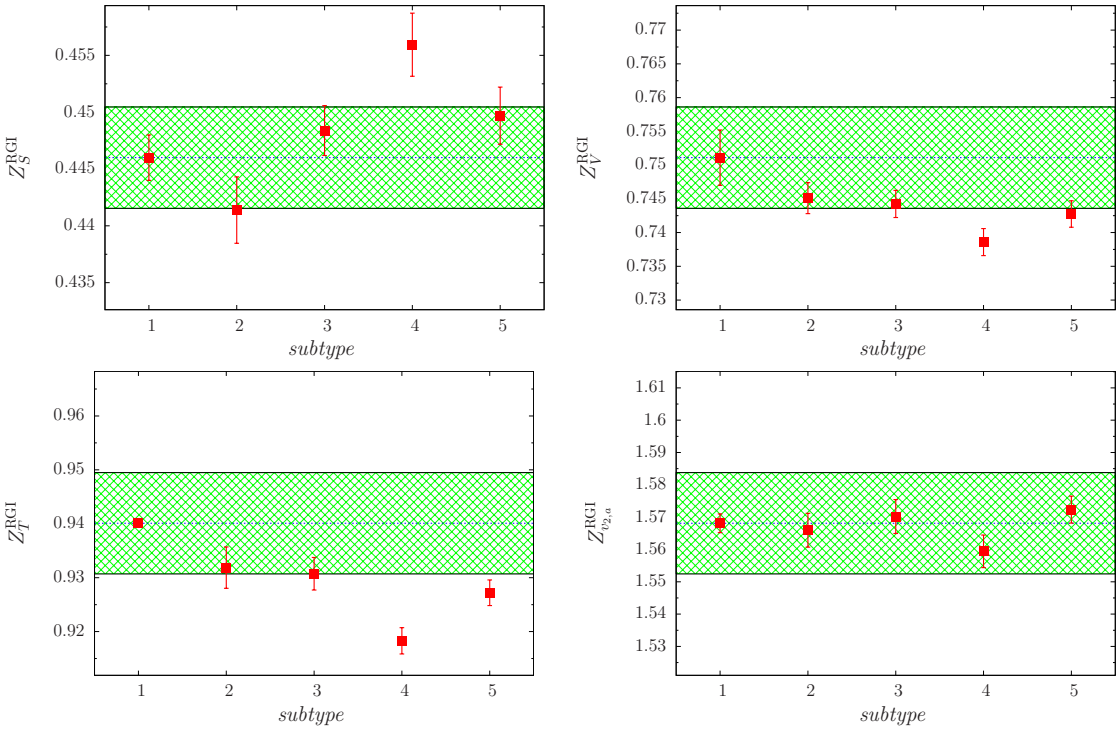

Figure 6.6: Z^{RGI} of selected operators at $\beta = 5.40$ as a function of the subtraction type (*subtype*): **1:** complete subtraction (6.14) with $g_\star = g_B$, **2:** (**s**) with $g_\star = g_B$, **3:** (**m**) with $g_\star = g_B$, **4:** (**s**) with $g_\star = g$, **5:** (**m**) with $g_\star = g$. The horizontal borders of the shaded area show a 1% deviation from case **1**.

and the gauge couplings coincide. The differences in the results for (**2**) and (**3**) can be used as an indication for a systematic uncertainty in the determination of Z^{RGI} based on the schemes (**s,m**). We observe that both subtraction approaches are numerically almost equivalent. Choices (**4**) and (**5**) lead to Z^{RGI} factors which are partly outside the 1 % deviation. Generally, we recognize that all subtraction procedures for both bare and boosted couplings produce fit results within a reasonable error band width.

In order to test the effect of subtraction we compare the g^2a^2 contributions as given in (6.17) with the remaining lattice artifacts of the Monte Carlo data fitted after subtraction, i.e. the result for (6.27) setting $Z^{\mathrm{RGI}}(a) = 0$. In Fig. 6.7 we show the results for the same selected operators choosing g_B. In the small p^2 region the remaining lattice artifacts are significantly smaller than the one-loop a^2 terms (operators $\mathcal{O}^S$, $\mathcal{O}^T$ and $\mathcal{O}^{v_{2,a}}$). In case of already small one-loop a^2 artifacts (operator $\mathcal{O}^V$) the final artifacts remain small. This behavior strongly suggests to subtract the one-loop a^2 terms before applying the fit procedure.

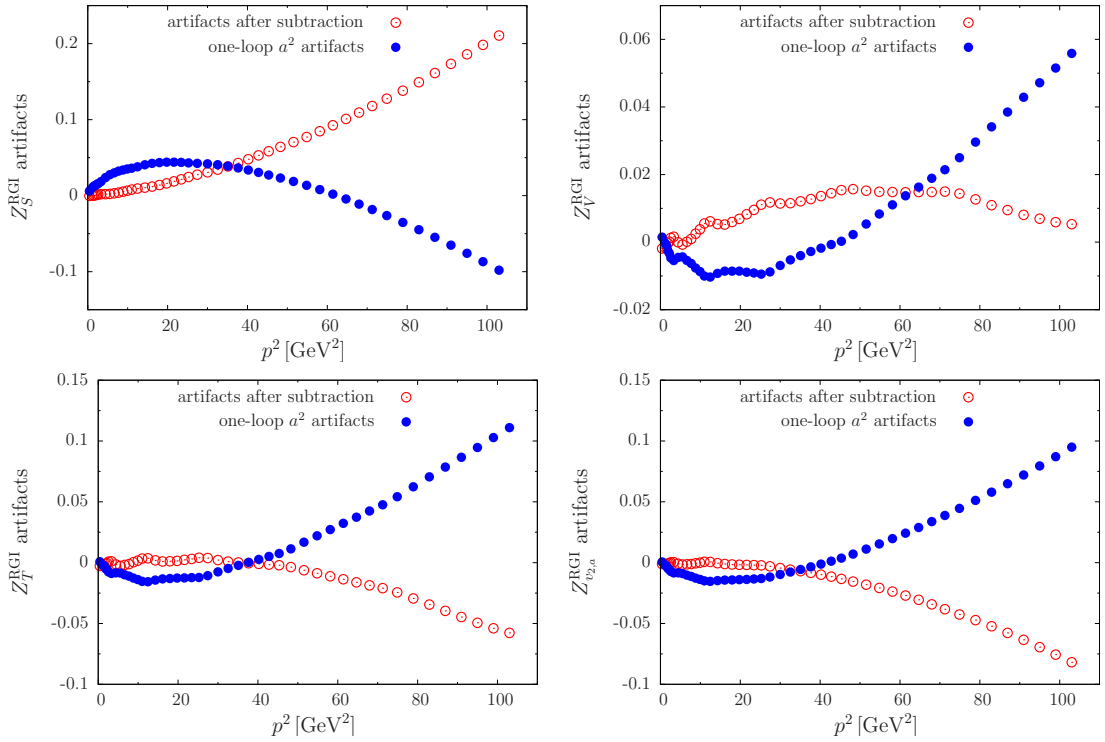

Figure 6.7: Lattice artifacts for Z^{RGI} of selected operators for $\beta = 5.40$ as a function of p^2 choosing $g_\star = g_B$. The blue filled circles are the corresponding g^2a^2 correction terms, the red open circles are the fit results for (6.27) setting $Z^{\mathrm{RGI}}(a) = 0$.

Since the boosted coupling g_B is assumed to remove large lattice artifacts due to tadpole contributions in the perturbative series, we will use g_B in the following. In addition, we restrict ourselves to subtraction type (**s**), which is closest in spirit to the complete one-loop subtraction studied in [117] (leading approximately to a plateau in the Z^{RGI} as a function of p^2).

6.5.2 Dependence on hypercubic invariants

Now we discuss the dependence on the hypercubic invariants included in the fit ansatz (6.27). The goal is to select a reasonable set of parameters to parametrize the remaining lattice artifacts. Figure 6.8 shows the fit results for some Z^{RGI} utilizing different parameter sets $\{c_k\}$. We use the subtraction type (**s**) with $g_\star = g_B$. In that case the results from the complete one-loop subtraction (**1**) serve as reference values.

Generally, we recognize that the resulting RGI renormalization factors do not vary significantly. Most fit results for Z^{RGI} are located in a 1 % deviation band around the

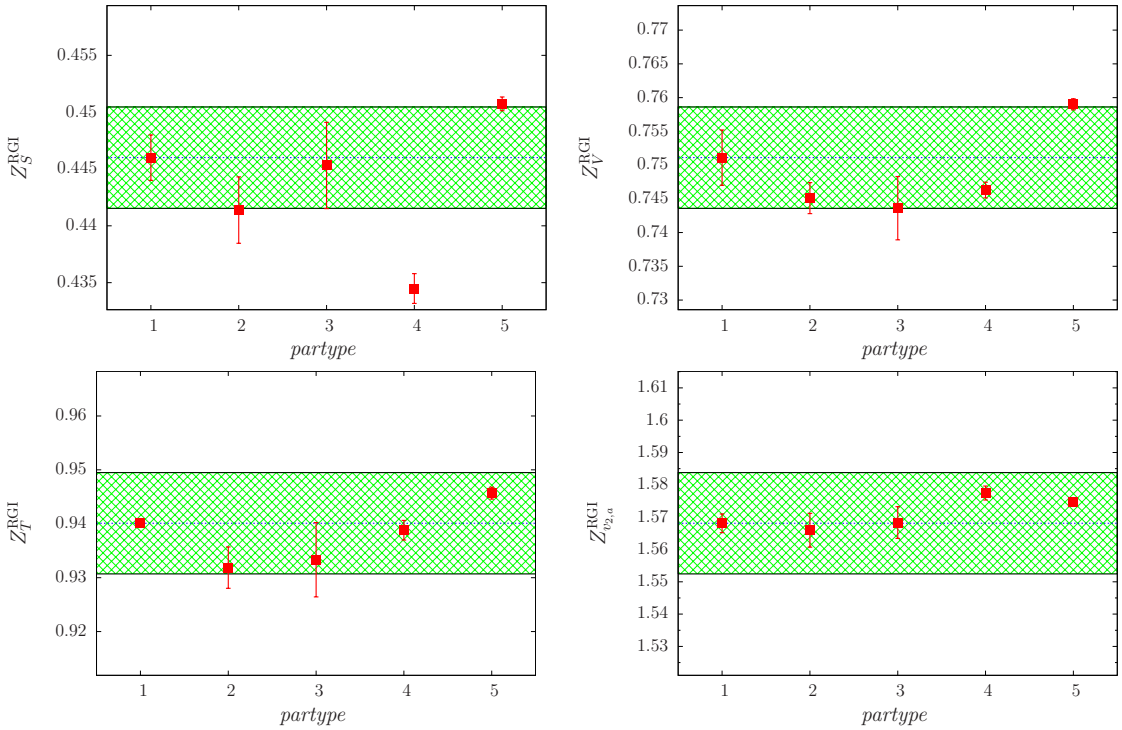

Figure 6.8: Z^{RGI} for selected operators at $\beta = 5.40$ as a function of the parameters included in the fit ansatz (6.27). The used parameter combinations (*partype*) are: **1:** complete one-loop subtraction of lattice artifacts (6.14) **2:** all c_i, **3:** (c_1, c_4, c_6) - $O(4)$ invariant, **4:** $(c_1, c_2, c_3, c_4, c_5)$ - (a^2, a^4)- hypercubic invariants, **5:** $(c_4, c_5, c_6, c_7, c_8)$ - (a^4, a^6)- hypercubic invariants. The horizontal borders of the shaded area show a 1% deviation from case **1**.

corresponding complete subtraction results (**1**). In addition, parametrizations (**2**) and (**3**) give almost identical fit results. This reflects, of course, the fact that our momenta are very close to the diagonal in the Brillouin zone. These restricted momentum sets might be the reason that even "incomplete" hypercubic invariant sets (**4, 5**) can be used to obtain reasonable fits. For the final results we use the fit with all $c_i \neq 0$ which would be natural in the case of more off-diagonal momenta.

In Figs. 6.9, 6.10 and 6.11 we show the results for all operators using the parameter sets with all c_i compared to the results obtained by the subtraction scheme based on (6.14).

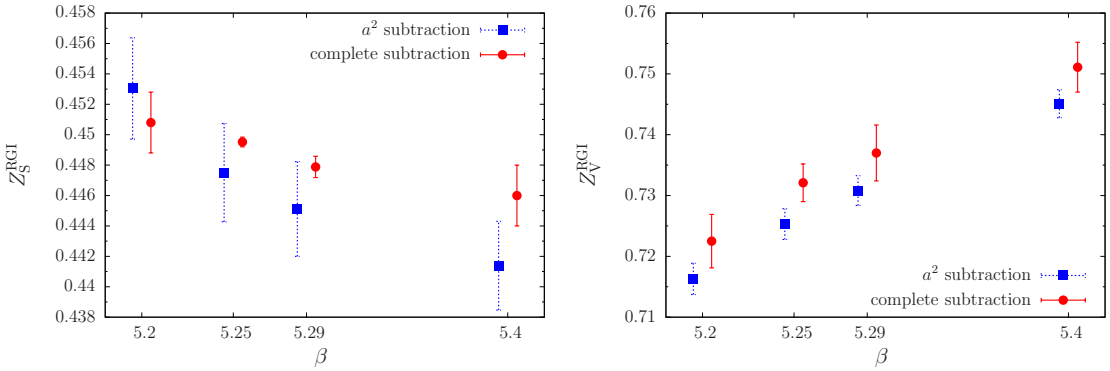

Figure 6.9: $Z_S^{\rm RGI}$ (left) and $Z_V^{\rm RGI}$ (right) at $r_0\,\Lambda_{\overline{\rm MS}} = 0.700$ as a function of β using all c_i compared to the complete one-loop subtraction.

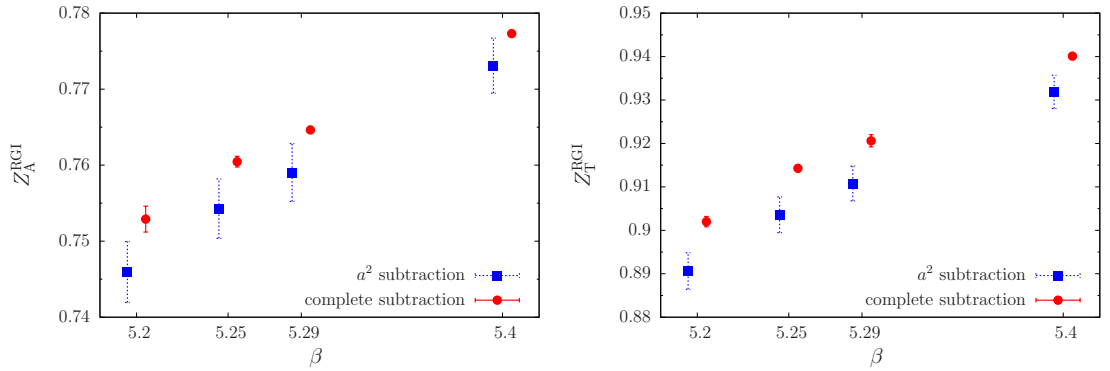

Figure 6.10: The same as in Fig. 6.9 for $Z_A^{\rm RGI}$ (left) and $Z_T^{\rm RGI}$ (right).

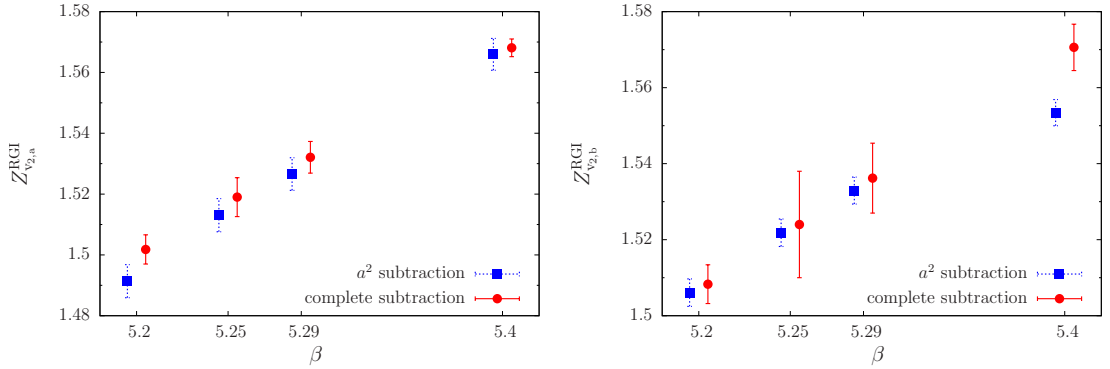

Figure 6.11: The same as in Fig. 6.9 for $Z_{v_{2,a}}^{\rm RGI}$ (left) and $Z_{v_{2,b}}^{\rm RGI}$ (right).

6.6 Results for local and one-link operators and conclusions

As a result of the preceding discussions we use subtraction type (**s**) (Eq. (6.25)) with boosted coupling g_B and the fitting formula (6.27) with all c_i and b_1 coefficients to determine the Z^{RGI}. The final renormalization factors are collected in Table 6.2 using the two different

Op.	$r_0\,\Lambda_{\overline{\mathrm{MS}}}$	$Z^{\mathrm{RGI}}\vert_{\beta=5.20}$	$Z^{\mathrm{RGI}}\vert_{\beta=5.25}$	$Z^{\mathrm{RGI}}\vert_{\beta=5.29}$	$Z^{\mathrm{RGI}}\vert_{\beta=5.40}$
$\mathcal{O}^S$	0.700	0.4530(34)	0.4475(33)	0.4451(32)	0.4414(30)
	0.789	0.4717(44)	0.4661(65)	0.4632(54)	0.4585(27)
$\mathcal{O}^V$	0.700	0.7163(26)	0.7253(26)	0.7308(25)	0.7451(24)
	0.789	0.7238(72)	0.7319(94)	0.7365(99)	0.7519(50)
$\mathcal{O}^A$	0.700	0.7460(41)	0.7543(40)	0.7590(39)	0.7731(37)
	0.789	0.7585(46)	0.7634(77)	0.7666(81)	0.7805(30)
$\mathcal{O}^T$	0.700	0.8906(43)	0.9036(42)	0.9108(41)	0.9319(39)
	0.789	0.8946(85)	0.9041(111)	0.9075(120)	0.9316(49)
$\mathcal{O}^{v_{2,a}}$	0.700	1.4914(55)	1.5131(55)	1.5266(54)	1.5660(53)
	0.789	1.4635(108)	1.4776(112)	1.4926(90)	1.5397(58)
$\mathcal{O}^{v_{2,b}}$	0.700	1.5061(37)	1.5218(37)	1.5329(36)	1.5534(35)
	0.789	1.4601(151)	1.4727(206)	1.4863(165)	1.5115(140)

Table 6.2: Z^{RGI} values using the subtraction (**s**) with g_B.

$r_0\,\Lambda_{\overline{\mathrm{MS}}}$ values 0.700 and 0.789. This shows the influence of the choice of $r_0\,\Lambda_{\overline{\mathrm{MS}}}$ (depending on the anomalous dimension of the operator). For the investigated operators and β values we found for the relative differences of the Z^{RGI}

$$\delta Z^{\mathrm{RGI}} = \left| \frac{Z^{\mathrm{RGI}}_{r_0\,\Lambda_{\overline{\mathrm{MS}}}=0.700} - Z^{\mathrm{RGI}}_{r_0\,\Lambda_{\overline{\mathrm{MS}}}=0.789}}{Z^{\mathrm{RGI}}_{r_0\,\Lambda_{\overline{\mathrm{MS}}}=0.700}} \right| \lesssim 0.04\,. \tag{6.29}$$

For comparison we collect in Table 6.3 the values for Z^{RGI} computed by means of fits with the ansatz (6.16) to data where a complete one-loop subtraction of lattice artifacts

(according to (6.14) with $g_\star = g_{\rm B}$) has been performed. Note that here the errors are determined from the variation of the subtracted data between the scales $\mu^2 = 10,\ 20,\ 30\,\mathrm{GeV}^2$ [117]. The reported renormalization factors are calculated for the values r_0/a given at the

Op.	$r_0\,\Lambda_{\overline{\rm MS}}$	$Z^{\rm RGI}\vert_{\beta=5.20}$	$Z^{\rm RGI}\vert_{\beta=5.25}$	$Z^{\rm RGI}\vert_{\beta=5.29}$	$Z^{\rm RGI}\vert_{\beta=5.40}$
$\mathcal{O}^S$	0.700	0.4508(20)	0.44952(32)	0.44788(70)	0.4460(20)
	0.789	0.4620(85)	0.4603(60)	0.4585(61)	0.4560(48)
$\mathcal{O}^V$	0.700	0.7225(44)	0.7321(31)	0.7370(46)	0.7511(41)
	0.789	0.7219(53)	0.7316(41)	0.7364(55)	0.7506(50)
$\mathcal{O}^A$	0.700	0.7529(17)	0.76046(70)	0.76463(33)	0.77731(20)
	0.789	0.7530(14)	0.76054(48)	0.7647(14)	0.7774(10)
$\mathcal{O}^T$	0.700	0.9020(12)	0.91427(24)	0.9206(14)	0.94009(69)
	0.789	0.8948(40)	0.9072(32)	0.9137(48)	0.9333(38)
$\mathcal{O}^{v_2,a}$	0.700	1.5018(48)	1.5190(64)	1.5321(52)	1.5681(29)
	0.789	1.473(18)	1.490(14)	1.504(12)	1.540(14)
$\mathcal{O}^{v_2,b}$	0.700	1.5083(51)	1.524(14)	1.5362(92)	1.5706(61)
	0.789	1.480(15)	1.497(28)	1.509(23)	1.5436(69)

Table 6.3: $Z^{\rm RGI}$ using a complete one-loop subtraction of lattice artifacts.

end of Section 6.4 and, therefore, differ from those given in [117]. The Z factors of the local operators in both tables agree within 1 %. The Z factors of the one-link operators differ at most by 2 %.

Let us compare our results in Table 6.3 for the local vector current with $Z_V^{\rm RGI}$ obtained from an analysis of the proton electromagnetic form factor [130] following [131], which are listed in Table 6.4. The numbers agree within less than 1 % with the numbers in Table 6.3 ($r_0\,\Lambda_{\overline{\rm MS}} = 0.700$), supporting the complete one-loop subtraction as our reference point.

From the present investigation we conclude: The alternatively proposed "reduced" subtraction algorithm can be used for the determination of the renormalization factors if the complete subtraction method is not available. Possible applications could be Z factors for $N_f = 2+1$ calculations with more complicated fermionic and gauge actions where one-loop

$Z^{\mathrm{RGI}}\vert_{\beta=5.20}$	$Z^{\mathrm{RGI}}\vert_{\beta=5.25}$	$Z^{\mathrm{RGI}}\vert_{\beta=5.29}$	$Z^{\mathrm{RGI}}\vert_{\beta=5.40}$
0.7296(4)	0.7355(3)	0.7401(2)	0.7521(3)

Table 6.4: Z^{RGI} values for operator V from the proton electromagnetic form factor analysis.

results to order a^2 are available (for the fermionic SLiNC action with improved Symanzik gauge action see Chapter 5 and Ref. [122]).

In this study we have analyzed data sets with momenta close to the diagonal of the Brillouin zone. The one-loop a^2 contributions to the Z factors are completely general and can be used for arbitrary (also non-diagonal) momentum sets. Our ansatz (6.27) allows to take into account the remaining artifacts after subtracting these one-loop a^2 terms. To get reasonable fit results the ratio (number of data points)/(number of fit parameters) has to be sufficiently large.

As we pointed out the subtraction type is not unique. With (**s**) and (**m**) we tested two different types. The resulting fits do not give a clear preference for one of these. Even the additional choice for the coupling ($g_\star = g$ or $g_\star = g_B$) does not lead to significantly different results. Therefore, our final choice (**s**) (Eq. (6.25) with $g_\star = g_B$) was supported by "external" arguments: the improved behavior of the boosted perturbative series and the results obtained by complete one-loop subtraction [117].

We have shown that already the one-loop a^2 subtraction improves the behavior of the Z factors significantly: In the small p^2 region the contributions of the remaining lattice artifacts are smaller than the corresponding one-loop a^2 terms. As mentioned above, the accuracy to determine the Z factors is already at the 1 % level for local operators and at the 2 % level for operators with one covariant derivative compared to the complete one-loop subtraction of lattice artifacts. Additional systematic uncertainties are due to the choice of the $r_0\,\Lambda_{\overline{\mathrm{MS}}}$ and r_0/a.

Chapter 7

Renormalization of the Chromomagnetic Operator on the Lattice

In this Chapter we describe our study of the chromomagnetic operator (CMO), which is defined as[1]:

$$\mathcal{O}_{CM} = g\,\overline{\psi}_s\,\sigma_{\mu\nu}\,G_{\mu\nu}\psi_d \tag{7.1}$$

This operator appears in effective Hamiltonians describing semileptonic processes in and beyond the Standard Model. We have computed its Green's functions with two (quark-antiquark) and three (quark-antiquark-gluon) external fields, at nonzero quark masses. Our calculations were performed using both the lattice and dimensional regularization.

Having dimension 5, the chromomagnetic operator is characterized by a rich pattern of mixing with other operators of equal and lower dimensionality, including also non gauge invariant quantities; it is thus quite a challenge to extract from lattice simulations a clear signal for the hadronic matrix elements of this operator.

The lattice computation is carried out using the maximally twisted-mass action for the fermions; for the gluons we employed the Symanzik improved gauge action, for different sets of values of the Symanzik coefficients. In order to find the mixing with other operators we examined the transformation properties of all operators which could possibly mix with $\mathcal{O}_{CM}$. We have identified these operators and we calculated those elements of the mixing matrix which are relevant for the renormalization of $\mathcal{O}_{CM}$. We also computed and present

[1]Notation: g_0: bare coupling constant, $\psi_{s,d}$: s- and d-quark fields, $G_{\mu\nu}$: gluon tensor, $\sigma_{\mu\nu} = (i/2)[\gamma_\mu, \gamma_\nu]$.

the renormalization of the fermion field Z_ψ, of the gluon field Z_A, of the ghost field Z_c and the coupling constant Z_g, which enter the renormalization conditions.

7.1 Introduction

The electroweak effective Hamiltonian describing strangeness changing ($\Delta S = 1$) processes, in the Standard Model (SM) and beyond, contains four "magnetic" operators of dimension 5:

$$H_{\rm eff}^{\Delta S=1,\ d=5} = \sum_{i=\pm} (C_\gamma^i Q_\gamma^i + C_g^i Q_g^i) + \text{h.c.} \tag{7.2}$$

$$Q_\gamma^\pm = \frac{Q_d\, e}{16\pi^2} \left(\bar\psi_{sL}\, \sigma_{\mu\nu}\, F_{\mu\nu}\, \psi_{dR} \pm \bar\psi_{s\,R}\, \sigma_{\mu\nu}\, F_{\mu\nu}\, \psi_{dL}\right), \tag{7.3}$$

$$Q_g^\pm = \frac{g}{16\pi^2} \left(\bar\psi_{sL}\, \sigma_{\mu\nu}\, G_{\mu\nu}\, \psi_{dR} \pm \bar\psi_{sR}\, \sigma_{\mu\nu}\, G_{\mu\nu}\, \psi_{dL}\right) \tag{7.4}$$

In the above expressions, $F_{\mu\nu}$ and $G_{\mu\nu}$ represent the electromagnetic and strong field strength tensors respectively, ψ_s and ψ_d are the strange and down quark fields and the subscripts R, L denote the left/right chiral structure $(1 \pm \gamma_5)$. The coefficients C_γ^i and C_g^i, multiplying the electromagnetic (EMO) and chromomagnetic (CMO) operators, respectively, may be calculated perturbatively via the OPE; they are suppressed within the SM, but become more pronounced beyond the SM, e.g. through penguin diagrams in SUSY.

Some of the most relevant matrix elements of the CMO are parameterized as [132]:

$$\langle \pi^0 | Q_g^+ | K^0 \rangle = \frac{-11}{32\sqrt{2}\pi^2} \frac{M_K^2 (p_\pi \cdot p_K)}{m_s + m_d} B_{g1} \tag{7.5}$$

$$\langle \pi^+\pi^- | Q_g^- | K^0 \rangle = \frac{11\,\mathrm{i}}{32\pi^2} \frac{M_K^2\, M_\pi^2}{f_\pi\, (m_s + m_d)} B_{g2} \tag{7.6}$$

$$\langle \pi^+\pi^+\pi^- | Q_g^+ | K^+ \rangle = \frac{-11}{16\pi^2} \frac{M_K^2\, M_\pi^2}{f_\pi^2\, (m_s + m_d)} B_{g3} \tag{7.7}$$

These matrix elements appear in the study of $K^0 - \bar K^0$ mixing, ϵ'/ϵ, the $\Delta I = 1/2$ rule, and $K \to 3\pi$ decays. To leading order in Chiral Perturbation Theory (χPT), the B-parameters are all related [133]:

$$Q_g^\pm = \frac{11}{256\pi^2} \frac{f_\pi^2\, M_K^2}{m_s + m_d} B_g \left[U(D_\mu U^\dagger)(D^\mu U) \pm (D_\mu U^\dagger)(D^\mu U) U^\dagger\right]_{23} \tag{7.8}$$

Thus, a lattice study of, say, Eq. (7.5), provides information for Eqs. (7.6), (7.7) as well.

The EMO has been studied in simulations with $N_f = 0$ [134] and $N_f = 2$ [135] dynamical flavors, focusing on:

$$\langle \pi^0 | Q_\gamma^+ | K^0 \rangle = \mathrm{i} \frac{Q_d \, e \sqrt{2}}{16\pi^2 \, M_K} \, p_\pi^\mu \, p_K^\nu \, F_{\mu\nu} \, B_T \, R_T(q^2) \qquad [R_T(0) = 1] \tag{7.9}$$

The parameter B_T appears, e.g., in the branching ratio of $K_L \to \pi^0 \, e^+ \, e^-$ in SUSY models.

We focused on the matrix elements of $\mathcal{O}_{CM}$ between a kaon and a pion state. The $K-\pi$ matrix element of $\mathcal{O}_{CM}$ has never been calculated before on the lattice. Its renormalization entails subtraction of operators, which can mix with power divergent coefficients. In general, the renormalization of effective operators is highly non trivial. A serious complication in this case is that operators with the same dimensions as $\mathcal{O}_{CM}$ or lower, and with the same quantum numbers, can mix with $\mathcal{O}_{CM}$ at the quantum level. In order to identify which operators can possibly mix, we exploited the fact that all candidate operators should have the same transformation properties as $\mathcal{O}_{CM}$, and we reduced the number of these operators to a minimal set of 13 operators.

We compute perturbatively the relevant Green's functions of $\mathcal{O}_{CM}$ to determine the renormalization mixing coefficients. The calculations were performed in the continuum (dimensional regularization) and on the lattice using the maximally twisted mass fermion action and the Symanzik improved gluon action. This computation is followed by the construction of the mixing matrix, which involves gauge invariant operators and operators that vanish by the equations of motion. In parallel, non-perturbative measurements of the $K - \pi$ matrix element are being performed by the Roma Tre group, in simulations with 2 dynamical ($N_f = 2$) twisted mass fermions and the Iwasaki improved gluon action.

7.2 Symmetries of the Action and Transformation Properties of operators

We study the mixing of the chromomagnetic operator:

$$\mathcal{O}_{CM} = g_0 \, \overline{\psi}_s \, \sigma_{\mu\nu} \, G_{\mu\nu} \psi_d, \tag{7.10}$$

using both dimensional regularization (DR) and lattice regularization (L). On the lattice we use the fermion setup studied by Frezzotti and Rossi [137, 138, 139]; in particular,

valence quarks are described by the twisted mass action, which in the physical basis reads:

$$S_F[\psi_f,\bar{\psi}_f,U] = a^4 \sum_f \sum_x \bar{\psi}_f(x)\Big[\gamma\cdot\widetilde{\nabla} - i\gamma_5 W_{\rm cr}(r_f) + m_f\Big]\psi_f(x)\,, \tag{7.11}$$

where

$$\gamma\cdot\widetilde{\nabla} \equiv \frac{1}{2}\sum_\mu \gamma_\mu(\nabla^\star_\mu + \nabla_\mu)\,, \tag{7.12}$$

$$W_{\rm cr}(r_f) \equiv -a\frac{r_f}{2}\sum_\mu \nabla^\star_\mu\nabla_\mu + M_{\rm cr}(r_f)\,, \tag{7.13}$$

r_f is the Wilson parameter for the flavor $f = u,\, d,\, s$ and $M_{\rm cr}(r_f)$ is the corresponding critical quark mass ($M_{\rm cr}(-r_f) = -M_{\rm cr}(r_f)$).

The full fermion action includes also a part describing sea quarks, as well as a ghost part (to compensate the valence quark determinant) [138]; these parts will not be needed in our one-loop calculation. For the gluon part we employ the Symanzik improved action described in Eq. (2.17). Our results (Section 7.3.2) will be provided for some of the most popular choices for the Symanzik coefficients.

There exist certain symmetries of the action (valid both in the continuum and lattice formulation of the theory) which reduce considerably the number of operators that can possibly mix with $\mathcal{O}_{CM}$ at the quantum level. These symmetries are defined by means of the discrete transformations $\mathcal{P}$ (continuum parity) and $\mathcal{D}_d$ in the physical basis,

$$\mathcal{P}: \begin{cases} U_0(x) \to U_0(x_{\mathcal{P}})\,, \qquad U_k(x) \to U_k^\dagger(x_{\mathcal{P}} - a\hat{k})\,, \qquad k = 1,2,3 \\ \psi_f(x) \to \gamma_0\psi_f(x_{\mathcal{P}}) \\ \bar{\psi}_f(x) \to \bar{\psi}_f(x_{\mathcal{P}})\gamma_0\,, \end{cases} \tag{7.14}$$

$$\mathcal{D}_d: \begin{cases} U_\mu(x) & \to U_\mu^\dagger(-x - a\hat{\mu}) \\ \psi_f(x) & \to e^{3i\pi/2}\psi_f(-x) \\ \bar{\psi}_f(x) & \to e^{3i\pi/2}\bar{\psi}_f(-x), \end{cases} \tag{7.15}$$

(where $x_{\mathcal{P}} = (-\mathbf{x}, x_0)$ and $\hat{\mu}$ is the unit vector in the μ-direction)

$$\mathcal{R}_5 = \prod_f \mathcal{R}_{f\,5}\,, \qquad \mathcal{R}_{f\,5} : \begin{cases} \psi_f & \to \gamma_5 \psi_f \\ \bar{\psi}_f & \to -\bar{\psi}_f \gamma_5\,, \end{cases} \tag{7.16}$$

$\mathcal{C}$ (charge conjugation; ^{T} means transpose)

$$\mathcal{C} : \begin{cases} \psi(x) \to i\gamma_0\gamma_2 \bar{\psi}(x)^T \\ \bar{\psi}(x) \to -\psi(x)^T i\gamma_0\gamma_2 \\ U_\mu(x) \to U_\mu^\star(x)\,, \quad \mu = 0,1,2,3\,, \end{cases} \tag{7.17}$$

and $\mathcal{S}$ (exchange between the s and the d quark)

$$\mathcal{S} : \begin{cases} \psi_s(x) & \leftrightarrow \psi_d(x) \\ \bar{\psi}_s(x) & \leftrightarrow \bar{\psi}_d(x) \\ m_s & \leftrightarrow m_d\,. \end{cases} \tag{7.18}$$

In terms of the above transformations, the symmetries of the action are[2]:

- $\mathcal{P} \times \mathcal{D}_d \times (m \to -m)$, where m are all masses except $M_{\rm cr}$
- $\mathcal{D}_d \times \mathcal{R}_5$
- $\mathcal{C} \times \mathcal{S}$, if $r_s = r_d$
- $\mathcal{C} \times \mathcal{P} \times \mathcal{S}$, if $r_s = -r_d$.

In order to identify which operators can possibly mix with $\mathcal{O}_{CM}$, we examine the transformation properties of all candidate operators under the above symmetries; admissible

[2]Note that, in the case of $r_s = -r_d$, $\mathcal{CPS}$ will not be a symmetry of the valence part of the action which contains a u quark, since it will require $r_u \to -r_u$. However, the u quark can be dropped from the valence part of the action, since our operator does not contain u quarks, and therefore the Green's functions of interest will also not contain any external u quarks. Nonetheless, it is important to note that the sea quark part of the action is symmetric even in the presence of u, since it is an even function of the Wilson r coefficients [138].

	Operators	$\mathcal{P}\times\mathcal{D}_d\times$ $(m\to -m)$	$\mathcal{D}_d\times\mathcal{R}_5$	$\mathcal{C}\times\mathcal{S}$ if $r_s=r_d$	$\mathcal{C}\times\mathcal{P}\times\mathcal{S}$ if $r_s=-r_d$
Dimension 3 operators					
✓	$\overline{\psi}_s\psi_d$	$-$	$+$	$+$	$+$
	$i\,\overline{\psi}_s\gamma_5\psi_d$	$+$	$+$	$+$	$-$
Dimension 4 operators					
	$(m_d+m_s)\overline{\psi}_s\psi_d$	$+$	$+$	$+$	$+$
	$(m_d-m_s)\overline{\psi}_s\psi_d$	$+$	$+$	$-$	$-$
$(+)$	$i\,(m_d+m_s)\overline{\psi}_s\gamma_5\psi_d$	$-$	$+$	$+$	$-$
$(-)$	$i\,(m_d-m_s)\overline{\psi}_s\gamma_5\psi_d$	$-$	$+$	$-$	$+$
	$\overline{\psi}_s(\vec{D}+m_d)\psi_d+\overline{\psi}_s(-\overleftarrow{D}+m_s)\psi_d$	$+$	$+$	$+$	$+$
	$\overline{\psi}_s(\vec{D}+m_d)\psi_d-\overline{\psi}_s(-\overleftarrow{D}+m_s)\psi_d$	$+$	$+$	$-$	$-$
$(+)$	$i\,\overline{\psi}_s\gamma_5(\vec{D}+m_d)\psi_d+i\,\overline{\psi}_s(-\overleftarrow{D}+m_s)\gamma_5\psi_d$	$-$	$+$	$+$	$-$
$(-)$	$i\,\overline{\psi}_s\gamma_5(\vec{D}+m_d)\psi_d-i\,\overline{\psi}_s(-\overleftarrow{D}+m_s)\gamma_5\psi_d$	$-$	$+$	$-$	$+$

Table 7.1: Transformation properties of dimension 3 and 4 operators. Included are gauge invariant operators and operators which vanish by the equations of motion, in the physical basis.

operators must transform in the same way as $\mathcal{O}_{CM}$. Furthermore, by general renormalization theorems, these operators must be gauge invariant, or else they must vanish by the equations of motion.

In Tables 7.1 and 7.2 we present all candidate operators along with their transformation properties. Operators marked by "✓" have the same properties as $\mathcal{O}_{CM}$ and thus may mix with it. Operators marked by "$(+)$" or "$(-)$" have the same transformation properties as $\mathcal{O}_{CM}$ only if $r_s=r_d$ or $r_s=-r_d$, respectively; for this reason the Wilson parameters r_s, r_d have been explicitly introduced in $\mathcal{O}_{11}$ and $\mathcal{O}_{12}$ below (see Eqs. (7.29) - (7.30)). There

	Dimension 5 Operators	$\mathcal{P}\times\mathcal{D}_d\times$ $(m\to -m)$	$\mathcal{D}_d\times\mathcal{R}_5$	$\mathcal{C}\times\mathcal{S}$ if $r_s=r_d$	$\mathcal{C}\times\mathcal{P}\times\mathcal{S}$ if $r_s=-r_d$
✓	$g_0\,\overline{\psi}_s\sigma_{\mu\nu}G_{\mu\nu}\psi_d$	−	+	+	+
	$i\,g_0\,\overline{\psi}_s\gamma_5\sigma_{\mu\nu}G_{\mu\nu}\psi_d$	+	+	+	−
✓	$(m_d^2+m_s^2)\overline{\psi}_s\psi_d$	−	+	+	+
	$i\,(m_d^2+m_s^2)\overline{\psi}_s\gamma_5\psi_d$	+	+	+	−
	$(m_d^2-m_s^2)\overline{\psi}_s\psi_d$	−	+	−	−
	$i\,(m_d^2-m_s^2)\overline{\psi}_s\gamma_5\psi_d$	+	+	−	+
✓	$m_d\,m_s\overline{\psi}_s\psi_d$	−	+	+	+
	$i\,m_d\,m_s\overline{\psi}_s\gamma_5\psi_d$	+	+	+	−
✓	$m_s\overline{\psi}_s(\vec{D}+m_d)\psi_d+m_d\overline{\psi}_s(-\overleftarrow{D}+m_s)\psi_d$	−	+	+	+
✓	$m_d\overline{\psi}_s(\vec{D}+m_d)\psi_d+m_s\overline{\psi}_s(-\overleftarrow{D}+m_s)\psi_d$	−	+	+	+
	$m_s\overline{\psi}_s(\vec{D}+m_d)\psi_d-m_d\overline{\psi}_s(-\overleftarrow{D}+m_s)\psi_d$	−	+	−	−
	$m_d\overline{\psi}_s(\vec{D}+m_d)\psi_d-m_s\overline{\psi}_s(-\overleftarrow{D}+m_s)\psi_d$	−	+	−	−
	$i\,m_s\overline{\psi}_s\gamma_5(\vec{D}+m_d)\psi_d+i\,m_d\overline{\psi}_s(-\overleftarrow{D}+m_s)\gamma_5\psi_d$	+	+	+	−
	$i\,m_d\overline{\psi}_s\gamma_5(\vec{D}+m_d)\psi_d+i\,m_s\overline{\psi}_s(-\overleftarrow{D}+m_s)\gamma_5\psi_d$	+	+	+	−
	$i\,m_s\overline{\psi}_s\gamma_5(\vec{D}+m_d)\psi_d-i\,m_d\overline{\psi}_s(-\overleftarrow{D}+m_s)\gamma_5\psi_d$	+	+	−	+
	$i\,m_d\overline{\psi}_s\gamma_5(\vec{D}+m_d)\psi_d-i\,m_s\overline{\psi}_s(-\overleftarrow{D}+m_s)\gamma_5\psi_d$	+	+	−	+
✓	$\overline{\psi}_s(\vec{D}+m_d)^2\psi_d+\overline{\psi}_s(-\overleftarrow{D}+m_s)^2\psi_d$	−	+	+	+
	$\overline{\psi}_s(\vec{D}+m_d)^2\psi_d-\overline{\psi}_s(-\overleftarrow{D}+m_s)^2\psi_d$	−	+	−	−
	$i\,\overline{\psi}_s\gamma_5(\vec{D}+m_d)^2\psi_d+i\,\overline{\psi}_s(-\overleftarrow{D}+m_s)^2\gamma_5\psi_d$	+	+	+	−
	$i\,\overline{\psi}_s\gamma_5(\vec{D}+m_d)^2\psi_d-i\,\overline{\psi}_s(-\overleftarrow{D}+m_s)^2\gamma_5\psi_d$	+	+	−	+
✓	$\overline{\psi}_s\overleftarrow{D}_\mu\overrightarrow{D}_\mu\psi_d$	−	+	+	+
	$i\,\overline{\psi}_s\gamma_5\overleftarrow{D}_\mu\overrightarrow{D}_\mu\psi_d$	+	+	+	−
✓	$\overline{\psi}_s(-\overleftarrow{D}+m_s)\,(\vec{D}+m_d)\psi_d$	−	+	+	+
	$i\,\overline{\psi}_s(-\overleftarrow{D}+m_s)\,\gamma_5\,(\vec{D}+m_d)\psi_d$	+	+	+	−
✓	$\overline{\psi}_s\overleftarrow{\not{D}}\,(\vec{D}+m_d)\psi_d-\overline{\psi}_s(-\overleftarrow{D}+m_s)\overrightarrow{\not{D}}\,\psi_d$	−	+	+	+
✓	$\overline{\psi}_s\overrightarrow{\not{D}}\,(\vec{D}+m_d)\psi_d-\overline{\psi}_s(-\overleftarrow{D}+m_s)\overleftarrow{\not{D}}\,\psi_d$	−	+	+	+
	$\overline{\psi}_s\overleftarrow{\not{D}}\,(\vec{D}+m_d)\psi_d+\overline{\psi}_s(-\overleftarrow{D}+m_s)\overrightarrow{\not{D}}\,\psi_d$	−	+	−	−
	$\overline{\psi}_s\overrightarrow{\not{D}}\,(\vec{D}+m_d)\psi_d+\overline{\psi}_s(-\overleftarrow{D}+m_s)\overleftarrow{\not{D}}\,\psi_d$	−	+	−	−
	$i\,\overline{\psi}_s\overleftarrow{\not{D}}\,\gamma_5(\vec{D}+m_d)\psi_d-i\,\overline{\psi}_s(-\overleftarrow{D}+m_s)\gamma_5\overrightarrow{\not{D}}\,\psi_d$	+	+	+	−
	$i\,\overline{\psi}_s\overrightarrow{\not{D}}\,\gamma_5(\vec{D}+m_d)\psi_d-i\,\overline{\psi}_s(-\overleftarrow{D}+m_s)\gamma_5\overleftarrow{\not{D}}\,\psi_d$	+	+	+	−
	$i\,\overline{\psi}_s\overleftarrow{\not{D}}\,\gamma_5(\vec{D}+m_d)\psi_d+i\,\overline{\psi}_s(-\overleftarrow{D}+m_s)\gamma_5\overrightarrow{\not{D}}\,\psi_d$	+	+	−	+
	$i\,\overline{\psi}_s\overrightarrow{\not{D}}\,\gamma_5(\vec{D}+m_d)\psi_d+i\,\overline{\psi}_s(-\overleftarrow{D}+m_s)\gamma_5\overleftarrow{\not{D}}\,\psi_d$	+	+	−	+

Table 7.2: Transformation properties of gauge invariant operators and of operators which vanish by the equations of motion, in the physical basis (Operator dimension = 5).

follows immediately that $\mathcal{O}_{CM} \equiv \mathcal{O}_1$ can only mix with the following operators:

$$\mathcal{O}_1 = g_0\,\overline{\psi}_s\sigma_{\mu\nu}G_{\mu\nu}\psi_d \tag{7.19}$$

$$\mathcal{O}_2 = (m_d^2 + m_s^2)\overline{\psi}_s\psi_d \tag{7.20}$$

$$\mathcal{O}_3 = m_d\, m_s\overline{\psi}_s\psi_d \tag{7.21}$$

$$\mathcal{O}_4 = \overline{\psi}_s\overleftarrow{D}_\mu\overrightarrow{D}_\mu\psi_d \tag{7.22}$$

$$\mathcal{O}_5 = \overline{\psi}_s(-\overleftarrow{D} + m_s)(\vec{D} + m_d)\psi_d \tag{7.23}$$

$$\mathcal{O}_6 = \overline{\psi}_s(\vec{D} + m_d)^2\psi_d + \overline{\psi}_s(-\overleftarrow{D} + m_s)^2\psi_d \tag{7.24}$$

$$\mathcal{O}_7 = m_s\overline{\psi}_s(\vec{D} + m_d)\psi_d + m_d\overline{\psi}_s(-\overleftarrow{D} + m_s)\psi_d \tag{7.25}$$

$$\mathcal{O}_8 = m_d\overline{\psi}_s(\vec{D} + m_d)\psi_d + m_s\overline{\psi}_s(-\overleftarrow{D} + m_s)\psi_d \tag{7.26}$$

$$\mathcal{O}_9 = \overline{\psi}_s\overleftarrow{\not{\partial}}\,(\vec{D} + m_d)\psi_d - \overline{\psi}_s(-\overleftarrow{D} + m_s)\overrightarrow{\not{\partial}}\,\psi_d \tag{7.27}$$

$$\mathcal{O}_{10} = \overline{\psi}_s\overrightarrow{\not{\partial}}\,(\vec{D} + m_d)\psi_d - \overline{\psi}_s(-\overleftarrow{D} + m_s)\overleftarrow{\not{\partial}}\,\psi_d \tag{7.28}$$

$$\mathcal{O}_{11} = i\,r_d\,\overline{\psi}_s\gamma_5(\vec{D} + m_d)\psi_d + i\,r_s\,\overline{\psi}_s(-\overleftarrow{D} + m_s)\gamma_5\psi_d \tag{7.29}$$

$$\mathcal{O}_{12} = i\,(r_d\,m_d + r_s\,m_s)\overline{\psi}_s\gamma_5\psi_d \tag{7.30}$$

$$\mathcal{O}_{13} = \overline{\psi}_s\,\psi_d\,, \tag{7.31}$$

where left and right covariant derivatives are defined in terms of the gluon field A_μ as follows:

$$\overrightarrow{D}_\mu = \overrightarrow{\partial}_\mu + ig_0A_\mu\,, \tag{7.32}$$

$$\overleftarrow{D}_\mu = \overleftarrow{\partial}_\mu - ig_0A_\mu\,. \tag{7.33}$$

For the parameters r_s, r_d, in our perturbative calculation we have made the (independent) choices of values $r_s = \pm 1,\ r_d = \pm 1$, consistently with their values in simulations.

Operators $\mathcal{O}_9$ and $\mathcal{O}_{10}$ are not gauge invariant, but they are admissible candidates for

mixing, since they vanish by the equations of motion; indeed, they will mix with $\mathcal{O}_{CM}$ both in dimensional regularization and on the lattice. The operators $\mathcal{O}_{11}$, $\mathcal{O}_{12}$, $\mathcal{O}_{13}$ are of lower dimension and thus they do not mix with $\mathcal{O}_1$ in dimensional regularization; they do however show up in the lattice formulation.

7.3 Renormalization functions

The operators $\mathcal{O}_i^R$ are related to the bare ones, $\mathcal{O}_i$ $(i = 1, \ldots, 13)$, through:

$$\mathcal{O}_i = \sum_{j=1}^{13} Z_{ij} \mathcal{O}_j^R \quad \text{(in matrix notation : } \mathcal{O} = Z\mathcal{O}^R\text{)}\,. \tag{7.34}$$

The 13×13 mixing matrix Z_{ij} should more properly be denoted as $Z_{ij}^{X,Y}$, where $X = DR, L, \ldots$ is the regularization and $Y = RI', \overline{\rm MS}, \ldots$ is the renormalization scheme. It obeys:

$$Z = \mathbb{1} + \mathcal{O}(g^2)\,, \tag{7.35}$$

where g is the renormalized coupling constant; in particular,

$$\mathcal{O}_i^R = \sum_{j=1}^{13} \left(Z^{-1}\right)_{ij} \mathcal{O}_j\,, \qquad Z^{-1} = 2 \cdot \mathbb{1} - Z + \mathcal{O}(g^4)\,. \tag{7.36}$$

Since we are interested in $\mathcal{O}_1^R$ we calculate the first row of the mixing matrix: $Z_i \equiv Z_{1i}$. We note that $Z_i = \mathcal{O}(g^2)$ for $i > 1$, and $Z_1 = 1 + g^2\, z_1 + \mathcal{O}(g^4)$.

Since renormalization conditions are typically imposed on amputated renormalized Green's functions, let us relate the latter to the bare ones. For the quark-antiquark Green's functions:

$$\begin{aligned}
\langle \psi^R\, \mathcal{O}_1^R\, \overline{\psi}^R \rangle_{\rm amp} &= \langle \psi^R\, \overline{\psi}^R \rangle^{-1}\, \langle \psi^R\, \mathcal{O}_1^R\, \overline{\psi}^R \rangle\, \langle \psi^R\, \overline{\psi}^R \rangle^{-1} \\
&= \left(Z_\psi\, \langle \psi\, \overline{\psi} \rangle^{-1}\right) \left(Z_\psi^{-1} \sum_{i=1}^{13} (Z^{-1})_{1i} \langle \psi\, \mathcal{O}_i\, \overline{\psi} \rangle\right) \left(Z_\psi\, \langle \psi\, \overline{\psi} \rangle^{-1}\right) \\
&= Z_\psi \sum_{i=1}^{13} (Z^{-1})_{1i} \langle \psi\, \mathcal{O}_i\, \overline{\psi} \rangle_{\rm amp}\,, \quad \psi = \sqrt{Z_\psi}\, \psi^R\,.
\end{aligned} \tag{7.37}$$

The one-loop Feynman diagrams contributing to $\langle \psi\, \mathcal{O}_1\, \overline{\psi} \rangle_{\rm amp}$ are shown in Fig. 7.1. Note that Eq. (7.37) holds for an arbitrary regularization and arbitrary renormalization scheme;

the only condition on the renormalization scheme is that it be mass-independent, in which case the quark field renormalization constant Z_ψ does not depend on flavor. To avoid heavy notation we have omitted coordinate/momentum arguments on ψ, $\mathcal{O}$, as well as Dirac/flavor indices on $\langle \psi\, \overline{\psi} \rangle$, $\langle \psi\, \mathcal{O}\, \overline{\psi} \rangle$, etc.

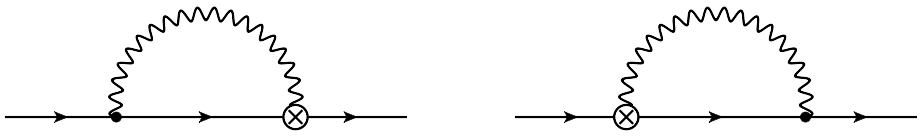

Figure 7.1: One-loop Feynman diagrams contributing to the 2-pt Green's function of the chromomagnetic operator, $\mathcal{O}_1$. A wavy (solid) line represents gluons (quarks). A cross denotes the insertion of $\mathcal{O}_1$.

Similarly for quark-antiquark-gluon Green's functions we have:

$$\langle \psi^R\, \mathcal{O}_1^R\, \overline{\psi}^R A_\nu^R \rangle_{\rm amp} = Z_\psi\, Z_A^{1/2} \sum_{i=1}^{13} (Z^{-1})_{1i} \langle \psi\, \mathcal{O}_i\, \overline{\psi}\, A_\nu \rangle_{\rm amp}\,, \quad A_\nu = \sqrt{Z_A}\, A_\nu^R\,. \tag{7.38}$$

[Strictly speaking, in the right-hand sides of Eqs. (7.37) and (7.38) one must take the regulator to its limit value (i.e. $\epsilon \to 0$ in dimensional regularization or $a \to 0$ on the lattice). This limit is convergent, provided all renormalization functions Z have been appropriately chosen. It is only in this limit that the right-hand sides of Eqs. (7.37) and (7.38) are equal to the corresponding left-hand sides.]

The one-loop Feynman diagrams contributing to $\langle \psi\, \mathcal{O}_1\, \overline{\psi}\, A_\nu \rangle_{\rm amp}$ are shown in Fig. 7.2 (one-particle irreducible (1PI)) and Fig. 7.3 (one-particle reducible (1PR)).

Imposing renormalization conditions of the above 2- and 3-pt Green's functions is sufficient[3] in order to obtain all Z_i.

In some definitions of $\mathcal{O}_{CM}$ (see, e.g., [136]) there is an extra factor of a quark mass:

$$\widetilde{\mathcal{O}}_{CM} \equiv m\, \mathcal{O}_{CM}\,, \tag{7.39}$$

where m is the mass of one of the quark flavors. The renormalized mass m^R is given by

[3] One could of course calculate also 4-pt Green's functions; in doing so, a number of consistency checks would emerge regarding the divergent part of the mixing coefficients Z_i. Further Green's functions (5-pt and above) will bring in no superficial divergences; thus the regulator (in our case, the lattice spacing a) can be taken to its limit right away and no further renormalization conditions or consistency checks will arise.

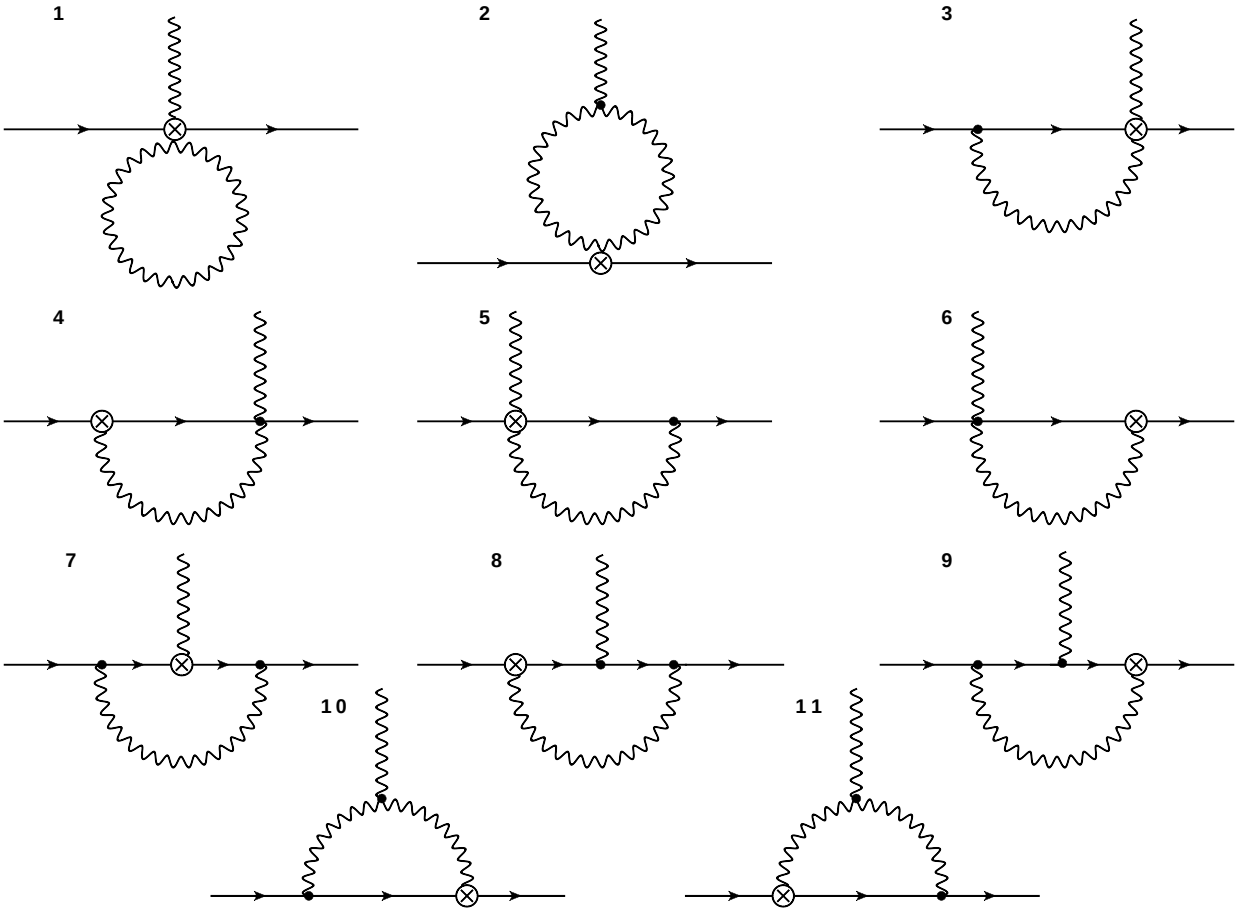

Figure 7.2: 1PI Feynman diagrams which contribute to the 3-pt Green's function of $\mathcal{O}_1$. Diagrams 1, 4, 6 do not appear in dimensional regularization. A wavy (solid) line represents gluons (quarks). A cross denotes the insertion of $\mathcal{O}_1$.

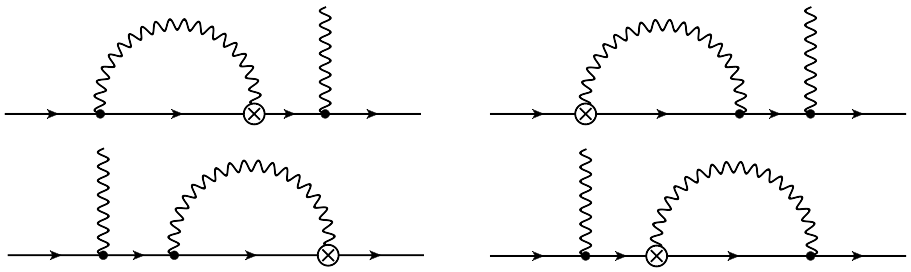

Figure 7.3: 1PR Feynman diagrams which contribute to the 3-pt Green's function of $\mathcal{O}_1$. A wavy (solid) line represents gluons (quarks). A cross denotes the insertion of $\mathcal{O}_1$.

$m^R = Z_m^{-1}\, m$; in a mass-independent scheme, Z_m is also flavor independent, by analogy with Z_ψ. In this case:

$$\begin{aligned}\tilde{\mathcal{O}}_1^R &= m^R\, \mathcal{O}_1^R = m^R \sum_{i=1}^{13} \left(Z^{-1}\right)_{1i} \mathcal{O}_i \\ &= \left(Z_m^{-1}\, m\right) \sum_{i=1}^{13} \left(Z^{-1}\right)_{1i} \mathcal{O}_i = \sum_{i=1}^{13} \left(Z^{-1}\right)_{1i} Z_m^{-1}\, (m\, \mathcal{O}_i)\ . \end{aligned} \tag{7.40}$$

Thus the renormalization matrix $\tilde{Z}_{ij}$ for $\tilde{\mathcal{O}}_{CM}$ is given by: $\tilde{Z}_{ij} = Z_m\, Z_{ij}$.

By analogy with Z_m, a multiplicative factor of Z_g must be included in Z_1, if the calculation of Green's functions involves the operator $\overline{\psi}_s\, \sigma_{\mu\nu}\, G_{\mu\nu}\, \psi_d$, rather than $g\, \overline{\psi}_s\, \sigma_{\mu\nu}\, G_{\mu\nu}\, \psi_d$. We will make use of this fact in Eq. (7.61). The calculation of Z_m and Z_g is presented in section 7.4.

In order to impose renormalization conditions, we need the expressions for the tree-level 2-pt and 3-pt Green's functions of $\mathcal{O}_i$, $i = 1, \ldots, 13$. The tree-level parts of the 3-pt amputated bare Green's functions $\langle \psi_s(q_2) \mathcal{O}_i(x) \overline{\psi}_d(q_3)\, A_\nu(q_1) \rangle_{\rm amp}$ are shown (apart from an overall factor of $e^{i\, x\cdot(-q_1-q_2+q_3)}$) in Table 7.3; similarly for the tree-level parts of the 2-pt bare Green's functions $\langle \psi_s(q_2) \mathcal{O}_i(x) \overline{\psi}_d(q_3) \rangle_{\rm amp}$. Note that the tree-level 3-pt Green's functions, despite being amputated, receive also contributions which are not 1PI, as shown in Fig. 7.4. We do not include these in Table 7.3; however, their value can be easily deduced from the corresponding tree-level 2-pt Green's functions.

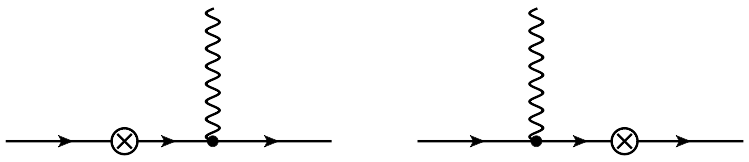

Figure 7.4: 1PR Feynman diagrams contributing to the tree-level 3-pt Green's functions; A wavy (solid) line represents gluons (quarks). A cross denotes the insertion of the operator $\mathcal{O}_i$, $i = 1, \ldots, 13$.

Operators	Tree Level 2-pt	Tree Level 3-pt (1PI)
$\mathcal{O}_1$	0	$-2ig_0\sigma_{\mu\nu}q_{1\mu}$
$\mathcal{O}_2$	$m_d^2+m_s^2$	0
$\mathcal{O}_3$	$m_d m_s$	0
$\mathcal{O}_4$	$q_2\cdot q_3$	$g_0(q_{3\nu}+q_{2\nu})$
$\mathcal{O}_5$	$-\not{q}_2\not{q}_3+i\not{q}_2 m_d+i\not{q}_3 m_s+m_s m_d$	$-g_0(\not{q}_2\gamma_\nu+\gamma_\nu\not{q}_3)+ig_0(m_s+m_d)\gamma_\nu$
$\mathcal{O}_6$	$-q_2^2-q_3^2+2i(m_d\not{q}_3+m_s\not{q}_2)+m_d^2+m_s^2$	$-2g_0 i\sigma_{\mu\nu}q_{1\mu}-2g_0(q_{3\nu}+q_{2\nu})-2ig_0(m_d+m_s)\gamma_\nu$
$\mathcal{O}_7$	$m_s(\ i\not{q}_3+m_d)+m_d(i\not{q}_2+m_s)$	$ig_0(m_s+m_d)\gamma_\nu$
$\mathcal{O}_8$	$m_d(\ i\not{q}_3+m_d)+m_s(i\not{q}_2+m_s)$	$ig_0(m_s+m_d)\gamma_\nu$
$\mathcal{O}_9$	$2\not{q}_2\not{q}_3-i(\not{q}_2 m_d+\not{q}_3 m_s)$	$g_0(\not{q}_2\gamma_\nu+\gamma_\nu\not{q}_3)$
$\mathcal{O}_{10}$	$-q_3^2-q_2^2+i(\not{q}_2 m_s+\not{q}_3 m_d)$	$-2g_0(q_{2\nu}+q_{3\nu})+g_0(\not{q}_2\gamma_\nu+\gamma_\nu\not{q}_3)-2ig_0\sigma_{\mu\nu}q_{1\mu}$
$\mathcal{O}_{11}$	$i\,r_d\gamma_5(i\not{q}_3+m_d)+i\,r_s(i\not{q}_2+m_s)\gamma_5$	$-g_0(r_d-r_s)\gamma_5\gamma_\nu$
$\mathcal{O}_{12}$	$i\,(r_d\,m_d+r_s\,m_s)\gamma_5$	0
$\mathcal{O}_{13}$	1	0

Table 7.3: Operators which will possibly mix with the chromomagnetic operator in the physical basis, along with their tree-level 2-pt and 3-pt (1PI) Green's functions. Here, q_1 is the external gluon momentum and $q_2(q_3)$ is the external quark (antiquark) momentum.

7.3.1 Dimensional Regularization

The next step in our renormalization procedure is to calculate the $\overline{\rm MS}$-renormalized 2-pt and 3-pt Green's functions of $\mathcal{O}_{CM}$; in order to do so, we must regularize the theory in D-dimensions ($D = 4 - 2\,\epsilon$), in the continuum. The general form of the $\mathcal{O}\,(1/\epsilon)$ part of the bare Green's functions is:

$$\begin{aligned}\langle \psi\, \mathcal{O}_1\, \overline{\psi} \rangle^{DR}_{\rm amp}\Big|_{1/\epsilon} &= \rho_1\,(q_2^2 + q_3^2) + \rho_2\,(m_s^2 + m_d^2) + \rho_3\, i\,(m_d\, \not{q}_3 + m_s\, \not{q}_2) \\ &\quad + \rho_4\, i\,(m_s\, \not{q}_3 + m_d\, \not{q}_2) + \rho_5\, q_2.q_3 + \rho_6\, \not{q}_2\, \not{q}_3 + \rho_7\, m_s\, m_d \qquad (7.41)\end{aligned}$$

$$\begin{aligned}\langle \psi\, \mathcal{O}_1\, \overline{\psi} A_\nu \rangle^{DR}_{\rm amp,1PI}\Big|_{1/\epsilon} &= R_1\, g\,(q_2 + q_3)_\nu + R_2\, g\,(\gamma_\nu\, \not{q}_3 + \not{q}_2\, \gamma_\nu) + R_3\, i\, g\,(m_s + m_d)\,\gamma_\nu \\ &\quad + R_4\,(-2\, i\, g\, \sigma_{\rho\nu}\, q_{1\rho}\,) \qquad (7.42)\end{aligned}$$

where g is the renormalized coupling constant in the $\overline{\rm MS}$ scheme, which is related to the bare coupling constant in dimensional regularization, g_0^{DR} , through: $g = \mu^{-\epsilon}\,(Z_g^{DR,\overline{\rm MS}})^{-1}\, g_0^{DR}$ and ρ_i, R_i are numerical coefficients. Computing ρ_i, R_i to one loop we find:

$$\rho_1 = \frac{g^2\,C_F}{16\,\pi^2}\left(-\frac{3}{\epsilon}\right) \tag{7.43}$$

$$\rho_2 = \frac{g^2\,C_F}{16\,\pi^2}\left(-\frac{6}{\epsilon}\right) \tag{7.44}$$

$$\rho_3 = \frac{g^2\,C_F}{16\,\pi^2}\left(\frac{3}{\epsilon}\right) \tag{7.45}$$

$$\rho_4 = \rho_5 = \rho_6 = \rho_7 = 0 \tag{7.46}$$

$$R_1 = \frac{g^2\,C_F}{16\,\pi^2}\left(\frac{-6}{\epsilon}\right) \tag{7.47}$$

$$R_2 = \frac{g^2}{16\,\pi^2}\left(\frac{3\,N_c}{4\,\epsilon}\right) \tag{7.48}$$

$$R_3 = \frac{g^2}{16\,\pi^2}\left(-\frac{3}{2\,N_c\,\epsilon}+\frac{3\,N_c}{4\,\epsilon}\right) \tag{7.49}$$

$$R_4 = \frac{g^2}{16\,\pi^2}\left(\frac{1}{N_c\,\epsilon}-\frac{\alpha}{2\,N_c\,\epsilon}+\frac{7\,N_c}{4\,\epsilon}+\frac{3\,\alpha\,N_c}{4\,\epsilon}\right)\,. \tag{7.50}$$

Here, N_c: number of colors, $C_F = (N_c^2-1)/(2\,N_c)$: quadratic Casimir operator in the fundamental representation, α: gauge parameter ($\alpha = 1 (\alpha = 0)$ corresponds to Feynman (Landau) gauge).

We have also computed the finite parts ($\mathcal{O}(\epsilon^0)$) for the above Green's functions, which are just the corresponding $\overline{\rm MS}$-renormalized Green's functions. These are irrelevant for the computation of the mixing coefficients in the $\overline{\rm MS}$ scheme in dimensional regularization; however, they are necessary in the calculation of Z_{ij} with lattice regularization and $\overline{\rm MS}$ renormalization, see Section 7.3.2. Using the form of Eqs. (7.41) - (7.42) and the tree-level Green's functions of the various operators (Table 7.3), we construct a set of equations for the disentanglement of the mixing coefficients; in particular, by demanding that the coefficients of $\mathcal{O}(1/\epsilon)$ in the left-hand sides of Eqs. (7.37) - (7.38) vanish, we obtain [4]:

[4]Note that Eq. (7.38) will also contain $\mathcal{O}\,(1/\epsilon)$ terms which are not polynomial in q_i, m; such terms arise from the 1PR one-loop 3-pt Green's function of $\mathcal{O}_1$ (Fig. 7.3) and from the 1PR tree-level Green's functions of $\mathcal{O}_2,\ldots,\mathcal{O}_{13}$ (Fig. 7.4). By Eq. (7.37) all such terms cancel out among themselves.

$$-\,Z_6^{DR,\overline{\rm MS}} - Z_{10}^{DR,\overline{\rm MS}} = \rho_1 \tag{7.51}$$

$$Z_2^{DR,\overline{\rm MS}} + Z_6^{DR,\overline{\rm MS}} + Z_8^{DR,\overline{\rm MS}} = \rho_2 \tag{7.52}$$

$$2\,Z_6^{DR,\overline{\rm MS}} + Z_8^{DR,\overline{\rm MS}} + Z_{10}^{DR,\overline{\rm MS}} = \rho_3 \tag{7.53}$$

$$-\,Z_5^{DR,\overline{\rm MS}} - Z_7^{DR,\overline{\rm MS}} + Z_9^{DR,\overline{\rm MS}} = \rho_4 \tag{7.54}$$

$$-\,Z_4^{DR,\overline{\rm MS}} = \rho_5 \tag{7.55}$$

$$-\,Z_5^{DR,\overline{\rm MS}} + 2\,Z_9^{DR,\overline{\rm MS}} = \rho_6 \tag{7.56}$$

$$-\,Z_3^{DR,\overline{\rm MS}} - Z_5^{DR,\overline{\rm MS}} - 2\,Z_7^{DR,\overline{\rm MS}} = \rho_7 \tag{7.57}$$

$$Z_4^{DR,\overline{\rm MS}} - 2\,Z_6^{DR,\overline{\rm MS}} - 2\,Z_{10}^{DR,\overline{\rm MS}} = R_1 \tag{7.58}$$

$$-\,Z_5^{DR,\overline{\rm MS}} + Z_9^{DR,\overline{\rm MS}} + Z_{10}^{DR,\overline{\rm MS}} = R_2 \tag{7.59}$$

$$Z_5^{DR,\overline{\rm MS}} - 2\,Z_6^{DR,\overline{\rm MS}} + Z_7^{DR,\overline{\rm MS}} + Z_8^{DR,\overline{\rm MS}} = R_3 \tag{7.60}$$

$$g^2\,z_1^{DR,\overline{\rm MS}} + Z_6^{DR,\overline{\rm MS}} + Z_{10}^{DR,\overline{\rm MS}} = R_4 + g^2\left(z_\psi^{DR,\overline{\rm MS}} + \frac{1}{2}\,z_A^{DR,\overline{\rm MS}} + z_g^{DR,\overline{\rm MS}}\right) \tag{7.61}$$

where

$$Z_\psi^{DR,\overline{\rm MS}} = 1 + g^2\,z_\psi^{DR,\overline{\rm MS}} + \mathcal{O}(g^4)\,, \quad z_\psi^{DR,\overline{\rm MS}} = \frac{1}{16\,\pi^2}\frac{1}{\epsilon}\,(-C_F\,\alpha) \tag{7.62}$$

$$Z_A^{DR,\overline{\rm MS}} = 1 + g^2\,z_A^{DR,\overline{\rm MS}} + \mathcal{O}(g^4)\,, \quad z_A^{DR,\overline{\rm MS}} = \frac{1}{16\,\pi^2}\frac{1}{\epsilon}\left(\frac{13\,N_c}{6} - \frac{\alpha\,N_c}{2} - \frac{2\,N_f}{3}\right) \tag{7.63}$$

$$Z_g^{DR,\overline{\rm MS}} = 1 + g^2\,z_g^{DR,\overline{\rm MS}} + \mathcal{O}(g^4)\,, \quad z_g^{DR,\overline{\rm MS}} = \frac{1}{16\,\pi^2}\frac{1}{\epsilon}\left(\frac{N_f}{3} - \frac{11\,N_c}{6}\right)\,. \tag{7.64}$$

In particular, Eq. (7.61) stems from the requirement that the coefficients of $(1/\epsilon)(-2ig\sigma_{\mu\nu}q_{1\mu})$

in the left-hand side and right-hand side of Eq. (7.38) coincide:

$$0 = \underbrace{(1+g^2\,z_\psi^{DR,\overline{\rm MS}})\left(1+\frac{1}{2}\,g^2\,z_A^{DR,\overline{\rm MS}}\right)\left(1+g^2\,z_g^{DR,\overline{\rm MS}}\right)(1-g^2\,z_1^{DR,\overline{\rm MS}})(1+R_4)}_{\text{only the } \mathcal{O}(1/\epsilon) \text{ part}}$$
$$- Z_6^{DR,\overline{\rm MS}} - Z_{10}^{DR,\overline{\rm MS}}\,. \tag{7.65}$$

As it stands, the system of 11 equations (Eq. (7.51) - (7.61)) for the 10 unknowns $Z_1^{DR,\overline{\rm MS}} - Z_{10}^{DR,\overline{\rm MS}}$ appears overconstrained; indeed, Eqs. (7.51), (7.55) and (7.58) can only be compatible if $2\,\rho_1 = R_1$. This relation is indeed confirmed by our results (Eq. (7.43) and Eq. (7.47)). The presence of $z_g^{DR,\overline{\rm MS}}$ in Eq. (7.61) stems from the fact that all one-loop Green's functions were calculated with an insertion of $\overline{\psi}_s\,\sigma_{\mu\nu}\,G_{\mu\nu}\,\psi_d$ (rather than $g\,\overline{\psi}_s\,\sigma_{\mu\nu}\,G_{\mu\nu}\,\psi_d$, see comment below Eq. (7.40)).

Solving the above equations, we obtain the mixing coefficients:

$$Z_1^{DR,\overline{\rm MS}} = 1 + \frac{g^2}{16\,\pi^2}\,\frac{1}{\epsilon}\left(-\frac{N_c}{2} + \frac{5}{2\,N_c}\right) \tag{7.66}$$

$$Z_2^{DR,\overline{\rm MS}} = \frac{g^2}{16\,\pi^2}\,\frac{1}{\epsilon}\left(-3\,N_c + \frac{3}{N_c}\right) \tag{7.67}$$

$$Z_3^{DR,\overline{\rm MS}} = 0 \tag{7.68}$$

$$Z_4^{DR,\overline{\rm MS}} = 0 \tag{7.69}$$

$$Z_5^{DR,\overline{\rm MS}} = \frac{g^2}{16\,\pi^2}\,\frac{1}{\epsilon}\left(\frac{3\,N_c}{2} - \frac{3}{N_c}\right) \tag{7.70}$$

$$Z_6^{DR,\overline{\rm MS}} = 0 \tag{7.71}$$

$$Z_7^{DR,\overline{\rm MS}} = \frac{g^2}{16\,\pi^2}\,\frac{1}{\epsilon}\left(-\frac{3\,N_c}{4} + \frac{3}{2\,N_c}\right) \tag{7.72}$$

$$Z_8^{DR,\overline{\rm MS}} = 0 \tag{7.73}$$

$$Z_9^{DR,\overline{\rm MS}} = \frac{g^2}{16\,\pi^2}\,\frac{1}{\epsilon}\left(\frac{3\,N_c}{4} - \frac{3}{2\,N_c}\right) \tag{7.74}$$

$$Z_{10}^{DR,\overline{\rm MS}} = \frac{g^2}{16\,\pi^2}\,\frac{1}{\epsilon}\left(\frac{3\,N_c}{2} - \frac{3}{2\,N_c}\right). \tag{7.75}$$

An immediate check of our results is the extraction of the correct anomalous dimension, $\widetilde{\gamma}_{CM}$, already known in the literature for the operator $\widetilde{\mathcal{O}}_{CM}$ (Eq. (7.39)), with a quark mass and a coupling constant in its definition [136]. The following relation holds between $z_1^{DR,\overline{\rm MS}}$ and $\widetilde{\gamma}_{CM}$:

$$\widetilde{\gamma}_{CM} = -2\,\epsilon\,g^2\,(z_1^{DR,\overline{\rm MS}} + z_m^{DR,\overline{\rm MS}}) = \frac{g^2}{16\,\pi^2}\left(4\,N_c - \frac{8}{N_c}\right), \tag{7.76}$$

$$\left(Z_m^{DR,\overline{\rm MS}} = 1 + g^2\,z_m^{DR,\overline{\rm MS}} + \mathcal{O}(g^4), \quad z_m^{DR,\overline{\rm MS}} = \frac{1}{16\,\pi^2}\frac{1}{\epsilon}\,(-3\,C_F)\right). \tag{7.77}$$

7.3.2 Lattice regularization – $\overline{\rm MS}$ renormalization

The computations of the 2-pt and 3-pt bare Green's functions of $\mathcal{O}_{CM}$ on the lattice are the most demanding part of the present work. This is particularly true for the 3-pt function, since it had to be calculated for arbitrary values of the external momenta, q_i , of the quark, antiquark and gluon. The algebraic expressions involved were split into two parts: a) Terms which can be evaluated in the $a \to 0$ limit: Included in this part are terms with polynomial dependence on q_i (with coefficients which depend on the lattice regularization), but also terms which exhibit a very complicated dependence on q_i , even for zero quark masses, involving Spence functions. These functions constitute a part of the regularization independent renormalized Green's functions. b) All remaining terms: These are divergent as $a \to 0$, however their dependence on q_i, m is necessarily polynomial. Our computations were performed in a covariant gauge, with arbitrary value of the gauge parameter α. Given that some of the operators which mix with $\mathcal{O}_{CM}$ contain powers of the quark masses, we have kept these masses different from zero throughout most of the computation; it is only in the final expressions for Z_i that we set $m \to 0$.

For the algebraic operations involved in evaluating Feynman diagrams, we make use of our symbolic package in Mathematica. A brief description of the computation of a Feynman diagram can be found, e.g., in Ref. [43] and references therein. The algebraic expressions for each Feynman diagram typically involve $\sim 10^5$ terms at intermediate stages. The requirements in terms of CPU time, both for algebraic manipulation and for numerical integration of momentum loop integrals, were rather modest as compared to human effort: A total of ~ 4 months on a single core CPU was required.

The computation on the lattice is performed in the twisted basis (χ, $\bar{\chi}$), and thus, before comparing with the results in dimensional regularization, we must rotate to the physical

basis (ψ, $\bar{\psi}$). This rotation amounts to the following transformation of the fermion field:

$$\chi = e^{-i\frac{\pi}{4}\gamma_5}\,\psi\,, \tag{7.78}$$

$$\bar{\chi} = e^{-i\frac{\pi}{4}\gamma_5}\,\bar{\psi}\,. \tag{7.79}$$

The rotation of the 2-pt Green's function is therefore:

$$\langle \psi\,\mathcal{O}\,\bar{\psi}\rangle_{\rm amp} = e^{-i\frac{\pi}{4}\gamma_5}\,\langle \chi\,\mathcal{O}\,\bar{\chi}\rangle_{\rm amp}\,e^{-i\frac{\pi}{4}\gamma_5}\,, \tag{7.80}$$

and similarly for the 3-pt Green's function.

We will make use, once again, of Eqs. (7.37) - (7.38), with $\overline{\rm MS}$ being the renormalization scheme; however, the regularization will now be the lattice. The above equations now take the form:

$$\langle \psi\,\mathcal{O}_1\,\overline{\psi}\rangle^{\overline{\rm MS}}_{\rm amp} = Z_\psi^{L,\overline{\rm MS}}\sum_{i=1}^{13}\left((Z^{L,\overline{\rm MS}})^{-1}\right)_{1i}\langle \psi\,\mathcal{O}_i\,\overline{\psi}\rangle^{L}_{\rm amp} \tag{7.81}$$

and

$$\langle \psi\,\mathcal{O}_1\,\overline{\psi}A_\nu\rangle^{\overline{\rm MS}}_{\rm amp} = Z_\psi^{L,\overline{\rm MS}}\,(Z_A^{L,\overline{\rm MS}})^{1/2}\sum_{i=1}^{13}\left((Z^{L,\overline{\rm MS}})^{-1}\right)_{1i}\langle \psi\,\mathcal{O}_i\,\overline{\psi}\,A_\nu\rangle^{L}_{\rm amp}\,. \tag{7.82}$$

The left-hand sides of the above equations are known from the calculations in dimensional regularization, see Subsection 7.3.1. The bare lattice Green's functions in these equations contain terms which diverge in the limit $a \to 0$; these divergent terms have a form similar to Eqs. (7.41) and (7.42), with two differences:

- $\dfrac{1}{\epsilon} \to -\log(a^2)$
- There are additional $\mathcal{O}\left(\dfrac{1}{a^2}\right)$, $\mathcal{O}\left(\dfrac{1}{a}\right)$ contributions:

$$\text{in } \langle \psi\,\mathcal{O}_1\,\overline{\psi}\rangle^{L}_{\rm amp}: \quad \rho_8\,(r_d\,\gamma_5\,\not{q}_3 + r_s\,\not{q}_2\,\gamma_5) + \rho_9\,i\,(r_d\,m_d + r_s\,m_s)\,\gamma_5 + \rho_{10}\cdot 1 \tag{7.83}$$

$$\text{in } \langle \psi\,\mathcal{O}_1\,\overline{\psi}A_\nu\rangle^{L}_{{\rm amp},1PI}: \quad R_5\,g\,(r_d - r_s)\,\gamma_5\,\gamma_\nu\,. \tag{7.84}$$

These contributions lead to mixing with $\mathcal{O}_{11}$, $\mathcal{O}_{12}$ and $\mathcal{O}_{13}$.

The renormalization functions $Z_\psi^{L,\overline{\rm MS}}$ ($Z_A^{L,\overline{\rm MS}}$) for the quark (gluon) field, as well as $Z_g^{L,\overline{\rm MS}}$, $Z_m^{L,\overline{\rm MS}}$, were only partially available in the literature; we computed them for a general covariant gauge, using the Symanzik improved gauge action for different sets of values for the

Symanzik coefficients. These results are presented in section 7.4, in the RI′ renormalization scheme along with conversion factors to the $\overline{\rm MS}$ scheme.

Renormalizability of the theory implies that the difference between the one-loop renormalized and bare Green's functions must only consist of expressions which are polynomial in q_i, m ; in this way, the right-hand sides of Eqs. (7.81) - (7.82) can be rendered equal to the corresponding left-hand sides, by an appropriate definition of the (q_i- and m-independent) renormalization functions $Z_i^{L,\overline{\rm MS}}$. These differences can be written as follows:

$$\langle\psi\,\mathcal{O}_1\,\overline{\psi}\rangle^{\overline{\rm MS}}_{\rm amp} - \langle\psi\,\mathcal{O}_1\,\overline{\psi}\rangle^{L}_{\rm amp} = g^2\Big(z_\psi^{L,\overline{\rm MS}} - z_1^{L,\overline{\rm MS}}\Big)\langle\psi\,\mathcal{O}_1\,\overline{\psi}\rangle_{\rm tree} - \sum_{i=2}^{13} Z_i^{L,\overline{\rm MS}}\langle\psi\,\mathcal{O}_i\,\overline{\psi}\rangle_{\rm tree} \quad (7.85)$$

and

$$\begin{aligned}\langle\psi\,\mathcal{O}_1\,\overline{\psi}A_\nu\rangle^{\overline{\rm MS}}_{\rm amp} - \langle\psi\,\mathcal{O}_1\,\overline{\psi}A_\nu\rangle^{L}_{\rm amp} = \;& g^2\;\Big(z_\psi^{L,\overline{\rm MS}} + \frac{1}{2}z_A^{L,\overline{\rm MS}} + z_g^{L,\overline{\rm MS}} - z_1^{L,\overline{\rm MS}}\Big)\langle\psi\,\mathcal{O}_1\,\overline{\psi}A_\nu\rangle_{\rm tree} \\ & - \sum_{i=2}^{13} Z_i^{L,\overline{\rm MS}}\langle\psi\,\mathcal{O}_i\,\overline{\psi}\,A_\nu\rangle_{\rm tree}\,. \qquad (7.86)\end{aligned}$$

Indeed, we have checked explicitly the polynomial character of the left-hand sides of Eqs. (7.85) - (7.86). This check is quite nontrivial, especially for Eq. (7.86), since both the bare and renormalized Green's functions, taken individually, exhibit a very complex dependence on the momenta q_i . The left-hand sides of Eqs. (7.85) - (7.86) have the same tensorial form as Eqs. (7.41) - (7.42), respectively, but with the additional contributions of Eqs. (7.83) - (7.84).

Each tensorial structure (multiplying $\rho_1 - \rho_{10}$, $R_1 - R_5$) will provide an equation; the set of these equations (a total of 15) can be solved for the 13 mixing coefficients Z_i. Two of the equations serve as consistency checks and the remaining 13 lead to a well determined system. Upon solving all equations we obtain for the tree-level Symanzik gluon action (see

Appendix D.1, for other gluon actions we have considered):

$$Z_1^{L,\overline{\rm MS}} = 1+\frac{g^2}{16\,\pi^2}\Big(N_c\big(-12.8455+\frac{1}{2}\,\log\big(a^2\,\bar{\mu}^2\big)\big)+\frac{1}{N_c}\big(9.3779-\frac{5}{2}\,\log\big(a^2\,\bar{\mu}^2\big)\big)\Big) \quad (7.87)$$

$$Z_2^{L,\overline{\rm MS}} = \frac{g^2\,C_F}{16\,\pi^2}\,\big(2.7677+6\,\log\big(a^2\,\bar{\mu}^2\big)\big) \quad (7.88)$$

$$Z_3^{L,\overline{\rm MS}} = 0 \quad (7.89)$$

$$Z_4^{L,\overline{\rm MS}} = 0 \quad (7.90)$$

$$Z_5^{L,\overline{\rm MS}} = \frac{g^2}{16\,\pi^2}\,\Big(N_c\Big(5.3894-\frac{3}{2}\,\log\big(a^2\,\bar{\mu}^2\big)\Big)+\frac{1}{N_c}\Big(-5.5061+3\,\log\big(a^2\,\bar{\mu}^2\big)\Big)\Big) \quad (7.91)$$

$$Z_6^{L,\overline{\rm MS}} = 0 \quad (7.92)$$

$$Z_7^{L,\overline{\rm MS}} = -\frac{Z_5^{L,\overline{\rm MS}}}{2} \quad (7.93)$$

$$Z_8^{L,\overline{\rm MS}} = \frac{g^2\,C_F}{16\,\pi^2}\,(-3.9654) \quad (7.94)$$

$$Z_9^{L,\overline{\rm MS}} = \frac{Z_5^{L,\overline{\rm MS}}}{2} \quad (7.95)$$

$$Z_{10}^{L,\overline{\rm MS}} = \frac{g^2\,C_F}{16\,\pi^2}\,\big(5.5061-3\,\log\big(a^2\,\bar{\mu}^2\big)\big) \quad (7.96)$$

$$Z_{11}^{L,\overline{\rm MS}} = \frac{1}{a}\,\frac{g^2\,C_F}{16\,\pi^2}\,(-4.0309) \quad (7.97)$$

$$Z_{12}^{L,\overline{\rm MS}} = -Z_{11}^{L,\overline{\rm MS}} \quad (7.98)$$

$$Z_{13}^{L,\overline{\rm MS}} = \frac{1}{a^2}\,\frac{g^2\,C_F}{16\,\pi^2}\,(47.7929)\ . \quad (7.99)$$

In these equations, $\bar{\mu}$ is the $\overline{\rm MS}$ renormalization scale which appears in $\langle\psi\,\mathcal{O}_1\,\overline{\psi}\rangle_{\rm amp}^{\overline{\rm MS}}$ and $\langle\psi\,\mathcal{O}_1\,\overline{\psi}A_\nu\rangle_{\rm amp}^{\overline{\rm MS}}$ by virtue of: $g=\mu^{-\epsilon}\,(Z_g^{DR,\overline{\rm MS}})^{-1}\,g_0^{DR}$, $\bar{\mu}=\mu(4\pi/e^{\gamma_E})^{1/2}$.

The above results for $Z_1^{L,\overline{\rm MS}}$ - $Z_{13}^{L,\overline{\rm MS}}$ are independent of the choices $r_s=\pm1$, $r_d=\pm1$. There is also a small systematic error originating from the numerical estimation of lattice integrals, however it is much smaller than the displayed accuracy of the results.

If one wants to renormalize in an (appropriately defined) RI′ scheme, the calculation in dimensional regularization is not necessary: it suffices to compute the bare Green's functions on the lattice. In this case the left-hand sides of Eqs. (7.37) - (7.38), for particular values of the external momenta, are dictated by the RI′ renormalization conditions.

The conversion factor between the RI′ and the $\overline{\rm MS}$ scheme will actually be a (13×13) matrix in this case: $C_{ij}^{RI',\overline{\rm MS}}$. Since this matrix is regularization independent, one may compute it through:

$$\mathcal{O}_R^{\overline{\rm MS}} \equiv C^{RI',\overline{\rm MS}}\, \mathcal{O}_R^{RI'} \,, \quad C^{RI',\overline{\rm MS}} = \left(Z^{DR,\overline{\rm MS}}\right)^{-1} Z^{DR,RI'}. \tag{7.100}$$

Thus, in RI′, the mixing coefficients read (in matrix notation):

$$Z^{L,RI'} = Z^{L,\overline{\rm MS}} C^{RI',\overline{\rm MS}} \,. \tag{7.101}$$

7.4 One-loop Renormalization of Z_c , Z_ψ , Z_m , Z_A , Z_g on the Lattice

In this section we provide the results of our one-loop calculation for the renormalization functions of the ghost field (Z_c), quark field (Z_ψ), gluon field (Z_A), coupling constant (Z_g), quark mass (Z_m). These functions enter the renormalization of the chromomagnetic operator through Eqs. (7.117), (7.37), (7.38), (7.86), (7.40). The computation was performed using twisted mass fermions, Symanzik improved gluons and a general covariant gauge. Here we present the results for the Wilson, tree-level Symanzik, TILW ($\beta\, c_0 = 8.30$), Iwasaki and DBW2 gluon actions. For the extraction of the renormalization functions, we applied the RI′ scheme at a scale $\bar{\mu}$. Once we have computed the renormalization functions in the RI′ scheme we can construct their $\overline{\rm MS}$ counterparts using conversion factors which are known (see, e.g., [121]), up to the required perturbative order.

The aforementioned renormalization functions are defined as follows:

$$\begin{aligned} g_0 &= Z_g\, g, && (7.102)\\ c &= \sqrt{Z_c}\, c^R, && (7.103)\\ \psi &= \sqrt{Z_\psi}\, \psi^R, && (7.104)\\ A_\mu &= \sqrt{Z_A}\, A_\mu^R, && (7.105)\\ \alpha &= Z_\alpha^{-1} Z_A\, \alpha^R, && (7.106)\\ m &= Z_m m^R . && (7.107) \end{aligned}$$

In the above, Z_g actually stands for $Z_g^{L,RI'}$; similarly for all other Z's. The renormalization function Z_α for the gauge parameter receives no one-loop contribution.

7.4.1 Ghost Field Renormalization Z_c

The ghost field renormalization enters the evaluation of Z_g (see subsection 7.4.4); it can be extracted from the RI′ condition:

$$\lim_{a\to 0}\left[Z_c^{L,\mathrm{RI}'}(a\bar{\mu}) \frac{\Sigma_c^L(q,a)}{q^2}\right]_{q^2=\bar{\mu}^2} = 1, \tag{7.108}$$

where $\Sigma_c^L(q,a)$ is the ghost self energy up to one-loop, computed from the diagrams in Fig. 7.5.

$$\Sigma_c^L(q,a) = q^2 + \mathcal{O}(g^2). \tag{7.109}$$

The generic form of $Z_c^{L,\mathrm{RI}'}$ is:

$$Z_c^{L,\mathrm{RI}'} = 1 + \frac{g^2 N_c}{16\pi^2}\Big[e_c - 1.2029\alpha - \frac{1}{4}\,(3-\alpha)\log\left(a^2\,\bar{\mu}^2\right)\Big]. \tag{7.110}$$

The numerical values of the coefficient e_c are listed in Table 7.4 for all gluon actions we have considered.

Figure 7.5: One-loop Feynman diagrams contributing to the renormalization of the ghost field. A wavy (dotted) line represents gluons (ghosts).

Coefficient	Wilson	Tree-level Symanzik	TILW ($\beta\, c_0 = 8.30$)	Iwasaki	DBW2
e_c	4.6086	3.7759	3.2208	2.5469	0.9433
e_ψ	16.6444	13.0233	10.7153	8.1166	2.9154
e_m	16.9524	13.6067	11.4247	8.8575	2.9060
$e_{A,1}$	22.3157	10.3088	2.4199	-7.2464	-28.5805
$e_{A,2}$	-19.7392	-6.6595	2.0039	11.8888	32.2815
$e_{g,1}$	-13.4192	-6.5831	-2.0835	3.4235	15.6942
$e_{g,2}$	9.8696	3.3297	-1.0019	-5.9444	-16.1407

Table 7.4: The coefficients e_c , e_ψ , e_m , $e_{A,1}$, $e_{A,2}$, $e_{g,1}$ and $e_{g,2}$ for five actions: Wilson, tree-level Symanzik, TILW ($\beta\, c_0 = 8.30$), Iwasaki and DBW2.

7.4.2 Renormalization of Fermion Field (Z_ψ) and Mass (Z_m)

In order to obtain the renormalization functions of fermionic operators we also compute the quark field renormalization, Z_ψ, as a prerequisite.

Z_ψ is extracted from an RI′ condition on the fermion self energy $\Sigma_\psi^L(q,a) = i\not{q} + m + \mathcal{O}(g^2)$:

$$\lim_{a\to 0}\left[Z_\psi^{L,\mathrm{RI}'}(a\bar{\mu})\,\mathrm{tr}\left(\Sigma_\psi^L(q,a)\,\not{q}\right)/(4i\,q^2)\right]_{q^2=\bar{\mu}^2} = 1. \tag{7.111}$$

The trace here is over Dirac indices; a Kronecker delta in color and in flavor indices has been factored out of the definition of Σ_ψ^L. The Feynman diagrams contributing to Σ_ψ^L are identical to those shown in Fig. 3.1. Our result for Z_ψ is:

$$Z_\psi^{L,\mathrm{RI}'} = 1 + \frac{g^2 C_F}{16\pi^2}\left[e_\psi - 4.7920\alpha + \alpha\log\left(a^2\,\bar{\mu}^2\right)\right]. \tag{7.112}$$

The part of Σ_ψ^L proportional to the unit matrix in Dirac space leads to the value of Z_m. Our result for Z_m is:

$$Z_m^{L,\mathrm{RI}'} = 1 + \frac{g^2 C_F}{16\pi^2}\Big[e_m + \alpha - 3\,\log\left(a^2\,\bar{\mu}^2\right)\Big]. \tag{7.113}$$

The numerical values of the coefficients e_ψ and e_m are listed in Table 7.4.

7.4.3 Gluon Field Renormalization Z_A

The renormalization for the gluon field, Z_A, can be evaluated from the gluon propagator $G^L_{\mu\,\nu}(q,a)$ with radiative corrections:

$$G^L_{\mu\,\nu}(q,a) = \frac{1}{q^2}\left[\frac{\delta_{\mu\,\nu} - q_\mu q_\nu/q^2}{\Pi_T(aq)} + \alpha\,\frac{q_\mu q_\nu/q^2}{\Pi_L(aq)}\right], \tag{7.114}$$

where the one-loop contributions to the transverse (Π_T) and longitudinal (Π_L) parts of the gluon self-energy, $\Pi_{T,L}(aq) = 1 + \mathcal{O}(g^2)$ are obtained from the diagrams of Fig. 7.6. The normalization condition is:

$$\lim_{a\to 0}\left[Z_A^{L,\mathrm{RI}'}(a\bar{\mu})\,\frac{1}{\Pi_T(aq)}\right]_{q^2=\bar{\mu}^2} \;=\; 1. \tag{7.115}$$

Our result up to one-loop is:

$$\begin{aligned} Z_A^{L,\mathrm{RI}'} \;&=\; 1 + \frac{g^2}{16\pi^2}\Big[N_c\left(e_{A,1} - 0.8863\alpha + \frac{1}{4}\alpha^2\right) + \frac{1}{N_c}e_{A,2} - 2.1685 N_f \\ &+\; \left(\frac{2}{3}N_f - \frac{13}{6}N_c + \frac{1}{2}\alpha N_c\right)\log\left(a^2\,\bar{\mu}^2\right)\Big], \end{aligned} \tag{7.116}$$

(N_f stands for the number of flavors). The numerical values of the coefficients $e_{A,1}$ and $e_{A,2}$ are listed in Table 7.4. From $\Pi_L(aq)$ one can deduce the value of Z_α , as mentioned before, this receives no contributions at one-loop.

7.4.4 Coupling constant renormalization Z_g

Z_g can be extracted either from the gluon-quark-antiquark Green's function, or equivalently from the gluon-ghost-antighost Green's function $G^L_{A\bar{c}c}$; we have chosen to compute the latter. However, the results of the two determinations coincide, as has been checked by us

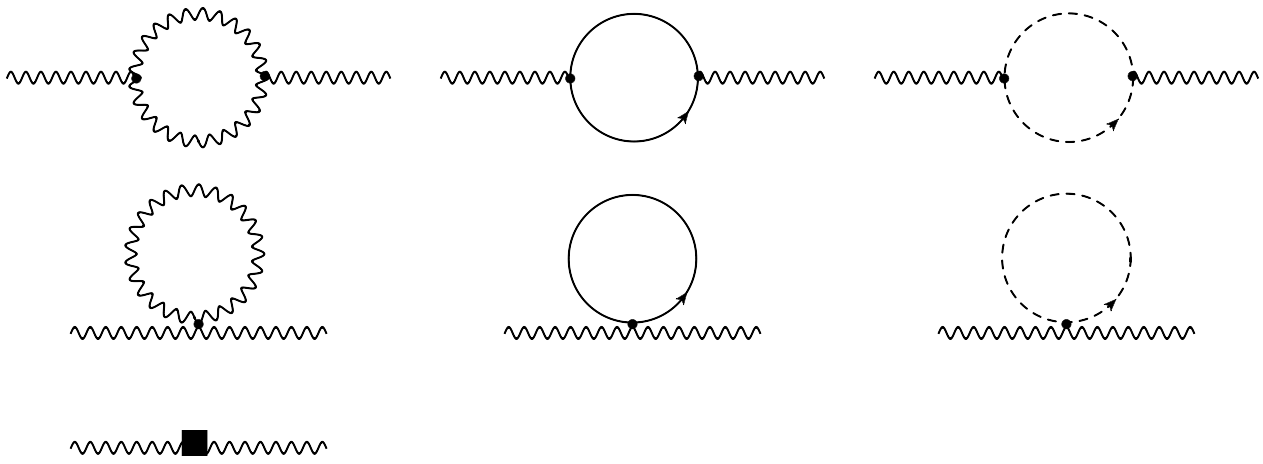

Figure 7.6: One-loop Feynman diagrams contributing to the renormalization of the gluon field. A wavy (solid, dotted) line represents gluons (fermions, ghosts). A solid box denotes a vertex from the measure part of the lattice action.

in the Feynman gauge. The corresponding normalization condition is [5]:

$$\lim_{a\to 0}\left[Z_c^{L,\mathrm{RI}'}\,(Z_A^{L,\mathrm{RI}'})^{1/2} Z_g^{L,\mathrm{RI}'} G^L_{A\bar{c}c}(q,a)\right]_{q^2=\bar{\mu}^2} = G^{\mathrm{finite}}_{A\bar{c}c}, \tag{7.117}$$

where the expression $G^{\mathrm{finite}}_{A\bar{c}c}$ is required to be the same as the one stemming from the continuum:

$$\lim_{\epsilon\to 0}\left[Z_c^{DR,\mathrm{RI}'}\,(Z_A^{DR,\mathrm{RI}'})^{1/2} Z_g^{DR,\mathrm{RI}'} G_{A\bar{c}c}(q)\right]_{q^2=\bar{\mu}^2} = G^{\mathrm{finite}}_{A\bar{c}c}. \tag{7.118}$$

[In the above equation $Z_g^{DR,\mathrm{RI}'}$ is required to eliminate only the pole parts of the left-hand side, without additional finite terms; hence, it is trivially equal to $Z_g^{DR,\overline{\mathrm{MS}}}$.] Calculating in dimensional regularization, $G^{\mathrm{finite}}_{A\bar{c}c}$ is found to be:

$$G^{\mathrm{finite}}_{A\bar{c}c} = 1 + \frac{g^2}{16\,\pi^2}\,\left[\left(\frac{169}{72} + \frac{3}{4}\alpha + \frac{1}{8}\alpha^2 + \frac{1}{2}\alpha\log\left(\frac{\bar{\mu}^2}{q^2}\right)\right)N_c - \frac{5}{9}N_f\right]. \tag{7.119}$$

The Feynman diagrams contributing to $G^L_{A\bar{c}c}$ are shown in Fig. 7.7. Our result for $Z_g^{L,\mathrm{RI}'}$ is:

$$Z_g^{L,\mathrm{RI}'} = 1 + \frac{g^2}{16\,\pi^2}\,\left[e_{g,1}\,N_c + \frac{1}{N_c}e_{g,2} + 0.5287 N_f + \left(\frac{11}{6}N_c - \frac{1}{3}N_f\right)\log(a^2\,\bar{\mu}^2)\right]. \tag{7.120}$$

[5] Eq. (7.117) is evaluated at vanishing ghost momentum; q stands for the antighost/gluon momentum.

The numerical values of the coefficients $e_{g,1}$ and $e_{g,2}$ are listed in Table 7.4.

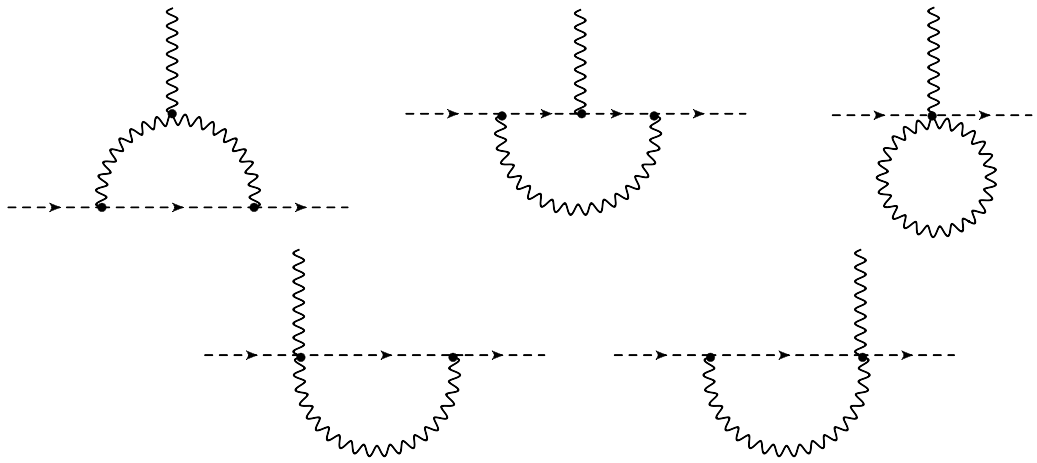

Figure 7.7: One-loop Feynman diagrams contributing to $G^L_{A\bar{c}c}$. A wavy (dotted) line represents gluons (ghosts).

7.4.5 Conversion to the $\overline{\rm MS}$ scheme

Each renormalization function on the lattice, $Z^{L,\rm RI'}$, may be expressed as a power series in the renormalized coupling constant $g^{RI'}$. For the purposes of our work the conversion of $g^{\rm RI'}$ to $\overline{\rm MS}$ is trivial since:

$$g^{RI'} = g^{\overline{\rm MS}} + \mathcal{O}\big((g^{\overline{\rm MS}})^9\big). \tag{7.121}$$

As already mentioned, our one-loop calculations for Z_c, Z_ψ, Z_m, Z_A and Z_g are performed in a generic gauge with parameter $\alpha^{RI'}$. The conversion of $\alpha^{RI'}$ to the $\overline{\rm MS}$ scheme is given by:

$$\alpha^{RI'} = \left(\frac{Z_\alpha^{L,\overline{\rm MS}}}{Z_\alpha^{L,\rm RI'}}\right)^{-1} \frac{Z_A^{L,\overline{\rm MS}}}{Z_A^{L,\rm RI'}}\, \alpha^{\overline{\rm MS}}. \tag{7.122}$$

Since $(Z_\alpha^{L,\overline{\rm MS}}/Z_\alpha^{L,RI'}) = (Z_\alpha^{DR,\overline{\rm MS}}/Z_\alpha^{DR,RI'}) = 1$ at three loops [140], there follows:

$$\alpha^{RI'} = (Z_A^{L,\overline{\rm MS}}/Z_A^{L,RI'})\, \alpha^{\overline{\rm MS}} \equiv \alpha^{\overline{\rm MS}} \,/\, C_A(g^{\overline{\rm MS}}, \alpha^{\overline{\rm MS}}). \tag{7.123}$$

Since the ratio of Z's appearing in Eq. (7.123) must be *regularization independent*, it may be calculated more easily in dimensional regularization [121]; to one loop, the

conversion factor C_A equals:

$$C_A(g,\alpha) = \frac{Z_A^{DR,\mathrm{RI}'}}{Z_A^{DR,\overline{\mathrm{MS}}}} = 1 + \frac{g^2}{36(16\pi^2)}\left[\left(9\alpha^2 + 18\alpha + 97\right)\, N_c - 40 N_f\right], \tag{7.124}$$

(Here, and below, both g and α are in the $\overline{\mathrm{MS}}$ scheme).

Thus, once we have computed the renormalization functions in the RI′ scheme we can construct their $\overline{\mathrm{MS}}$ counterparts using conversion factors which, up to the required perturbative order, are given by:

$$C_c(g,\alpha) \equiv \frac{Z_c^{L,\mathrm{RI}'}}{Z_c^{L,\overline{\mathrm{MS}}}} = \frac{Z_c^{DR,\mathrm{RI}'}}{Z_c^{DR,\overline{\mathrm{MS}}}} = 1 + \frac{g^2}{16\pi^2}\, N_c\,, \tag{7.125}$$

$$C_\psi(g,\alpha) \equiv \frac{Z_\psi^{L,\mathrm{RI}'}}{Z_\psi^{L,\overline{\mathrm{MS}}}} = \frac{Z_\psi^{DR,\mathrm{RI}'}}{Z_\psi^{DR,\overline{\mathrm{MS}}}} = 1 - \frac{g^2}{16\pi^2}\, C_F\, \alpha, \tag{7.126}$$

$$C_m(g,\alpha) \equiv \frac{Z_m^{L,\mathrm{RI}'}}{Z_m^{L,\overline{\mathrm{MS}}}} = \frac{Z_m^{DR,\mathrm{RI}'}}{Z_m^{DR,\overline{\mathrm{MS}}}} = 1 + \frac{g^2}{16\pi^2}\, C_F\,(4+\alpha). \tag{7.127}$$

$$\tag{7.128}$$

7.4.6 Non-perturbative results – Preliminary

In the calculation of on-shell matrix elements, by virtue of the equations of motion, some of the operators $\mathcal{O}_1 - \mathcal{O}_{13}$ will not appear. The remaining ones: $\mathcal{O}_1$, $\mathcal{O}_2$, $\mathcal{O}_3$, $\mathcal{O}_4$, $\mathcal{O}_{12}$, $\mathcal{O}_{13}$ will be present, and it is imperative to have a stringent estimate of the corresponding mixing coefficients. For operators of the same dimensionality as the chromomagnetic one, i.e. $\mathcal{O}_1$, $\mathcal{O}_2$, $\mathcal{O}_3$, $\mathcal{O}_4$, our one-loop results are expected to provide satisfactory accuracy; however, for operators of lower dimensionality ($\mathcal{O}_{12}$, $\mathcal{O}_{13}$), given that their coefficients are power divergent, perturbation theory is expected to provide only a ballpark estimate at best. Fortunately, it is precisely for the coefficients of these latter operators that we can have best access to non-perturbative estimates.

Imposing conditions such as:

$$\lim_{m_s\,,\; m_d\to 0} \langle \pi(0)|\mathcal{O}_1^{\mathrm{sub}}|K(0)\rangle = \lim_{m_s\,,\; m_d\to 0} \langle \pi(0)|\mathcal{O}_1 + \frac{c_{13}}{a^2}\mathcal{O}_{13}|K(0)\rangle = 0 \tag{7.129}$$

$$\langle 0|\mathcal{O}_1^{\mathrm{sub}}|K(0)\rangle_{m_s\,,\; m_d} = \langle 0|\mathcal{O}_1 + \frac{c_{13}}{a^2}\mathcal{O}_{13} + \frac{c_{12}}{a}\mathcal{O}_{12}|K(0)\rangle_{m_s\,,\; m_d} = 0 \tag{7.130}$$

we can fit the values of $c_{13}(g_0)$, $c_{12}(g_0)$ to data from simulations with varying quark masses.

In a preliminary series of simulations, by our collaborators in University of Roma Tre, the coefficient c_{13} extracted at different values of the coupling ($\beta \equiv 6/g_0^2 = 1.90,\ 1.95,\ 2.10$) using the Iwasaki gluon action. The results for c_{13} closely follow a quadratic dependence on g_0 , thus resembling a one-loop effect; nevertheless there is some difference, as was expected:

$$Z_{13}^{\text{non-pert}} \sim a^{-2}\,\frac{g^2 C_F}{16\pi^2}\,(33.7) \tag{7.131}$$

$$Z_{13}^{\text{pert}} = a^{-2}\,\frac{g^2 C_F}{16\pi^2}\,(36.061) \tag{7.132}$$

7.5 Summary – Extensions

On the lattice, the mixing pattern of the CMO can become considerably more complicated, given that certain symmetries are violated; there can be mixing with additional operators of dimension five (with logarithmically divergent coefficients) or less (with power-divergent coefficients). A generic hypercubic- and gauge-invariant lattice discretization will result in mixing with 2+8+32 candidate operators of dimension 3, 4, 5, respectively. It is thus imperative to make a judicious choice of lattice action, with a large set of discrete symmetries, so as to exclude as many as possible of these candidates.

We calculated the 2- and 3-pt bare Green's functions of the CMO, first in DR and then in the far more complicated case of the lattice. The purpose of the calculation in DR is twofold: First, it provides the mixing coefficients $Z_i^{DR,\overline{\text{MS}}}$, which are interesting on their own right; second, and most important, it leads to the renormalized Green's functions in $\overline{\text{MS}}$, which are then necessary for extracting the real quantities of interest: $Z_i^{L,\overline{\text{MS}}}$.

The renormalization functions Z_ψ, Z_A (as well as those for the coupling constant (Z_g), the fermion mass (Z_m), and the ghost field (Z_c)) were not all available for the actions considered in this work, and had to be calculated as a prerequisite. We mention in passing that Z_ψ and Z_m do not depend on flavor in mass-independent schemes. We also note that both the 2-pt and 3-pt functions are necessary in order to fix all Z_i , but they are also sufficient.

Besides a series of controls which we have applied to our results, some further ones may be applied: (i) A calculation of 4-point Green's functions will provide important consistency checks, but no new information, on Z_i . On the other hand, 5-point functions and beyond are irrelevant: Being superficially convergent, they have a straightforward continuum limit. (ii) Non-perturbative estimates of all mixing coefficients would be very

important cross checks.

Depending on the method one wishes to employ for computing matrix elements of the CMO non-perturbatively, a renormalization scheme other than $\overline{\text{MS}}$ may be more appropriate. In particular, one may employ an extension of the RI' scheme, in which RI'-like conditions need to be imposed on both 2-point and 3-point functions. The new mixing coefficients $Z_{ij}^{L,RI'}$ are related to $Z_{ij}^{L,\overline{\text{MS}}}$ via a (13×13) regularization-independent conversion matrix, whose elements are finite functions of the renormalized coupling. In fact, all relevant matrix elements are directly obtainable from our results on the renormalized Green's functions, with no further calculation required.

A further extension of the present work would be to apply methods of improved perturbation theory ("boosted" coupling, "cactus" diagrams, etc.) to our results. Another direction is to compute $\mathcal{O}(a^2 g^2)$ corrections to Green's functions; these, combined with non-perturbative evaluations, lead to an improvement in the non-perturbative estimates of the mixing coefficients.

Chapter 8

Summary and Conclusions

In this Thesis we have performed a series of calculations in Lattice Perturbation Theory, as a tool for connecting results from lattice simulations to physical predictions for strong interaction processes. Each computation was performed employing improved actions for fermions (staggered, SLiNC, clover and Twisted mass action) and/or gluons (Symanzik action).

Let us mention the main computations of this Thesis. We began in Chapter 3 with the perturbative calculation of the renormalization functions for the quark field and for a complete set of ultralocal fermion bilinears. This was the first one-loop calculation using staggered fermions with stout links, and it proved to be extremely demanding in human and CPU time, due to the fact that the vertices of the staggered operators with stout links involve lengthy expressions. More specifically, we calculated the fermion propagator and the quark-antiquark Green's functions of the bilinears. We presented the matrix elements of these operators and the renormalization functions for the quark field and for all ultralocal taste-singlet bilinear operators with general values of the action's and operator's stout smearing parameters ω_{A_1}, ω_{A_2}, $\omega_{\mathcal{O}_1}$, $\omega_{\mathcal{O}_2}$. Our perturbative results of Z_S and Z_T have been used, in Chapter 4, for the determination of the quark condensates ($\langle\bar{\psi}_f\sigma_{xy}\psi_f\rangle$ and $\langle\bar{\psi}_f\psi_f\rangle$), in order to study the response of the QCD vacuum to an external magnetic field, at zero and finite temperature. Magnetic fields probe the QCD vacuum in several ways, by affecting its fundamental properties like chiral symmetry breaking and restoration, the phase diagram, as well as the vacuum polarization. Together with our collaborators in Regensburg and Wuppertal, we aimed at a determination of the magnetic susceptibility of the vacuum. This quantity was evaluated for a wide range of temperatures applying fully dynamical lattice simulations. We performed the renormalization of the tensor coefficient

and carried out the continuum extrapolation using results obtained at different lattice spacings. We extracted the value of the magnetic susceptibilities χ_f at zero temperature for the up, down and strange quarks in the $\overline{\text{MS}}$ scheme at a renormalization scale of 2 GeV. The magnetic susceptibilities at $T = 0$ were negative, indicating the spin-diamagnetic nature of the QCD vacuum. We also found that the polarization changes smoothly with temperature in the confinement phase and is then drastically reduced around the transition region.

In Chapter 5 we discussed improvement to second order in the lattice spacing a, in one-loop perturbation theory. In particular, we focused on the fermion propagator, local and extended fermion bilinear operators; employing the fermionic part of the SLiNC action and the Symanzik improved gauge action for different sets of values of the Symanzik coefficients. These operators are of great phenomenological interest, since they are employed in the calculation of certain transition amplitudes among hadrons and in the extraction of meson and baryon form factors. We provided the expression for the inverse fermion propagator (in the massless case) S^{-1}, the 2-pt Green's function of local bilinears Λ_Γ^{1-loop} as functions of the coupling constant, the number of colors, the gauge fixing parameter, the clover and the stout parameter. The dependence of these quantities on the Symanzik coefficients is not expressible in closed form, thus we provided results for a selected list of the most commonly used values for these coefficients; for economy of space, we presented our results for tree-level Symanzik gluons. We also presented the Z factors for the quark field and for all local fermion bilinears in the case of tree-level Symanzik gluons, along with the renormalization of the extended bilinear operators. Our $\mathcal{O}(a^2)$ perturbative results are applicable to data extracted from numerical simulations performed by the QCDSF collaboration. Our results will be useful for many collaborations worldwide: By setting the stout parameter to zero, the SLiNC action reduces to the clover action; setting both the stout and the clover parameter equal to zero we obtain the Wilson action (where the Wilson parameter r is henceforth set to $r = 1$), and finally setting only the clover parameter equal to zero we obtain the Wilson action with one stout smearing step.

In Chapter 6 we used perturbative results to correct nonperturbative renormalization factors in the RI′-MOM scheme. We investigated a method to suppress lattice artifacts by subtracting one-loop contributions to renormalization factors, calculated in lattice perturbation theory, from simulation data. The perturbative Z factors of local and one-link operators had been calculated using clover fermions and Wilson gluons up to $\mathcal{O}(g^2\,a^2)$. These results can be used in order to construct improved versions of the operators, with

reduced lattice artifacts. In doing so, however, one must bear in mind that, unlike the $\mathcal{O}(a^1)$ case, corrections to $\mathcal{O}(a^2)$ include expressions which are non-polynomial in the external momentum and thus cannot be eliminated by local counterterms for all momentum values. As an alternative stratergy, we subtracted the $\mathcal{O}(a^2)$ effects which we calculated from the corresponding nonperturbative Green's functions and this procedure allows for an improved extrapolation to the limit $a \to 0$.

Finally, in Chapter 7 we studied matrix elements of the chromomagnetic operator on the lattice. This operator is contained in the strangeness-changing part of the effective Hamiltonian which describes electroweak effects of semileptonic processes. This study on the lattice has been hampered up to now by the exceedingly complex pattern of operator mixing. We identify these operators and subtract their contributions, which are typically divergent. There is mixing with lower dimensional operators (power divergent), as well as with gauge non-invariant operators. We computed all relevant mixing coefficients to one loop in lattice perturbation theory; this necessitates calculating both 2-pt (quark-antiquark) and 3-pt (gluon-quark-antiquark) Green's functions at nonzero quark masses. We used the twisted mass lattice formulation (at maximal twist), with Symanzik improved gluon action. In our approach, the nonperturbative mixing coefficients will be determined through a combination of simulations and perturbative calculations. In a preliminary series of simulations, by our collaborators in University of Roma Tre, one mixing coefficient (c_{13}) was extracted at different values of the coupling ($\beta \equiv 6/g_0^2 = 1.90,\ 1.95,\ 2.10$) using the Iwasaki gluon action showing a better-than-expected agreement with our perturbative results. The continuation of these simulations, along with our perturbative results, will allow a clean interpretation of lattice data on the Green's functions of the chromomagnetic operator.

There are several future plans in which this dissertation could be extended. A natural extension would be the computation of the Green's functions for operators including more covariant derivatives in their definitions. Such Green's functions provide more detailed information on the structure of hadrons, being related to higher moments of structure functions and parton distributions.

We also can study the mixing of $\mathrm{Tr}\,(F_{\mu\rho}\,F_{\rho\nu}) - \frac{1}{4}\delta_{\mu\nu}\mathrm{Tr}\,(F_{\sigma\rho}\,F_{\rho\sigma})$ with $\overline{\psi}\gamma_{\{\mu}\overleftrightarrow{D}_{\nu\}}\psi$. By analogy with the chromomagnetic operator, we will obtain a 2×2 mixing matrix in order to compute the renormalization functions of these operators which will be applied to the nonperturbative lattice evaluation of the fraction of the nucleon momentum, $\langle x\rangle_f$ carried by quarks ($f \equiv q = u, d, s, \ldots$) and gluons ($f \equiv g$).

It would be also interesting to calculate the Green's functions of staggered operators and of the chromomagnetic operator up to second order in the lattice spacing. These extensions are useful in order to construct improved versions of the operators, but also to remove $\mathcal{O}(g^2\,a^2)$ contributions from the non-perturbative data of the operators.

A further extension of the present work would be to compute the existing Green's functions up to two loops. Computing higher loops in perturbation theory is a difficult task due to the increased number of Feynman diagrams and the appearance of more complicated terms as well as due to the more intricate structure of (sub)divergences. Also flavor singlet results become different from nonsinglet ones because of a diagrams with closed fermion loop.

We could also apply methods of improved perturbation theory such as "boosted" coupling [142] or "cactus" diagrams [141] to our results. Such improvements lead to an agreement with nonperturbative estimates, which is typically comparable to what is obtained by two-loop computations.

Finally, further improved actions are continuously being implemented in simulations by international lattice collaborations; as a simple example, further steps of stout smearing are being currently tested. It would thus be important to extend our computations to these actions as well.

Appendix A

Stout smeared links

Here we present the 1-gluon part of the doubly-stout link, $U^{(1)}$, for general values of ω_1 and ω_2, as well as the 2-gluon part, $U^{(2)}$, (only for $\omega_2 = 0$, to simplify the latter's lengthy expression):

$$\begin{aligned}
\tilde{\tilde{U}}^{(1)}_{\mu}(x;\omega_1,\omega_2) \;=\; & \\
ig\Big[A_\mu(x) \;+\; & (\omega_1+\omega_2)\Big(-8A_\mu(x)+\sum_{\rho=\pm1}^{\pm4}\Big(A_\mu(x+a\hat{\rho})+A_\rho(x)-A_\rho(x+a\hat{\mu})\Big)\Big) \\
+\; & (\omega_1\,\omega_2)\Big[64A_\mu(x)+\sum_{\rho=\pm1}^{\pm4}\Big(-16A_\mu(x+a\hat{\rho})-8A_\rho(x)+8A_\rho(x+a\hat{\mu})\Big) \\
+\; & \sum_{\rho=\pm1}^{\pm4}\sum_{\sigma=\pm1}^{\pm4}\Big(A_\rho(x+a\hat{\sigma})-A_\rho(x+a\hat{\mu}+a\hat{\sigma})+A_\mu(x+a\hat{\rho}+a\hat{\sigma})\Big)\Big]\Big] \qquad \text{(A.1)}
\end{aligned}$$

$$
\begin{aligned}
\tilde{U}_\mu^{(2)}(x;\omega_1,\omega_2=0) \;=\;& \\
g^2\Big[-\frac{A_\mu(x)^2}{2} \;+\;& \omega_1\big(8A_\mu(x)^2-\sum_{\rho=\pm1}^{\pm4}A_\mu(x)(A_\mu(x+a\hat{\rho})+A_\rho(x)-A_\rho(x+a\hat{\mu}))\big) \\
+\;& \omega_1^2\Big[-32A_\mu(x)^2+\sum_{\rho=\pm1}^{\pm4}\Big(8A_\mu(x)(A_\mu(x+a\hat{\rho})+A_\rho(x)-A_\rho(x+a\hat{\mu}))\Big) \\
+\;& \sum_{\rho=\pm1}^{\pm4}\sum_{\sigma=\pm1}^{\pm4}\Big(-\frac{1}{2}A_\mu(x+a\hat{\rho})A_\mu(x+a\hat{\sigma})-A_\mu(x+a\hat{\rho})A_\sigma(x) \\
-\;& \frac{1}{2}A_\rho(x)A_\sigma(x)+\frac{1}{2}A_\rho(x+a\hat{\mu})A_\sigma(x)+\frac{1}{2}A_\rho(x+a\hat{\mu}-a\hat{\rho})A_\sigma(x+a\hat{\mu}) \\
+\;& A_\mu(x+a\hat{\rho})A_\sigma(x+a\hat{\mu})-\frac{1}{2}A_\rho(x-a\hat{\rho})A_\sigma(x+a\hat{\mu})\Big)\Big]\Big] \qquad \text{(A.2)}
\end{aligned}
$$

where we define $A_{-\rho}(y)=-A_\rho(y-a\hat{\rho})$, $\rho>0$.

Note: The order in which a product of gluon fields appear in $\tilde{U}_\mu^{(2)}$ is irrelevant for the particular diagrams which we compute (since these two gluons are contracted among themselves); we have used this fact in order to simplify the expression for $\tilde{U}_\mu^{(2)}$.

Appendix B

Results and proofs using Staggered fermions

B.1 Numerical results for the staggered propagator and for $\lambda_{\mathcal{O}}$ in the case of the Wilson gluon action

In this Appendix we present the numerical coefficients e_1 and e_2 appearing in Eq. (3.27) for the Wilson gluon action. For economy of space, we do not list our results for the remaining gluon actions which we have considered; however, they are publicly available. The coefficients e_1 and e_2 are polynomials in the 2 stout smearing parameters of the action $(\omega_{A_1}, \omega_{A_2})$:

$$\begin{aligned} e_1 &= -9.83170 + 167.367\,(\omega_{A_1} + \omega_{A_2}) - 710.612\,(\omega_{A_1}^2 + \omega_{A_2}^2) \\ &- 2842.45\,\omega_{A_1}\,\omega_{A_2} + 13134.2\,(\omega_{A_1}^2\omega_{A_2} + \omega_{A_1}\,\omega_{A_2}^2) - 64757.6\,\omega_{A_1}^2\omega_{A_2}^2\,, \end{aligned} \tag{B.1}$$

$$\begin{aligned} e_2 &= 33.3933 - 342.525\,(\omega_{A_1} + \omega_{A_2}) + 1174.37\,(\omega_{A_1}^2 + \omega_{A_2}^2) \\ &+ 4697.49\,\omega_{A_1}\,\omega_{A_2} - 18790.0(\omega_{A_1}^2\omega_{A_2} + \omega_{A_1}\,\omega_{A_2}^2) + 82920.9\,\omega_{A_1}^2\omega_{A_2}^2\,. \end{aligned} \tag{B.2}$$

B.2 Results for $\lambda_{\mathcal{O}}$

We provide the expressions for $\lambda_{\mathcal{O}}$ in the case of the Wilson gluon action; these are polynomials in the 4 stout smearing parameters (ω_{A_1}, ω_{A_2}, $\omega_{\mathcal{O}_1}$, $\omega_{\mathcal{O}_2}$):

$$\begin{aligned}\lambda_S &= -43.2250 + 509.892\,(\omega_{A_1}+\omega_{A_2}) - 1884.98\,\left(\omega_{A_1}^2+\omega_{A_2}^2\right) - 7539.93\,\omega_{A_1}\,\omega_{A_2} \\ &+ 31924.1\,\left(\omega_{A_1}^2\,\omega_{A_2}+\omega_{A_1}\,\omega_{A_2}^2\right) - 147678\,\omega_{A_1}^2\,\omega_{A_2}^2 \end{aligned} \tag{B.3}$$

$$\begin{aligned}\lambda_V &= 118.435\,[(\omega_{A_1}+\omega_{A_2}) - (\omega_{\mathcal{O}_1}+\omega_{\mathcal{O}_2})] - 473.741\,\left[\left(\omega_{A_1}^2+\omega_{A_2}^2\right) - \left(\omega_{\mathcal{O}_1}^2+\omega_{\mathcal{O}_2}^2\right)\right] \\ &- 1894.96\,(\omega_{A_1}\,\omega_{A_2} - \omega_{\mathcal{O}_1}\,\omega_{\mathcal{O}_2}) + 8527.33\,\Big[\left(\omega_{A_1}^2\,\omega_{A_2}+\omega_{A_1}\,\omega_{A_2}^2\right) \\ &- \left(\omega_{\mathcal{O}_1}^2\,\omega_{\mathcal{O}_2}+\omega_{\mathcal{O}_1}\,\omega_{\mathcal{O}_2}^2\right)\Big] - 41689.2\,\left(\omega_{A_1}^2\,\omega_{A_2}^2 - \omega_{\mathcal{O}_1}^2\,\omega_{\mathcal{O}_2}^2\right) \end{aligned} \tag{B.4}$$

$$\begin{aligned}\lambda_T &= 11.4655 + 157.914\,(\omega_{A_1}+\omega_{A_2}) - 276.349\,(\omega_{\mathcal{O}_1}+\omega_{\mathcal{O}_2}) - 728.589\,\left(\omega_{A_1}^2+\omega_{A_2}^2\right) \\ &+ 1105.42\,\left(\omega_{\mathcal{O}_1}^2+\omega_{\mathcal{O}_2}^2\right) - 2869.44\,\omega_{A_1}\,\omega_{A_2} + 4466.53\,\omega_{\mathcal{O}_1}\,\omega_{\mathcal{O}_2} \\ &+ 44.9165\,(\omega_{A_1}+\omega_{A_2})\,(\omega_{\mathcal{O}_1}+\omega_{\mathcal{O}_2}) + 13709.5\,\left(\omega_{A_1}^2\,\omega_{A_2}+\omega_{A_1}\,\omega_{A_2}^2\right) \\ &- 20212.9\,\left(\omega_{\mathcal{O}_1}^2\,\omega_{\mathcal{O}_2}+\omega_{\mathcal{O}_1}\,\omega_{\mathcal{O}_2}^2\right) - 402.837\,\Big((\omega_{A_1}+\omega_{A_2})\,\omega_{\mathcal{O}_1}\,\omega_{\mathcal{O}_2} \\ &+ \omega_{A_1}\,\omega_{A_2}\,(\omega_{\mathcal{O}_1}+\omega_{\mathcal{O}_2})\Big) - 68173.3\,\omega_{A_1}^2\,\omega_{A_2}^2 \\ &+ 100117\,\omega_{\mathcal{O}_1}^2\,\omega_{\mathcal{O}_2}^2 + 3865.46\,\omega_{A_1}\,\omega_{A_2}\omega_{\mathcal{O}_1}\,\omega_{\mathcal{O}_2} \end{aligned} \tag{B.5}$$

$$\begin{aligned}\lambda_A &= 22.5089 + 157.914\,(\omega_{A_1}+\omega_{A_2}) - 434.263\,(\omega_{\mathcal{O}_1}+\omega_{\mathcal{O}_2}) - 710.612\,\left(\omega_{A_1}^2+\omega_{A_2}^2\right) \\ &+ 1737.05\,\left(\omega_{\mathcal{O}_1}^2+\omega_{\mathcal{O}_2}^2\right) - 2797.53\,\omega_{A_1}\,\omega_{A_2} + 6993.12\,\omega_{\mathcal{O}_1}\,\omega_{\mathcal{O}_2} \\ &+ 44.9165\,(\omega_{A_1}+\omega_{A_2})\,(\omega_{\mathcal{O}_1}+\omega_{\mathcal{O}_2}) + 13300.9\,\left(\omega_{A_1}^2\,\omega_{A_2}+\omega_{A_1}\,\omega_{A_2}^2\right) \\ &- 31582.7\,\left(\omega_{\mathcal{O}_1}^2\,\omega_{\mathcal{O}_2}+\omega_{\mathcal{O}_1}\,\omega_{\mathcal{O}_2}^2\right) - 298.982\,\Big((\omega_{A_1}+\omega_{A_2})\,\omega_{\mathcal{O}_1}\,\omega_{\mathcal{O}_2} \\ &+ \omega_{A_1}\,\omega_{A_2}\,(\omega_{\mathcal{O}_1}+\omega_{\mathcal{O}_2})\Big) - 66424.5\,\omega_{A_1}^2\,\omega_{A_2}^2 \\ &+ 155387\,\omega_{\mathcal{O}_1}^2\,\omega_{\mathcal{O}_2}^2 + 2004.59\,\omega_{A_1}\,\omega_{A_2}\omega_{\mathcal{O}_1}\,\omega_{\mathcal{O}_2} \end{aligned} \tag{B.6}$$

$$
\begin{aligned}
\lambda_P &= 34.3567 + 157.914\,(\omega_{A_1}+\omega_{A_2}) - 592.176\,(\omega_{\mathcal{O}_1}+\omega_{\mathcal{O}_2}) - 710.612\,\left(\omega_{A_1}^2+\omega_{A_2}^2\right)\\
&+ 2368.71\,\left(\omega_{\mathcal{O}_1}^2+\omega_{\mathcal{O}_2}^2\right) - 2797.53\,\omega_{A_1}\,\omega_{A_2} + 9519.74\,\omega_{\mathcal{O}_1}\,\omega_{\mathcal{O}_2}\\
&+ 44.9166\,(\omega_{A_1}+\omega_{A_2})\,(\omega_{\mathcal{O}_1}+\omega_{\mathcal{O}_2}) + 13134.2\,\left(\omega_{A_1}^2\,\omega_{A_2}+\omega_{A_1}\,\omega_{A_2}^2\right)\\
&- 42952.5\,\left(\omega_{\mathcal{O}_1}^2\,\omega_{\mathcal{O}_2}+\omega_{\mathcal{O}_1}\,\omega_{\mathcal{O}_2}^2\right) - 298.982\Big(\,(\omega_{A_1}+\omega_{A_2})\,\omega_{\mathcal{O}_1}\,\omega_{\mathcal{O}_2}\\
&+ \omega_{A_1}\,\omega_{A_2}\,(\omega_{\mathcal{O}_1}+\omega_{\mathcal{O}_2})\Big) - 63289.9\,\omega_{A_1}^2\,\omega_{A_2}^2\\
&+ 210973\,\omega_{\mathcal{O}_1}^2\,\omega_{\mathcal{O}_2}^2 + 2371.72\,\omega_{A_1}\,\omega_{A_2}\omega_{\mathcal{O}_1}\,\omega_{\mathcal{O}_2}
\end{aligned}
\tag{B.7}
$$

B.3 Spin- and orbital angular momentum- contributions

The appendices B.3 and B.4 contain some material elaborated by F. Bruckmann, and included here for completeness. The partition function of QCD is given by the functional integral,

$$\mathcal{Z} = \int \mathcal{D}U e^{-\beta S_g} \prod_f \det(\not{D}_f + m_f), \tag{B.8}$$

with the massless Dirac operator $\not{D}_f = \gamma_\mu D_{\mu,f}$ and covariant derivative $D_{\mu,f} = \partial_\mu + iq_f A_\mu + igA_\mu^a T^a$. For an external magnetic field in the z-direction one has $\partial_x A_y - \partial_y A_x = B$ and $A_z = A_t = 0$.

The derivative of the logarithm of Eq. (B.8) with respect to B is

$$\frac{\partial \log \mathcal{Z}}{\partial B} = \sum_f \left\langle \mathrm{Tr} \frac{1}{\not{D}_f + m_f} \frac{\partial \not{D}_f}{\partial B} \right\rangle . \tag{B.9}$$

We manipulate this using $\mathrm{Tr}\,\partial\not{D}_f/\partial B \propto \mathrm{Tr}\,\gamma_\mu = 0$ and the cyclicity of the trace:

$$
\begin{aligned}
\frac{\partial \log \mathcal{Z}}{\partial B} &= \sum_f \frac{1}{m_f} \left\langle \mathrm{Tr}\left(\frac{m_f}{\not{D}_f + m_f} - 1\right) \frac{\partial \not{D}_f}{\partial B} \right\rangle \\
&= -\sum_f \frac{1}{m_f} \left\langle \mathrm{Tr} \frac{1}{\not{D}_f + m_f} \not{D}_f \frac{\partial \not{D}_f}{\partial B} \right\rangle \\
&= -\frac{1}{2} \sum_f \frac{1}{m_f} \left\langle \mathrm{Tr} \frac{1}{\not{D}_f + m_f} \frac{\partial \not{D}_f^2}{\partial B} \right\rangle .
\end{aligned}
\tag{B.10}
$$

The derivative of the square of the Dirac operator in the magnetic field background, after

a standard simplification involving γ-matrices, reads

$$\frac{\partial \not{D}_f^2}{\partial B} = \frac{\partial D_f^2}{\partial B} - q_f \sigma_{xy}, \tag{B.11}$$

where $D_f^2 = D_{\mu,f} D_{\mu,f}$ with summation over μ but not over f. This implies,

$$\frac{T}{V}\frac{\partial \log \mathcal{Z}}{\partial B} = \frac{1}{2}\sum_f \frac{q_f}{m_f}\left(\langle \bar{\psi}_f \sigma_{xy} \psi_f \rangle + \langle \bar{\psi}_f L_{xy} \psi_f \rangle\right), \tag{B.12}$$

where we defined

$$L_{xy} \equiv -\frac{\partial D_f^2}{\partial (q_f B)}. \tag{B.13}$$

This operator corresponds to a generalized angular momentum, as for the choice $A_x = -By/2$, $A_y = Bx/2$ (such that $\partial_\mu A_\mu = 0$), it assumes the form $L_{xy} = -i(x\partial_y - y\partial_x) + q_f B(x^2+y^2)/2 - yA_x^a T^a + xA_y^a T^a$.

Altogether, using the definition of the (total) magnetic susceptibility, Eqs. (4.2) and (4.3), we get

$$\xi_f = \frac{q_f/e}{2m_f}\left(\frac{\partial \langle \bar{\psi}_f \sigma_{xy} \psi_f \rangle}{\partial (eB)} + \frac{\partial \langle \bar{\psi}_f L_{xy} \psi_f \rangle}{\partial (eB)}\right)\Bigg|_{eB=0}, \tag{B.14}$$

showing two separate contributions $\xi^S + \xi^L$ to the total susceptibility, cf. Eq. (4.4).

The conventional calculation of the spin- and orbital momentum-related contributions to ξ yields the same result. Below we demonstrate this for the free case. Here the spin-related contribution to the change in the free energy density due to the magnetic field at zero temperature is given by [102, 144, 145],

$$\begin{aligned} \Delta f^S \quad &= -N_c \int \frac{d^3p}{(2\pi)^3} \\ &\times \sum_{f,s=\pm 1}\left(\sqrt{p^2 + m_f^2 + s\, q_f B} - \sqrt{p^2 + m_f^2}\right). \end{aligned} \tag{B.15}$$

Employing the definition of the total susceptibility, Eq. (4.2), the spin-dependent contribution equals

$$\xi^S = -\frac{\partial^2 \Delta f^S}{\partial (eB)^2}\Bigg|_{eB=0} = -N_c \sum_f \frac{(q_f/e)^2}{2\pi}\int \frac{d^2p}{(2\pi)^2}\frac{1}{p^2 + m_f^2}. \tag{B.16}$$

In Appendix B.4 we will calculate the tensor polarization in the free case. Comparing

Eq. (B.16) with Eq. (B.22) below, we see that the first term of Eq. (B.14) is indeed the spin-related contribution, ξ^S. The second term of Eq. (B.14) is then identified with the orbital momentum coupling. The two contributions to Eq. (4.3) then read,

$$\xi^S = \sum_f \frac{(q_f/e)^2}{2m_f}\tau_f, \qquad \xi^L = \sum_f \frac{q_f/e}{2m_f}\frac{\partial \langle \bar{\psi}_f L_{xy} \psi_f \rangle}{\partial(eB)}, \tag{B.17}$$

where we used the definition of the tensor coefficient, Eq. (4.5). This shows that the tensor coefficient of the quark condensate is responsible for the spin contribution of the total magnetic susceptibility. Recalling the relation between the sign of ξ^S and para/diamagnetism as discussed in Chapter 4, we conclude that with our sign conventions $\tau_f > 0$ ($\chi_f > 0$) corresponds to paramagnetism, while $\tau_f < 0$ ($\chi_f < 0$) to diamagnetism. We remark that on the lattice ξ^L cannot directly be computed from Eq. (B.13), due to the quantization of the magnetic flux.

B.4 Logarithmic divergence in the tensor polarization

In this appendix we will demonstrate the appearance of a logarithmic divergence in the tensor polarization of the condensate. We consider one free quark with electric charge q_f and mass m_f at vanishing temperature.

The negative square of the Dirac operator in the background of a constant magnetic field is well-known to have eigenvalues [66, 146]

$$-\not{D}_f^2 \to \lambda^2 = p_0^2 + p_z^2 + (2n+1)|q_f B| + s\, q_f B, \tag{B.18}$$

being twice degenerate (incorporating particle and antiparticle). Here p_0, p_z are momenta, $n = 0, 1, \ldots$ labels the Landau levels and $s = \pm 1$ is twice the spin (these are the eigenvalues of σ_{xy}), which is coupled to the magnetic field (here we do not consider anomalous magnetic moments). The sum over the eigenvalues is performed according to (see e.g. Ref. [102]),

$$\sum_{\lambda^2} = 2N_c \frac{1}{2\pi T}\int_{-\infty}^{\infty} dp_0 \frac{L_z}{2\pi}\int_{-\infty}^{\infty} dp_z \frac{L_x L_y |q_f B|}{2\pi}\sum_{n=0}^{\infty}\sum_{s=\pm 1}. \tag{B.19}$$

For the tensor polarization of Eq. (4.10) we note that due to chirality (and since γ_5

commutes with σ_{xy}),

$$\begin{aligned} \mathrm{Tr}\frac{1}{\not{D}_f + m_f}\sigma_{xy} &= \mathrm{Tr}\,\gamma_5\frac{1}{\not{D}_f + m_f}\gamma_5\sigma_{xy} \\ &= \mathrm{Tr}\frac{1}{-\not{D}_f + m_f}\sigma_{xy} = m_f\,\mathrm{Tr}\frac{\sigma_{xy}}{-\not{D}_f^2 + m_f^2}, \end{aligned} \tag{B.20}$$

which results in the spectral representation,

$$\begin{aligned} \left\langle\bar{\psi}_f\sigma_{xy}\psi_f\right\rangle &= N_c\frac{m_f|q_fB|}{\pi}\int\frac{d^2p}{(2\pi)^2} \\ &\times\sum_{n,s}\frac{s}{p^2 + \big(2n+1+s\,sign(q_fB)\big)|q_fB| + m_f^2}. \end{aligned} \tag{B.21}$$

In the sum the contributions $\{n = k, s\,sign(q_fB) = 1\}$ and $\{n = k+1, s\,sign(q_fB) = -1\}$ cancel leaving only the unpaired lowest Landau level $\{n = 0, s\,sign(q_fB) = -1\}$, as was also noted in Ref. [85]. Hence we get

$$\left\langle\bar{\psi}_f\sigma_{xy}\psi_f\right\rangle = -N_c\frac{m_f\,q_fB}{\pi}\int\frac{d^2p}{(2\pi)^2}\frac{1}{p^2 + m_f^2}. \tag{B.22}$$

This cancellation can be confirmed via zeta function regularization and is absent for other observables like the free energy or the condensate. As the eigenvalue of the lowest Landau level is B-independent, the free tensor polarization is exactly linear in the magnetic field.

We evaluate the remaining logarithmically divergent integral with dimensional regularization in $d = 2 - \epsilon$ dimensions,

$$\left\langle\bar{\psi}_f\sigma_{xy}\psi_f\right\rangle = N_c\frac{m_f\,q_fB}{4\pi^2}\left[-\frac{2}{\epsilon} + \gamma + \log\left(\frac{m_f^2}{4\pi}\right)\right] + \mathcal{O}(\epsilon). \tag{B.23}$$

A $\log m_f^2$-term has appeared, whose coefficient is scheme-independent; for 3 colors its coefficient is $3/(4\pi^2)\cdot m_f\,q_fB$ (cf. Ref. [67] with different sign conventions). Also the singularity for $\epsilon \to 0$ has been isolated and can be subtracted through a particular renormalization scheme, introducing a cut-off Λ such that $\left\langle\bar{\psi}_f\sigma_{xy}\psi_f\right\rangle \propto \log(m_f^2/\Lambda^2)$, or, on the lattice $\log(m_f^2a^2)$. The finite term ($\gamma - \log(4\pi)$ in Eq. (B.23)) is scheme-dependent (in our lattice scheme it reads $0.1549\,\pi^2 - \log 4$) but, together with the logarithmic contribution, it

disappears from the combination

$$(1 - m_f \partial_{m_f}) \left\langle \bar{\psi}_f \sigma_{xy} \psi_f \right\rangle = -\frac{m_f \, q_f B}{2\pi^2}, \tag{B.24}$$

as we also emphasized in the body of Chapter 4, Eq. (4.18). Note that $(1 - m_f \partial_{m_f})$ acting on Eq. (B.22) renders the integral finite and allows for a direct computation of the coefficient of the logarithmic term.

Appendix C

The derivation of renormalization condition for Chapter 6

In this Appendix we show that the definition (6.6) leads to renormalization factors which are invariant under the hypercubic group $H(4)$.

We consider a multiplet of local quark-antiquark operators $\mathcal{O}_i(x)$ $(i = 1, 2, \ldots, d)$ in position space which transform according to

$$\mathcal{O}_i(x) \to S_{ij}(R)\, \mathcal{O}_j(R^{-1}x) \tag{C.1}$$

when

$$\psi(x) \to D(R)\, \psi(R^{-1}x)\ ,\ \bar{\psi}(x) \to \bar{\psi}(R^{-1}x)\, D(R)^\dagger \tag{C.2}$$

for all $N = 384$ elements R of $H(4)$. Here $D(R)$ denotes the (unitary) spinor representation of $H(4)$ (or $O(4)$):

$$D(R)^\dagger \gamma_\mu D(R) = R_{\mu\nu}\gamma_\nu\,. \tag{C.3}$$

We assume that the operators $\mathcal{O}_i(x)$ have been chosen such that the $d \times d$-matrices $S(R)$ form a unitary irreducible representation of $H(4)$.

Denoting the unrenormalized vertex function at external momentum p of the operator $\mathcal{O}_i$ by $\Lambda_i(p)$ we have

$$\Lambda_i(p) = \sum_{j=1}^{d} S_{ij}(R)\, D(R)\, \Lambda_j(R^{-1}p)\, D(R)^\dagger \tag{C.4}$$

for all $R \in H(4)$, and analogously for the corresponding tree-level term $\Lambda_i^{\mathrm{tree}}(p)$. Conse-

quently we get

$$\sum_{i=1}^{d} \mathrm{Tr}\left[\Lambda_i(p)\Lambda_i(p)^\dagger\right] = \sum_{i=1}^{d} \mathrm{Tr}\left[\Lambda_i(Rp)\Lambda_i(Rp)^\dagger\right] \ . \tag{C.5}$$

Using the orthogonality relations for the matrix elements of irreducible representations one finds in addition

$$\sum_{R} \mathrm{Tr}\left[\Lambda_i(Rp)\Lambda_j(Rp)^\dagger\right] = \frac{1}{d}\delta_{ij} \sum_{k=1}^{d}\sum_{R} \mathrm{Tr}\left[\Lambda_k(Rp)\Lambda_k(Rp)^\dagger\right] \ , \tag{C.6}$$

where the sum extends over all $R \in H(4)$. The same relations hold when one of the vertex functions or both are replaced by the corresponding tree-level terms, e.g.,

$$\sum_{i=1}^{d} \mathrm{Tr}\left[\Lambda_i(p)\Lambda_i^{\mathrm{tree}}(p)^\dagger\right] = \sum_{i=1}^{d} \mathrm{Tr}\left[\Lambda_i(Rp)\Lambda_i^{\mathrm{tree}}(Rp)^\dagger\right] \ . \tag{C.7}$$

Therefore the renormalization condition

$$Z^{-1}Z_q = \frac{\sum_{i=1}^{d} \mathrm{Tr}\left[\Lambda_i(p)\,\Lambda_i^{\mathrm{tree}}(p)^\dagger\right]}{\sum_{j=1}^{d} \mathrm{Tr}\left[\Lambda_j^{\mathrm{tree}}(p)\,\Lambda_j^{\mathrm{tree}}(p)^\dagger\right]} \tag{C.8}$$

or, equivalently,

$$Z^{-1}Z_q\delta_{ij} = \frac{d}{N}\frac{\sum_{R} \mathrm{Tr}\left[\Lambda_i(Rp)\,\Lambda_j^{\mathrm{tree}}(Rp)^\dagger\right]}{\sum_{k=1}^{d} \mathrm{Tr}\left[\Lambda_k^{\mathrm{tree}}(p)\,\Lambda_k^{\mathrm{tree}}(p)^\dagger\right]} \tag{C.9}$$

respects the hypercubic symmetry, i.e., writing more precisely $Z = Z(p)$ we have $Z(Rp) = Z(p)$ for all $R \in H(4)$, and all lattice artefacts in Z must be invariant under the hypercubic group. Of course, here it has been assumed that $Z_q(Rp) = Z_q(p)$, as is the case for our definition (6.3) of Z_q.

Appendix D

Results from the calculation of the chromomagnetic operator on the lattice

D.1 Mixing coefficients Z_i

In this Appendix we present our results for the mixing coefficients, Z_i $(i = 1, \ldots, 13)$ in the $\overline{\text{MS}}$ scheme, for the following gluon actions: Wilson, tree-level Symanzik, Tadpole Improved Lüscher-Weisz (TILW, at $\beta\, c_0 = 8.30$; $\beta = 2N_c/g^2$), Iwasaki and Doubly Blocked Wilson (DBW2). The values of the Symanzik coefficients corresponding to these actions are shown in table D.1.

Coefficient	Wilson	Tree-level Symanzik	TILW ($\beta\, c_0 = 8.30$)	Iwasaki	DBW2
c_0	1	5/3	2.386978	3.648	12.2688
c_1	0	-1/12	-0.159128	-0.331	-1.4086
c_2	0	0	0	0	0
c_3	0	0	-0.014244	0	0

Table D.1: Symanzik coefficients for various choices of gluon actions.

Our calculation has been performed in an arbitrary covariant gauge. All the mixing coefficients Z_i $(i = 1, \ldots, 13)$ in the $\overline{\text{MS}}$ scheme are gauge independent. To one loop, the

generic forms of the mixing coefficients are:

$$Z_1^{L,\overline{\rm MS}} = 1 + \frac{g^2}{16\,\pi^2}\left(N_c\left(e_{1,1} + \frac{1}{2}\,\log(a^2\,\bar{\mu}^2)\right) + \frac{1}{N_c}\left(e_{1,2} - \frac{5}{2}\,\log(a^2\,\bar{\mu}^2)\right)\right) \quad \text{(D.1)}$$

$$Z_2^{L,\overline{\rm MS}} = \frac{g^2\,C_F}{16\,\pi^2}\,\left(e_2 + 6\,\log\left(a^2\,\bar{\mu}^2\right)\right) \quad \text{(D.2)}$$

$$Z_3^{L,\overline{\rm MS}} = 0 \quad \text{(D.3)}$$

$$Z_4^{L,\overline{\rm MS}} = 0 \quad \text{(D.4)}$$

$$Z_5^{L,\overline{\rm MS}} = \frac{g^2}{16\,\pi^2}\left(N_c\left(e_{5,1} - \frac{3}{2}\,\log(a^2\,\bar{\mu}^2)\right) + \frac{1}{N_c}\left(e_{5,2} + 3\,\log(a^2\,\bar{\mu}^2)\right)\right) \quad \text{(D.5)}$$

$$Z_6^{L,\overline{\rm MS}} = 0 \quad \text{(D.6)}$$

$$Z_7^{L,\overline{\rm MS}} = -\frac{Z_5^{L,\overline{\rm MS}}}{2} \quad \text{(D.7)}$$

$$Z_8^{L,\overline{\rm MS}} = \frac{g^2\,C_F}{16\,\pi^2}\,\left(e_8\right) \quad \text{(D.8)}$$

$$Z_9^{L,\overline{\rm MS}} = \frac{Z_5^{L,\overline{\rm MS}}}{2} \quad \text{(D.9)}$$

$$Z_{10}^{L,\overline{\rm MS}} = \frac{g^2\,C_F}{16\,\pi^2}\,\left(-e_{5,2} - 3\,\log\left(a^2\,\bar{\mu}^2\right)\right) \quad \text{(D.10)}$$

$$Z_{11}^{L,\overline{\rm MS}} = \frac{1}{a}\,\frac{g^2\,C_F}{16\,\pi^2}\,\left(e_{11}\right) \quad \text{(D.11)}$$

$$Z_{12}^{L,\overline{\rm MS}} = -Z_{11}^{L,\overline{\rm MS}} \quad \text{(D.12)}$$

$$Z_{13}^{L,\overline{\rm MS}} = \frac{1}{a^2}\,\frac{g^2\,C_F}{16\,\pi^2}\,\left(e_{13}\right)\,. \quad \text{(D.13)}$$

The values of e_i, $e_{i,j}$ are shown explicitly in Table D.2.

Coefficient	Wilson	Tree-level Symanzik	TILW ($\beta\, c_0 = 8.30$)	Iwasaki	DBW2
$e_{1,1}$	-16.8770	-12.8455	-10.4920	-7.9438	-3.2465
$e_{1,2}$	13.4540	9.3779	7.0022	4.4851	-0.5102
e_2	1.9290	2.7677	3.4589	4.5370	8.5250
$e_{5,1}$	5.9806	5.3894	4.9311	4.2758	2.2834
$e_{5,2}$	-6.4047	-5.5061	-4.8014	-3.7777	-0.5292
e_8	-4.0626	-3.9654	-3.8894	-3.7760	-3.4713
e_{11}	-4.4977	-4.0309	-3.6792	-3.2020	-1.9216
e_{13}	54.9325	47.7929	42.6253	36.0613	19.9812

Table D.2: Results for the mixing coefficients at one-loop using the $\overline{\text{MS}}$ scheme on the lattice. The finite parts e_i and $e_{i,j}$ are given for five actions: Wilson, tree-level Symanzik, TILW ($\beta\, c_0 = 8.30$), Iwasaki and DBW2.

Bibliography

[1] D.J. Gross and F. Wilczek, Phys. Rev. Lett. **30** (1973) 26.

[2] K. Wilson, Phys. Rev. **D10** (1974) 2445.

[3] S. Capitani, Phys. Rept. **382** (2003) 113, [hep-lat/0211036].

[4] N. Su, Commun. Theor. Phys. **57** (2012) 409, [arXiv:1204.0260].

[5] C. Bernard and M. Golterman, Phys. Rev. **D88** (2013) 014004, [arXiv:1304.1948].

[6] Q. Mason, H. D. Trottier, R. Horgan, C. Davies and P. Lepage, Phys. Rev. **D73** (2006) 114501, [hep-ph/0511160].

[7] A. Skouroupathis and H. Panagopoulos, Phys. Rev. **D76** (2007) 094514, [arXiv:0707.2906].

[8] A. Skouroupathis and H. Panagopoulos, Phys. Rev. **D79** (2009) 094508, [arXiv:0811.4264].

[9] M. Brambilla and F. Di Renzo, Eur. Phys. J. **C73** (2013) 2666, [arXiv:1310.4981].

[10] M. Brambilla, M. Brida, F. Di Renzo, D. Hesse and S. Sint, [arXiv:1310.8536].

[11] S. Narison, Phys. Lett. **B721** (2013) 269, [arXiv:1212.5544].

[12] T. Reisz, Nucl. Phys. **B318** (1989) 417; T. Reisz and H. Rothe, Nucl. Phys. **B575** (2000) 255, [hep-lat/9908013].

[13] H.B. Nielsen and M. Nimomiya, Nucl. Phys. **185** (1981) 20.

[14] C. Alexandrou, M. Constantinou, T. Korzec, H. Panagopoulos and F. Stylianou, Phys. Rev. **D86** (2012) 014505, [arXiv:1201.5025].

[15] B. Sheikholeslami and R. Wohlert, Nucl. Phys. **B259** (1985) 572.

[16] K. Jansen and C. Liu, Computer Phys. Communications **99** (1997) 221.

[17] N. Cundy, M. Göckeler, R. Horsley, T. Kaltenbrunner, A. D. Kennedy, Y. Nakamura, H. Perlt, D. Pleiter, P. E. L. Rakow, A. Schäfer, G. Schierholz, A. Schiller, H. Stüben and J. M. Zanotti, Phys. Rev. **D79** (2009) 094507.

[18] W. Bietenholz, Nucl. Phys. **B644** (2002) 223, [hep-lat/0204016].

[19] C. Morningstar and M. Peardon, Phys. Rev. **D69** (2004) 054501, [hep-lat/0311018].

[20] J. Kogut and L. Susskind, Phys. Rev. **D11** (1975) 395.

[21] R. Frezzotti, P. Grassi, S. Sint and P. Weisz, JHEP **08** (2001) 058, [hep-lat/0101001].

[22] A. Shindler, Phys. Rept. **461** (2008) 37, [arXiv:0707.4093].

[23] R. Frezzotti and G. Rossi, Nucl. Phys. (Proc. Suppl.) **128** (2004) 193, [hep-lat/0311008].

[24] C. Pena, S. Sint and A. Vladikas, JHEP **09** (2004) 069, [hep-lat/0405028].

[25] P. Hägler, Phys. Rept. **490** (2010) 49, [arXiv:0912.5483].

[26] T. Doi, PoS **LATTICE2012** (2012) 009, [arXiv:1212.1572].

[27] H. W. Lin, PoS **LATTICE2012** (2012) 013, [arXiv:1212.6849].

[28] J. B. Kogut and L. Susskind, Phys. Rev. **D11** (1975) 395.

[29] A. Bazavov, C. Bernard, C. DeTar, W. Freeman, S. Gottlieb et al., (2012), [arXiv:1212.4768].

[30] I. Allison, E. Dalgic, C. Davies, E. Follana, R. Horgan et al., Phys. Rev. **D78** (2008) 054513, [arXiv:0805.2999].

[31] G. Bali, F. Bruckmann, G. Endrődi, Z. Fodor, S. Katz et al., JHEP **1202** (2012) 044, [arXiv:1111.4956].

[32] G. Bali, F. Bruckmann, M. Constantinou, M. Costa, G. Endrődi et al., Phys. Rev. **D86** (2012) 094512, [arXiv:1209.6015].

[33] Y. Aoki, Z. Fodor, S. D. Katz and K. K. Szabó, JHEP **01** (2006) 089, [hep-lat/0510084].

[34] S. Borsányi, Z. Fodor, S. Katz, S. Krieg, C. Ratti et al., J. Phys. **G38** (2011) 124060, [arXiv:1109.5030].

[35] A. Bazavov, T. Bhattacharya, M. Cheng, C. DeTar, H. Ding, et al., Phys. Rev. **D85** (2012) 054503, [arXiv:1111.1710].

[36] A. Patel and S. Sharpe, Nucl. Phys. **B395** (1993) 701, [hep-lat/9210039].

[37] S. Aoki, T. Izubuchi, Y. Kuramashi and Y. Taniguchi, Phys. Rev. **D67** (2003) 094502, [hep-lat/0206013].

[38] Q. Mason, H. Trottier, R. Horgan, C. Davies and G. Lepage, Phys. Rev. **D73** (2006) 114501, [hep-ph/0511160].

[39] C. Alexandrou, M. Constantinou, T. Korzec, H. Panagopoulos and F. Stylianou, Phys. Rev. **D83** (2011) 014503, [arXiv:1006.1920].

[40] W. Lee and S. R. Sharpe, Phys. Rev. **D66** (2002) 114501, [hep-lat/0208018].

[41] J. Kim, W. Lee and S. R. Sharpe, Phys. Rev. **D81** 114503, [arXiv:1004.4039].

[42] S. Capitani, M. Göckeler, R. Horsley, H. Perlt, P. Rakow et al., Nucl. Phys. **B593** (2001) 183, [hep-lat/0007004].

[43] M. Constantinou, V. Lubicz, H. Panagopoulos and F. Stylianou, **JHEP** 0910 (2009) 064, [arXiv:0907.0381].

[44] D. Daniel and S. Sheard, Nucl. Phys. **B302** (1988) 471.

[45] N. Ishizuka and Y. Shizawa, Phys. Rev. **D49** (1994) 3519, [hep-lat/9308008].

[46] J. Gracey, Nucl. Phys. **B662** (2003) 247, [hep-ph/0304113].

[47] A. Buras and P. Weisz, Nucl. Phys. **B333** (1990) 66.

[48] G. 't Hooft and M. Veltman, Nucl. Phys. **B44** (1972) 189.

[49] S. Larin, Phys. Lett. **B303** (1993) 113, [hep-ph/9302240, containing an extra section].

[50] J. Kim, W. Lee and S. Sharpe, Phys. Rev. **D83** (2011) 094503, [arXiv:1102.1774].

[51] S. Borsányi, Z. Fodor, C. Hoelbling, S. Katz, S. Krieg et al., PoS **LATTICE2011** (2011) 209, [arXiv:1111.3500].

[52] M. Constantinou, M. Costa, M. Göckeler, R. Horsley, H. Panagopoulos et al., Phys. Rev. **D87** (2013) 096019, [arXiv:1303.6776].

[53] For the MILC collaboration's public lattice gauge theory code, see http://physics.utah.edu/∼detar/milc.html.

[54] V. P. Gusynin, V. A. Miransky and I. A. Shovkovy, Nucl. Phys. **B462**(1996) 249, [hep-ph/9509320].

[55] M. Chernodub, Phys. Rev. **D82** (2010) 085011, [arXiv:1008.1055].

[56] Y. Hidaka and A. Yamamoto, [arXiv:1209.0007].

[57] M. Chernodub, [arXiv:1209.3587].

[58] G. Bali, F. Bruckmann, G. Endrődi, Z. Fodor, S. Katz et al., PoS **LATTICE2011** (2011) 192, [arXiv:1111.5155].

[59] G. Bali, F. Bruckmann, G. Endrődi, Z. Fodor, S. Katz et al., [arXiv:1206.4205].

[60] M. D'Elia, S. Mukherjee and F. Sanfilippo, Phys. Rev. **D82** (2010) 051501, [arXiv:1005.5365].

[61] E.-M. Ilgenfritz, M. Kalinowski, M. Muller-Preussker, B. Petersson and A. Schreiber, Phys. Rev. **D85** (2012) 114504, [arXiv:1203.3360].

[62] Y. Aoki, G. Endrődi, Z. Fodor, S. D. Katz and K. K. Szabó, Nature **443** (2006) 675, [hep-lat/0611014].

[63] T. Vachaspati, Phys. Lett. **B265** (1991) 258.

[64] V. Skokov, A. Y. Illarionov and V. Toneev, Int. J. Mod. Phys. **A24** (2009) 5925, [arXiv:0907.1396].

[65] R. C. Duncan and C. Thompson, Astrophys. J. **392** (1992) L9.

[66] L. Landau, Zeitschrift für Physik A, Hadrons and Nuclei **64** (1930) 629.

[67] B. L. Ioffe and A. V. Smilga, Nucl. Phys. **B232** (1984) 109.

[68] P. Colangelo, F. De Fazio and A. Ozpineci, Phys. Rev. **D72** (2005) 074004, [hep-ph/0505195].

[69] A. Czarnecki, W. J. Marciano and A. Vainshtein, Phys. Rev. **D67** (2003) 073006, [hep-ph/0212229].

[70] V. M. Braun, S. Gottwald, D. Y. Ivanov, A. Schäfer and L. Szymanowski, Phys. Rev. Lett. **89** (2002) 172001, [hep-ph/0206305].

[71] B. Pire and L. Szymanowski, [arXiv:0909.0098].

[72] A. Nyffeler, PoS **CD09** (2009) 080, [arXiv:0912.1441].

[73] J. Rohrwild, JHEP **09** (2007) 073, [arXiv:0708.1405].

[74] V. Belyaev and Y. Kogan, Yad. Fiz. **40** (1984) 1035.

[75] I. Balitsky, A. Kolesnichenko and A. Yung, Sov. J. Nucl. Phys. **41** (1985) 178.

[76] P. Ball, V. M. Braun and N. Kivel, Nucl. Phys. **B649** (2003) 263, [hep-ph/0207307].

[77] O. Bergman, G. Lifschytz and M. Lippert, JHEP **0805** (2008) 007, [arXiv:0802.3720].

[78] A. Gorsky and A. Krikun, Phys. Rev. **D79** (2009) 086015, [arXiv:0902.1832].

[79] A. Vainshtein, Phys. Lett. **B569** (2003) 187, [hep-ph/0212231].

[80] H.-C. Kim, M. Musakhanov and M. Siddikov, Phys. Lett. **B608** (2005) 95, [hep-ph/0411181].

[81] A. E. Dorokhov, Eur. Phys. J. **C42** (2005) 309, [hep-ph/0505007].

[82] K. Goeke, H.-C. Kim, M. Musakhanov and M. Siddikov, Phys. Rev. **D76** (2007) 116007, [arXiv:0708.3526].

[83] S.-i. Nam, H.-Y. Ryu, M. Musakhanov and H.-C. Kim, J.Korean Phys.Soc. **55** (2009) 429, [arXiv:0804.0056].

[84] B. Ioffe, Phys.Lett. **B678**m(2009) 512, [arXiv:0906.0283].

[85] M. Frasca and M. Ruggieri, Phys. Rev. **D83** (2011) 094024, [arXiv:1103.1194].

[86] P. Buividovich, M. Chernodub, E. Luschevskaya and M. Polikarpov, Nucl. Phys. **B826** (2010) 313, [arXiv:0906.0488].

[87] V. Braguta, P. Buividovich, T. Kalaydzhyan, S. Kuznetsov and M. Polikarpov, PoS **LATTICE2010** (2010) 190, [arXiv:1011.3795].

[88] M. D'Elia and F. Negro, Phys. Rev. **D83** (2011) 114028, [arXiv:1103.2080].

[89] G. Martinelli, G. Parisi, R. Petronzio and F. Rapuano, Phys. Lett. **B116** (1982) 434.

[90] C. W. Bernard, T. Draper, K. Olynyk and M. Rushton, Phys. Rev. Lett. **49** (1982) 1076.

[91] G. 't Hooft, Nucl. Phys. **B153** (1979) 141.

[92] M. H. Al-Hashimi and U. J. Wiese, Annals Phys. **324** (2009) 343, [arXiv:0807.0630].

[93] S. Borsányi et al., JHEP **11** (2010) 077, [arXiv:1007.2580].

[94] H. Leutwyler and A. V. Smilga, Phys. Rev. **D46** (1992) 5607.

[95] G. S. Bali and K. Schilling, Phys.Rev. **D47** (1993) 661, [hep-lat/9208028].

[96] G. S. Bali and P. Boyle, [hep-lat/0210033].

[97] S. Borsányi et al., JHEP **1009** (2010) 073, [arXiv:1005.3508].

[98] G. Colangelo and S. Dürr, Eur. Phys. J. **C33** (2004) 543, [hep-lat/0311023].

[99] S. Dürr, Z. Fodor, C. Hoelbling, S. Katz, S. Krieg, et al, Phys. Lett. **B701** (2011) 265, [arXiv:1011.2403].

[100] M. Jamin, Phys. Lett. **B538** (2002) 71, [hep-ph/0201174].

[101] Y. Y. Balitsky, V. M. Braun and A. Kolesnichenko, Sov. J. Nucl. Phys. **48** (1988) 348.

[102] N. Nielsen, Am. J. Phys. **49** (1981) 1171.

[103] Xiang-Dong Ji, J. Phys. **G24** (1998) 1181, [hep-ph/9807358].

[104] LHPC Collaboration: Ph. Hagler, J.Negele, D. Renner, W. Schroers, Th. Lippert, K. Schilling, Phys. Rev. **D68** (2003) 034505, [hep-lat/0304018].

[105] J. D. Bjorken, Phys. Rev. **148** (1966) 1467.

[106] A. H. Mueller, Phys. Rev. **D9** (1974) 963.

[107] V. M. Braun, A. N. Manashov and J. Rohrwild, Nucl. Phys. **B807** (2009) 89, [arXiv:0806.2531].

[108] M. Göckeler, R. Horsley, T. Kaltenbrunner, Y. Nakamura, D. Pleiter, P. E. L. Rakow, A. Schäfer, G. Schierholz, H. Stüben, N. Warkentin and J. M. Zanotti, Nucl. Phys. **B812** (2009) 205, [arXiv:0810.3762].

[109] D. Dolgov, R. Brower, S. Capitani, P. Dreher, J. W. Negele et al, Phys. Rev. **D66** (2002) 034506, [hep-lat/0201021].

[110] K.G. Chetyrkin and F.V. Tkachov, Nucl. Phys. **B192** (1981) 159.

[111] A. Efremov and A. Radyuskin, Phys. Lett. **A24** (2009) 2803.

[112] C. Diaconu, Int. J. Mod. Phys. **A24** (2009) 1069.

[113] H. Kawai, R. Nakayama and K. Seo, Nucl. Phys. **B189** (1981) 40.

[114] G. Martinelli, C. Pittori, C. T. Sachrajda, M. Testa and A. Vladikas, Nucl. Phys. **B445** (1995) 81, [hep-lat/9411010].

[115] R. Arthur and P. A. Boyle (RBC and UKQCD Collaborations), Phys. Rev. **D83** (2011) 114511, [arXiv:1006.0422].

[116] H. Panagopoulos and E. Vicari, Nucl. Phys. **B332** (1990) 261.

[117] M. Göckeler, R. Horsley, Y. Nakamura, H. Perlt, D. Pleiter, P. E. L. Rakow, A. Schäfer, G. Schierholz, A. Schiller, H. Stüben and J. M. Zanotti (QCDSF/UKQCD Collaboration), Phys. Rev. **D82** (2010) 114511 [Erratum-ibid. **D86** (2012) 099903], [arXiv:1003.5756].

[118] M. Göckeler, R. Horsley, E.-M. Ilgenfritz, H. Perlt, P. E. L. Rakow, G. Schierholz and A. Schiller, Phys. Rev. **D54** (1996) 5705, [hep-lat/9602029].

[119] S. A. Larin, T. van Ritbergen and J. A. M. Vermaseren, Nucl. Phys. **B427** (1994) 41.

[120] A. Retey and J. A. M. Vermaseren, Nucl. Phys. **B604** (2001) 281, [hep-ph/0007294].

[121] J. A. Gracey, JHEP **0610** (2006) 040, [hep-ph/0609231].

[122] A. Skouroupathis and H. Panagopoulos, PoS **LATTICE2010**, 240 (2010).

[123] Mathematica, Version 9.0, Wolfram Research, Inc., Champaign, IL (2012).

[124] MINUIT, Reference Manual, F. James, CERN Geneva, Switzerland (1994).

[125] QCDSF collaboration, in preparation.

[126] P. Fritzsch, F. Knechtli, B. Leder, M. Marinkovic, S. Schaefer, R. Sommer and F. Virotta (ALPHA Collaboration), Nucl. Phys. **B865** (2012) 397, [arXiv:1205.5380].

[127] G. S. Bali, P. C. Bruns, S. Collins, M. Deka, B. Gläßle, M. Göckeler, L. Greil, T.R. Hemmert, R. Horsley, J. Najjar, Y. Nakamura, A. Nobile, D. Pleiter, P. E. L. Rakow, A. Schäfer, R. Schiel, G. Schierholz, A. Sternbeck and J. M. Zanotti (QCDSF Collaboration), Nucl. Phys. **B866** (2013) 1, [arXiv:1206.7034].

[128] P. Boucaud, F. de Soto, J. P. Leroy, A. Le Yaouanc, J. Micheli, H. Moutarde, O. Pene and J. Rodriguez-Quintero, Phys. Lett. **B575** (2003) 256, [hep-lat/0307026].

[129] F. de Soto and C. Roiesnel, JHEP **0709** (2007) 007, [arXiv:0705.3523].

[130] S. Collins, M. Göckeler, P. Hägler, R. Horsley, Y. Nakamura, A. Nobile, D. Pleiter, P. E. L. Rakow, A. Schäfer, G. Schierholz, W. Schroers, H. Stüben, F. Winter and J. M. Zanotti (QCDSF/UKQCD Collaboration), Phys. Rev. **D84** (2011) 074507, [arXiv:1106.3580].

[131] T. Bakeyev, M. Göckeler, R. Horsley, D. Pleiter, P. E. L. Rakow, G. Schierholz and H. Stüben (QCDSF/UKQCD Collaboration), Phys. Lett. **B580** (2004) 197, [hep-lat/0305014].

[132] G. D'Ambrosio, G. Isidori and G. Martinelli, Phys. Lett. **B480** (2000) 164, [hep-ph/9911522].

[133] S. Bertolini, J.O. Eeg and M. Fabbrichesi, Phys. Lett. **B449** (1995) 197, [hep-ph/9409437].

[134] D. Becirevic, V. Lubicz, G. Martinelli and F. Mescia, Phys. Lett. **B501** (2001) 98, [hep-ph/0010349].

[135] I. Baum, V. Lubicz, G. Martinelli, L. Orifici and S. Simula, Phys. Rev. **D84** (2011) 074503, [arXiv:1108.1021].

[136] M. Ciuchini, E. Franco, L. Reina and L. Silvestrini, Nucl. Phys. **B421** (1994) 41, [hep-ph/9311357].

[137] R. Frezzotti and G. C. Rossi, JHEP **0408** (2004) 007, [hep-lat/0306014].

[138] R. Frezzotti and G. C. Rossi, JHEP **0410** (2004) 070, [hep-lat/0407002].

[139] R. Frezzotti and G. C. Rossi, [hep-lat/0507030].

[140] K. G. Chetyrkin and A. Rétey, [hep-ph/0007088].

[141] H. Panagopoulos and E. Vicari, Phys. Rev. **D58** (1998) 114501, [hep-lat/9806009].

[142] G. P. Lepage and P. B. Mackenzie, Phys. Rev. **D48** (1993) 2250, [hep-lat/9209022].

[143] G. I. Egri, Z. Fodor, C. Hoelbling, S. D. Katz, D. Nógrádi et al, Comput. Phys. Commun. **177** (2007) 631, [hep-lat/0611022].

[144] F. Wilczek, [hep-th/9609099].

[145] A. Grozin, [arXiv:0803.2589].

[146] W. Heisenberg and H. Euler, Z. Phys. **98** (1936) 714.